The Determination of Subtle Deformation Signals Using a Permanent CGPS Network in the Aegean

Nicholas David Forrest

Thesis submitted for the degree of Doctor of Philosophy of University College London

Department of Civil, Environmental and Geomatic Engineering

University College London

Abstract

Geophysical motions can occur over a broad temporal spectrum, from high frequency seismic movements to very long period tectonic deformation. The Aegean region is tectonically one of the most active areas on Earth. There have, over the past 15 years, been a range of campaign style GPS studies which have looked to increase our knowledge of the area and better define the geodynamic processes involved. In 2002 the Center for the Observation and Modelling of Earthquakes and Tectonics (COMET) established a network of continuously operating GPS receivers (CGPS) throughout the region in order to add to the knowledge gained from previous studies.

This thesis focuses on which tectonic motions can be observed using the COMET continuous GPS network. Approaches for the precise analytical estimation of subtle tectonic motion are presented. Daily coordinate estimates of COMET sites and a number of ITRF (International Terrestrial Reference Frame) sites around Europe were calculated using a precise point positioning strategy and ambiguity resolution using NASA's GIPSY – OASIS II processing software and IGS (International GPS Service) precise products. Time series produced showed post fit standard deviations of 2-3 mm in the horizontal and 6-8 mm in the vertical. Significant annual periodic variation is observed in the time series.

The coordinate time series studies were further refined using a selection of filters. Firstly, gross and sigma filters were applied to remove outliers, the data then had a range of regional filters applied looking to best define and remove the common mode error in the area. These filters produced mixed results with time series improvement occurring on a site by site basis. In some cases noise was reduced by a factor of 2 whilst in other cases there was little or no improvement. This combined with a lack of knowledge of the individual site movements led to the use of a filtered baseline method, whereby common mode error was removed purely on a site by site basis. This method revealed expansion across the Hellenic arc of the order of a few millimetres per year and sub millimetre north-south compaction behind the arc. It also revealed first evidence of transient motion at a number of sites parallel to the Hellenic arc. The

transient signals occurred every 12 months ±1.5 and lasting for 40 – 100 days. These signals were not so much a reversal of tectonic motion akin to the silent earthquakes observed in Cascadia, Japan and Mexico, instead they appeared more as a pause in the otherwise consistent movement of the Aegean microplate overriding the subducting African lithosphere. In addition to the observed tectonic signals, the effects and implications of the two post processing strategies are analysed and discussed.

Higher temporal frequency positioning is carried out on seismic events (M_w 6.7 earthquake Kithera, M_w 8.1 and M_w 6.7 earthquakes, Macquarie island) using instantaneous positioning followed by "sidereal filtering" whereby integer-cycle phase ambiguities are resolved using only single epochs of dual frequency phase and pseudorange data. These positions are then siderealy stacked to reduce the effects of geometry related error. The technique reduces geometry related noise by a factor ≈2 using epoch by epoch 30 second data. The feasibility of the technique for observing pre, co and post seismic signals is demonstrated.

A visualisation tool was developed to allow the simultaneous observation of the tectonic motion of a CGPS network data over any spatial and temporal regimes.

Acknowledgements

I would like to thank the many people who helped and contributed to make this work possible. Firstly to my supervisor Marek Ziebart for his enthusiasm, encouragement, support and for sharing his vast geodetic knowledge as well as creating an environment conducive to developing my ideas. Thanks also for the hours spent reading, correcting and commenting on this manuscript.

I am also very grateful to my colleagues, in particular Anthony Sibthorpe who provided advice on a wide array of subjects but in particular C++, C-scripts, AWK and the use of the Generic Mapping Tool (GMT). In addition I would like to thank him for his contribution to the programming of the visualisation tool developed as part of my research.

Furthermore I would like to thank Geoff Blewitt for his help with all aspects of GIPSY-OASIS, the additional scripts he wrote and for welcoming me on my visit to Reno.

Thanks to the Center for the Observation and Modelling of Earthquakes and Tectonics (COMET) group, in particular to Michael Floyd for the provision of much of the data used in the course of my research. This was furnished by the National Technical University of Athens (NTU) and the International GPS Service (IGS).

This Thesis was funded by a Natural Environmental Research Council (NERC) studentship.

Special thanks to my wife Michelle for putting up with my moods and for pretending to listen as I talked about a subject that doesn't hold quite so much interest for her.

Contents

List of Figures

List of Tables

Glossary

AC	Analysis Center
ARTA	Aspect Repeat Time Adjustment
CEFMO	Code aux Elements Finis pour la Maree Oceanique
CGPS	Continuous GPS
COMET	Center for the Observation and Modelling of Earthquakes and Tectonics
CORS	Continuously Operating Reference Stations
COTS	Commercial off the shelf
DORIS	Doppler Orbitography and Radiopositioning Integrated by Satellite system
ECEF	Earth Centered Earth Fixed
ECI	Earth Centered Inertial
EOP	Earth Orientation Parameters
ERA	Earthquake Risk Assessment
EUREF	European Reference (Network of CORS)
f_1, f_2	The GPs signal frequencies (L1 1575.42 MHz; L2 1227.6 MHz)
GIPSY-OASIS	GPS Inferred Positioning SYstem – Orbit Analysis and SImulation Software
GMT	Generic Mapping Tool
GNSS	Global Navigation Satellite System
GPS	Global Positioning Service
GRACE	Gravity Recovery and Climate Experiment
GSHAP	Global Seismic Hazard Assessment Program
IAG	International Association of Geodesy
ICRF	International Celestial Reference Frame
ICSU	International Council of Scientific Unions
IERS	International Earth Rotation Service
IGS	International GPS Service
ILP	International Lithosphere Program
InSAR	Interferometric Synthetic Aperture Radar

ITRF	International Terrestrial Reference Frame
JPL	Jet Propulsion Laboratory
LEGOS	Laboratoire d'Etudes en Geophysique et Oceanographie Spatiales
NASA	National Aeronautics and Space Administration
NTU	National Technical University of Athens
PANGA	Pacific Northwest Geodetic Array
PCO	Phase Center Offset
PCV	Phase Center Variation
PGA	Peak Ground Accelerations
RINEX	Receiver Independent EXchange Service
SESAME	Seismotectonics and Seismic Hazard Assessment of the Mediterranean
SINEX	Solution Independent EXchange Service
SLR	Satellite Laser Ranging
SRTM	Shuttle Radar Topography Mission
SV	Satellite Vehicle
USGS	United States Geological Survey
UTC	Universal Time Coordinated
VLBI	Very Long Baseline Interferometry

Chapter 1

Introduction

1.1 Observing Ground Motion

Geodesy is the science related to the determination of the size, shape and gravity field of the Earth. In recent years technology has allowed us to focus in greater and greater detail at not just the size and shape of the Earth but how the Earth deforms. Key to these deformations is the theory of continental drift proposed by Alfred Wegener in 1915. His theory that the Earth's crust is comprised of a number of plates that move throughout time was eventually termed plate tectonics and gained credibility due to evidence such as the symmetrical nature of magnetic anomalies either side of the Earths mid ocean ridges and the concentration of seismology around continental edges. Historically the movements of the Earth's tectonic plates were determined from the geological record, using for example plate boundary data such as magnetic anomalies and directions determined from transform fault azimuths and earthquake slip vectors (*Demets et al. 1990*). Spreading rates and average directions of plate movement determined from these phenomena are derived over long timescales and give little information about deformations within the plate boundary zones. The development of space Geodetic technologies such as VLBI (Very Long Baseline Interferometry), SLR (Satellite Laser Ranging), InSAR (Interferometric Synthetic Aperture Radar), DORIS (Doppler Orbitography and Radiopositioning Integrated by Satellite system) and GPS (Global Positioning System) have allowed us to observe the Earth's movement and deformation with greater accuracy and a higher temporal resolution. This has enabled us to refine the plate tectonic theory with the quantification of plate motions such as the formation of the NNR-Nuvel1 and NNR-Nuvel-1a models of tectonic motion (*DeMets et al 1990, 1994*).

GPS in particular has allowed us to observe plate motion at finer and finer spatial and temporal resolutions. Rather than using data derived from the geological record that represents, on average, millions of years of plate movement which may not accurately reflect current plate motion, GPS needs only a short period of data to define not only the general movement of the Earth's plates, but also to more accurately quantify deformations and interactions in the plate boundary zones. This tectonic motion in plate boundary zones can occur over a wide range of spatial regimes from the large movements associated with major earthquakes to subtle stresses and strains. This has in turn placed greater demands on the accuracy and precision of the GPS observing technique to better define and observe these subtle movements.

GPS measurements are either collected in field campaigns, whereby an area is surveyed for a short period and later reoccupied over a number of years to observe the displacement and hence velocity field of a network over time, or by continuously occupied arrays of GPS receivers designed to provide an uninterrupted history of all ground motions over an extended period of time. Modern Geodesy recognises that ground motion can occur at practically all temporal regimes from seismic to geologic, which has led to many more continuously occupied GPS (CGPS) networks. In the past ten years these CGPS arrays have revealed a number of aseismic transient crustal movements that have been termed "silent" or "slow" earthquakes. They have been detected in a number of places around the world but in particular on the subduction interfaces in Cascadia and Japan (*Dragert et al. 2001; Ozawa et al. 2004*). This has led to debate into their origins, triggers, stress and strain fields and in particular whether they are potentially releasing or removing strain from the seismogenic part of the subduction interface and therefore their potential as a seismic earthquake precursor.

1.2 The Study Area

The Aegean region of the eastern Mediterranean is in the collision zone of the African, Arabian and Eurasian lithospheric plates. This has led to a number of microplates forming a broad zone of continental deformation, with the westerly movement of the Anatolian microplate leading to the extrusion of the Aegean which in turn over rides the subducting African lithosphere (Figure 1.1). This complex area of continental collision

is therefore one of the most seismically active areas in the world. This is reflected in the large number (> 4500) of earthquakes with magnitude >4 over the last 30 years (*Hollenstein, 2007*).

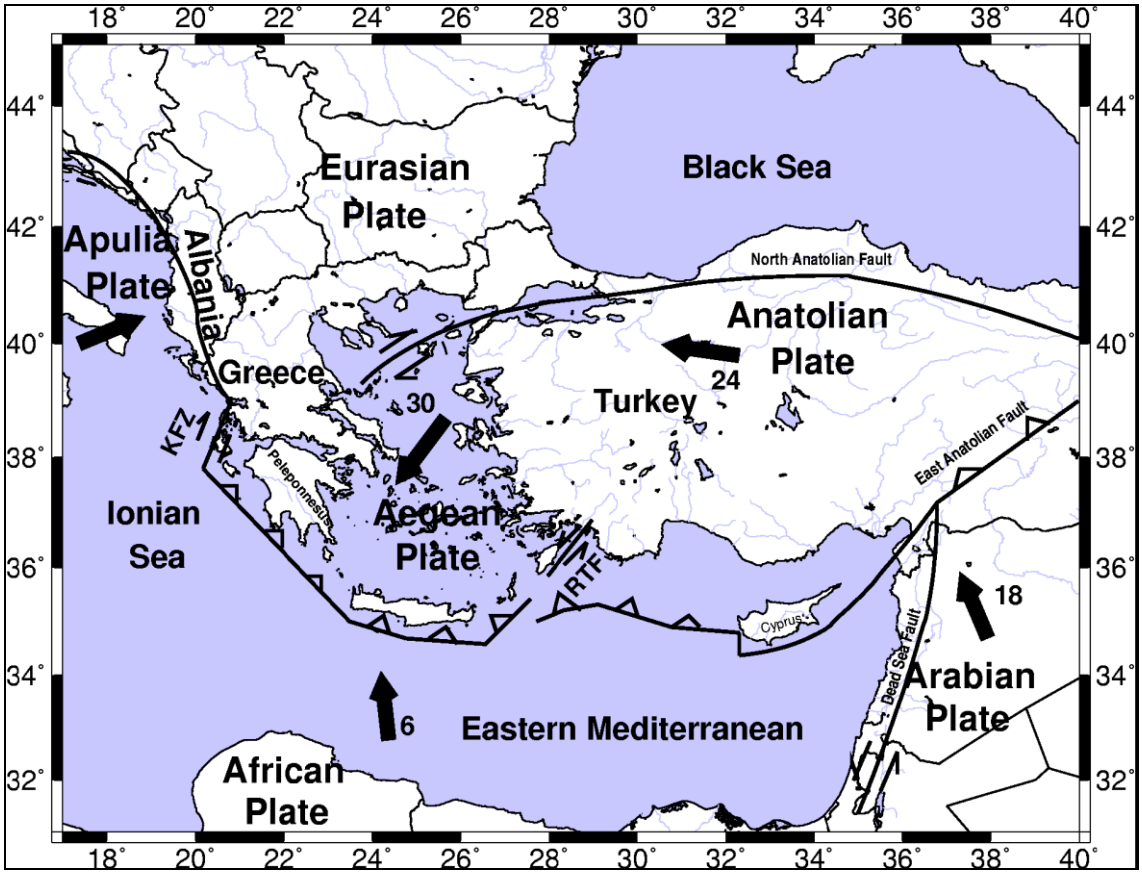

Figure 1.1: Geological setting of the Aegean region. Arrow indicate the motion relative to Eurasia, mm/yr (from McClusky et al. 2000)

Because of this, many geological and geophysical models have been made describing the kinematics of the area (*McKenzie et al. 1983; Jackson et al. 1992*) and in more recent times direct measurement of the present kinematic movements of the plates and microplates have been determined using space geodetic techniques such as SLR, VLBI and in particular GPS. The GPS data largely consist of campaign style measurements aquired over roughly a ten year period (*Clarke et al. 1998; Cocard et al. 1999; McClusky et al. 2000; Meade et al. 2002; Nyst and Thatcher, 2004*). These results and others in the surrounding area have constrained the current velocity fields in the area. They have revealed 30-40 mm per year of southerly movement along the Hellenic arc relative to Eurasia. This amount of tectonic movement produces a lot of earthquakes, however, despite the high levels of seismicity around the Hellenic arc, studies have shown that seismic slip on the Hellenic subduction zone can only account for between 10% and 45% of that necessary to accommodate the subduction of the oceanic

Mediterranean Sea floor beneath the continental lithosphere of the Aegean region (*Jackson and McKenzie, 1988b; Main and Burton, 1989; Koaros et al. 2003; Jenny et al. 2004*).

This disparity can be explained as evidence of either occasional large seismic events or the presence of aseismic slip. There is a good historical record of seismicity around Greece which confirms there are occasional large seismic events but these are not frequent enough to account for all the slip on the subduction interface therefore there has to be the presence of aseismic slip in the region. This aseismic slip could either take the form of continuous stable slip or be of a more transient nature.

The COMET group (Centre for the Observation and Modelling of Earthquakes and Tectonics) has for a number of years, been involved in determining the velocities and deformations of the Aegean area. To assist this, a continuous GPS network was established throughout Greece in 2003 (figure 1.2).

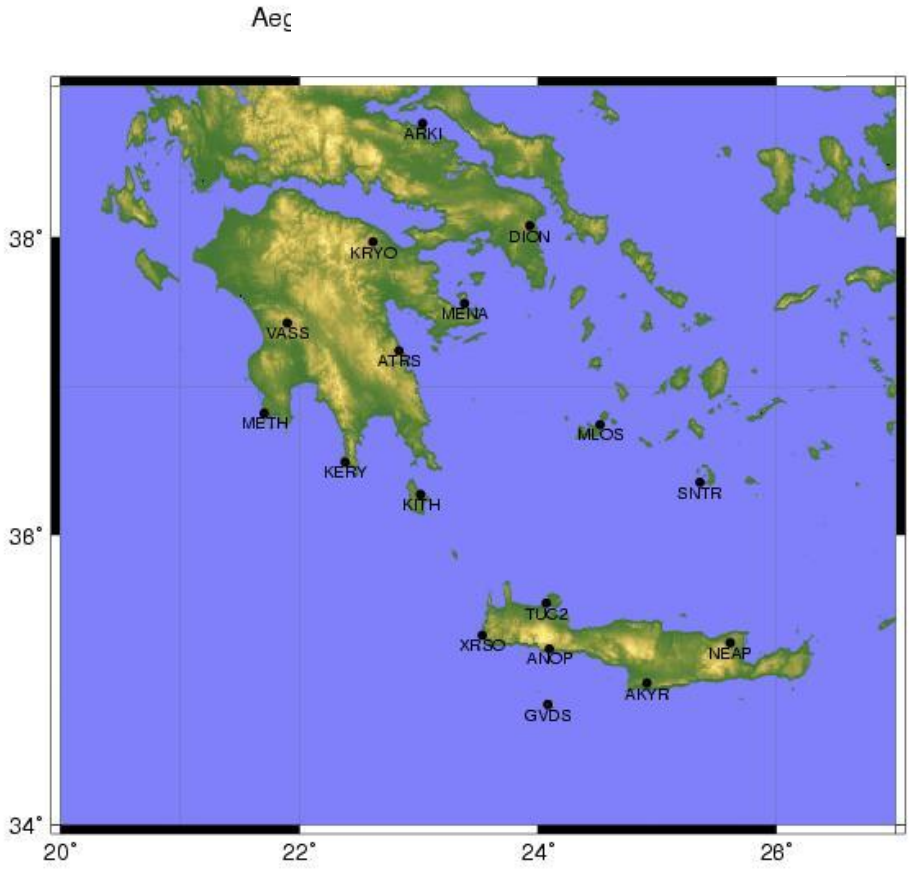

Figure 1.2: The CGPS sites established by the COMET group around the Aegean. (ARKI and DION established by NTU, TUC2 is a EUREF site)

The use of CGPS has a number of advantages compared to the campaign measurements and geological and geophysical models mentioned above:

- It allows the examination of tectonic signals at all temporal resolutions. This potentially allows the study of pre, post and co seismic signals as well as any transient motion that may occur.
- The low number of campaigns and short observation times in each of those campaigns, as well as set up problems, result in relatively high levels of uncertainty in any parameters estimated from the data collected, for example strain rate. CGPS eliminates these problems.
- Vertical accuracies are notoriously inaccurate in GPS campaign networks (*Leick, 2004*).

The aim of this thesis is therefore to determine what can be gained from the use of CGPS in the Aegean region for the detection and characterisation of tectonic signals. Within this a particular emphasis was to be made on how CGPS can be used to best determine seismic or transient events as well as adding to the knowledge of the general velocities and strain fields in the region. The reported achievable scatter in daily GPS coordinate solutions is currently 1-3 mm in the north, and 3-5 mm in the east components. It is worse in the vertical, 7-10 mm, due to the weaker satellite geometry and the fact that many systematic errors and biases have a greater effect on this component (*Nikolaidis, 2002*). These values can be improved in post processing by reducing noise through the application of suitable filters such that subtle geophysical signals can be observed. Measurements at this level are sufficiently precise to determine transient motion around other tectonic subduction zones (*Blewitt,1993*), the study therefore looks to prove or discount the presence of similar transient movements within the Aegean, as well as to better define the general velocities and strain fields in the region.

The use of CGPS allows the analysis of seismic signals in the Aegean region. An additional aim of the thesis is therefore to apply filtering techniques, in particular sidereal filtering, to reduce noise levels in sub twenty four hour time series to see if any earthquakes during the study period are of sufficient magnitude to show co or post seismic signals.

The visualisation of GPS data is at present fairly limited when looking at a large quantity of data over a wide area and long duration. In general subtle signals are identified using time series, either of baseline variation or variation in the baseline components. In the process of investigating geophysical signals in the Aegean the development of a visualisation technique to simultaneously display large amounts of GPS data over a range of temporal and spatial regimes will also be investigated.

1.3 Summary of Aims

- To determine what can be gained from the use of CGPS in the Aegean region for the detection and characterisation of transient tectonic signals.
- Define the baseline variation and hence strain rates across the COMET network in the Aegean.
- The determination of what can be gained from the use of CGPS in the Aegean region for the detection and characterisation of seismic signals.
- Investigate the visualisation of GPS data when looking at geophysical signals.

1.4 Overview of Thesis Structure

Chapter 1 is the introduction explaining the basis and focus of the research

Chapter 2 looks into the relevant geological background, the setting of the Aegean study region and the area around Maquarie Island which is used to compare the sidereal filtering technique. The current understanding of aseismic motion is outlined. Asiesmic motion is observed as stable slip in most faults in the world, there are however a number of examples of transient aseismic slip in subduction zones, transform faults and around volcanic activity.

The geodetic background necessary to observe ground motion at yearly, daily and sub-daily timescales is discussed in chapter 3, in particular considering the various Earth movements and other error sources, as well as the choice of reference frame necessary

to mitigate these error sources. The chapter also gives some background regarding the processing strategies and processing software available to undertake this kind of study.

Chapter 4 explains the exact processing strategies employed by the author to evaluate the daily GPS data from the Aegean. A precise point positioning technique with ambiguity resolution was applied to determine the general time series of the COMET sites and a range of IGS/EUREF sites. These were processed using the GIPSY-OASIS II software and precise JPL and IGS products. The search for any possible transient movements and the analysis of the general tectonic velocity and strain fields involved the use of a range of regional filters and differencing to remove general common mode errors without averaging out potential subtle tectonic movements. The results of these studies are then displayed and discussed. The spatial coherence of common error, and its often assumed homogeneity is a subject this thesis aims to address.

Chapter 5 looks at the sidereal filtering technique. A number of examples of its application, namely the M_w 6.7 earthquake on the 8th of January 2006, located near the island of Kithira and two other examples near Macquarie Island, the M_w 8.1 event on the 23rd of December 2004 and the M_w 6.5 quake on the 10th of November 2007. The sidereal filter was applied to look at the benefits and limitations of the technique when studying co and post seismic motion using 30 second GPS data.

The subject of visualising and displaying CGPS data is looked at in chapter 6. The traditional use of time series and velocity vectors is discussed and a new technique for the simultaneous visualisation of large quantities of CGPS data over a range of spatial and temporal scales is presented. The benefits and drawbacks of this technique are analysed and discussed.

The daily GPS results and the sidereal filtering are discussed with respect to their geodetic and geological implications in chapter 7. Conclusions and closing remarks are covered in chapter 8.

Chapter 2

Geological Background

This chapter highlights the geological motivation behind the thesis, firstly introducing some of the general geological theories that are discussed and examined in later chapters and secondly giving the reader a background of the specific geological concepts studied within this thesis, in particular those pertinent to the Aegean region and the range of tectonic movements that can affect it.

2.1 Seismic Hazard Assessment

Earthquakes represent a major natural hazard, resulting in loss of life and economic losses due to damage to buildings, infrastructure and businesses. Seismic hazard is defined as the probable level of ground shaking associated with the occurrence of earthquakes (*Giardini et al. 2000*). The assessment of seismic hazard is the first step in the evaluation of seismic risk, obtained by combining the seismic hazard with local soil conditions and with vulnerability factors (type, value and age of buildings and infrastructures, population density, land use). Frequent, large earthquakes in remote areas result in high seismic hazard but pose no risk; on the contrary, moderate earthquakes in densely populated areas entail small hazard but high risk (*Giardini et al. 2000*).

For people living in areas affected by earthquakes, risk management decisions need to be made. For example decisions regarding the level of the determination of aseismic design (earthquake-resistant design developed to limit the potential damage of buildings to a tolerable level) (*Park et al. 1987*), whether or not the structural upgrading

of buildings is appropriate or how to cost insurance premiums. These decisions need to be based on some prediction of the likelihood and magnitude of future earthquake events, which are derived through an Earthquake Risk Assessment (ERA), in order to develop strategies which will help manage or mitigate future seismic events.

There are two different approaches that can be used to assess the risk associated with a particular seismic hazard, deterministic and probablistic. Deterministic is a more conservative approach which looks at the worst possible senario. For this reason it is mainly used in the plans for emergency response or the assessment of structures such as dams or nuclear plants which require very high safety measures (*McGuire, 2001*). Probablistic analysis on the other hand accepts uncertainties in features such as earthquake magnitude, location and duration and using this knowledge gives a quantitative assessment of risk which leads to its use in descisions such as seismic design levels and insurance premiums (*Banitsiotou et al. 2004*). The basic elements of modern probabilistic seismic hazard assessment can be grouped into four main categories:

1. *Earthquake Catalogue*: the compilation of a uniform database and catalogue of seismicity for the historical (pre-1900), early-instrumental (1900-1964) and instrumental periods (1964-today).

2. *Earthquake Source Model*: the creation of a master seismic source model to describe the spatial-temporal distribution of earthquakes, integrating the earthquake history with evidence from seismotectonics, paleoseismology, mapping of active faults, geodesy and geodynamic modeling.

3. *Strong Seismic Ground Motion*: the evaluation of ground shaking as a function of earthquake size and distance, taking into account propagation effects in different tectonic and structural environments.

4. *Seismic Hazard*: the computation of the probability of occurrence of ground shaking in a given time period, to produce maps of seismic hazard and related uncertainties at appropriate scales (*Giardini et al. 2000*).

In reality both techniques are generally used with the probablistic analysis guiding the deterministic events (*McGuire, 2001*).

Over the last fifteen years several projects on seismic hazard assessment have been undertaken on global and regional scales (*Jiminez et al. 2003*). On a world scale the Global Seismic Hazard Assessment Program (GSHAP) compiled the hazard results from a wide range of national and multinational programs. The ILP/ICSU's (International Lithosphere Project / International Council of Scientific Unions) Global Seismic Hazard Assessment Program is a demonstration program of the UN's International Decade for Natural Disaster Reduction. The GSHAP was implemented in the 1992-1997 period (*Grunthal et al. 1999. Giardini et al. 2000. Jiminez et al. 2003*). The generation of a uniform seismic hazard model for the whole of the Mediterranean has been carried out under the International Geological Correlation Program project n.382 "Seismotectonics and seismic hazard assessment of the Mediterranean basin" (SESAME). This was completed in 2000 but the work was taken further by the European Seismological Commission (ESC), which created a unified seismic hazard model for Europe and the Mediterranean in 2002 (*Jiminez et al. 2003*). An example of this work can be seen in figure 2.1.

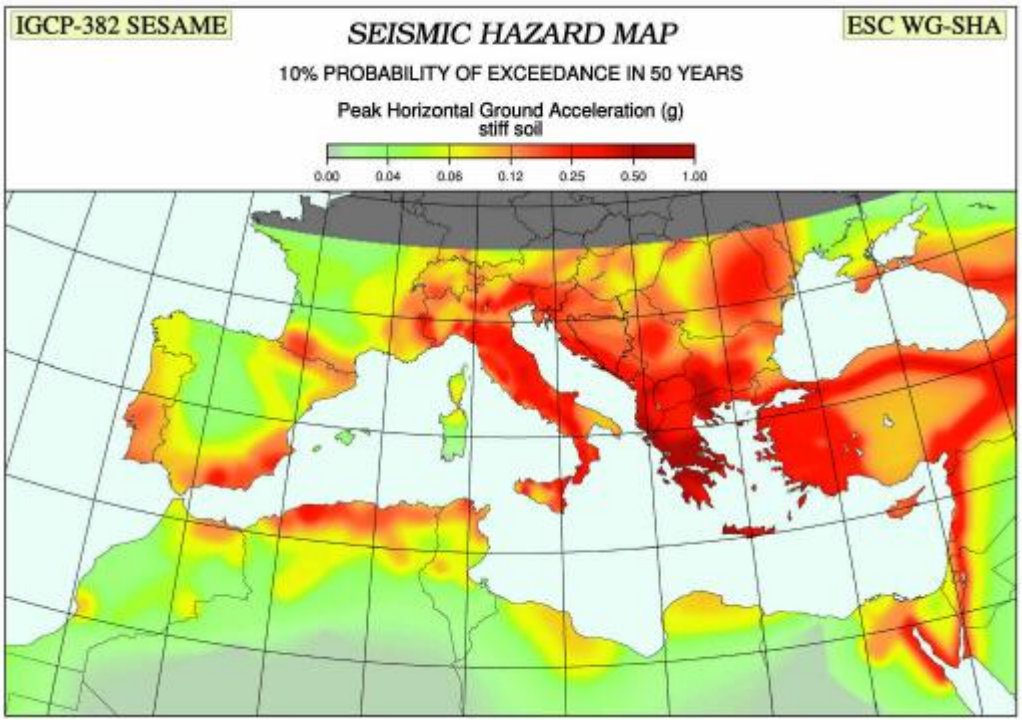

Figure 2.1: Seismic hazard map of the Mediterranean depicting PGA on stiff soil in g units for a 10% probability of exceedance in 50 years (*Jiminex et al. 2001*)

For these sorts of publications to be relevant a complete understanding of all the processes that affect these tectonically active areas must be applied.

2.2 Earthquakes and the Earthquake cycle

An earthquake is the result of the sudden release of energy stored in the Earth's crust that creates seismic waves. At the Earth's surface they manifest themselves by the shaking and displacement of the ground that can result in the loss of life and the destruction of property. The most common cause is the strain build up associated with tectonic plates, the strain becomes so great that the rock gives way by breaking and sliding along fault planes. Other smaller earthquakes can also be caused by volcanic activity, landslides or human activities such as mine blasts or nuclear tests.

There are two types of seismic wave, Body Waves and Surface Waves. Other modes of wave propagation exist, but they are of comparatively minor importance (*Chapman 2004*).

2.2.1 Seismic Waves

Body Waves

Body waves, as their name suggests travel through the Earth. They follow raypaths bent by the varying density and modulus (elasticity of the Earth) of the Earth's interior. The Earth's interior varies according to temperature, composition and phase. The body waves are felt as the first arriving tremors of an earthquake, as well as many later arrivals. There are two kinds of body wave, the primary (P-waves) and secondary (S-waves).

P-waves are longitudinal or compressional waves, which means that the ground is alternately compressed and dilated in the direction of propagation. In solids these waves generally travel slightly less than twice as fast as S waves (typically between 1 and 14 km/s) and can travel through any type of material. When generated by an earthquake they are less destructive than the S waves and surface waves that follow them, due to their lesser amplitude.

S-waves are transverse or shear waves, which means that the ground is displaced perpendicularly to the direction of propagation. In the case of horizontally polarized S waves, the ground moves alternately to one side and then the other. S waves can travel only through solids, as fluids (liquids and gases) do not support shear stresses.

Surface Waves

Surface waves are analogous to water waves and travel just under the Earth's surface. They travel more slowly than body waves (typically between 1 and 8 km/s). Because of their low frequency, long duration, and large amplitude, they can be the most destructive type of seismic wave. There are two types of surface waves, Rayleigh waves and Love waves.

Rayleigh waves are also known as ground roll. They are waves that travel analogously to ripples on water. They travel at roughly 70% of the velocity of S waves (typically between 2 and 6 km/s).

Love waves are surface waves that cause horizontal shearing of the ground. They usually travel slightly faster than Rayleigh waves, about 90% of the S-wave velocity. A summary of these wave types can be seen in figure 2.2.

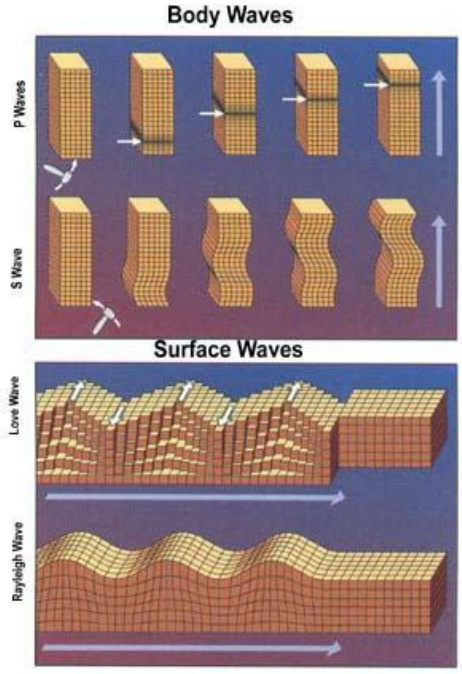

Figure 2.2: The major seismic wave forms (figure from USGC, http://www.usgs.gov)

The amplitude and duration of these seismic waves in turn determines the earthquake magnitude. Earthquakes range broadly in size. A rock burst in a mine may involve the fracture of 1 meter of rock; the 2004 Sumatra-Andaman earthquake ruptured approximately 1,600 kilometers of the Earth's crust. Earthquakes can be even smaller and even larger. If an earthquake is felt or causes perceptible surface damage, then its intensity of shaking can be subjectively estimated (The Mercalli Scale). But many large earthquakes occur in oceanic areas or at great focal depths and are either simply not felt or their felt pattern does not really indicate their true size (*Spence et al 1989*). As such a more quantitative method of defining the magnitude of any given earthquake was developed. This was pioneered by Charles Richter who studied and noted the maximum signal amplitude of one particular seismograph in California.

2.2.2 Earthquake Magnitude

Seismologists calculate the size of an earthquake using a range of magnitude scales. This is largely due to the variation in the seismometers, each of which is designed to measure different wave types and different magnitudes. All of the methods are designed to agree well over the range of magnitudes where they are reliable. A summary of the magnitude types and their respective scales can be seen in table 2.1.

Magnitude type	**Applicable magnitude range**	**Comments**
Duration (Md)	< 4	Based on the duration of shaking as measured by the time decay of the amplitude of the seismogram. Often used to compute magnitude from seismograms with "clipped" waveforms due to limited dynamic recording range of analog instrumentation, which makes it impossible to measure peak amplitudes.
Local (ML)	2-6	Based on the maximum amplitude of a seismogram recorded on a Wood-Anderson torsion seismograph. Although these instruments are no longer widely in use, ML values are calculated

		using modern instrumentation with appropriate adjustments.
Surface wave (Ms)	5-8	A magnitude for distant earthquakes based on the amplitude of Rayleigh surface waves measured at a period near 20 sec.
Moment (Mw)	> 3.5	Based on the moment of the earthquake, which is equal to the rigidity of the Earth times the average amount of slip on the fault times the amount of fault area that slipped.
Energy (Me)	> 3.5	Based on the amount of recorded seismic energy radiated by the earthquake.
Moment (Mi)	5-8	Based on the integral of the first few seconds of P wave on broadband instruments (Tsuboi method).
Body (Mb)	4-7	Based on the amplitude of P body-waves. This scale is most appropriate for deep-focus earthquakes.
Surface wave (MLg)	5-8	A magnitude for distant earthquakes based on the amplitude of the surface waves.

Table 2.1: Magnitudes used in determining earthquake size (Taken from USGS)

These scales of magnitude combine to define the size of an earthquake which is defined by the Richter scale. The scale most frequently quoted in scientific writing is the moment magnitude (M_w).

2.2.3 The Richter Scale

The Richter magnitudes are based on a logarithmic scale (base 10). Using this scale, a magnitude 5 earthquake would result in ten times the level of ground shaking as a magnitude 4 earthquake (and 32 times as much energy would be released). Although Richter originally proposed this way of measuring an earthquake's "size," he only used a certain type of seismograph and measured shallow earthquakes in Southern California. Scientists have now made other magnitude scales, all calibrated to Richter's original method, to use a variety of seismographs in order to measure the depths of earthquakes

of all sizes. A summary of the Richter scale and the subjectively estimated Mercalli scales of earthquake magnitude can be seen in table 2.2.

Mercalli Intensity	**Equivalent Richter Magnitude**	**Witness Observations**
I	1.0 to 2.0	Felt by very few people; barely noticeable.
II	2.0 to 3.0	Felt by a few people, especially on upper floors.
III	3.0 to 4.0	Noticeable indoors, especially on upper floors, but may not be recognized as an earthquake.
IV	4.0	Felt by many indoors, few outdoors. May feel like heavy truck passing by.
V	4.0 to 5.0	Felt by almost everyone, some people awakened. Small objects moved. trees and poles may shake.
VI	5.0 to 6.0	Felt by everyone. Difficult to stand. Some heavy furniture moved, some plaster falls. Chimneys may be slightly damaged.
VII	6.0	Slight to moderate damage in well built, ordinary structures. Considerable damage to poorly built structures. Some walls may fall.
VIII	6.0 to 7.0	Little damage in specially built structures. Considerable damage to ordinary buildings, severe damage to poorly built structures. Some walls collapse.
IX	7.0	Considerable damage to specially built structures, buildings shifted off foundations. Ground cracked noticeably. Wholesale destruction. Landslides.
X	7.0 to 8.0	Most masonry and frame structures and their foundations destroyed. Ground badly cracked. Landslides. Wholesale destruction.
XI	8.0	Total damage. Few, if any, structures standing. Bridges destroyed. Wide cracks in ground. Waves seen on ground.
XII	8.0 or greater	Total damage. Waves seen on ground. Objects thrown up into air.

Table 2.2: The two recognised earthquake magnitude scales and their equivalent effects (Taken from USGS, http://www.usgs.gov)

Earthquakes can occur practically anywhere on the Earth's surface, however the vast majority and the most destructive occur around plate margins. The reason for this is explained by the theory of plate tectonics.

2.2.4 Earthquake Prediction

Earthquake prediction has for a long time been a cherished goal of seismologists, with scientific and unscientific predictions dating back for hundreds of years, with precursors such as weather conditions, animal behaviour, electrical effects, earth tides and temperatures of hot springs all being touted as a solution (*Geller 1997, Gupta et al 2001*).

The definition of prediction generally used is: to be able to specify the location, size and time of reoccurrence, all with error windows (*Allen, 1976; Wyss, 2001*). This allows a fairly broad range of accuracies and timescales therefore the IASPEI (International Association for Seismology and Physics of the Earth's Interior) defines the categories of scientific information thought necessary to predict earthquakes and evaluates the reliability of various suggested precursors (*Wyss et al 1997*).

There is much debate as to whether prediction at any useful level is possible. Some people state that faulting is a non-linear process which is highly sensitive to immeasurably fine details of the state of the Earth, small earthquakes thus have some probability of cascading into a large event which is effectively impossible to predict (*Geller 1997*). Others argue that despite the large non-linear complexity of the lithosphere there are certain mesoscale regularities and therefore similarity and collective behaviour and the possibility of earthquake prediction (*Keilis-Borok et al 2001*).

At present earthquake forecasting is hardly better than a statistical prediction of reoccurrence from historical records. A number of models have been applied to this including stationary Poisson, the non-stationary Poisson, Markov chain models and Bayesian probabilities (*Stavrakakis et al 1995*). This has allowed the prediction of the last eight earthquakes across the globe with a magnitude of 8 or more but the error margins are such that it allows an area time to undertake earthquake preparedness rather than prediction, this method also produces a large rate of false alarms. What all groups are agreed upon is the need for better understanding and a greater resolution of the processes and pressures around plate margins.

2.3 Plate Tectonics

Plate tectonics is a theory of geology that has been developed to explain the observed evidence for large scale motions of the Earths lithosphere. The theory encompassed and superseded the older theory of continental drift, proposed by Alfred Wegener in 1912 (*Oreskes, 2003*) and the concept of seafloor spreading developed during the 1960s by Harry Hess.

The outermost part of the Earth's interior is made up of two layers, the lithosphere and the asthenosphere. The lithosphere is comprised of the crust and the rigid uppermost part of the mantle. The asthenosphere is a solid but has a low velocity and shear strength that allows it to flow like a liquid over geological time scales. The lithosphere is broken into a number of major and minor tectonic plates that ride on the asthenosphere. These plates move relative to one another and where they meet there is the formation of one of three boundaries, either convergent, divergent or transform. Each of these boundaries is associated with certain geological features and processes, for example earthquakes, volcanoes, mountain building or oceanic trenches.

What is driving this plate motion is still poorly understood and the active subject of research and discussion within the geophysical community. Dissipation of heat from the mantle is acknowledged to be the original source of energy driving plate tectonics, but it is no longer thought that the plates ride passively on asthenospheric convection currents. There has to be a way this energy is transferred to the lithospheric material in order for tectonic plates to move. There are essentially two types of forces that are thought to influence plate motion, friction and gravity (*Schubert et al 2001*). Frictional forces take two forms:

Basal drag – Whereby large convection currents in the semi plastic upper mantle are transmitted through the asthenosphere, plate motion is then driven by the friction between the asthenosphere and the lithosphere.

Slab Suction - Local convection currents exert a downward frictional pull on plates in subduction zones. This is not dissimilar to Basal drag but would act on both the upper and lower part of the lithosphere as it subducts.

Gravitational sliding - In addition to these frictional effects gravity is thought to drive plate motion (*Schubert et al. 2001*). The tectonic plates have a higher elevation at ocean ridges. As oceanic lithosphere is formed at spreading ridges from hot mantle material it gradually cools and thickens with age (and thus distance from the ridge). Cool oceanic lithosphere is significantly denser than the hot mantle material from which it is derived and so with increasing thickness it gradually subsides into the mantle to compensate the greater load. The result is a slight lateral incline with distance from the ridge axis (*Schubert et al. 2001*). This can also have an effect around the flexural bulging of lithosphere before it subducts under an adjacent plate and around mantle plumes.

Slab-pull - This states that the weight of cold, dense plates sinking into the mantle at trenches drives the plates and is thought to be the greatest force acting on the plates (*Carlson et al 1983, Heuret & Lallemand 2005*).

There are some theories that external forces, particularly the moon have an effect on plate motion. In a study published in the January-February 2006 issue of the Geological Society of America Bulletin, a team of Italian and U.S. scientists argued that the general westward component of plates is from Earth's rotation and consequent tidal friction of the moon. As the Earth spins eastward beneath the moon, the moon's gravity ever so slightly pulls the Earth's surface layer back westward (*Scoppola et al. 2006*).

The relative significance or contribution of each of these processes to a plate's movement is debatable, however it has been noted that lithospheric plates attached to downgoing (subducting) plates move much faster than plates not attached to subducting plates. The Pacific plate, for instance, is essentially surrounded by zones of subduction and moves much faster than the plates that comprise Atlantic basin, which are attached to adjacent continents instead of subducting plates. There are no absolute values of motion due to velocity variations around large plates such as the Pacific but figures of $\approx$ 1 cm/yr for the North Atlantic and $\approx$ 4 cm/yr for the Pacific are listed (*Kanamori and Brodsky, 2001*). It is thus thought that forces associated with the downgoing plate (slab pull and slab suction) are the driving forces which determine the motion of plates.

2.4 Tectonic Understanding

Our understanding of the processes surrounding tectonics and plate margins is limited by our ability to look inside the earth. The deepest mines in the world are only three or four kilometres deep, since it is roughly 6370 kilometers to the centre of the Earth this is only 0.06% of the Earth's depth. To investigate deeper a number of techniques have been developed to determine what is happening below the Earth's surface. Most notable amongst these is seismic tomography.

Seismic tomography is the process of studying the arrival times of the various seismic waves created by earthquakes or nuclear explosions in order to "illuminate" the interior of the earth. If the source of this seismic disturbance is well known the waves' arrival time at various seismic stations can be used to calculate the waves' speed through the earth and hence determine the density of the medium through which the waves travelled (*Nolet 1990, Stewart 1991*). With sufficient seismic stations and seismic sources a 3D image of the Earth's interior can be developed, although the non-linear nature of the problem means it is very sensitive to small errors in data collection, processing, or analysis (*van der Hilst et al 1991*). The method does, however, give a view of the Earth all the way to the mantle / core interface.

Similar to this, but on a smaller scale is reflection seismology which uses the same basic principle that when a seismic wave encounters a boundary between two different materials with different impedances, some of the energy of the wave will be reflected off the boundary, while some of it will be transmitted through the boundary. Again the seismic waves are measured using a number of seismometers, but the seismic sources are initiated (for example using dynamite explosions). By this process a finer model of the Earth's crust can be developed.

2.5 Fault Monitoring

There are a range of instruments used to measure deformation around fault zones (*Oreskes 2003*), for example:

Creepmeters - A creepmeter measures the displacement between 2 piers or monuments that are located on opposite sides of a fault. Typically, an invar wire is anchored to one pier and is stretched across the fault. Its displacement relative to the second pier is measured electronically and checked periodically with a mechanical measurement. Using the angle of the wire from the strike of the fault, the change in distance between the two piers is directly proportionally to fault slip (*Tarbuck and Lutgens, 1999*).

Tiltmeters - Tiltmeters are highly sensitive instruments with precisions of less than 1 part per billion at short periods. These instruments are used to measure ground tilt near active faults and volcanoes (*Tarbuck and Lutgens, 1999*).

Dilatometers and Tensor strainmeters - Strainmeters that measure the volumetric stretching and squeezing of the ground near active faults. Over short time periods they can detect changes of 1-part-per-billion (*Tarbuck and Lutgens, 1999*).

Although each of the above instruments is an accurate method of determining strain rates and movements around individual faults they are rather limited when looking at movements of tectonic plates and regions within those plates. In the past twenty or so years there has been a major increase in the use of satellite technology, in particular remote sensing, for monitoring tectonic movements over a wide range of scales, from the drift of the continents down to monitoring individual faults.

The main technologies utilised for this are GNSS (Global Navigation Satellite Systems), particularly GPS, and INSAR (Interferometric Synthetic Aperture Radar). GPS will be covered in more detail in chapter 3.

InSAR – Interferometric Synthetic Aperture Radar from Earth-orbiting spacecraft provides a new tool to map global topography and deformation. If the Earth's surface deforms between two radar image acquisitions, a map of the surface displacement with tens of meters resolution and sub centimeter accuracy can be constructed (*Burgmann et al 2000*). Typical image point (pixel) spacing in SAR images is 20-100 m within a 100km wide swath. InSAR distinguishes itself from other tectonic monitoring techniques by firstly mapping at very dense pixel spacing, 20-100 m over almost unlimited spatial distances, secondly INSAR is particularly sensitive to vertical

displacements, roughly 2-5mm which is comparable to the precision of levelling. Most importantly it requires no presence in the field, making its availability practically worldwide and measurements of deformation events in previously remote, dangerous or inaccessible areas possible. The InSAR method does however have a range of problems and limitations. Most significant of these is variations in the tropospheric delay noise as any difference in the atmosphere (troposphere or ionosphere) between two dates translates as a change in the apparent length between ther satellite and the ground, which is hard to distinguish from geophysical variation (*Massonnet and Fiegl, 1998; Xu et al. 2006*). Decorrelation of surface scatterers due to vegetation or other surface change processes can also add error to the process. In addition to these significant error sources in the estimation of interferograms (InSAR images of surface deformation or digital elevation, using differences in the phase of the waves returning to the satellite) there are also a number of other considerations when choosing InSAR as a method of monitoring geophysical variation. Firstly the temporal resolution of the technique, InSAR is limited by the approximately monthly repeat time of satellite flyovers (*Ferretti et al. 2004*). In addition the applied nominal satellite angle leads to an incidence angle for flat terrain equal to 23°. This high angle favours the observation of vertical displacements but makes it hard to recognize or distinguish horizontal displacements.

2.6 Aegean Tectonics

The Aegean region forms part of the major Alpine-Himalayan mountain belt, formed by the northward motion of Africa, Arabia and India relative to the Eurasian plate (*Jackson, 1994*). The Aegean region sits in a tectonically complex setting with the interactions of the African, Arabian, and Eurasian plates affecting a number of microplates in a broad zone of continental deformation (*Nyst and Thatcher 2004)*. Due to the collision of these three plates in the Greek area, the majority of the seismic activity of the eastern Mediterranean area occurs in the Aegean territory (*Jackson and McKenzie, 1988: 1988b*).

The present day tectonic framework of the area is controlled by the latest phase of the diachronous collision between the African and Eurasian plates which in turn affects the smaller Arabian, Anatolian and Aegean microplates (figure 2.3). The collision of the

Arabian microplate with the Eurasian plate along the Blitlis-Zagros zone (figure 2.3) around the time of the late Miocene initiated the westward tectonic escape of the Anatolian and Aegean microplates along two transform faults, the North and East Anatolian transform faults (*Dewey et al., 1986; Reilinger et al., 1997; McClusky et al. 2003: Kreemer et al., 2004*). The North Anatolian fault is a dextral intra-continental transform fault whilst the East Anatolian fault complements this with sinistral motion. This westward extrusion of the Anatolia – Aegean microplates leads to a collision with the Apulia-Adriatic platform which forces the Aegean microplate to progressively rotate anticlockwise toward the Hellenic arc (*Clews, 1989: Kissel et al. 1988; Underhill, 1989*). This rapid westward motion of Anatolia does not however result in a compressional stress field in the Aegean. Instead the Aegean is in general dominated by extensional stress as it moves in a relatively coherent manner at 30mm/yr with respect to Eurasia. A summary of these general eastern Mediterranean movements can be seen in figure 2.3.

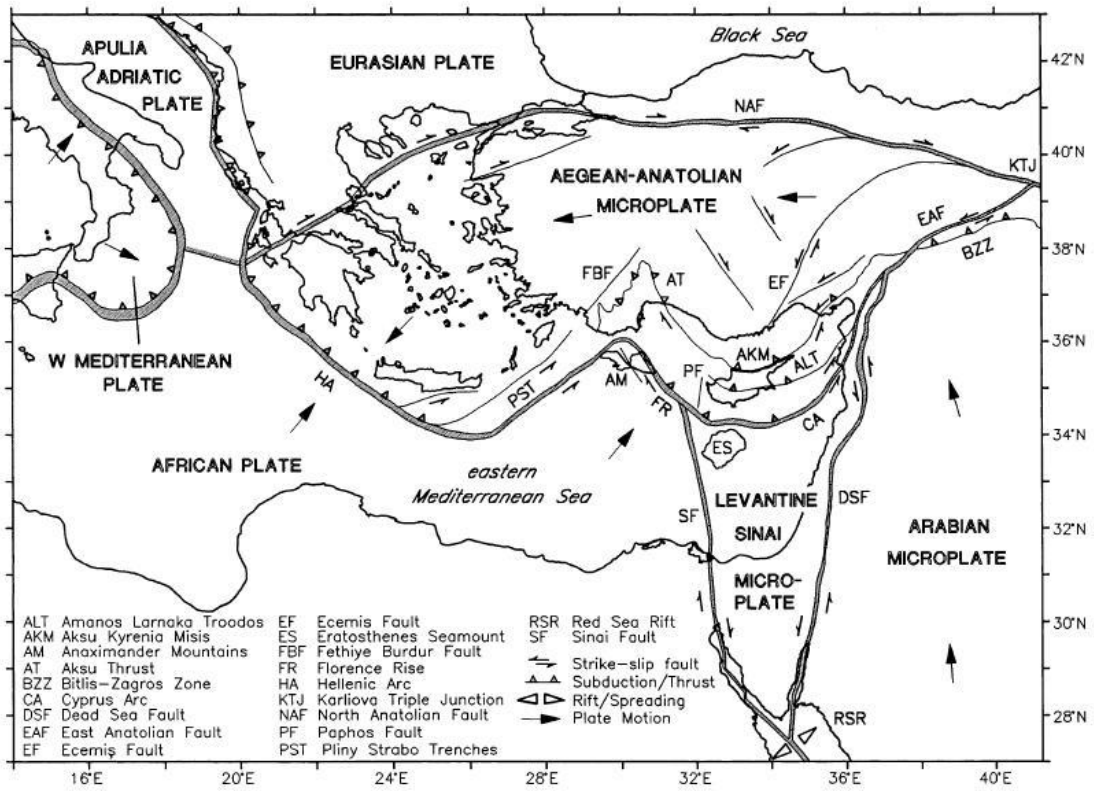

Figure 2.3: Simplified tectonic map of the eastern Mediterranean Sea (Aksu et al. 2005). Note that the position of several plate boundaries and the origin of particular structures are still controversial.

The most recent work looking to define the movements and stress fields across the region are by Le Pichon et al (1995), Reilinger et al (1997), Clarke et al (1998), Cocard et al (1999), McClusky et al (2000; 2003), and Meade et al (2002) who all incorporate

GPS campaign measurements to define movement with respect to Eurasia. Le Pichon et al used a combination of SLR and GPS at seven sites as well data from two triangulation networks to better define the extrusion of the Anatolian-Aegean block with respect to Europe as well as some of the deformation in the Aegean area. Reilinger et al used a more extensive network of 54 sites in a campaign style network to define the velocities of sites from the Caucasus Mountains in Russia and Georgia to the western coast of Turkey. They combined this with SLR data from the Aegean to show the northward motion of Arabia and the eastward extrusion of Anatolia as well as to suggest the driving forces for the motion in the study area as the pushing effect of Arabia and the pulling, or basal drag associated with the African plate in the Hellenic subduction zone. Clarke et al and Cocard et al filled in more detail by analysing data from campaign networks in central and western Greece respectively. Cocard et al integrated their campaign data with data from permanent GPS stations around the Ionian Islands. McClusky et al (2000) used data spanning nine years from 450 stations (189 in the Mediterranean) to give the most comprehensive cover of the Aegean region and followed this in 2003 with a study showing the relative motions of the African, Eurasian and Nubian plates. Kahle et al (1998; 1999; 2000) combined the results of a number of authors campaign GPS data to build up spatially denser pictures of the ground motion in the Eastern Mediterranean. For example in Kahle et al (2000) the networks of McClusky et al (2000) and Cocard et al (1999) are combined to determine the crustal deformation strain rate field in an area from 35ºN to 43ºN and 20ºE to 48ºE. Other studies have focused GPS campaign networks in other areas such as Meade et al (2002) and Ayhan et al (2002) in the Marmara Sea area and Western Turkey. Nyst and Thatcher (2004) have collated many of these field campaigns within the same reference frame to form a coherent picture of tectonic movements across the region. They hypothesise that the Aegean region is comprised of four relatively rigid microplates in the broad band of continental deformation between the converging African and Eurasian plates. In addition they compare their results with many previously hypothesised tectonic arrangements of Greece such as those by McKenzie (1978), McKenzie and Jackson (1983) and Goldsworthy et al (2002).

Articles describing the use of CGPS in the Aegean are less common due to the limited number of permanent networks and the immaturity of sites within those networks. A number of authors have looked to describe the motion in the area using the available IGS and EUREF sites. Nocquet and Calais (2004) presented a study using 64 sites

around Europe and published estimates for African plate kinematics to define convergence rates between Africa and stable Europe. Studies by Hollenstein et al and Hollenstein (2006, 2007) used the extended CION permanent network now called the HELLAS continuous network as a continuation of the works mentioned above to present a consistent solution for the strain rates velocities and trajectories in the area of Greece and Southern Italy. The Hellas network is focused in the Kefalonia Fault Zone with a number of sites across the Hellenic Arc to the islands of Rhodes and Kastelorizo.

Although there is some disagreement between previous studies of the Aegeanit is evident that the Aegean region is not a homogenous microplate. It consists of a wide range of deformation zones with normal, reverse and strikeslip faulting as well as the seismicity associated with the Hellenic subduction zone and the volcanism across the south Aegean Sea. Details of a number ofthe Aegean areas and features are summarized below.

2.6.1 The Southern Aegean / Hellenic Subduction Zone

One of the most obvious features of the Aegean area is the Hellenic trench which stretches across south western Greece from the Cephalonia fault to south of Crete where it forms the Pliny and Strabo trenches which in turn continue towards the south western Turkish coast. The trench itself is parallel to the Hellenic arc which consists of an outer sedimentary arc and an inner volcanic arc. This geomorphology combined with a range of earthquake studies and geophysical investigations of gravity and magnetic and seismic wave velocities (*Papazachos et al. 1995, 2000; Widiyantoro et al. 2004; Benetatos et al. 2004*) all show the existence of northerly dipping lithospheric material towards the concave side of the Hellenic arc. This lithospheric material is the subducting Oceanic lithosphere of the African plate (*Wortel et al. 1990; Wortel and Spakman, 2000; Widiyantoro et al. 2004*).

Tomographic studies such as that by Papazachos and Nolet (1997) have revealed interesting features and details of this subducting slab. On the Western section the slab subducts at a very shallow angle (≈10°) until a depth of roughly 70 km where there is a prominent kink followed by a new subduction angle of roughly 25°. The as you move eastwards across the Aegean the steeper the angle of subduction becomes (*Tiberi et al.*

2000; Sodoudi et al. 2006). It should be noted that although this is the commonly held theory, there are others for instance Knapmeyer et al (*2000*) suggest that the Hellenic trench system is a set of undulations in an accretionary wedge that has formed as the African oceanic crust subducts much nearer Africa, south of the Mediterranean ridge.

The Hellenic trench itself is not a stable feature and is believed to be migrating southwards due to slab roll-back. The downgoing slab exerts a slab-pull force on the rest of the oceanic lithosphere and causes a bend in the slab to migrate seawards as subduction continues, this is known as roll-back (*Wortel and Spakman, 2000*). This slab roll-back is leading to the consumption of the oceanic lithosphere between Africa and Europe and to the extension in the lithosphere above the subduction zone. This process is hypothesised to be the major driving force in the south westward motion of the southern Aegean and Hellenic Arc, the westward pushing affect of Turkey and the Anatolian microplate is seen as a secondary contribution to this movement (*Wortel and Spakman, 2000*). Davies et al. (1997) argue that the deformation in the area is consistent with that expected of a sheet of fluid moving toward the low pressure boundary at the Hellenic trench. A simple calculation implies that if the region does behave as a fluid, then its effective viscosity is $\sim 10^{22}$-10^{23}Pas. Such viscosities are consistent with the deformation of a lithosphere obeying a rheological law similar to that obtained for olivine in the laboratory.

In addition to the variation of the angle of the subducting plate and its southward migration there is a significant kink in the trench caused by this subduction. South of Crete, the Hellenic trench veers to become the Pliny and Strabo trenches. This curvature of the Hellenic arc is hypothesised to have been created during an earlier period of extension (during the Oligo-Miocene time). At this time there was extension in the southern Aegean, attested by the creation of deep basins and the exhumation of metamorphic core complexes as well as the paleomagnetic rotations of rock units in an opposite sense on either side of the Aegean (*Gautier, 1994; Jolivet, 2001; Sodoudi et al. 2006*). The curve in turn affects the tectonics by acting as a rupture barrier. Rupture barriers along large seismogenic faults are classified as either inhomogeneous or geometrical. Inhomogeneous barriers refer to the stopping point of earthquake rupture where no geometrical discontinuity exists. Geometrical barriers represent jogs or bends in the fault zone (*Poulimenos and Doutos, 1996*).

2.6.2 Mainland Greece and the North Aegean Sea

The North of the region is characterised by strike-slip faulting which propagates on from the North Anatolian fault into the Aegean Sea where the north-south extension creates the Strymon and Skyros basins and the North Aegean Trough (*Sengor et al. 2005*). These extensional features can be clearly seen in bathymetric images of the area and are reflected in the crustal thickness (figure 2.4). In general the thickness of the crust varies between Greece and the Aegean Sea. Thicker crust (40-45km) exists beneath Greece and the Peloponnesus along the Hellenides mountain range (*Papazachos & Nolet, 1997; Tiberi et al. 2000; Karagianni et al. 2005; Sodoudi et al. 2006*). Eastern Greece is 30-34 km thick while thinner crust exists below the Aegean Sea (20-30 km in the South, 25-30 km in the North. This thinning is particularly prevalent under the metamorphic belts that comprise the Menderes Massif in western Turkey and the Cycladic Massif (*Zhu et al. 2006*), indicating the extension across this part of the Aegean.

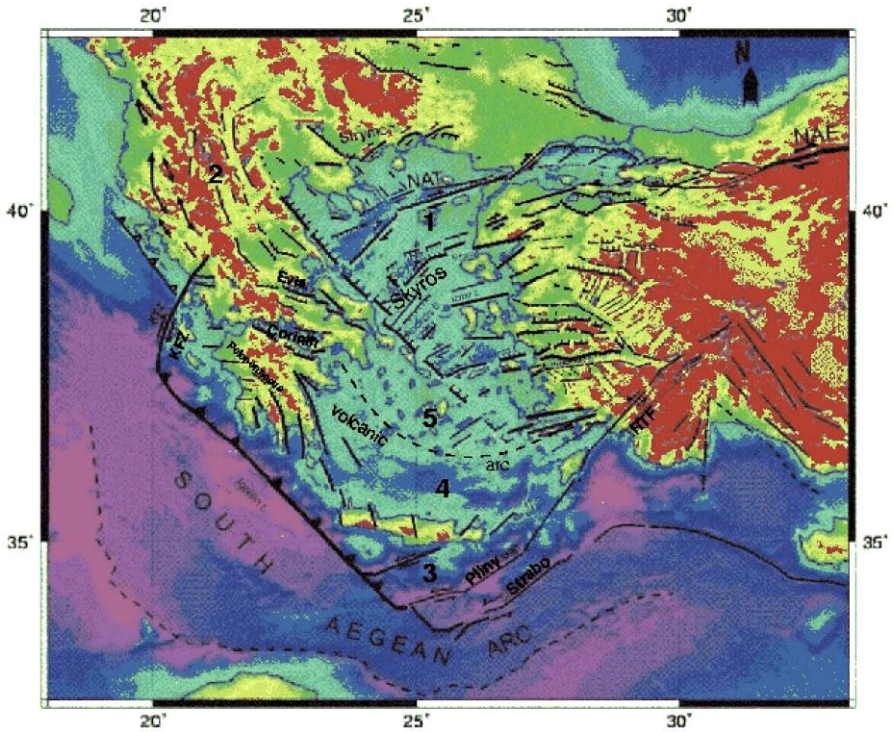

Figure 2.4: The general topography and bathymetry of the Aegean overlain with the major fault systems (From USGS, http://www.usgs.gov)

The geomorphology, distribution of large earthquakes and evidence from geodetic measurements all suggest that the active faulting in mainland Greece and the Northern

Aegean area are distributed around linear zones that bound relatively rigid blocks (*Goldsworthy et al. 2002; Nyst & Thatcher, 2004;*).

2.6.3 Greek Seismicity

Figure 2.5 shows the recent seismicity around the Aegean. The figure highlights the fact that Greece is one of the most seismically active regions on Earth but also that this seismicity is not limited to discrete zones. With the exception of the area of the Aegean Sea just behind the Hellenic arc, shallow seismicity is prevalent throughout the region. This seismicity is dominated by, but not limited to, the stresses around the Hellenic arc, where the subduction of the down going African plate leads to earthquakes over a wide range of depths. This can be seen in figure 2.5 where the depths of the earthquakes increase the further north you move from the subduction zone, essentially moving downdip around the subduction interface.

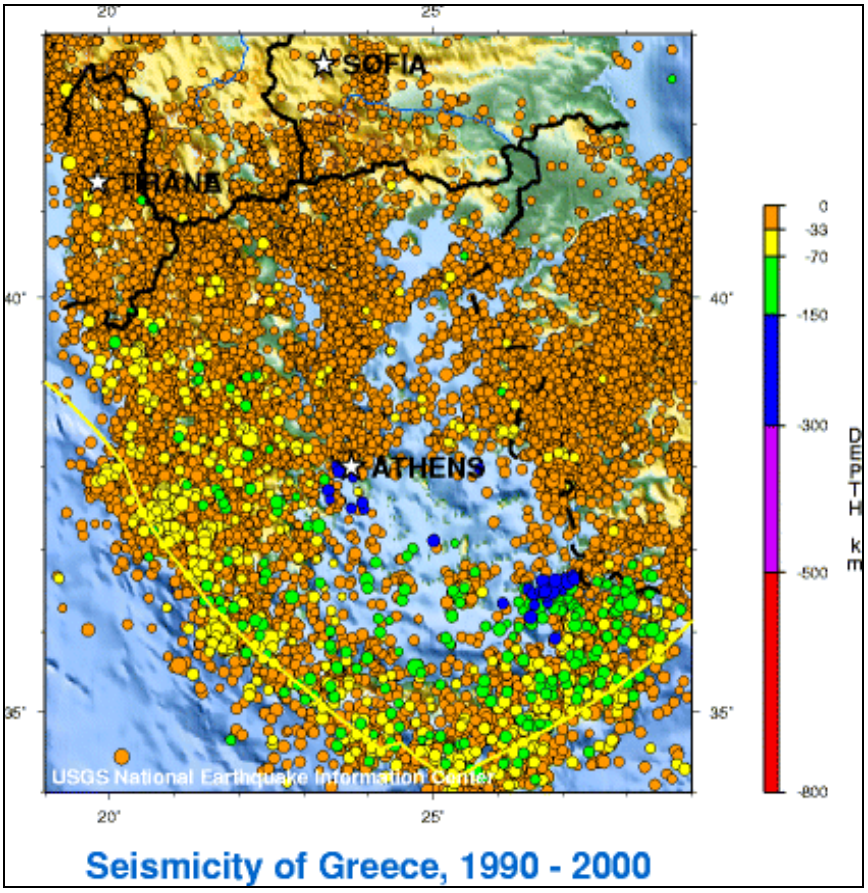

Figure 2.5: The recent seismic record in Greece (From USGS)

This seismicity associated with the subduction interface shows a range of moment tensor solutions with the epicentres of normal, strike-slip and thrust faulting located next to each other around the Hellenic arc (figure 2.6). The focus of each of these types of earthquake is however at different depths. The overriding Aegean plate is dominated by extensional normal faulting. At around 30km depth in the subduction interface there is strike-slip faulting to accommodate the arc shape of the subduction interface and the oblique angle with which the African plate meets the overriding Aegean microplate. The sense of this strike-slip faulting changes along the arc. The western parts have shown dextral motion whereas the eastern part of the arc near Rhodes shows sinistral strike-slip motion (*Benetatos et al. 2004*). At greater depth within the subduction interface there is thrust faulting (*Jackson, 2008*).

It is well-known that seismic slip on the Hellenic subduction zone can not account for the movement necessary to accommodate the subduction of the oceanic Mediterranean Sea floor beneath the continental lithosphere of the Aegean region. Jackson and McKenzie (1988) originally stated that only 10% of the subduction of the Mediterranean Sea floor beneath the continental lithosphere of the Aegean region is accounted for by seismic slip. This figure has been revised by Main and Burton (1989), Koaros et al (2003) and Jenny et al (2004) who all agree that the that the Hellenic arc convergence has a large aseismic component but place the figure for seismic slip closer to 45%. These figures were formed without the inclusion of the largest seismic moment release events which would normally dominate the total seismic release therefore making the estimation of seismic hazard inherently uncertain. The studies suggest that either the movement is accounted for aseismically or through occasional large earthquake events.

Figures 2.5 and 2.6 also highlight the other seismically active areas. Firstly the active normal faulting across the Peloponnese and mainland Greece which leads to East – West extension as well as the significant normal faulting across the Gulf of Corinth which relates to the north-south expansion across the region. To the West of the Peloponnese around Cephalonia the area is dominated by dextral strike-slip faulting that accommodates the meeting of the Aegean, Eurasian and Adriatic plates. In the northern Aegean the expansion is accommodated by strike-slip faulting which is an extension of the North Anatolian fault. The seismicity throughout western Turkey is also related to

north-south extension and has created normal fault related features such as the Menderes Massif.

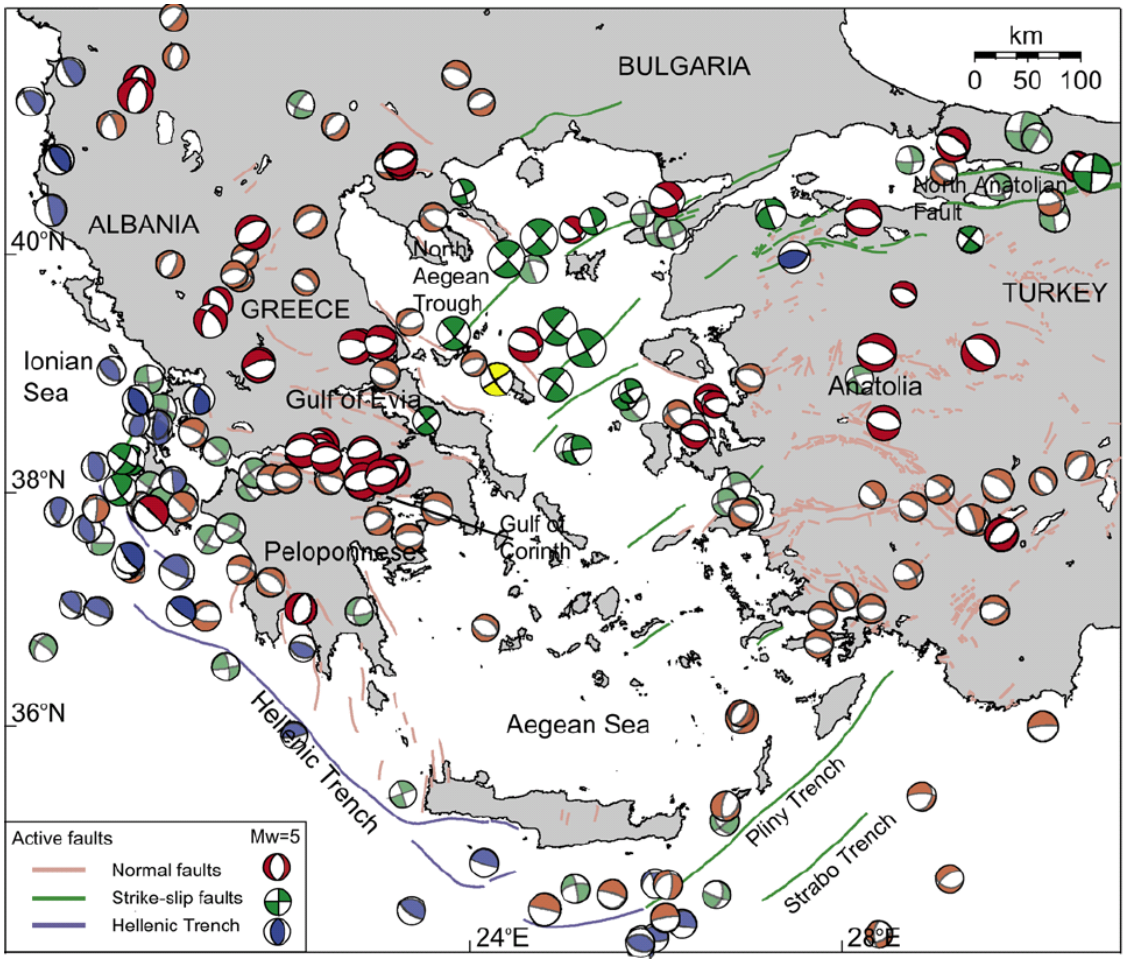

Figure 2.6: Moment Tensor solutions for the Aegean region taken from Nyst and Thatcher (2004)

2.7 Macquarie Island

The Macquarie Island earthquake on the 23rd of December 2004 was a major seismic event that occurred during the time of this study. As such it was used as a measure of the effectiveness of the Sidereal filtering technique and as a comparrison with seismic events in the Aegean region (Chapter 5).

Macquarie Island is situated between the Tasman Sea ocenic crust and the continental crust of the Campbell Plateau and runs coincident with the Indo-Australia / Pacific plate margin. This is an arcuate 2100km long crustal fracture system connecting the Pacific/Antarctic and the Indo-Australian/Antarctic spreading ridges with the Alpine fault system in New Zealand (Figure 2.7). The focal mechanisms shown in figure 2 are

predominantly strike-slip with less common thrust events indicating that the plate margin is transcurrent, evolving from a dextral strike-slip system into a subduction zone (*Goscombe and Everard, 2001*).

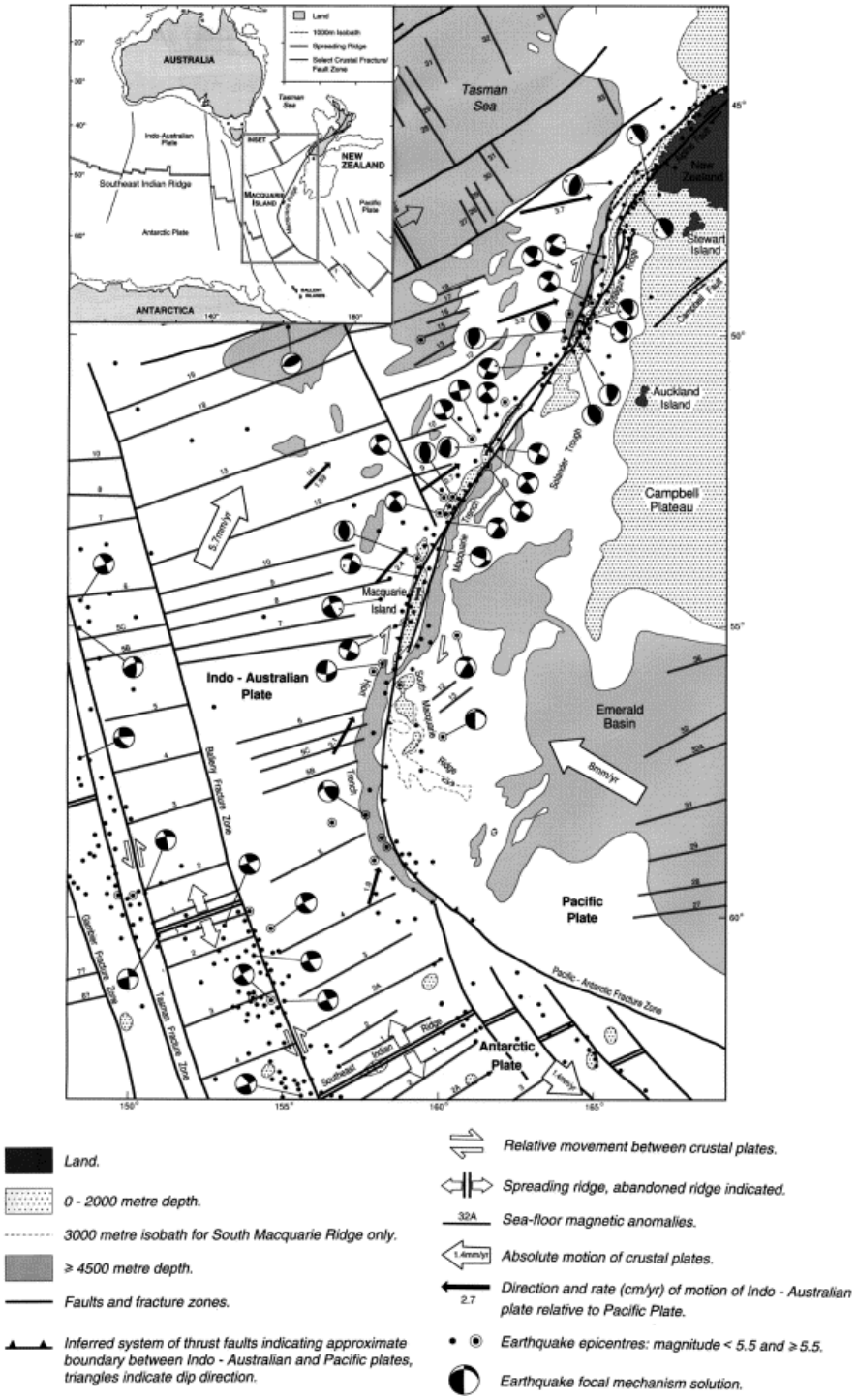

Figure 2.7: Tectonic map of the Macquarie Ridge region with an inset of the wider Southern Ocean region and major crustal features. The200m depth contour of campbell Plateau and New Zealand approximately outlines the continental crust;the rest of the map is oceanic crust (from *Goscombe and Everard, 2001*).

2.8 Seismic and Aseismic Crustal Movements

Earthquakes and their effects are well documented around the world. Seismic events of this nature are identified and logged. Less understood are the effects, causes and locations of aseismic plate motions. As the name suggests aseismic events are those that are not detectable using a seismograph, or those that are of a sufficiently small magnitude to be lost in the noise associated with the use of seismographs.

There are a number of variations in aseismic tectonic movements. In some cases it is regarded as creep or stable slip, even if there is a certain amount of seismicity associated with the fault in question (North Anatolian fault). In other cases aseismic movements have been identified that are of a more transient nature. These exhibit a wide range of magnitudes and periods and are the subject of much research both in terms of quantifying the stress and strain in an area but also as a potential precursor to a seismic event.

Changes in the rates of aseismic crustal deformation could facilitate warnings of impending earthquakes, as well as potentially discriminating between theories of the earthquake generation process. Obara suggested there may be a temporal link between transient deep tremor associated with aseismic slip and earthquakes in the Kii peninsula and the Shikoku area of Japan (figure 2.8). He stated that earthquakes led to an increase in pore pressure or the creation of new cracks that resulted in the tremor. Other authors, such as Roeloffs (2006), state that the silent slip and associated tremor can cause pressure changes in a fault zone resulting in potentially harmful seismic events.

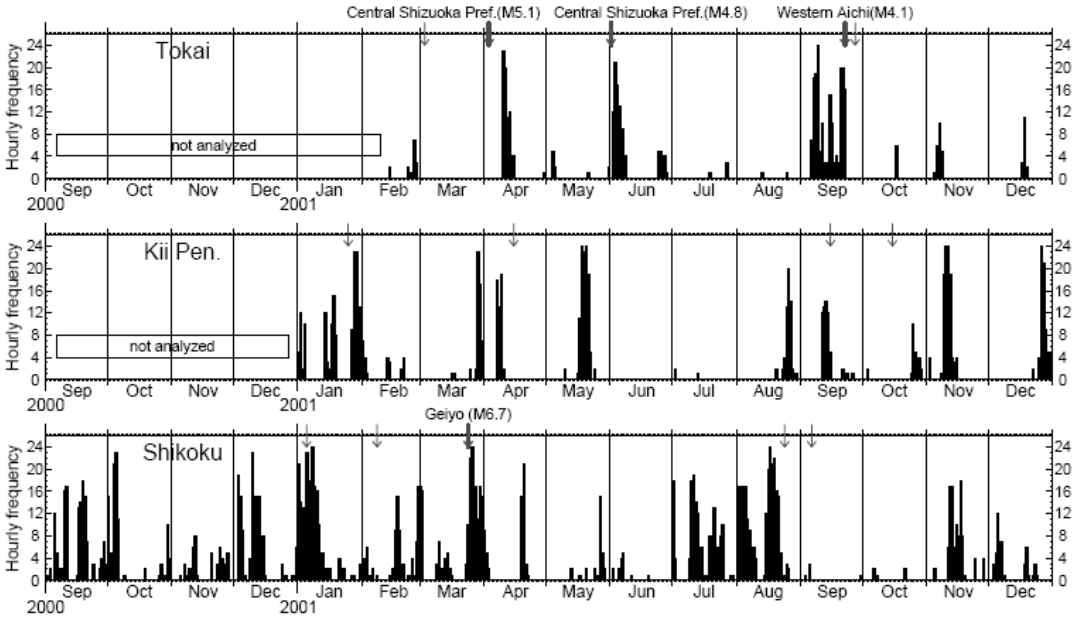

Figure 2.8: Time sequence of tremor activity in Japan. The arrows indicate major earthquakes greater than M_w4 which occurred near the tremor activity zone.

Transient events take place over timescales ranging from hundreds of seconds to over a decade. Deformation rate changes have been measured using a wide range seismological, geological and geodetic techniques in an attempt to identify earthquake precursors, examples of which are given below.

2.8.1 Evidence for Aseismic Crustal Movements Prior to Seismic Events

i. Microfossil Evidence

Microfossil diatom and pollen data was collected from a number of cores around the Girdwood flats and Kenai flats in Alaska. The relative sea level history of the area was deduced from this data as well as from Caesium (^{137}C) dating records. These records showed a long period of gradual uplift since the last large earthquake (approximately 800 years ago), until approximately 1952 when the record indicates relative sea level rise averaging 0.12 ± 0.13m occurred up until the great 1964 Alaskan earthquake ($M_w9.2$) (*Zong et al. 2003; Hamilton and Shennan 2005a,b*).

Another event was also hypothesised by Shennan (1998) for the occurrence in 1700 of a great (M9) subduction interplate earthquake along the Pacific coast of Oregon and Washington. Microfossils from cores along coastal Oregon showed evidence of preseismic rising relative to sea levels preceding the co-seismic deformation.

ii. Levelling

A levelling survey was established in 1944 by Mr Imamura along the Eastern section of the Nankai trough (Tonankai). Levelling misclosures averaged 0.01mm along a 700m section of this survey, however the day before the 1944, M8.2 Tonankai earthquake these same misclosures were measured at 2.9mm and measurements taken hours before the quake had misclosures of 4mm (*Sagiya,1998; Linde and Sacks, 2002*). These closure errors were all consistent with a preseismic north-down tilt. East-West oriented sections in the same area showed no significant closure error. This was supported by post-seismic surveys of these same lines in the days following the earthquake which again showed large misclosures but with an opposite tilt from the pre-seismic changes.

Tidal levels have also suggested aseismic uplift before a major quake. For example tide-gauge records at Tosahimizu indicated that the ground there rose 10 cm before the M_w 8.3 at Nankaido earthquake (*Kobayashi et al. 2002*)

iii. Water levels and Borehole strain

Small relative water level rises have been recorded in a number of wells monitored near Parkfield in California three days before the 1985 M_w 6.1 Kettleman hills earthquake. In addition to this borehole dilatometers recorded a contractional pre-earthquake strain transient of a similar duration. These readings returned to normal after the quake (*Roeloffs and Quilty, 1997; Roeloffs, 2006*).

Transient strain measured using borehole dilatometers was also observed an hour before seismic waves from an M_w 3.5 earthquake in a seismic swarm in the Gulf of Corinth in 2002 (*Bernard et al. 2004*). Although it has been hypothesised that this resulted from fluid or magma movements rather than a tectonic shift.

These two events were noted days or hours before an earthquake. Anomalous strain was measured using strainmeters for 6 months before the M_s 7.8,1983 Japan Sea earthquake. In that period 86 anomalous strain events were recorded. The strain meters had been placed to monitor the accelerating coastal uplift around the Oga / Fukaura peninsular where levelling surveys had shown up to 4cm of uplift. After the earthquake the aseismic strain events stopped and the uplifted peninsulas subsided (*Mogi, 1985*).

iv. CGPS

There have been a number of cases where CGPS have identified aseismic movement. A number of these cases have been described as possible precursors to seismic events. For example Melbourne and Webb (2002) claim that the post seismic movement of the M_w 8.4 Peru earthquake was 1cm per week until 18 hours before the largest of the aftershocks (M_w 7.6). At this point the deformation accelerated to around 2.0 ± 0.5 cm until the earthquake.

Although there are numerous examples of techniques demonstrating the potential prediction of seismic events, as yet they are all fairly site specific and applying the same techniques to other events shows no similar results. In addition a number of the techniques occur over a period of time that could be interpreted as being neither "transient" or "slip" events for example the microfossil evidence in Alaska and the

2.8.2 CGPS for the detection of aseismic and transient aseismic movements

Seismic deformation rates are often used to define strain rates across a region. This extrapolation of seismic deformation to geological deformation has inherent problems. Obviously only the seismic strain rate tensor can be calculated from this information and this only describes part of the tectonic cycle. Faults in general are described with smooth interseismic motion whereas in reality aseismic motion often occurs over fault zones. This aseismic motion can either be a state of relatively smooth, stable slip or in a number of cases, of a more transient nature. This leads to a difference between geological and seismic strain, which leads to an inaccurate picture of the tectonic risk associated with an area (*Masson et al. 2005*).

The establishment of CGPS networks across the globe has led to a better understanding of the movements of the Earth's crust and in particular the discovery of transient aseismic movements. This has led to the revision of the idea that earthquakes and postseismic slip are events that punctuate steady interseismic strain or displacement rates. These events were often undetectable by campaign GPS measurements and therefore it is only since the widespread establishment of CGPS networks in the 90's

that GPS data has had sufficient resolution to detect transient movements. Since then there has been widespread detection of aseismic transient events, particularly in the United States and Japan due to the extensive CGPS networks established there.

One of the first examples of aseismic transient motion or "silent earthquakes / slip" events as they have been termed was detected using the PANGA array. It was occurred in 1999 in Northwest America where the Juan de Fuca plate subducts beneath the North American plate. This subduction results in the landward movement (eastward) of the sites in the PANGA array relative to the site DRAO located in Penticton. It was noted by Dragert et al (2001) that a cluster of seven sites briefly reversed their direction of motion. No seismicity was associated with this event which involved horizontal displacements of 2-4 mm at each site over a period of 6-15 days. The event did not occur simultaneously across the region but instead propagated from the southeast to the northwest (essentially parallel to the strike of the subducting slab) over a period of 35 days. With further investigation this event was shown to not be an isolated event but one of a series of episodic events that occurred with a repeat period of 13–16 month intervals (figure 2.9). It has also been found that although they are referred to as silent events there is a unique nonearthquake seismic signature correlated temporally and spatially with these events (*Rogers and Dragert, 2003*). This surface movement is thought to arise from slip on the subduction interface downdip from the seismogenic zone where the interface is hotter and more plastic. It does open up the possibility that stress loading of the seismogenic zone (where megathrust earthquakes are located) can occur in discrete pulses.

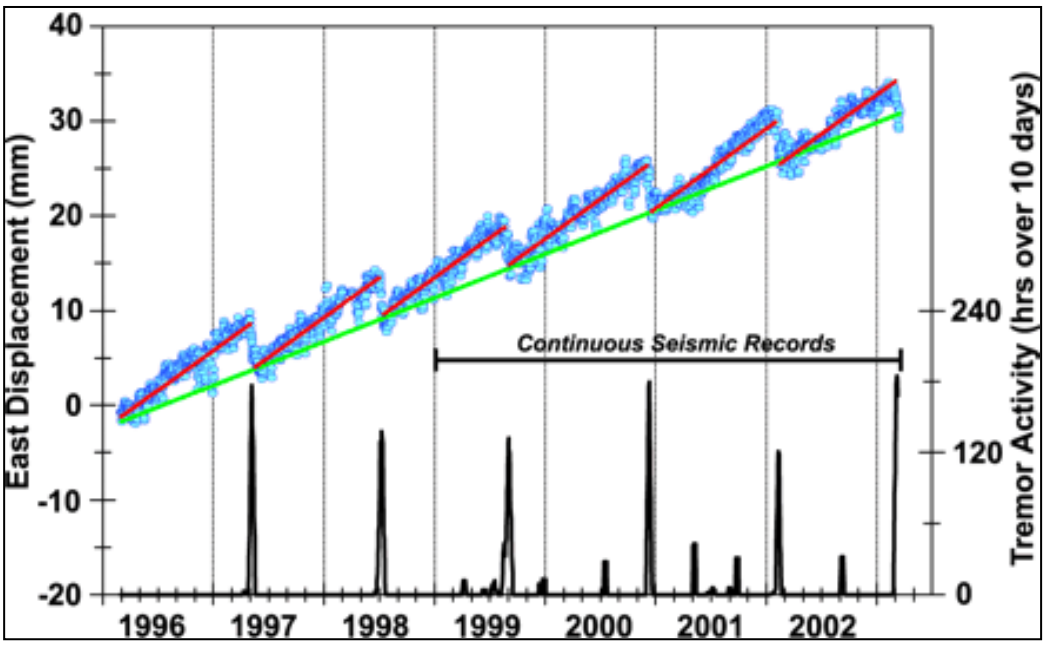

Figure 2.9: Episodic silent slip on the Juan de Fuca / North American subduction interface (Rogers and Dragert, 2003)

Similar events to this have been observed in Japan, particularly in the Tokai region (*Ozawa et al. 2002, 2004*). These show a similar pattern to Cascadia with a reversal in the normal direction of site movements. Their duration is however significantly longer with Ozama monitoring an event for almost two years and suggesting the possibility of similar transients in the periods 1978-83 and 1987-91. It was in Japan that the low-frequency tremors associated with these events were first noted. Katsumata and Kamaya (2003) stated that there was a belt of low-frequency continuous tremors in southwestern Japan. They stated this was caused by ascending water produced by dehydration of chlorite and amphibole in the subducting Philippine Sea plate. Obara (2002) suggested that the tremor may be caused by changes in pore pressure or the creation of new cracks through hydraulic fracturing when fluid levels reach saturation or are stimulated by nearby shaking. Obara showed strong relationships between deep tremor and earthquakes greater than M 4 in south western Japan. Kostoglodov et al (2003) reported a 6-7 month transient event along the Guerrero seismic gap on the Pacific coast of Mexico in 2001-2002 (*Kostoglodov et al. 2003; Franco et al. 2005*). The authors state that the process increases the stress at the base of the seismogenic zone which may have caused the M_w 5.9 and 6.7 earthquakes that occurred during their study period. They also state that the transient events here along the interface of the subducting Cocos plate beneath continental North America repeat, not in the regular pattern observed in Cascadia but instead have slipped in 1972, 1979, 1998, 2001-2002 and most recently in

2006 when horizontal displacements of nearly 6cm in the direction opposite to that recorded interseismically were reported (*Larlson et al. 2007*). As with other Aseismic slow slip events in subduction zones associated low frequency tremors have been recorded for both the 2001 -2002 and 2006 event (*Payero et al. 2008*).

Due to the temporal and spatial coherence detected between transient aseismic slip and tremor a better understanding of their origins and mechanics is being researched as they could potentially lead to better seismic hazard forecasting.

At present there are two hypotheses for their origins. One is that the tremor is the result of fluid movements at depth. This fluid is either rupturing or coupling with the rock resulting in the tremor. This fluid flow either triggers the aseismic slip or the fluid flow is a direct response to changes in stress and strain induced by shear slip on the plate interface (*Shelly et al. 2006*). In this scenario fluids may play an auxiliary role, altering conditions on the interface to allow transient slip events without generating a seismic signal directly (*Sagiya, 2004*). Payero et al (2008) state that although low frequency tremors activity and aseismic slow slip are related they are not of the same origin as when the activity of the two phenomena are compared it is seen that in Guerro, Mexico some highly energetic tremor episodes do occur during the “quiet” inter aseismic slip periods. The authors state that the long-term tremor is still clearly modulated by aseiesmic slip events.

The transient aseismic events mentioned above occurred downdip of the seismogenic zones on subducting plate margins. These are not the only events to have been detected. Aseismic slip has also been reported in shallow faults around volcanoes and in strike-slip faulting. The dense Kilauea CGPS array located on the flank of the Kilauea volcano, Hawaii (*Cervalli et al 2002; Segall et al. 2006*) has recorded a number of transient events each lasting 1-2 days. These were different to the events recorded in subduction zones in that they were smaller, shorter, shallower, (5km as opposed to 30-50km) and faster (slip rates of ≈ 20 mm/yr compared to ≈ 1 mm/yr in Cascadia). There was a clear increase in microseismicity within the region accompanying the slow slip event that appears to be triggered by the otherwise aseismic shift (*Segall et al. 2005*). Due to its different setting the trigger for this event differs from that found around plate margins. Cervalli hypothesises that the one meter of rain that fell nine days before the November 2000 event affected the slope stability. Firstly by increasing surface loading

in the volcano flank and secondly by elevating the water table in the area leading to an increase in pore pressure that decrease the effective normal stress on faults bringing them closer to failure.

The San Andreas Fault is another active tectonic area where aseismic slip is inferred. Although no GPS measurements have definitively shown surface deformation, deep tremor has been recorded (20-40 km) below the seismogenic zone. These tremors show a very similar signal to that seen in subduction zone tremor (*Nadeau and Dolenc, 2005*) but occur on a dextral strike-slip fault. The San Andreas Fault (SAF) tremors do show some variations from those documented in subduction zones. Firstly they are less frequent (less than five detected in a twenty-four hour period), they are shorter in duration (less than 20 minutes), they have smaller peak amplitudes ($<M_w$ 0.5 earthquakes) and they release less energy (equivalent to $< M_w$ 1.5). As fluid from the subduction process is deemed important for subduction zone tremor the SAF fault must either not rely on fluid or an alternative fluid source must be present below the seismogenic zone in the area. Linde et al (1996) reported the presence of a week long slow earthquake sequence on this same fault inferred from borehole strainmeters.

The importance of slow earthquakes in the seismogenic process remains open to debate, but their presence in a range of fault systems, at different depths and over a wide range of temporal regimes make them an important factor when defining the stress and strain fields of an area. The proximity of a subduction zone, major strike-slip faulting as well as the presence of volcanism makes the Aegean region an area potentially susceptible to transient seismic events.

2.8.3 CGPS for the detection of seismic movements

As well as looking at pre and post seismic deformation high rate CGPS is now being utilised as a method of looking at co seismic and seismic earth movements. GPS can measure the size of an earthquake by inverting the co-seismic displacement. High rate GPS (1Hz or greater) has the potential to recover both dynamic and static earth movements accurately. Traditionally GPS measurements have been averaged over a day in order to determine long term deformation rates. This is sufficient to measure the co-seismic displacements from an earthquake but this only constrains the cumulative slip of

a seismic event. Larson et al (2003) demonstrated that 1-Hz GPS data could be analysed with sufficient precision to measure seismic waves. In their study there were however, insufficient high rate GPS receivers to determine full rupture models for the Denali fault earthquake, which still relied on seismic data to constrain the quake.

Ji et al (2004) took this further by combining the results of strong motion instruments (accelerometers) and 1-Hz GPS, teleseismic data and GPS static offset measurements to construct the full slip history of the 2003 San Simeon earthquake. They found that in measuring an earthquake of this size 1-Hz GPS had several advantages when compared to strong motion data. Firstly GPS has very accurate timing information (strong motion sensors were found to disagree with UTC by as much as 20 seconds), near field strong motion horizontal measurements were also found to be contaminated by co-seismic ground tilts and analogue to digital conversion. Strong motion instruments are good at constraining detailed slip histories but their ability to recover long period motions and an inability to distinguish between linear accelerations and rotations mean that GPS is a powerful tool to help distinguish fault slip histories (*Miyazahi et al. 2004*).

These techniques are being applied to tsunami warning systems. At present the time in which the magnitude of an earthquake can be determined from seismic data is too slow for tsunami warning purposes. CGPS can greatly improve this, as shown by the M_w 9.2-9.3 Sumatra-Andaman earthquake. Seismic magnitude estimates after 15 minutes determined the quake to be M_w 8.0 and therefore not a tsunami risk, GPS data analysed 15 minutes after the event indicated a quake of M_w 9.0 (*Blewitt et al 2006*). JPL has recently researched this further, developing a method that estimates the energy an undersea earthquake transfers to the ocean to generate a tsunami by using data from coastal GPS stations near the epicenter. With these data, ocean floor displacements caused by the earthquake can be inferred (*Song, 2008*). In this way it is hoped that tsunami warning systems can be developed that won't give false positives.

Chapter 3

Geodetic Background

Chapter 3 looks to introduce the reader to the science related to the determination of the size and shape of the Earth. This background focuses on GPS and the factors that affect both the GPS signal and our ability to accurately measure that signal on the earth. The specific GPS processing software and the processing strategies employed in this study are also explained.

3.1 Introduction

GPS is a precision navigation and positioning system based on one-way ranging derived from timing signals. It was originally developed in the 1970s primarily as a military tool for the purpose of global navigation but was also always intended to have limited civil access and applications. To achieve real-time global positioning and to serve an unlimited number of users, a constellation of 24 satellites was established in near circular orbits at an altitude of roughly 20000 kilometers. The satellites were placed four to an orbit, with a 60º separation between orbital planes at the equator which are inclined to the equator at 55°. This allowed a view of at least four satellites almost everywhere on Earth, which in turn allowed the resolution of the three dimensional location of the receiver and the timing error associated with the low accuracy receiver clock used in most GPS receivers.

A wide range of uses for the system were developed and spurred on rapid development of both software and hardware (summarised in Blewitt, 1993; Leick, 2004), which have

in turn led to the rise of GNSS as a geodetic tool. The sub-centimetre precisions now achievable mean that it is no longer a just a navigational tool but also one capable of measuring ground motion.

3.2 The Global Positioning System for Observing Ground Motion

The theory of continental drift was put forward as far back as 1596 and reappeared many times throughout history, most notably expanded upon by Alfred Wegener who proposed the theory of plate tectonics in 1912. It was not however until the 1960s that the theory, research, data collection and analysis came together to prove the idea of plate tectonics.

Plate tectonics is a relatively new scientific concept, but it has revolutionized our understanding of the dynamics of the planet. Plate tectonics theory describes the motion of rigid plates that make up the lithosphere over the comparatively weak asthenosphere. This movement is believed to be driven by a combination of gravity, friction and convection cells located in the mantle and results in the constant movement of the Earth's surface and the some of the resulting forces and features that characterize it. Plates meet at boundaries that are either divergent convergent or conservative. Each of these boundary types in turn has its own signature of crustal deformation, for example crustal manufacture or destruction, mountain building or earthquakes.

Since the formation of the theory there has been much study into the number and location of these plates, their movements relative to one another and hence the positions of their boundaries and the stresses that are located there. Initially this was done using the geological record.

The first global tectonic motion model, known as AMO-2 was put forward by Minster and Jordan in 1978, more recently the Nuvel1 and NNR-Nuvel1 models were put forward by DeMets *et al (1990)* and Argus and Gordan (1991). In the Nuvel1 model the Pacific plate was held stationary whilst the NNR-Nuvel1 model imposed a no-net-rotation condition. More recently a revision of the paleomagnetic time scale has led to a re-scaling of both the Nuvel1 and NNR-Nuvel1 rates. A multiplying factor of 0.9562 has led to the formation of the "Nuvel-1a" and "NNR-Nuvel-1a" models (*DeMets et al. 1994)*. This NNR-Nuvel-1a model is still used by the International Earth Rotation Service (IERS) as the standard plate velocity model in its maintenance of the International Terrestrial Reference Frame (ITRF). The ITRF is an important bench mark

for researching global and regional motions of the Earth despite suggestions it may not be a truly rigorous and accurate no net rotation (NNR) model (*Jin and Zhu, 2004).*

All the models mentioned above have the disadvantage that they describe only the motions of the 14 major rigid plates and do not take into account the movements within the diffuse zones of deformation at the plate boundaries. This is largely due to the data sources used to compile their velocities and Euler poles. In the case of the NNR-Nuvel-1a model this was geomagnetic data and geological data such as quaternary fault slip rates. Over the past couple of decades space geodetic techniques have developed and provided large quantities of measurements both in the stable interiors of plates as well as in plate boundary zones. This data largely supports that shown in the long term geological record for example, a comparison of SLR geodetic rates with those from NUVEL-1 and AMO-2 models showed high correlations between tracking sites that are well within plate interiors (*Smith et al. 1990*) this is true for Very Long Baseline Interferometry (VLBI) and GPS measurements as well.

This development of space geodetic techniques, especially InSAR and GPS, has allowed the observation of ground motion to a finer and finer resolution, both spatially and temporally. Modern geodesy recognizes that ground motion can occur at practically all temporal regimes between geologic and seismic.

This section looks to give a brief outline of the recognised ground motions affecting the lithosphere at present, as well as introductioning conventional models used to describe them.

3.2.1 Tectonic Plate Motion

As mentioned in the previous section there are a number of standard models of tectonic plate motion. They describe the motion as a rotation of a given rigid plate about its rotation (Euler) pole on the surface of a spherical earth. Time dependence of the cartesian station coordinates of station "*i"* residing on plate "*j"* are expressed as

$$x_i = x_i^o + (w_y^j z_i^o - w_z^j y_i^o)(t - t_o) \quad (3.1)$$
$$y_i = y_i^o + (w_z^j x_i^o - w_x^j z_i^o) (t - t_o)$$
$$z_i = z_i^o + (w_x^j y_i^o - w_y^j x_i^o) (t - t_o)$$

where *x* , *y* and *z* are the Cartesian positions in an topocentric reference system, "w_{xyz}^{j}" are the angular velocities and t and t_o are the time of interest and initial positions in a given reference system i.e. ITRF 2000.

3.2.2 Solid Earth Tides

Just as the gravitational attraction of the sun and the moon distorts the shape of the ocean surface, it also distorts the shape of the earth. This distortion can be as great as 30 centimeters in the vertical and 5 centimeters in the horizontal. Whereas the shape of the ocean basins influences ocean tides, solid earth tides are accurately computable with periodicities calculated from the motion of celestial bodies. These calculations are well documented by McCarthy (1996).

$$\Delta X = \sum_{j=2}^{3} \frac{GM_j}{GM_E} \frac{\|r_E\|^4}{\|r_j\|^3} \{ h_2 \mathbf{e} \left(\frac{3}{2} (r_j . \mathbf{e})^2 - \frac{1}{2} \right) + 3 l_2 (r_{j_j} \cdot \mathbf{e}) [r_j - (r_j \cdot \mathbf{e}) \mathbf{e}] \} \quad (3.2)$$

Where $\mathbf{GM_E}$ is the gravitational constant of the earth, $\mathbf{GM_j}$ is the gravitational constant of the moon (j = 2) and the sun (j = 3), **e** is the unit vector of the station and **r** denotes the unit vector of the celestial body. $\mathbf{h_2}$ and $\mathbf{l_2}$ are the nominal degree 2 love numbers that describe the elastic properties of the earth.

To determine precise station coordinates these effects must be accounted for, especially over longer baselines where any movement will not difference away.

In addition to these periodic tidal effects there is a permanent (time independent) tidal effect. This tide generating potential has a mean (time average) value which is non zero, therefore this permanent potential produces a permanent deformation which is reflected in the static figure of the earth (*Poutanen et al. 1996; McCarthy, 1996*).

Because of its permanent character it can not be separated in any unique way from the background shape of the Earth's crust. It is therefore important to state from a modeling perspective whether any ground point coordinates have been corrected for solid Earth tides including permanent tides, or whether coordinates refer to the "non-tidal crust".

3.2.3 Pole Tides

Pole tides are the response of the Earth's crust to shifts in the spin axis orientation. The spin axis is known to describe a circular path of roughly 20 meters diameter and a period in excess of a year. This polar motion is slightly periodic due to a major 434 day constituent known as the Chandler period (*Leick, 2004*). The finer motion is however still the subject of ongoing research. This motion shifts the centrifugal effect felt at a given ground point and therefore shifts the point as the Earth's elastic crust responds. The displacement of a point can be derived from the expressions formulated by Wahr (1985) or by the IERS standards (*McCarthy, 1996)*

3.2.4 Ocean Loading

As well as the solid Earth tide deformations, ocean tides cause a periodic surface mass loading which can cause an elastic response of a few centimetres in the Earth's crust. This deformation has a vertical component and also a horizontal component, which is typically smaller by a factor of 3 or more. The displacements are dependent on time and location and constitute a combination of semidiurnal, diurnal and long-period tides (*Baker et al. 1995*). There are traditionally eleven designated tidal harmonics M_2, S_2, N_2, K_2 (Semi-diurnal) K_1, O_1, P_1 (diurnal) M_f, M_m, S_{sa} (long-periodic). Of these the M_2 (the principal lunar tide) loading deformations are typically the largest with up to 5cm in the vertical and 2cm in the horizontal. McCarthy (1996) lists the following expression for site displacement components.

$$\Delta c = \sum_j f_j A_{cj} \cos\left(\omega_j \mathbf{t} + \chi_j + \mathbf{u}_j - \Phi_{cj}\right) \tag{3.3}$$

$\boldsymbol{j}$ represents the eleven tidal harmonics, $\boldsymbol{\omega_j}$ are the angular velocities and astronomic arguments at time, $\mathbf{t.}\ \boldsymbol{\chi_j}$ reflect the position of the sun and moon. $\boldsymbol{f_j}$ and $\mathbf{u_j}$ depend on the longitude of the lunar node. The station specific amplitudes $\mathbf{A_{cj}}$ and phases $\mathbf{\Phi_{cj}}$ are computed using ocean tide models and coastal outline data.

Epoch by epoch CGPS station positions require ocean loading models. In daily solutions for CGPS network station positions, unmodelled ocean tide effects may not simply average out. Residual biases can be attributed to the M_2 and K_2 harmonics whose periods of 12.42 and 11.97 hours differ from the 12 hour, half day cycle related to the 24 hour RINEX observation format.

In addition to these oceanic loading effects, which display periodic signatures, either semi-diurnal annual or long term periods, there are deformations caused by redistribution of water mass in storms and more significantly storm surges. Storm surges are pronounced increases in water level due to a strong wind set-up and low barometric value travelling over the ocean surface. This can create a long surface wave which when combined with the certain ocean basin shapes can produce an event lasting 12 to 48 hours. Vertical displacements of as much as 20mm have been measured during these events (*Dong et al. 2002*).

3.2.5 Atmospheric Loading

Atmospheric pressure loading is a time and space varying effect that can induce crustal deformation (*Rabbel and Schuh, 1985*). The effects of pressure loading are of a very long wavelength (1000 - 2000 km) and are linked with the movement of pressure systems, particularly at higher latitudes (where pressure variations are larger in amplitude and more spatially coherent) leading to vertical displacements of up to 3cm (*van Dam et al. 1994)*. In general these pressure systems have periods of approximately two weeks but there is some evidence of an annual component with amplitudes between 0.5 and 3mm (*van Dam et al. 2002*). Effects are smaller at mid-latitudes and at locations within 500 km of the sea or ocean due to the inverted barometer response of the ocean. In all situations with pressure loading effects, horizontal crustal deformations are about one-third the amplitude of the vertical effects (*McCarthy et al. 2003*).

With such a long wavelength it is fair to assume that the effect of these earth movements will be negligible on short baselines (those of a few hundred kilometres), if however baseline lengths are comparable to wavelength (i.e. 1000-2000 km) they must be accounted for in any analysis. At present the IERS Conventions do not contain a clear recommendation of how to account for atmospheric loading in the determination of the ITRF (*van Dam et al. 2002*), although it is a key project for organisations such as the Special Bureau for Loading (SBL) (*Van Dam et al. 2002*).

3.2.6 Hydrological Loading

Hydrological loading is the deformation of the Earth due to water mass envelopes stored in continental water reservoirs (soil moisture, groundwater, snow and ice). This effect can cause site-dependant vertical displacements of up to ± 30 mm (*van Dam et al. 2001*). These vertical displacements are found to have a strong annual harmonic which is in phase and comparable amplitude with the seasonal variability in the hydrological cycle, but also there are some longer period variations which could be mistaken for other ground motions such as post glacial rebound or secular tectonic trends. These long term variations in the water mass load can be averaged out with a sufficient data time-series. (*van Dam et al. 2001*).

There are several new global models existing for soil moisture and snow cover, for example Milly et al (2002), which may be able to refine the long-wavelength hydrological loading effects (*Schuh et al. 2003*), however at present the Special Bureau for Loading within the Global Geophysical Fluid Centre (GGFC) of the IERS (*Van Dam et al. 2002*) has not produced any consistent models of the deformation of the solid Earth due to loading of the terrestrial hydrosphere. This is reflected in the IERS Conventions 2000 (2003) where no standard procedure is recommended for the case of hydrological surface loading effects. Therefore, whilst a family of loading effects have been identified the laws of consensus on their modelling means that any regional or global scale network analysis carried out for tectonic or seismic projects needs to consider carefully the aliasing of unmodelled loading effects in the time series analysis (Steigenberger et al. 2006).

3.2.7 Post Glacial Rebound

Thick glacial ice sheets covered large areas of Northern Europe, Siberia, Greenland and Canada. These melted roughly 10,000 years ago but the removal of their weight pressing on the Earth's crust results in a rebound that continues at present (*Tushingham and Peltier, 1991. Severs et al. 1995*). The rate and amount of rebound depends on a number of factors such as the original depth of ice, or thickness of the lithosphere but it is estimated that some areas may still have 10s of meters to rise with areas rising by approximately 1cm a year. In addition to these crustal deformations post glacial rebound also results in changes in the gravitational field, polar motion and the Earths rotation (*Mitrovicia et al. 2001, 2005*).

Current theories of the effects of deglaciation are not sufficiently developed to produce unambiguous results. This is largely due to an incomplete idea of the factors describing deglaciation and the rheological parameters of the crust, lithosphere and mantle (*Vermeesen, 2002. Mitroviciaet al. 2005*). With projects such as Gravity Recovery and Climate Experiment (GRACE) and Gravity Field and Stady-State Ocean Circulation Explorer (GOCE) this understanding will improve but at present there is no IERS recommendation for a post-glacial rebound model (*McCarthy et al. 2003*).

3.2.8 Aseismic Motion

Aseismic motions are measurable surface displacements without the presence of earthquakes. They are generally seen as a stable slip or creep in a fault zone but can also be of a more transient nature. Aseismic motion is covered in depth in section 2.7

3.2.9 Seismic Motion

Seismic waves are waves that travel through the Earth, most often as the result of a tectonic earthquake. Seismic motion is covered in depth in chapter 2.2

3.2.10 Other Deformations

In addition to the motions mentioned above there are a range of deformations that are often quite localised and often man-made. In particular subsidence due to mining, drilling activity or large scale construction projects. Landslides and slip can also shift bench marks or survey monuments and deform the surface in localised areas over a range of timescales (*Parry & Campbell 2007*).

Significant local land movements occur around volcanoes. If magma rises to a shallow level beneath a volcano, the ground surface above it will swell, causing survey monuments around the center of the intrusion to move horizontally and vertically away from the source. The pattern of displacements enables us to sometimes estimate the location, depth, and amount of magma intruded and therefore assess any risk of eruption. The amount of movement can and does vary significantly, from millimeters to tens of meters (*Janssen 2007*).

3.3 Reference Systems

When observing any ground motion, the movement of a given site or point has to be described relative to a reference. A subject of fundamental importance in geodetic positioning is the definition and realisation of a reference system. A reference system is realised by a reference frame, which is a catalogue of Cartesian station positions at an arbitrary and fundamental epoch, t_o (*Bock, 1996*). The basic properties of this Cartesian coordinate space are the origin, scale and orientation. Once the station positions have been defined the reference frame must be maintained by relating the rotated, translated and deformed positions at a later epoch back to the fundamental epoch. The definition of the frame therefore includes descriptions of anything that influence these positions e.g. plate motion models, gravity models, precession and nutation models.

3.3.1 The International Terrestrial Reference System and Frame

For work on the scale of global tectonic and geophysical monitoring the International Terrestrial Reference Frame (ITRF) is the frame favoured by most analysis for modern geodetic studies due to its ability to uniquely reference different locations, times and observation techniques. It has been maintained by the International Earth Rotation Service (IERS) since 1988 when the first realisation of the ITRF was released, ITRF88 (*Boucher et al 1996, 1999*).

The International Terrestrial Reference System (ITRS) is realised by the ITRF with the orientation of its Cartesian axes such that the z-axis coincides with the mean pole of rotation for the period 1900-1905 and the x-axis combining with this to form a plane through the Greenwich meridian consistent with the orientation stated by the Bureau International de l'Heure (BIH) at the epoch 1984.0. The ITRS origin is the dynamic centre of mass of the whole Earth (including oceans and atmosphere) and the unit of length is the metre (SI). The axes are then fixed to the crust such that there is no residual global rotation with respect to the lithosphere. This has traditionally been achieved using the NNR Nuvel-1a model (*DeMets et al. 1994; McCarthy, 1996)*.

The ITRF is created by the IERS by combining station positions and velocities determined by a range of space geodetic techniques. These include very long baseline interferometry (VLBI), lunar and satellite laser ranging (LLR, SLR), Doppler orbit determination and radio positioning integrated on satellites (DORIS) and GPS. Each technique has certain strengths and weaknesses when determining the reference frame parameters (*Angermann et al 2006*). VLBI defines accurate Earth orientation in an inertial frame but does not contribute to the determination of the geocentre (*Angermann et al 2002*). SLR and LLR allow for accurate positioning with respect to the geocentre and accurate determination of the scale (*Altamimi et al 2002; 2003*). By combining data from numerous observation techniques and analysis centres, the independent errors in the combined solution should be smaller than those from the individual solutions. Also the use of the full variance-covariance information provides a gauge of the true precision of each measurement type (*Boucher et al 1999*).

GPS does not contribute to the definition of the scale or the origin but makes a large contribution to the velocity field, particularly in the most recent frame, ITRF05. Unlike the previous versions of the ITRF, the ITRF2005 is constructed with input data in the form of time series of station positions and Earth orientation parameters. This has been implemented due to various reports stating that the NNR NUVEL-1A definition of the velocity model does not fulfil the no-net-rotation condition of the reference frame with respect to the Earth's lithosphere, especially when compared to the lithosphere deformation models derived using GPS. The NNR NUVEL-1A provides motions averaged over the past 3 million years rather than present day motions, in addition to this it only takes into account the rigid plates and not the deformation areas at plate boundaries (*Lavallee, 2000; Angermann et al. 2001; Altamimi et a, 2003*). A number of reports such as Angermann et al (2002) and Altamimi et al (2003) have stated rate differences of up to 2mm /yr between the various ITRF frames. Due to the uncertainty in the velocity field determination, coordinate errors will in turn grow as positions are extrapolated from the fundamental epoch. For example the ITRF2000 shows significant disagreement with the geological model NUVEL-1A in terms of relative plate motions (*Altamimi et al. 2002*). Although the ITRF2000 orientation rate alignment to NNR-NUVEL-1A is ensured at the 1 mm/y level, regional site velocity differences between the two may exceed 3 mm/y. Despite these draw backs the ITRF is still recognised as the standard solution for geo-referencing and all Earth science applications and with the increase in the number of sites and collocations (VLBI, SLR and LLR) the ITRF position and velocity precisions continue to be improved (figure 3.1).

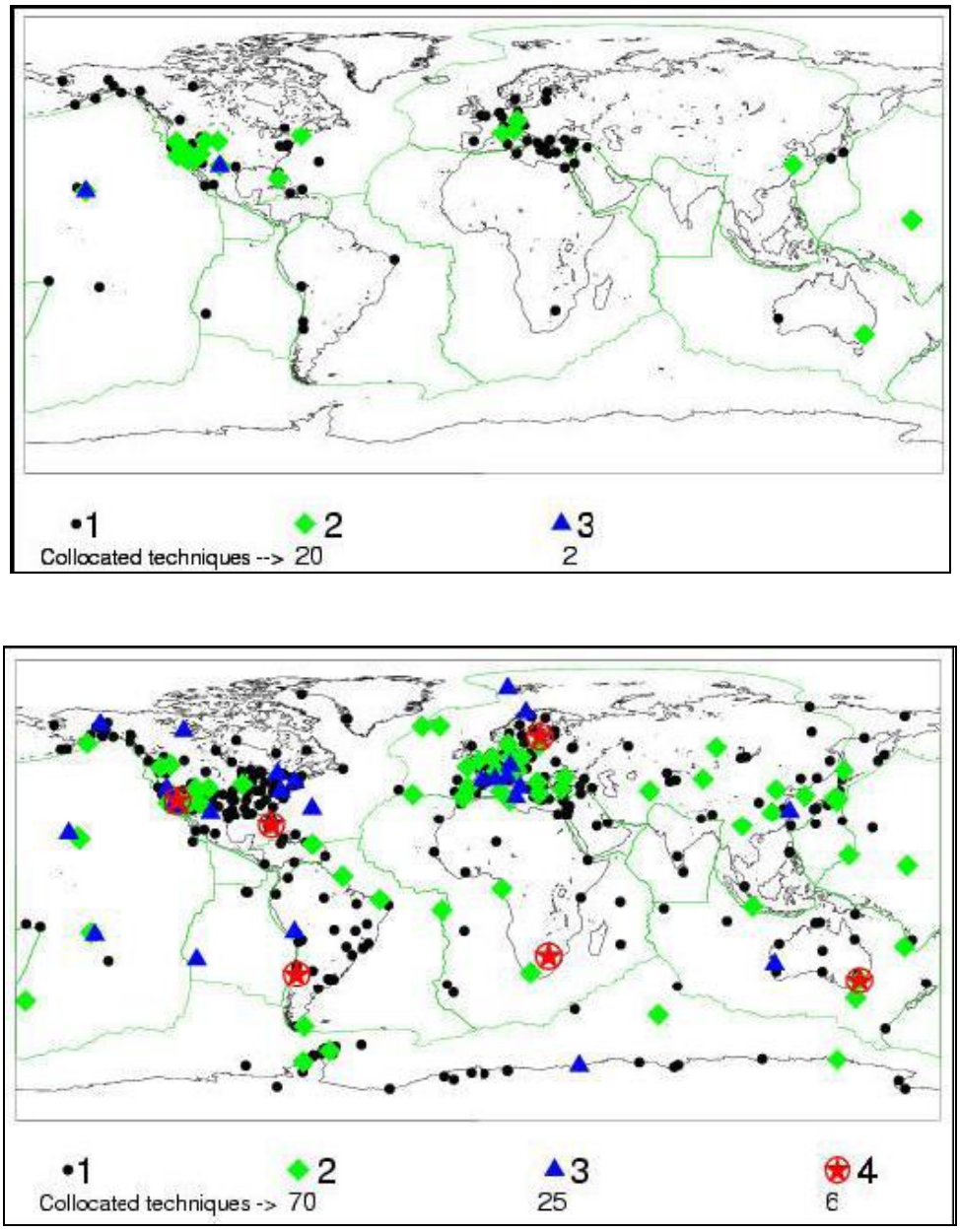

Figure 3.1: The ITRF 88 (top) and ITRF 2000 (bottom) sites and collocated techniques (IERS Technical note 33)

3.4 GPS Systematic Biases and Errors

There are a wide range of GPS systematic biases and errors that can corrupt a GPS measurement if they are not mitigated. In general these can be seen as:

- Receiver error
- Satellite error
- Atmospheric error
- Multipath error

3.4.1 Receiver Error

3.4.1.1 Receiver Clocks

The GPS pseudorange measurement is calculated by correlating identical PRN (Pseudorandom noise) codes generated by the satellite and a receiver. The Receiver clocks normally use a relatively cheap quartz oscillator which can lead to significant variation between the receiver generated codes and the transmitted codes generated by the satellite clock. These unavoidable timing errors cause the measured pseudorange to differ from the geometric distance (*Leick, 2004*).

3.4.1.2 Antenna Issues

The distance estimated between a receiver antenna and the transmitting satellite antenna is the range between the electrical phase centres of both antennas. The electrical phase centre of an antenna is not however a physical or stable point, and differs from the geometric antenna centres of receiver antennas by centimetres and satellite antennas by up to a metre (*Mader and Czopek, 2001; 2002*). This offset between the electrical phase centre and the geometric centre can be described using a constant and a varying component. The constant offset is the distance between the mean phase centre and an antenna reference point (generally the base of the receiving antenna and the centre of mass of a satellite). The variable offset depends on a range of factors such as satellite elevation angle and azimuth, intensity of the incoming signal, each of which vary on the L1 L2 or LC (ionospheric free combination) (*Rothacher et al. 1995*).

Each of these offsets vary from antenna type to antenna type but are approximately consistent in the same models. Similarly the offsets are assumed to be constant for specific satellite block types, although studies have shown inconsistencies of up to a decimeter within the same block type (*Steigenberger et al. 2004*). For short baselines this means that by using identical antennas and orientating them in the same direction the effect of antenna phase centre variations can be mitigated. If baselines are longer the elevation angle of satellites will vary between stations and any biases will not therefore difference out. In these cases antenna phase centre models must be applied. Antenna

phase center models used in this thesis are all calculated as relative phase center offsets calculated from GPS data over a short baseline with an AOAD/M_T (Allen Osborne Associates Dorne Margolin T) antenna as a reference at one end of the baseline and the antenna to be calibrated at the other (*Mader, 1999*). These corrections were used in GPS processing until 5th November, 2006 (*Schmid et al. 2006*). Since then there has been a switch to absolute phase center variations (PCVs) in the international terrestrial reference frame 2005. This subject is discussed in greater depth in chapter 8.3.1.

3.4.1.3 Noise

The assumption that CGPS measurements improve station coordinate estimates by a factor of $1/\sqrt{N}$, with N being the number of measurements, has been shown to be unrealistic. Although a lot of the noise inherent in a GPS signal such as thermal noise, high frequency multipath signals and signal scattering are Gaussian and are therefore average's out over a day's processing, the idea that GPS coordinate solutions are purely random or "white" noise has been shown to be incorrect as errors have also been characterised as coloured (time-correlated) noise (*Teferle. 1996*). There are a number of noise sources which mean GPS noise can be described as a power-law process, or one with time-domain behaviour (*Agnew, 1992; Zhang et al. 1997; Calais, 1999; Lavallee, 2000; Nikolaidis, 2002*). In particular flicker and random walk noise have been observed as fluctuations in GPS coordinate solutions. Flicker noise has been observed in dynamical processes such as sunspot variability the wobble of the Earth about its axis, undersea currents, average seasonal temperature and the ammount of annual rainfall (*Williams et al. 2003*). Naturally occurring processes often have more noise power at lower frequencies such as monument stability or transient tectonic motion and have been observed to follow a random walk process (*Zhang et al. 1997*).

Williams et al (2003) analysed a total of 954 continuous GPS position time series from 414 individual sites in nine different GPS solutions using maximum likelihood estimation (MLE). In their study they found that global GPS solutions could best be described by a combination of white noise plus flicker noise. Both these noise components showed latitudinal dependence in their amplitudes (higher at equitoral sites) combined with a bias to larger values for sites situated in the Southern Hemisphere. In regional solutions, where a common mode error signal had been removed using the

regional filtering technique the noise was significantly lowered. The spectral index of noise sources was more varied than in the the global solutions and probably reflected a mixture of local effects, for example residual common mode noise (white noise plus flicker noise), monument instabilies (random walk noise), and localized deformation due to changes in groundwater (unknown power law noise plus repeating signals).

The general conclusion is that as with the Gaussian noise sources many of these features will average out given enough data and time, but particularly for short time series, if not accounted for station velocity uncertainties may be underestimated by an order of magnitude (*Mao et al. 1999*).

3.4.2 Satellite Error

3.4.2.1 Satellite Clocks

Fundamental to GPS is the one-way ranging that ultimately depends on satellite clock predictability. The control segment of GPS maintains GPS time (to within 1μ s of UTC, not counting leap seconds). GPS satellites use atomic clocks (caesium and rubidium oscillators), and broadcast their offset and frequency offset from GPS time in the navigation files. More refined versions of these corrections are included in the precise orbits and clock corrections published with a 13 day latency.

3.4.2.2 Satellite Ephemeris

Ephemeris errors result when the GPS message does not transmit the correct satellite location. It is typical that the radial component of this error is the smaller, the tangential and cross-track errors may be larger by an order of magnitude. Fortunately, the larger components do not affect ranging accuracy to the same degree. Because satellite ephemeris errors reflect a position prediction, they tend to grow with time from the last control station upload. As such for precise applications it is recommended that that the precise orbits such as those available from the IGS (http://igscb.jpl.nasa.gov) are used (*Warren and Raquet, 2003*).

3.4.2.3 Satellite Geometry

GPS works best, or is at its most accurate, when there is a good angular separation between satellites. The measure of the angular separation is called the dilution of precision (DOP) and is a measure of the geometrical strength of the GPS satellite configuration. There are a variety of DOPs :

- PDOP = Position Dilution Of Precision (Most Commonly Used)
- VDOP = Vertical Dilution Of Precision
- GDOP = Geometric Dilution Of Precision
- HDOP = Horizontal Dilution Of Precision
- TDOP = Time Dilution Of Precision

If "x" number of satellites that can see a receiver are all arranged in the same section of the sky this will lead to a "bad" geometry and consequently greater error in positioning (figure 3.2)

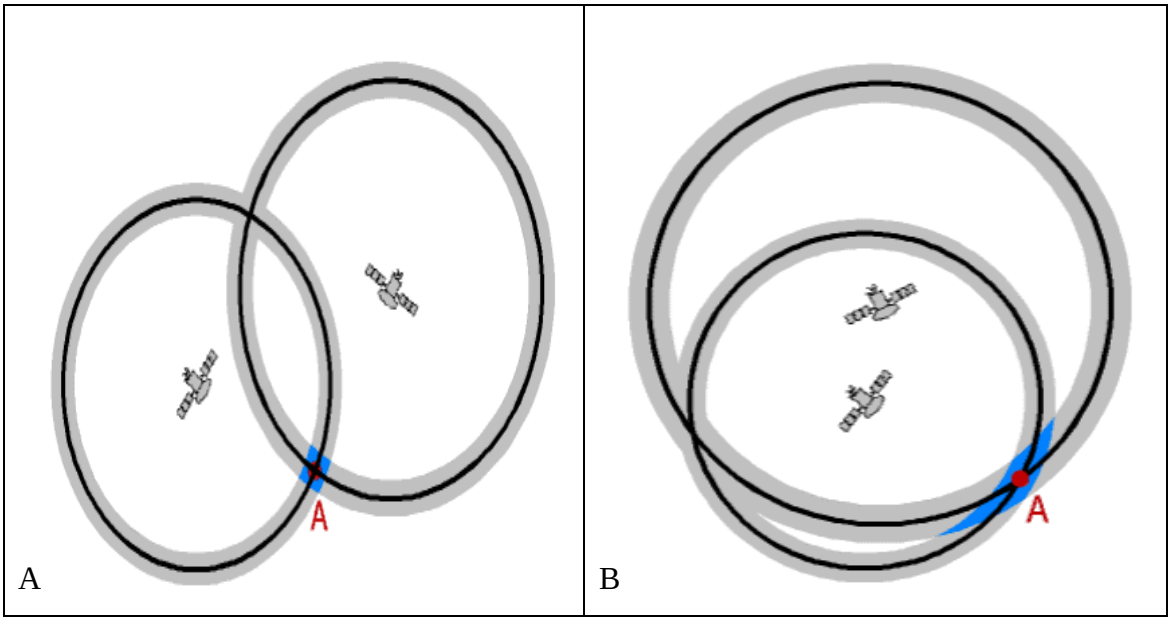

Figure 3.2: 2D example of "good" (A) and "bad" (B) geometrical precision and the corresponding errors encured (blue)

This error source affects receivers with a constrained view of the sky such as those in built up areas or receivers located at high latitudes. It is also a significant factor in the greater inaccuracy of the vertical component of GPS (*Santerre, 1991*).

The DOP values are calculated from the covariance matrix formed in the least squares computation on the GPS pseudorange measurement.

$$\mathrm{cov}(dx) = \begin{bmatrix} \sigma_x^2 & \sigma_{xy}^2 & \sigma_{xz}^2 & \sigma_{x\delta t}^2 \\ \sigma_{xy}^2 & \sigma_y^2 & \sigma_{yz}^2 & \sigma_{y\delta t}^2 \\ \sigma_{xz}^2 & \sigma_{yz}^2 & \sigma_z^2 & \sigma_{z\delta t}^2 \\ \sigma_{x\delta t}^2 & \sigma_{y\delta t}^2 & \sigma_{z\delta t}^2 & \sigma_{\delta t}^2 \end{bmatrix} \tag{3.4}$$

From this covariance matrix the various DOP parameters can be calculated as follows (*Kaplan and Hegarty, 2006*):

$$GDOP = \frac{\sqrt{\sigma_x^2 + \sigma_y^2 + \sigma_z^2 + \sigma_{\delta t}^2}}{\sigma_{VERE}} \tag{3.5}$$

$$PDOP \times \sigma_{VERE} = \sqrt{\sigma_x^2 + \sigma_y^2 + \sigma_z^2} \tag{3.6}$$

$$HDOP \times \sigma_{VERE} = \sqrt{\sigma_x^2 + \sigma_y^2 +} \tag{3.7}$$

$$VDOP \times \sigma_{VERE} = \sigma_z^2 \tag{3.8}$$

$$TDOP \times \sigma_{VERE} = \sigma_{\delta t}^2 \tag{3.9}$$

An example of how much affect satellite geometry and numbers can have on the DOP values can be seen in table 3.1 and graphically in figure 3.3. In this example the loss of only two satellites results in double the dilution of precision.

Time	No. of satellites	GDOP	PDOP	Satellites
10/03/06 14:30	10	2.8	2.3	G01, G11, G17, G20, G23, G24, R03, R04, R18, R19
10/03/06 14:40	10	2.9	2.3	G01, G11, G17, G20, G23, G24, R04, R05, R18, R19
10/03/06 14:50	10	3.0	2.4	G01, G11, G17, G20, G23, G24, R04, R05, R18, R19
10/03/06 15:00	8	6.7	5.2	G11, G17, G20, G23, G24, R04, R05, R19
10/03/06 15:10	8	7.3	5.7	G11, G17, G20, G23, G24, R04, R05, R19
10/03/06 15:20	8	6.7	5.3	G11, G17, G20, G23, G24, R04, R05, R19
10/03/06 15:30	9	3.0	2.5	G04, G11, G17, G20, G23, G24, R04, R05, R19
10/03/06 15:40	10	2.3	1.9	G04, G11, G13, G17, G20, G23, G24, R04, R05, R21
10/03/06 15:50	10	2.3	2.0	G04, G11, G13, G17, G20, G23, G24, R04, R05, R21
10/03/06 16:00	9	3.4	2.8	G04, G13, G17, G20, G23, G24, R04, R05, R21

Table 3.1: Satellite numbers and their respective GDOP and PDOP values (From LGO, printed document 4.0)

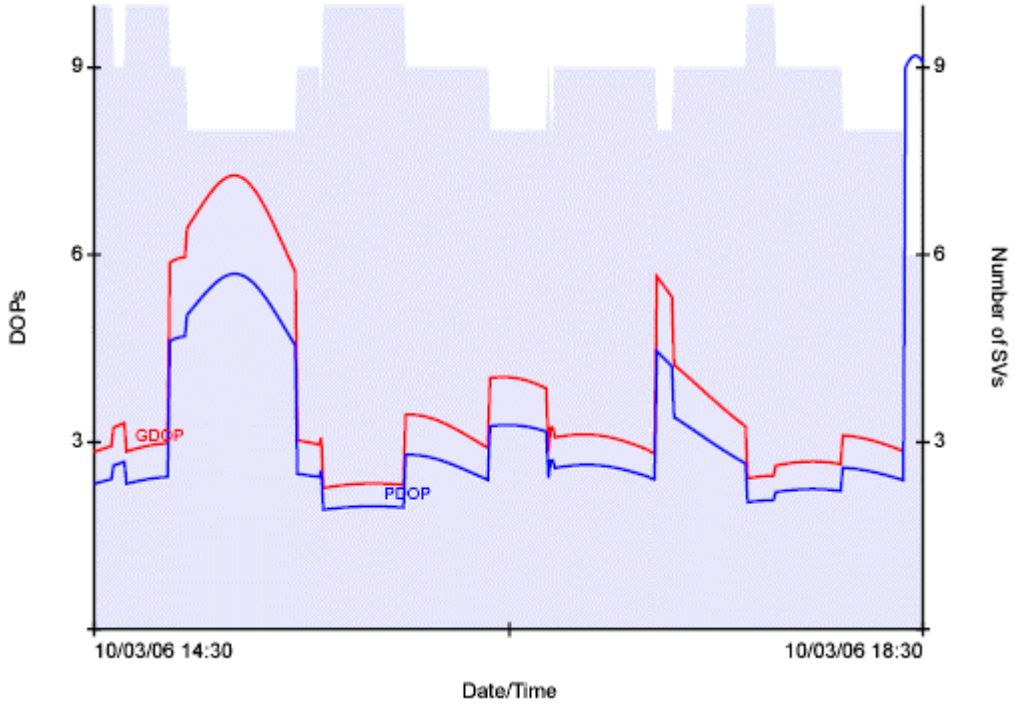

Figure 3.3: Satellite numbers and their respective GDOP and PDOP values (From LGO, printed document 4.0)

3.4.3 Atmospheric Biases

Radio signals travel with the speed of light in a vacuum, however on their path through the atmosphere GPS signals are affected by bending, refraction, scintillation, advances of the carrier phases and other changes. If not accounted for this will propagate into station coordinate estimates essentially introducing a scale error into the measurements.

Whilst geometric bending of the signal path causes minor delays that are negligible for elevation angles above 5˚, the affects of the Ionosphere and Troposphere can have a significant effect. This topic is still the subject of active research but is extensively discussed in numerous papers and textbooks (*Langley, 1996; Leick, 2004*).

3.4.3.1 Ionospheric Delay

The ionosphere covers the region between ≈ 50 and 1500 km above the Earth (*kelley, 1989*). It is characterised by the presence of free electrons and ions created by a combination of coronal mass ejections (CMEs) and extreme ultraviolet solar radiation (solar flux). The free electrons delay the pseudoranges and advance the carrier phases

along the GPS signal path by an equal amount. The size of any delays depends on the total electron count (TEC, the number of free electrons) in the column along which any signal propagates and the carrier frequency of that signal. It is a dispersive medium, therefore the refractive index of a signal is dependent on the signals frequency. TEC values vary between 10^{16} and 10^{19} electrons m^2 with a peak around 14:00 local time each day, decaying to a minimum just before sunrise. They also have a greater effect 20º above and below the magnetic equator (figure 3.4) (*Cross, 2004*).

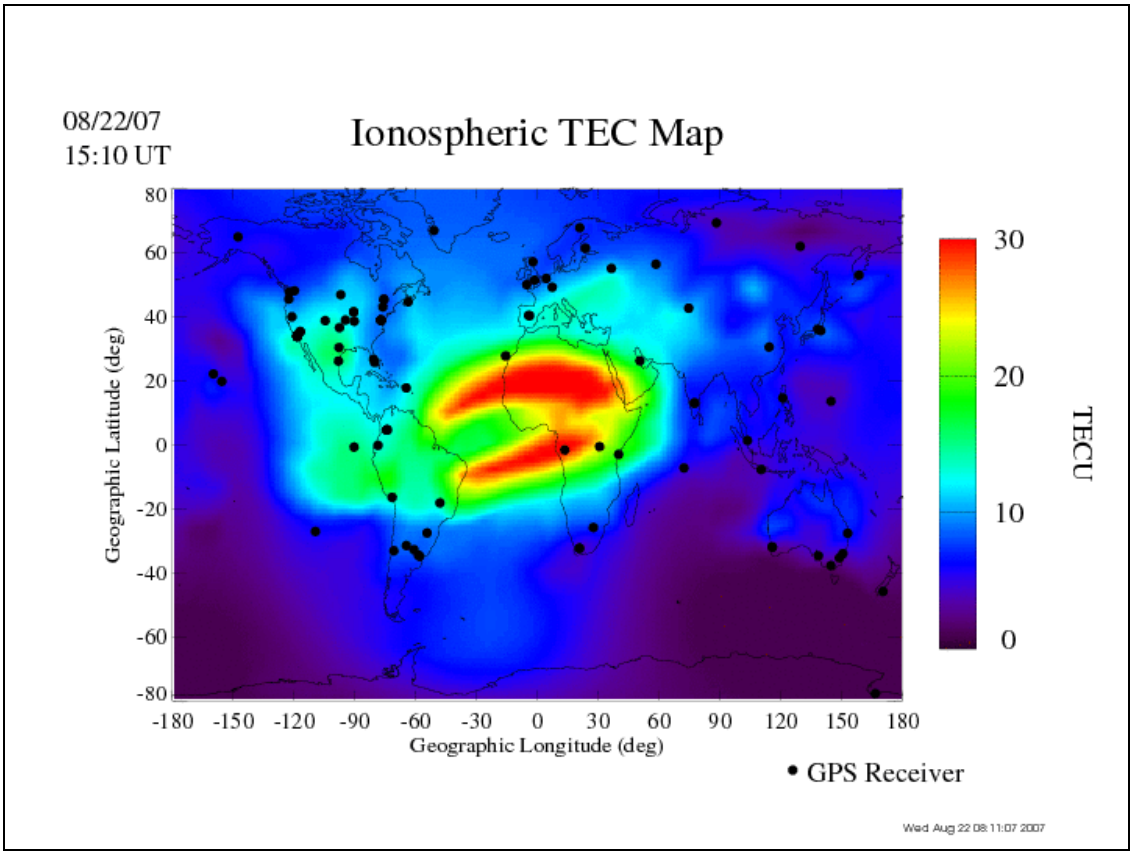

Figure 3.4: Example TEC map showing the characteristic double hump equatorial bias that appears at low latitudes (from http://iono.jpl.nasa.gov)

The first order ionospheric term, signal group delay (or phase advance) can be between 1-50 meters. There is also a second-order term (I_2), caused by the Faraday rotation effect induced by the Earth's magnetic field, which is about 1000 times smaller and usually ignored (*Kedar et al. 2003*). With increasing needs for improvements in precise GPS positioning the impact of the 2nd order term is becoming more relevant. The I_2 is proportional to the magnetic field projection along the transmitter-receiver direction and the ionospheric delay of the signal (*Hernandez-Pajares et al. 2007*). Fritsche et al (2005) and Hernandez-Pajares et al (2007) have both shown deviations in receiver position of the order of several millimeters for sub-daily differential positioning. The

impact on daily positions has been shown to be less than a millimeter but with a latitudinal dependence. In addition, although the term has little effect on receiver parameters the satellite parameters can be affected, in particular the satellite clock which can show deviations in excess of 1cm. Satellite orbits have been shown to be affected by a southward displacement of the orbits of several millimeters. There are now algorithms being developed to account for the I_2 using TEC maps (*Kedar et al. 2003; Fritsche et al. 2005*)or based on the GPS geometry free combinations in phase and code (*Hernandez-Pajares et al. 2007*).

There are also local disturbances in the atmosphere that can significantly impact the TEC such as Travelling Ionospheric Disturbances (TIDs) and scintillation effects (*Soicher, 1988; Warnant and Pottiaux, 2000*). TIDs appear as waves in the electron density (and consequently the TEC) due to interactions between the solar wind, or more specifically the magnetic field it carries and the ionosphere. These waves typically travel at 450 km/s with wavelengths ranging from a few tens of kilometres to more than a thousand kilometres. Their occurrence often causes large gradients in the TEC even over short distances. Scintillation can result in rapid variation in signal amplitude and phase which in some cases can cause receivers to lose, or be unable to maintain lock for a prolonged period of time (*Kunches & Klobuchar, 2000*).The amount of this ionospheric activity depends on the number of sunspots which follow a cycle of between 9 and 14 years. This scintillation generally follows the 11-year cycle of sunspot activity that last peaked in 2001 and as with the background flux has much greater effects in equatorial regions (*Kunches & Klobuchar, 2000*).

The first order ionospheric errors are corrected using dual frequency receivers. A linear combination of the L1 and L2 pseudorange measurements may be formed to estimate and remove the ionospheric bias from the L1 measurements (*Langley, 1996*).

$$d_{ion,1} = \frac{f_2^2}{f_2^2 - f_1^2}\left[p_1 - p_2\right] + e \tag{3.10}$$

$\mathbf{f_1}$ and $\mathbf{f_2}$ are the L1 and L2 carrier frequencies, **p1** and **p2** are the L1 and L2 pseudorange measurements and **e** represents unmodelled biases and measurement errors. Similarly the carrier phase measurements can be corrected with:

$$d_{ion,1} = \frac{f_2^2}{f_2^2 - f_1^2}\left[\left(\lambda_1 N_1 - \lambda_2 N_2\right) - \left(\phi_1 - \phi_2\right)\right] + e \tag{3.11}$$

Φ_1 and Φ_2 are the L1 and L2 carrier phase measurements, λ_1 and λ_2 are the L1 and L2 carrier wavelengths and N_1 and N_2 are the L1 and L2 integer phase ambuiguities.

Single frequency receivers can remove ionospheric errors by differencing the observations made simultaneously at different receivers, although there will be errors associated with this as any signals will not have propagated through the same part of the atmosphere and therefore their TEC will vary. There are also emphirical models to correct for ionospheric bias but for scientific studies dual frequency receivers are required.

3.4.3.2 Tropospheric Delay

The troposphere is the area of the Earth's atmosphere up to approximately 15km that contains most of the mass of the atmosphere. Above this the density is too small to have a measurable effect. This area behaves as a non-dispersive medium at microwave frequencies, i.e. the refractive index is independent of the signal frequency. Typically tropospheric refraction is treated in two parts, the hydrostatic and the nonhydrostatic wet component. Tropospheric delay models estimate the tropospheric zenith delay (TZD), which is the delay at 90˚ to the horizon (*Langley, 1996; Leick, 2004*). It is typically responsible for a zenith delay of approximately 2.4 to 2.8 m at sea level locations (≈ 2.4 m hydrostatic, ≈ 0.4 m nonhydrostatic wet component) (*Mendes, 1999*).

The large (≈ 90%) hydrostatic component follows the laws of ideal gases and as such can be computed accurately from a pressure observation at the receiver antenna, assuming the atmosphere is in a state of hydrostatic equilibrium (*Langley, 1996*). Examples of such models for the zenith hydrostatic delay (ZHD) are Hopfield (1969) or Saastamoinen (1972), see equation 3.12

$$ZHD_m = \frac{0.0022768_{p0[mbar]}}{1 - 0.00266\cos 2\varphi - 0.00028H_{[km]}} \tag{3.12}$$

Where ρ_0 is the total pressure at the site, *H* is the orthometric height and φ is the latitude.

Zenith models regarding the wet refractivity are far more problematic. It is a function of the water vapour content along the path of the electromagnetic signal and is highly variable, both temporally and spatially. Field observations of conditions can be influenced by significant surface layer biases and are not necessarily representative of adjacent layers.

Mapping functions have to be applied to both components as satellites can appear at elevation angles between 0 and 90˚ relative to a GPS receiver and therefore signals at lower elevation angles will propagate through more atmosphere and experience greater delay (*Dodson et al. 2000*). A function in common use is Niell's (1996) Mapping Function (NMF), which is independent of surface meterology and therefore requires only site location and time of year as input. This has recently been revised with the formation of the Global Mapping Function (GMF) which is based on data from the global ECMWF (The European Centre for Medium-Range Weather Forecasts) numerical weather model and improves the height biases and annual errors of NMF significantly (*Boehm et al. 2006*). More recently still Vienna mapping functions have been developed (*Boehm and Schuh, 2004*). The continued fraction form for the hydrostatic and wet mapping function for an elevation angle **e** is shown below

$$\mathrm{mf}(\mathrm{e}) = \frac{1 + \frac{\mathrm{a}}{1 + \frac{\mathrm{b}}{1+\mathrm{c}}}}{\sin \mathrm{e} + \frac{\mathrm{a}}{\sin \mathrm{e} + \frac{\mathrm{b}}{\sin \mathrm{e}+\mathrm{c}}}} \tag{3.13}$$

Three coefficients **a, b** and **c** are sufficient to map zenith delays down to elevations of 3º. VMF determines these coefficients using raytracing through numerical weather models (NWM) such as that produced by ECMWF. Every six hours the hydrostatic and wet mapping functions are determined by raytracing through the pressure levels at ten different initial elevation angles (90, 70, 50, 30, 20, 15, 10, 7, 5, 3.3). The coefficients in equation XX are calculated in a least squares procedure (*Boehm and Schuh, 2004*). This procedure is likely to improve as the NWM's receive more data and improve.

.

Although mapping functions do reduce biases they have a number of drawbacks, in particular they assume azimuthal symmetry around a receiver. In reality the water vapour in an area has an azimuthal dependency due to factors such as terrain and wind. To counter this there has been the development of horizontal gradient models (*Bar-Sever et al. 1998*)

The seasonal character of the troposphere is primarily described by the wet tropospheric component, therefore residual tropospheric delay biases may be responsible for some of the annual signals observed in coordinate time series (*Dong et al. 2002a*).

3.4.4 Multipath Effects

Objects in a GPS receiver's vicinity may reflect some signals before they enter an antenna. The reflected signals are delayed compared with the line of sight observations as they travel longer paths (*Leick, 2004*). Signals can also be reflected at the satellite (satellite multipath), although this largely cancels itself in single difference observables over short baselines.

There is a range of methods to mitigate multipath such as choosing appropriate hardware, receiver locations and suitable horizon cut off angles, or in post processing. Since the geometry between the GPS constellation and a receiver repeats every sidereal day, multipath shows the same pattern between consecutive days. As such the presence of multipath can in principle be verified, modelled or removed. In practical terms the attenuation properties of reflecting objects generally vary making multipath a difficult error source to deal with. Multipath effects are covered in greater detail by Meehan and Young (1992) or Zhdanov et al (2001) and the reader is referred to their work for a more complete discussion.

3.5 GPS Data

In scientific GPS data processing it is necessary to utilise a range of data sources describing features such as Earth orientation parameters, phase centre offsets, and satellite orbits in order to maximise the accuracy and minimise the errors inherent in any GPS positioning. This section describes the data available.

3.5.1 GPS Observations

GPS satellites transmit at two frequencies, L1 (1575.42 MHz) and L2 (1227.6 MHz). These frequencies are modulated with two types of code, the civilian / coarse acquisition (C/A) code and the precise code (P). The L1 frequency is modulated with both types of code whilst the L2 is modulated with only the P-code. In addition both frequencies have a navigation message (*Leick, 2004*). The most important GPS observations for the purpose of positioning are the pseudoranges and carrier phases which can be used independently or in conjunction with each other to obtain accurate surveying solutions. The pseudorange relates to the measured distance implied by the epochs of emission and reception of the GPS pseudo-random codes (C/A and P). The travel time of the codes is measured by correlating identical PRN codes generated by the satellite and the receiver. This process introduces unavoidable timing errors due to the differences in the receiver and the satellite clocks that generate the signal which in turn lead to a difference between the measured pseudorange and geometric distance corresponding to the instants of signal emission at the satellite and reception at the receiver.

The basic equation for this process, without any other factors such as ionospheric or tropospheric effects is as follows (*Leick, 2004*):

$$\rho_r^s(\hat{t}^\rho) = (\hat{t}_r - \hat{t}^s)c = (t_r + d\underline{t}_r - t^s - d\bar{t}^s)c \tag{3.14}$$

$\rho_r^s(\hat{t}^\rho)$ The geometric distance in a vacuum traveled by the code from satellite (s) to receiver (r).

$\hat{t}_r$ True time at the receiver measured at the epoch the code entered the antenna. The nominal time (t_r) is in error by dt_r.

$\hat{t}^s$ The true time at satellite transmission. The nominal time is t^s which is in error by dt^s.

c The velocity of light in a vacuum.

The code itself is generated by a feedback shift method (*Cross, 2004*) that corresponds to a one millisecond period (≈ 293 km) on the C/A code and a 38 week period on the P code.

The phase observation is the sum of the fractional carrier phase which arrives at the antenna at the nominal time and an unknown integer constant representing full waves. The wave lengths on the L1 and L2 are 19.03 or 24.45 cm respectively. The distance measurement of this is expressed in equation 3.15, where the carrier phase has been scaled to a unit of length by $\lambda_1 = c/f_1$.

$$\Phi^s_{r,1}(t_r) = \rho^s_r(\hat{t}^p) + \lambda_1 \mathrm{N}^s_r(1) - c\underline{dt}_r + c\bar{dt}^s + \mathrm{I}^s_{r,1,\Phi}(t_r) + \mathrm{T}^s_r(t_r) + \delta^s_{r,1,\Phi}(t_r) + \varepsilon_{1,\Phi} \tag{3.15}$$

$\Phi^s_{r,1}(t_r)$ The geometric distance as measured on the L1 carrier phase signal.

$\rho^s_r(\hat{t}^p)$ The fractional carrier phase which arrives at the receiver.

$\lambda_1 \mathrm{N}^s_r(1)$ The integer ambiguity. In particular the first epoch of observations (1) until a cycle slip occurs.

$\mathrm{I}^s_{r,1,\Phi}(t_r)$ Ionospheric carrier phase advance (a negative value).

$\mathrm{T}^s_r(t_r)$ Tropospheric delays.

$\delta^s_{r,1,\Phi}(t_r)$ Hardware delays and multipath effects on the L1 carrier phase.

$\varepsilon_{1,\Phi}$ L1 phase measurement noise (0.01 cycles).

This information is recorded in a range of formats, depending on antenna type. In 1989 a standard GPS format, RINEX (Receiver Independent Exchange Format) was created for the easy exchange of GPS data regardless of receiver manufacturer. A description of the RINEX Version 3.0 is outlined by Gunter and Estey (2007). This version consists of three ASCII file types, the observation data file, the navigation file and the meteorological data file.

The observation files contain more than just the measurement of the pseudorange, the phase and the time signature. They also give information on Doppler shifts, signal strength and ionospheric phase delays.

Likewise the meteorological file can contain data on:

- Pressure (mbar)
- Dry temperature (deg Celsius)
- Relative humidity (%)
- The wet zenith path delay (mm)
- Dry component of the zenith path delay (mm)
- Total zenith path delay (mm)
- Wind azimuth (deg)
- Wind speed (m/s)
- Rain increment (1/10 mm)
- Hail indicator

You can get RINEX files from many servers around the world for example at the NASA Goddard Space Flight Center or at SOPAC (Scripps Orbit and Permanent Array Center).

The L1 and L2 frequencies combined with the navigation message and the meteorological file are the current signals provided by GPS satellites. The system is at present going through a modernisation program utilising advances in satellite technology and adding to the current broadcast frequencies. The L2 frequency will be shared between civil and military signals with a L2CM (civil moderate length) and L2CL (civil long) added which should increase robustness and improve accuracy. In addition new military codes will be added to the L1 and L2 and satellites will transmit

on a third civilian frequency called L5. This frequency (1176.45 MHz) is in the protected Aeronautical Radio Navigation Service (ARNS) band and will be used as a civilian "safety of life" signal (Leick, 2004).

This GPS modernisation will be complemented by the launch of the European GNSS system, Galileo. GPS and Galileo are designed to share similar frequency space and be interoperable which will greatly increase the availability of GNSS satellites thereby increasing accuracy and reducing the number of satellite black spots such as urban canyons.

3.5.2 Earth Orientation and Satellite Position Data

For precise applications a range of information is required to achieve accurate estimates of station positions. In particular data describing the orientation of the Earth and the position of the satellites around that Earth.

The terrestrial reference system and frame described in section 3.3.1 was developed and is maintained with reference to a celestial reference system. The celestial reference system is realised by a catalogue of celestial coordinates of extragalactic radio sources (quasars) determined from astrometric observations (VLBI). This frame is maintained through a number of the International Association of Geodesy's (IAG) umbrella organisations, particularly the International Earth Rotation Service (IERS)

To transform between the celestial (CRF) and terrestrial reference frames (TRF) requires knowledge of how the Earths celestial pole moves in the celestial reference frame, particularly the precessions and nutations caused by the gravitational attraction of the sun, moon and planets (*McCarthy and Petit, 2003*), also the variation in the instantaneous rotation axis (polar motion) and variations in the rotation of the Earth around the axis of the pole. Of fundamental importance to many of these calculations are the time systems used to measure and define them.

The relationship between the celestial and terrestrial reference frames is defined by Greenwich apparent sidereal time (GAST). Sidereal time (also called universal time) was a time system based on the Earth's diurnal rotation and was used prior to the advent

of atomic time (UTC) Today it is not used as a practical time system as it is too irregular when compared to atomic clocks, it is however used as an angular measurement in the transformation between the CRF and TRF. This relates the Greenwich mean astronomic meridian to the vernal equinox (the direction of the TRF's "X" axis) (*Bock, 1998; Leick, 2004*) Atomic time is a uniform time scale known as International Atomic Time (TAI). Because TAI is a continuous time scale it does not maintain synchronization with universal time as the Earth's rotation rate is slowing down, for civilian convenience this is solved by Universal Time Coordinated (UTC), which runs at the same rate as TAI but is incremented by leap seconds occasionally. Time signals broadcast by GPS are referred to as Global Positioning Time System (GPST) and run within 5 nanoseconds of TAI but with an offset.

GPST + 19 Seconds = TAI

Having determined the position of the TRF, accurate knowledge of the positions of the satellites within this Cartesian system is of fundamental importance, as any error will translate directly to the positioning of a receiver. The accurate determination of satellites must consider a range of perturbing accelerations that deviate the satellite from its normal orbit. These include the nonsphericity of the gravitational potential, the attraction of the sun and moon, solar radiation pressure and smaller factors that are still the subject of on going research such as the Earth's albedo and thermal reradiation.

The operational control system for GPS, located in Colorado Springs is responsible for satellite control as well as the determination, prediction and dissemination of satellite ephemerides and clock information. This information is periodically updated and broadcast as part of the GPS navigation message. The generation of the navigation message starts with the OCS's use of a Kalman filter to estimate satellite position, velocity, solar radiation pressure coefficients, clock bias, clock drift and clock drift rate. These estimated parameters are then used to propagate the satellite position and clock corrections into the future. The propagated values are then fit to a set of equations and the fit coefficients are distributed as broadcast ephemerides in the navigation message (*Warren and Raquet, 2003*). The accuracy of this message is at present calculated to be around 1.1 meter. This is a real time message sufficient for many GPS applications but for surveying and scientific purposes more accurate satellite ephemeris and clock data is required.

This task is performed by the IGS (International GNSS Service) who collate earth orientation data and satellite positional data from a large number of data centres and process it in order to provide a range of more accurate products some of which are listed in table 3.1.

Product	**Accuracy**	**Latency**	**Updates**
GPS Satellite Ephemeris and Satellite Clocks			
Predicted (ultra rapid)	~ 10 cm; ~5 ns	Real time	4 Times daily
	~ 5 cm; ~0.1 ns	17 hrs	Daily
Rapid	~ 5 cm; ~0.1 ns	~ 13 days	Weekly
Final			
Geocentric Coordinates of IGS Tracking Stations			
Final Positions	3mm horizontal 6mm vertical	12 days	Weekly
Final Velocities	2mm/yr horizontal 3mm/yr vertical	12 days	Weekly
Earth Rotation Parameters			
Rapid polar motion	< 0.1 mas	17 hours	Daily
Polar motion rates	< 0.2 mas/day		
Length-of-day	0.03 mas		
Rapid polar motion	0.05 mas	~ 13 days	Weekly
Polar motion rates	< 0.2 mas/day		
Length-of-day	0.02 mas		

Table 3.1: The various IGS products (from http://igs.jpl.nasa.gov)

The Predicted, Rapid and Final orbit products differ mainly by their latency and the extent of the tracking network used for their computation. The Final orbits are formed from the combined contributions of 7 IGS Analysis Centers (AC's).

Other data required includes information on time, polar motion (x and y pole position and rates) and earth rotation (Length of day, LOD), time dependant parameters such as station and satellite clock biases, and satellite positions at known times and in a

recognised reference frame. There are a range of files that can provide this information. The most common are SP3 files which describe satellite orbits in terms of their X, Y, Z coordinates and errors in an Earth centered Earth fixed frame (WGS84). They also contain information relating to the clock errors.

Other systems use Earth centered inertial systems, such as processing using the GIPSY-OASIS software package. This requires a number of files, firstly an "eci" (earth centered inertial) file containing satellite positions and their velocity, a "tpeo" file that contains information on time, polar motion, and earth rotation and a "tdpc" file which contains information on all the time-dependant parameters. These files can be used in conjunction with an "x" file to convert from the Earth centered inertial frame to any given reference (ITRF). In addition to "shadow files" containing information on when each satellite will be moving through the penumbra and umbra in order to mitigate the effect of varying yaw attitudes.

3.6 Processing Strategies

When studying a problem such as tectonic movements using GNSS technology the choice of processing strategy is of fundamental importance. A data processing strategy starts with the choice of network observation style.

GPS networks can either be comprised of permanent continually operating reference stations (CORS) or sites that are periodically observed in a campaign style. Both techniques have advantages and disadvantages. CORS have no setting up error, and as they are continuous, pick up movements at all temporal scales. They are however expensive and can have serious logistical problems regarding power and data retrieval. Campaign observations are cheap and don't have the same logistical problems but do have significant error sources. These are partly due to set up errors if the monument used is not a maintained or permanent structure but more significantly are due to the duration and epoch of any observations made. The length of a reoccupation session directly affects the accuracy of a position as solutions based on short observation sessions are generally less reliable than those from longer sessions. In general campaign style GPS observations are less than twenty four hours and are often less than ten

(*Cross, 2004*). The positional errors introduced using the campaign style of reoccupation can give false images of the secular trends in a time series and being intermittent do not detect transient motion. The choice of observation technique is therefore determined by the application and resources available.

Once the GNSS data has been collected a suitable choice of processing strategy must be made. In general, processing strategies can be defined as absolute or relative.

Absolute positioning is with respect to a coordinate system (i.e., ITRF). This coordinate system is realised by the coordinates of the monitoring stations and subsequently transferred to users via the changing positions of the GNSS satellites. As any range measurement made between a satellite and a receiver will contain a number of error sources such as satellite and receiver clock offsets, tropospheric and ionospheric refraction and multipath, in absolute positioning these must be modelled or averaged to achieve improved positioning accuracy (*Evans et al. 2002; Rizos, 1999; Leick, 2004*).

Relative (differential) positioning takes advantage of the fact that many errors will affect the absolute position of two or more GPS receivers to almost the same degree. These errors largely cancel out when relative or differential positioning is applied. Typically one or more stations are held fixed and a set of correlated vectors are determined between these and other estimated stations. There are a range of GNSS processing strategies, the principles of each of these are outlined below.

3.6.1 Differential GPS (DGPS)

Differential positioning is the determination of a point with respect to a coordinate system formed by a reference station(s) (*Kaplan and Hegarty, 2006*). In general this involves the use of a process known as double differencing to remove satellite clock and receiver clock errors as well as other errors that cancel over short distances (such as the ionosphere and troposphere). In differential GPS a reference station at a known location is used to observe the GPS signals from two satellites at the same time. If these signals are differenced the receiver clock error is removed. If this process is repeated at an unknown receiver all receiver clock errors are removed. In a similar way observing signals from the same satellite at the same time using two receivers and differencing,

the satellite clock error is removed. If this is repeated for all sites (known and unknown) and satellites, all clock errors can be removed. This process obtains precise baselines. The coordinates of unknown receivers can then be determined relative to the known site locations. Hence the phrase differential positioning (*Zumberge et al. 1997; King et al. 2002; Leick, 2004*).

3.6.2 Fiducial (Network) Positioning

Fiducial positioning is a form of differential GPS. The technique utilizes the ITRF stations as a subset of reference points with known coordinates to precisely calculate the coordinates of other unknown GPS stations. When compared to non fiducial processing the stations used as reference points in a fiducial network are tightly constrained to some *a priori* coordinates in the estimation strategy. These initial coordinates were traditionally determined by a range of other space-based techniques such as SLR and VLBI but with increases in the time series of permanent GPS stations these are now commonly seen as known coordinates. This fiducial network therefore provides a well defined reference frame in which to study other sites (*Heflin et al. 1992*). This can however lead to a number of problems as any error in the position of the reference stations translates directly into undesired errors in the resulting coordinates for the non fiducial stations. In particular changes in antennas (and therefore absolute phase centers), earthquakes or other significant changes in the position of antenna reference points results in errors and noise in non – fiducial sites through the least squares process. In addition on a global scale it becomes hard to interpret GPS solutions which are strongly constrained *a priori* (*Blewitt et al. 1992*) and prevents study of the fiducial stations themselves (*Rius et al. 1995*).

3.6.3 Non-fiducial (free-network) Positioning

Terrestrial reference frames require an origin, scale and orientation. These do not need to be defined by a fiducial network as the satellite force models imply an origin as the center of mass for the earth and a scale is implied by the satellite force model, radio propagation model and the GPS data. In addition fiducial coordinates do not affect rotationally invariant quantities such as baselines and geocentric radii. As such non-

fiducial sites can be used to form a rigid closed polyhedron with known origin and scale, but with a poorly known orientation (*Heflin et al. 1992*).

Non-fiducial processing therefore differs from fiducial in that its *a priori* station coordinate values are very loosely constrained (10 m to 1 km). This means that positions are far less prone to errors resulting from antenna phase center changes and gives very good relative network site geometry. The positions then need to be transformed from this internal frame to an external one such as the ITRF. This is achieved with a Helmert transformation (*Heflin et al. 1992; Blewitt et al. 1992*). As the frame is loosely defined this transformation modelling can lead to some problems.

As a service, JPL obtains the loosely constrained coordinates of roughly 40 globally distributed IGS stations using a non-fiducial approach. Using these loosely constrained solutions and the ITRF coordinates of these stations the seven parameters necessary for a helmert transformation from loose solutions to the ITRF are calculated. These are then published over the internet as the so called x files (*Zhang et al. 2002*).

The transformation from one reference frame to another is performed using a seven parameter Helmert transformation (3 translations, 3 rotations and scale).

$$\begin{bmatrix} x \\ y \\ z \end{bmatrix} = \begin{bmatrix} T_x \\ T_y \\ T_z \end{bmatrix} + \begin{bmatrix} 1+S & -\theta_z & \theta_y \\ \theta_z & 1+S & -\theta_x \\ -\theta_y & \theta_x & 1+S \end{bmatrix} \cdot \begin{bmatrix} X \\ Y \\ Z \end{bmatrix} \tag{3.16}$$

Where T are translations, θ are rotations and S is scale.

3.6.4 Precise Point Positioning

Precise Point Positioning (PPP) is a form of GPS processing originally devised to reduce the computational burden of processing large and ever growing GPS networks (*Zumberge et al. 1997*). In principle PPP works by estimating receiver and transmitter parameters (such as orbits, satellite clocks and Earth rotation parameters (*Blewitt, 1998*)) from a globally distributed network of **R** receivers. If an additional receiver is added to this network (**R+1)** and the receiver and transmitter parameters are once again

estimated, the data from this extra receiver will have a negligible effect on the values of the estimated transmitter parameters. When GPS orbits (in an earth fixed frame) and GPS clock corrections are not estimated but fixed at some predetermined values there is no need to analyse data from all receivers simultaneously and therefore parameters specific to any additional receivers can be analysed in a more efficient secluded fashion.

As such precise absolute coordinates for a single receiver at an unknown position may be obtained without the need of relative positioning from a second receiver at a known location. This has a number of advantages over differential positioning. Firstly as relative positioning produces baseline solutions any change in that baseline could relate to a change in either the reference or unknown station or both, PPP provides absolute solutions. Secondly the accuracies of relative positioning degrade with distance from the reference station, this is not the case with PPP as it is base station independent (*King et al. 2002*).

PPP has some drawbacks in particular the need to use the precise satellite position and clock solutions which are only made available two weeks after data has been collected. In addition differential positioning may be more appropriate for smaller networks (< 50 km) where the double differencing process can cancel errors such as tropospheric and ionospheric delay or tidal and non-tidal loading that are common to the network (*Zumberge et al. 1997; King et al. 2002*).

3.6.5 Sidereal Filtering

Sidereal filtering is a method of removing GPS time series noise in order to study geophysical signals over sub daily periods of time, for example volcanic deformation or seismic waves (*Ji et al. 2004*). This requires the removal of error sources normally mitigated by averaging, in particular those associated with site and satellite geometry such as multipath effects (*Bock, 1991; Bock et al. 2000, 2004; Choi et al. 2004*). Due to the sidereal repeatability of the GPS orbits and hence groundtracks, these errors also repeat on a day to day basis.

The sidereal filtering process involves the estimation of positions at the desired rate (i.e., 1Hz) on day one. These positions are then shifted by the sidereal time period (23

hours, 56 minutes, 4 seconds) and subtracted from estimated positions of a second day. In this manner an average of the error associated with a particular satellite geometry, at a particular site can be built up and differenced from a period of interest to reduce the noise level hiding a transient signal.

It should be noted that although ground tracks are designed to repeat exactly over a sidereal period, in reality satellite repeat periods are not sidereal. The orbits are designed to repeat the ground track and not the nominal sidereal period (23 hours, 56 minutes, 4 seconds). Seeber et al (1997) noted that the satellite orbits were not optimal and in addition varied for different satellites. There are various techniques developed to account for this effect such as modified sidereal filtering (*Choi et al. 2004*), aspect repeat time adjustment (*Larson et al. 2007*) and autocorrelating the phase (*Ragheb et al. 2007*) developed to take this into account which are discussed in more depth in chapter 8.2.

As this technique requires the positioning of sites on an epoch by epoch basis the traditional batch least squares or similar multi-epoch estimation methods are not applicable (*Bock et al. 2000; Nikolaidis, 2002*). Instead the instantaneous positioning technique has to be applied.

3.6.6 Instantaneous Positioning

The instantaneous positioning technique requires the resolution of the integer phase ambiguity using only a single epoch of dual frequency phase and pseudorange data. Other techniques such as kinematic and rapid static methods require only a short span of data but are not instantaneous and often require very short (<10 km) baselines. For example kinematic processing requires 30-45s to resolve the integer cycle phase ambiguity and must be reinitialised in the event of a cycle slip. Instantaneous positioning requires a number of tightly constrained sites which in turn provide the relative positions of an unknown site or sites on an epoch by epoch basis (*Bock et al. 2000; Nikolaidis, 2002*).

3.6.7 Regional Filtering

Regional filtering is a way of improving coordinate time series by removing the so called common mode errors and therefore achieving better resolution to study weak or transient signals. This method was originally put forward in 1997 by Wdowinski et al and updated by Dong et al in 2006. The process works by assuming that modelling of common mode errors such as ionospheric and tropospheric delay, solid Earth tides, ocean loading and hydrological loading are spatially uniform over areas of a few hundred kilometres.

The process involves the removal of outliers from the time series of the positional components of a site (eastings, northings and vertical), followed by the fitting of a linear regression line to the time series by simple least squares. For each day "d" and site "s" calculate the residual, i.e. the difference between the observed position and value predicted by the regression line.

$$\varepsilon_s(d) = O^s(d) - C^s(d) \tag{3.17}$$

$O^s(d)$: The observed topocentric site position (easting, northing or vertical)

$C^s(d)$: The predicted topocentric site position determined from a least squares fitted regression line.

Then calculate the day to day common mode bias by averaging $\varepsilon_s(d)$ from all sites, s (equation 3.18)

$$\varepsilon(d) = \frac{\sum_{s=1}^{S} \varepsilon_s(d)}{S} \tag{3.18}$$

For each site then subtract the common mode error from the observed position to obtain the regionally filtered estimate (*Wdowinski et al. 1997; Dong et al. 2006*).

$$\hat{O}_s(d) = O_s(d) - \varepsilon(d) \tag{3.19}$$

$\hat{O}_s(d)$ = The regionally filtered estimate

This process should be used with caution as short time series have been shown to produce inaccurate regression lines which in turn affect the accuracy of the common mode bias estimate. Blewitt and Lavallee (2002) showed that GPS site coordinates in a global reference frame show annual variation with typical amplitudes of 2 mm in the horizontal. This annual component is largely caused by hydrological and atmospheric loading (*Van Dam et al. 2001*). Unless accounted for these annual signals can significantly bias estimation of site velocities and hence regression lines defining these velocities. As such Blewitt and Lavallee (2002) recommend at least 2.5 years of observations to mitigate the annual variations in a signal sufficiently for the site velocities to be defined (figure 3.4) and therefore for the regional filtering technique to be applicable. Marquez-Azua and DeMets (2003) found that common mode errors were spatially correlated over 1000km, this spatial coherence drops to zero over 6000km. For regional CGPS networks such as the COMET network in the Aegean, the technique has been used in the study of various tectonic processes from fault movement to strain accumulation and volcanism (*Wdowinski et al. 1997; Calais, 1999; Miller et al. 2001; Wdowinski et al. 2004; Smith et al. 2004*).

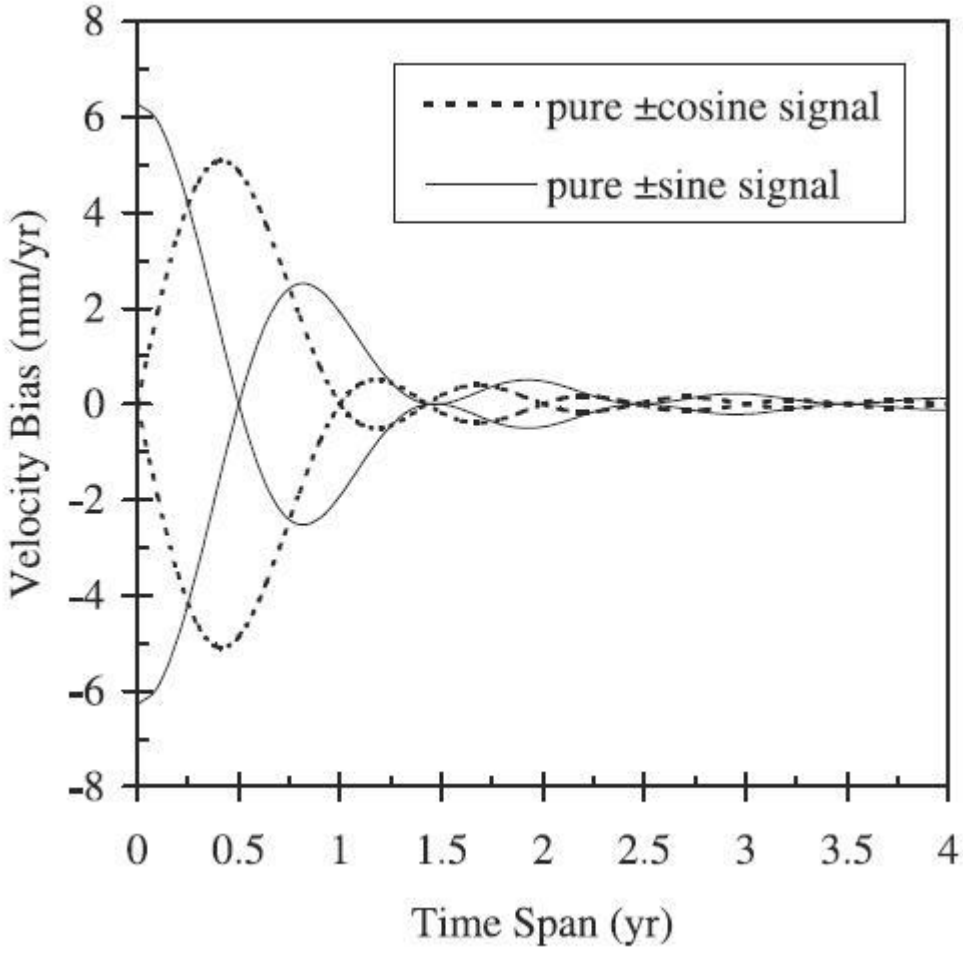

Figure 3.5: Velocity bias from an annual sinusoidal signal versus data span (Blewitt and Lavallee 2002).

3.7 Processing Software

GPS processing software packages tend to fall into one of three broad classes. Commercial software packages that are generally developed by instrument manufacturers to address standard land surveying applications, otherwise known as commercial off-the-shelf (COTS) software. Scientific software developed by third parties such as government or academic institutions intended for high precision or geodetic applications and specialist software intended for unusual or one off applications such as GPS systems integrated with other sensors.

There are several distinctions to be made between the commercial and scientific software.

- Commercial software is invariably written to handle data from one instrument type. Scientific software is instrument independent and uses the RINEX format.
- The commercial software tends to be "user-friendly", requiring a minimum of analyst input and running on a windows based system. The scientific software tends to have been developed for research and precise positioning purposes, offering many options and requiring more analyst skill to use. It is normally command line based and scriptable to enhance automation. In addition, because such software has many more features and supports more complex data modeling, the computer requirements are generally more demanding.
- The commercial software is optimised for GPS surveying accuracies (a few parts per million relative positioning accuracy), whereas scientific software generally addresses very high accuracy applications.
- The scientific software has more sophisticated modeling and processing strategies, such as the ability to adjust orbital parameters, resolve long baseline ambiguities, estimate tropospheric scale factors, process more than one observation session simultaneously, etc.
- The commercial software tends to use sub-optimal data processing algorithms, typically processing data on a single baseline mode (even if more than two receivers were operating simultaneously), whereas the scientific software has multi-baseline and multi-session capability.
- Scientific software is normally highly adjustable, with options over any numbers of parameters. Commercial software is normally limited in this respect with little knowledge of which algorithms and factors are achieving a given result (*Rizos, 1999*).

All results shown in this thesis were produced by the author using the GIPSY-OASIS II (GPS Inferred Positioning SYstem and Orbit Analysis SImulation Software) precise GPS positioning software developed by the Jet Propulsion Laboratory (JPL) (*Webb and Zumberge, 1993*). It is a collection of independent processing modules each designed to undertake a separate part of the GPS processing load. There are a range of differences between GIPSY and other precise GPS software packages such as BERNESE or GAMIT/GLOBK. The following sections will look to highlight some of the modules that are unique to the GIPSY-OASIS II software.

3.7.1 GIPSY – User Input Processing

GIPSY was developed as a UNIX command line based software package. As such it is accessible, with sections of code open for adjustment, and fully automatable such that scripts can be written to input, process and output any set of data and processing strategy. It does contain user manual and help pages but these are often rather limited which in turn does impede its commercial applicability and ease of use.

3.7.2 GIPSY – Data Preprocessing

GIPSY takes GPS observation files in the RINEX format and initially runs the TurboEdit algorithm. This deletes outliers, detects and corrects cycle slips, independent of clock instability, receiver-satellite kinematics and tropospheric conditions (*Blewitt, 1990*) and outputs the data in a range of formats with the desired output interval. This process is important for any GPS processing as at some stage ambiguity resolution is applied and with out a phase corrected set of data each outlier and cycle slip would represent a distance error of an integer number of phase cycles. In order to achieve this TurboEdit requires undifferenced data from dual frequency receivers as it utilizes the P code pseudorange data on both the L1 and L2 frequencies. A smoothly varying ionospheric content is also required. Two linear combinations are used to achieve this, firstly the wide-lane combination, and secondly the ionospheric or narrow-lane combination.

“Wide-lane” Combination

This is also sometimes referred to as the “L5” combination and is defined by the phase difference $\Phi(L1) - \Phi(L2) = \Phi(L5)$. This is referred to as the wide-lane combination because the effective wavelength of the resulting observable is $\lambda_\delta = c / f_1 - f_2 \approx 0.86$ meters. The wide-lane phase biases which can change spontaneously by integer values (cycle-slips) are defined as $b_\delta = b_1 - b_2$ and is an integer as both b_1 and b_2 are integers.

$$\begin{aligned} L_\delta &\equiv -\Phi_\delta \lambda_\delta \\ &= \left(f_1 L_1 - f_2 L_2\right) / \left(f_1 - f_2\right) \\ &= \rho + I\, f_1 f_2 / \left(f_1^2 - f_2^2\right) + \lambda_\delta b_\delta \end{aligned} \tag{3.20}$$

Where $\mathbf{L_\delta}$ is the wide-lane combination, $\mathbf{L_1}$ and $\mathbf{L_2}$ are the carrier phases expressed as ranges, $\boldsymbol{f_1}$ and $\boldsymbol{f_2}$ are the carrier frequencies (154 * 10.23 MHz and 120 * 10.23 MHz respectively), **I** is the ionospheric delay parameter, $\boldsymbol{\rho}$ refers to all the non-dispersive delays that affect all data types equally (*Blewitt, 1990; Gregorius, 1996)*.

In order to detect wide-lane cycle slips we subtract the following pseudorange combination from L_δ (the wide-lane combination). This does require the measured pseudorange to be more accurate than one wide-lane wavelength (86cm) which in turn requires a low noise environment or long observation periods.

$$\begin{aligned} P_\delta &\equiv \left(f_1 P_1 - f_2 P_2\right) / \left(f_1 - f_2\right) \\ &= \rho + I\, f_1 f_2 / \left(f_1^2 - f_2^2\right) \end{aligned} \tag{3.21}$$

By subtracting equations 3.21 from 3.20 we can write

$$b_\delta \equiv \frac{1}{\lambda_\delta}\left(L_\delta - P_\delta\right) \tag{3.22}$$

TurboEdit uses equation 3.22 independently at each data epoch and calculates time averages of b_δ both before and after a cycle slip with the difference required to be close to an integer. For that reason an a priori RMS scatter of 0.5 wide-lane cycles is assumed. The algorithm then sequentially updates (b_δ) (the mean wide-lane bias) and σ (the RMS scatter) using the following recursive formula.

$$\left\langle b_\delta \right\rangle_i = \left\langle b_\delta \right\rangle_{i-1} + \frac{1}{i}\left(b_{\delta_i} - \left\langle b_\delta \right\rangle_{i-1}\right) \tag{3.23}$$

$$\sigma_i^2 = \sigma_{i-1}^2 + \frac{1}{i}\left[\left(b_{\delta_i} - \left\langle b_\delta \right\rangle_{i-1}\right)^2 - \sigma_{i-1}^2\right] \tag{3.24}$$

The "i" in the above equations refers to the current number of points in the data arc. Subsequent epoch estimates are required to lie within 4σ of the running mean. Isolated outliers are deleted and any two consecutive outliers within one cycle indicate that a cycle slip has occurred (*Blewitt, 1990; Gregorius, 1996).* Starting with these points a new average is started and continues until another potential cycle slip occurs.

The integer offset between each phase connected arc is determined by differencing the (b_δ) values with the smallest standard error in the mean $\sigma_n / \sqrt{(n-1)}$, where n is the number of data in the arc. The integer offset between the two arcs is then determined by rounding off this difference if its standard error is less than 0.15 cycles, and if the standard error of the fractional part of the difference is less than 0.30 cycles (= 2 standard errors).

As the arcs are phase connected the (b_δ) of the aggregate arc is calculated to statistically enhance subsequent phase connections. For multiple cycle slips in a short period of time, this data is deleted and the time gap treated as one cycle slip and the phase is connected across this gap, which is typically a couple of minutes.

Ionospheric "narrow-lane" Combination

The ionospheric combination is defined as the difference between L_1 and L_2, as follows:

$$\begin{aligned} L_I &\equiv L_1 - L_2 \\ L_I &= I + \lambda_1 b_1 - \lambda_2 b_2 \\ L_I &= I + \lambda_1 (b_1 - b_2) + (\lambda_1 - \lambda_2) b_2 \\ L_I &= I + \lambda_1 b_\delta - \lambda_I b_2 \end{aligned} \qquad (3.25)$$

The ionospheric wavelength is short, $\lambda_I \equiv (\lambda_2 - \lambda_1) \approx 5.4$ cm and is therefore often referred to as the "narrow-lane" combination. The pseudorange is therefore not quite accurate enough to successfully calibrate the ionospheric carrier phase as it would require centimetric control of multipath. The ionospheric parameter "*I"* can however be expressed as the difference between both the P-code pseudoranges.

$$P_I \equiv P_2 - P_1 = I \tag{3.26}$$

The approach taken by GIPSY assumes that "*I*" behaves as a reasonably smooth function (*Blewitt, 1990*). TurboEdit firstly makes the hypothesis that cycle slips occur simultaneously in the ionospheric and wide-lane combinations. At the same time TurboEdit has to guard against the fact that a cycle slip occurs but the wide-lane discontinuity $\Delta n_\delta = 0$ (ie, the difference before and after the cycle slip is zero cycles). This is achieved by subtracting a polynomial fit (Q to P_I) from L_I and then searching for discontinuities in the residual (L_I - Q). Outliers and cycle slips are then identified using the following equations (*Blewitt, 1990*):

$$(L_{I\,i} - Q_i) - (L_{I\,i-1} - Q_{i-1}) > \kappa \text{ cycles} \tag{3.27}$$

$$(L_{I\,i+1} - Q_{i+1}) - (L_{I\,i} - Q_i) < 1 \text{ cycles} \tag{3.28}$$

The value of "κ" defaults to six cycles (ie. 6 × 5.4 cm) to account for large phase variations of receivers at high latitudes which are not to be confused with cycle slips. Phase connection is achieved by fitting a polynomial to the L_I before the cycle slip and extrapolating to data after the slip. The cycle slip on L_2, Δn_2 can then be determined by subtracting the extrapolated fit from the first few data points after the cycle slip.

After this each carrier phase data point is corrected by an integer number of cycles to form "phase connected ranges".

3.7.3 GIPSY – Observation Models

GIPSY uses a module known as "qregres" to apply a wide range of earth and other observation models. The earth models applied include receiver location time dependence, tidal effects (solid earth tides, ocean loading and pole tides), UT1 and polar motion, nutation, precession, perturbation rotation, geocenter offset and coordinate scaling. The current observation models observed by GIPSY can be viewed on the GIPSY OASIS homepage (https://gipsy-oasis.jpl.nasa.gov) and are summarized in table 3.2

Observation	Data / Data Source
Elevation cut off	15 degrees
Station Information	JPL Database
Antenna Phase center	JPL Database
Troposphere Mapping Function	Niell mapping Function
Earth Orientation	IERS (Bulletin B)
Ocean Loading	FES2002 Ocean tide predict

Table 3.2: GIPSY observation models and data (https://gipsy-oasis.jpl.nasa.gov)

3.7.4 GIPSY – Parameter Estimation

A common technique used in geodetic software is to estimate the receiver clock offset using a linearised pseudorange model. This yields an estimate of the observation epoch then remove all the clock parameters by double-differencing. The receiver clock time must be determined precisely in order to know when the data was collected (*Blewitt, 1998*). This technique has the disadvantage of cancelling out the receiver clock offsets which prevents the production of a high precision clock solution.

GIPSY uses an alternative technique by processing the undifferenced carrier phase and pseudorange data simultaneously. The models for both these observables are the same (apart from the phase bias, nominally set to zero, and the phase wind-up effect). Similarly the parameters are identical or at least no extra parameters are required. This technique effectively uses the pseudorange as a consistency check on the carrier phase solution, decorrelating the undifferenced carrier phase data from the carrier phase bias parameters. This process is run through a sequential filter algorithm called a Square Root Information Filter (SRIF) which is a modified Kalman filter (*Bierman, 1977*).

The SRIF filter avoids the problem of having to invert one big matrix, which is inherent in least squares processing of large GPS networks, by inverting lots of smaller matrices that are created sequentially for each time interval. A typical time interval is five minutes. That is the filter solves for the parameters in each interval and accumulates the solutions. In addition this allows it to use the solutions from the previous interval as the a priori values for the next interval. All the parameters are allowed stochastic behaviour

which is constant in each interval. After each interval the filter updates the parameter estimates and covariance matrix and performs a time update whereby process noise is added to the parameter uncertainties to allow for unmodeled or mismodeled effects (*Gregorius, 1996*).

3.7.5 GIPSY – Solution Processing

3.7.5.1 Ambiguity Resolution

The GPS carrier-phase ambiguity represents the arbitrary counter setting (an integer value) of the carrier-phase cycle tracking register at the start of observations of a satellite (phase lock), which biases all measurements in an unbroken sequence of that satellite's carrier-phase observations. Once the integer ambiguities are fixed correctly, the carrier phase observations are conceptually turned into millimeter-level high-precision range measurements and hence it is possible to attain sub-centimeter-level positioning solutions (*Kim and Langley, 2000*). This has been shown to improve the horizontal accuracy of regional networks by a factor 1.5 to 2 (*Blewitt, 1989*).

The traditional method of resolving ambiguities is the double-differencing approach which cancels out the large receiver clock errors as well as cancelling the satellite clock errors. GIPSY estimates the clock parameters stochastically and therefore double-differencing is performed on processed undifferenced data. This is a problem as undifferenced processing results in non integer double-difference phase biases. To resolve this, the correct integer values are estimated using the sequential approach (*Blewitt, 1989*).

3.7.5.2 The Sequential Approach

The longer the wavelength of the L1/L2 linear combination, the greater the confidence with which the phase bias can be fixed to an integer. Ambigon2, the module within GIPSY that carries out ambiguity resolution therefore applies a sequential approach, first fixing the wide-lane bias due to its relatively long wavelength, then fixing the narrow-lane (ionospheric) bias in order to achieve greater accuracy.

After resolving the wide-lane combination (if any biases can't be fixed to their integer value they are fixed to their decimal value), the parameter estimation is redone. This reduces the number of unresolved parameters which raises the confidence level with which the narrow-lane biases can be fixed. The phase ambiguities are then resolved again with any unresolved figures again fixed to their decimal value. The parameter estimation is then calculated again to produce the strongest solution.

This approach can lead to a number of dilemmas. Firstly in fixing the wide-lane bias two different methods can be followed, the ionospheric approach whereby ionospheric constraints are applied through the use of an ionospheric model. This is good for short baselines (< 300 km) but fails over longer distances due to the unpredictable variations in the ionosphere. Alternatively there is the pseudorange approach which is baseline independent but requires low noise environments (*Blewitt, 1990; Gregorius, 1996*).

To then resolve the narrow-lane bias then raises another dilemma. Either using the ionospheric approach which gives integer ambiguities but they may be wrong due to the unmodelled ionospheric delay, or using the ionosphere free approach which neutralises the ionosphere but gives non-integer biases

To overcome these problems GIPSY uses the following approach starting with the undifferenced estimates:

- Double-Differencing - This produces non-integer, double differenced phase biases.

- Wide-laning - Pseudorange method followed by ionospheric method. As the ionospheric method is not good enough on long base lines a "boot strapping" approach is applied to larger networks. This utilises the fact that biases on short and long baselines are correlated, therefore determining the best short baselines reduces the number of parameters in the network and eases the ambiguity resolution of the longer baselines.

- Narrow-laning – The Ionosphere-free method, due to the spatial unpredictability of the ionosphere.

These procedures leave us with the real values of the bias parameters. They still need to be fixed to integer values. GIPSY estimates these integers in a couple of ways.

3.7.5.3 Sequential Bias Fixing

Bias fixing constrains the phase biases to integer values using a confidence test. This effectively removes the biases as parameters from the solution. The method used calculates the cumulative probability that all the fixed biases (wide and narrow lane) have the correct value and won't subsequently fix another bias unless the cumulative probability that all biases are fixed to the correct integer remains above 99%. The estimates and uncertainties of all the remaining unfixed biases are constantly updated to reflect the improving quality of the solution as biases become fixed to their true values (*Blewitt, 1989; Gregorius, 1996*). The order of bias fixing is not random instead the probability of fixing a bias correctly is determined from its distance to the nearest integer and its formal error.

3.7.5.4 Sequential Bias Optimising

Bias optimising is recommended only when bias fixing fails. In this case the wide-lane biases are fixed using the bias fixing technique but the narrow-lane solutions are optimised in order to avoid arbitrary confidence tests such as the 99% value used before. The technique utilises the principle that if the expected parameters are all integers then the expectation value is a minimum variance solution where the weights are derived from the formal errors. In this way an expectation value for the real bias is estimated and requires no subjective decisions (*Blewitt, 1989; Gregorius, 1996*).

Summary

There are a wide range of ground motions and error sources that affect the estimation of a GPS receiver's position in a given reference frame. In this chapter the background of error sources and estimates of their effect have been given. Processing strategies and the software needed to implement these strategies are also presented.

Chapter 4

Daily CGPS Data Analysis in the Aegean

The chapter explains the processes and techniques applied to the CGPS Rinex data collected from the COMET network as well as a range of IGS and EUREF sites. Firstly there is an introduction to the data used and the generic precise point positioning and ambiguity resolution processing technique that was performed on this data before a range of post processing filters were applied. The specific post processing filters include the regional filtering method and the filtered baseline technique. The chapter is separated into the methods used and results achieved in the daily estimate of CGPS station coordinates and some analysis and discussion of those results.

4.1 Introduction – The COMET Network

The Aegean has been studied numerous times using GPS campaign style studies. These have each been referenced to the ITRF using a fiducial network of ITRF reference stations (*Pichon et al. 1995; McClusky et al. 2000; Meade et al. 2002; Pichon et al. 2003*) and generally all show consistent movements with respect to the Eurasian plate. These studies provided great insight into the long term movements of the Aegean but being campaign studies could not provide any information regarding transient motion, or subtle changes in velocity over time due to the inherent errors associated with campaign style observations.

Campaign style observations potentially lead to a range of errors in the estimation of the position of a point and hence the modelled movement or deformation of an area. These are partly due to set up errors if the monument used is not a maintained or permanent structure but more significantly are due to the epoch and duration of any site occupations. The length of a reoccupation session directly affects the accuracy of a position as solutions based on short observation sessions are generally less reliable than those from longer sessions. This is due to a range of error sources such as:

- Changes in receiver-satellite geometry (as experienced through the day).
- Different numbers of available satellites due the temporal variance in the GPS orbits and the various changes in the active GPS satellites as well as signal obstructions.
- Day and night observations (induce differences in atmospheric conditions).
- Varying temperature and pressure conditions as well as other seasonal effects.
- Varying site conditions leading to a variety of multipath and signal jamming scenarios.
- Tidal variations (both solid Earth tides and ocean tides)

In general campaign style GPS observations are less than twenty four hours and are often less than ten (*Cross, 2004*). The positional errors introduced using the campaign style of reoccupation can give false images of the secular trends in a time series, for example figure 4.1 shows approximately a year's worth of continuous data and its linear regression (0.029 m/yr). Also included are the hypothetical worst case scenarios for a campaign observation whereby the regression lines formed by the first day and the modified Julian days 53792 (pink) and 53805 (yellow). These lines suggest northerly variation of 0.010 m/yr and 0.033 m/yr respectively which are significantly different from the variation shown by the CGPS data. These are extreme cases shown using outliers in the time series but it should also be noted that they are formed using CGPS (24hr) data rather than data collected over a shorter period which may be affected by the potential error and noise sources mentioned above.

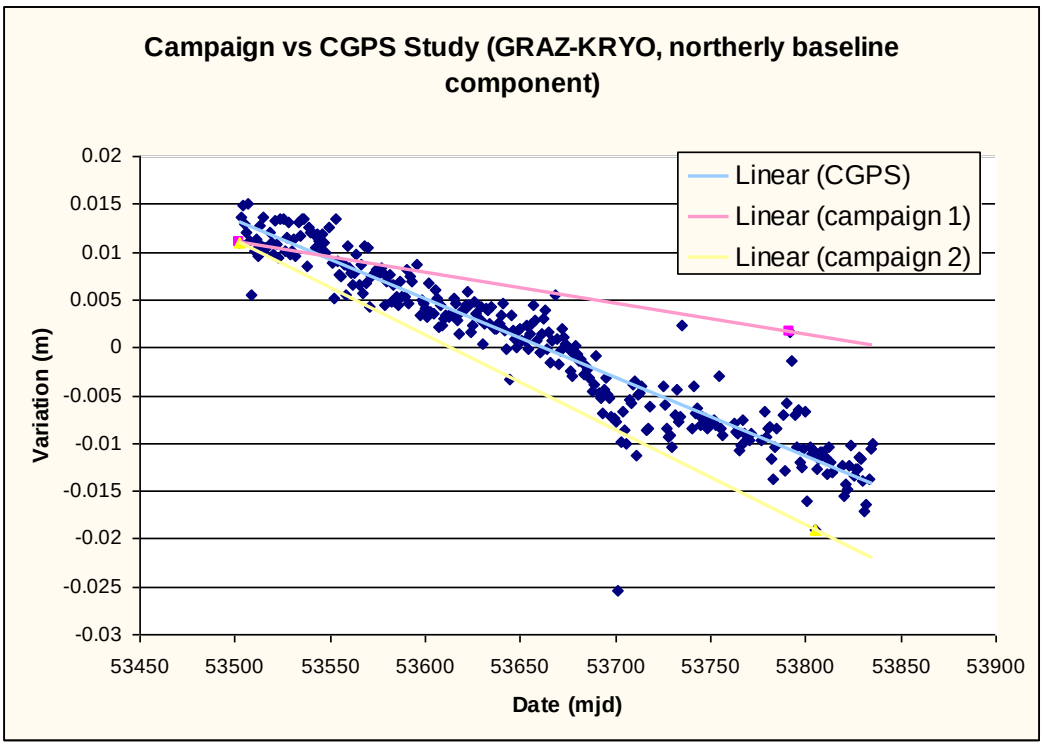

Figure 4.1: A comparison of secular motion interpretation between CGPS (blue) and two potential campaign style GPS studies (pink and yellow)

Figure 4.1 demonstrates how campaign style GPS studies can mis interpret secular trends. In the figure the blue line represents the trend derived using all the data collected during the period. The red and yellow lines represent extreme examples of possible regression lines formed from only two points showing significant variation. The nature of reoccupation can also lead to inaccurate estimates of periodic effects, for example figure 4.2 demonstrates how roughly annual reoccupations could point toward a very different phase and amplitude of periodic effects (black) when compared to an annual signal (blue).

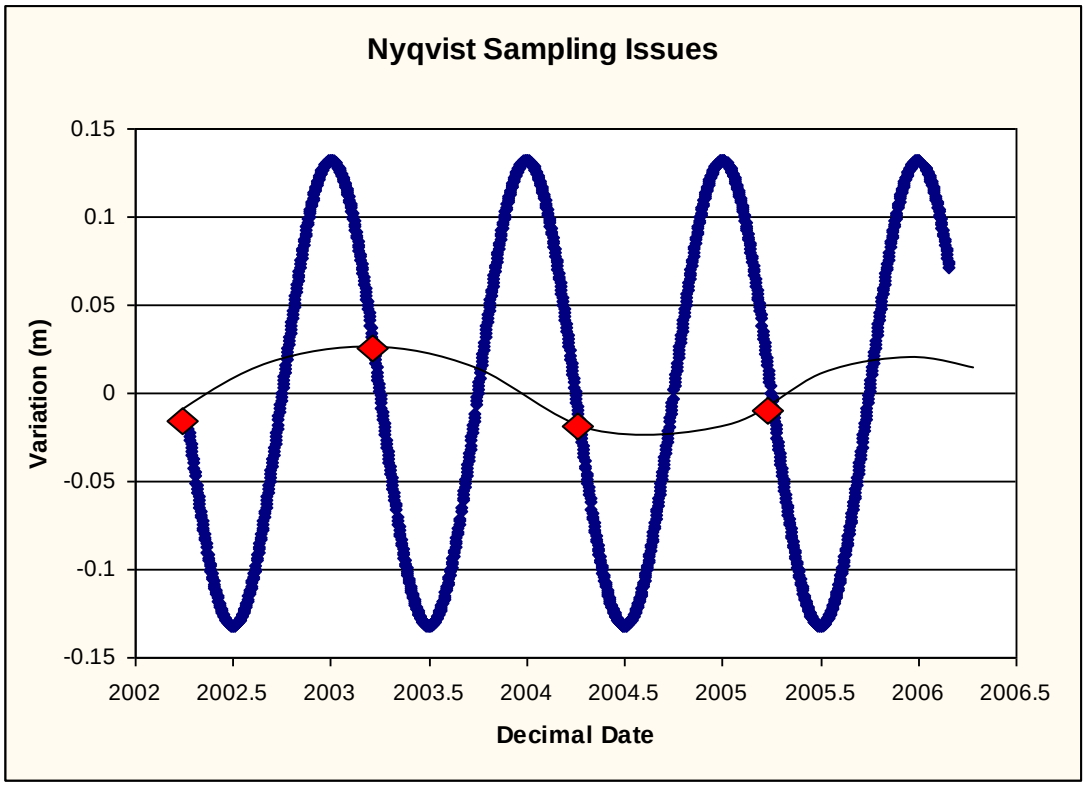

Figure 4.2: A comparison of periodic motion interpretation between CGPS (blue) and campaign style GPS studies (grey)

What distinguishes this study from models derived using campaign approaches is the facility to determine more rigorously the long term trends in regional deformation by using CORS (Continuously Operating Reference Stations) data and therefore to examine subtle departures from the long term trend. Of particular concern to this study is the inability of campaign data in the detection of transient signals. For the reasons mentioned above the use of CGPS data for the determination of tectonic regimes as well as the detection of transient motion is increasingly being used.

To better understand the Hellenic area the COMET group (Centre for the Observation and Modelling of Earthquakes and Tectonics) established a permanent network of CORS throughout the Aegean and Western Turkey from the 1st of January 2002. A summary of these sites can be seen in figure 4.3. In general each of the sites are building located trimble TRM41249.00 antennas with Trimble 5700 receivers. Comprehensive site descriptions are shown in Appendix A.

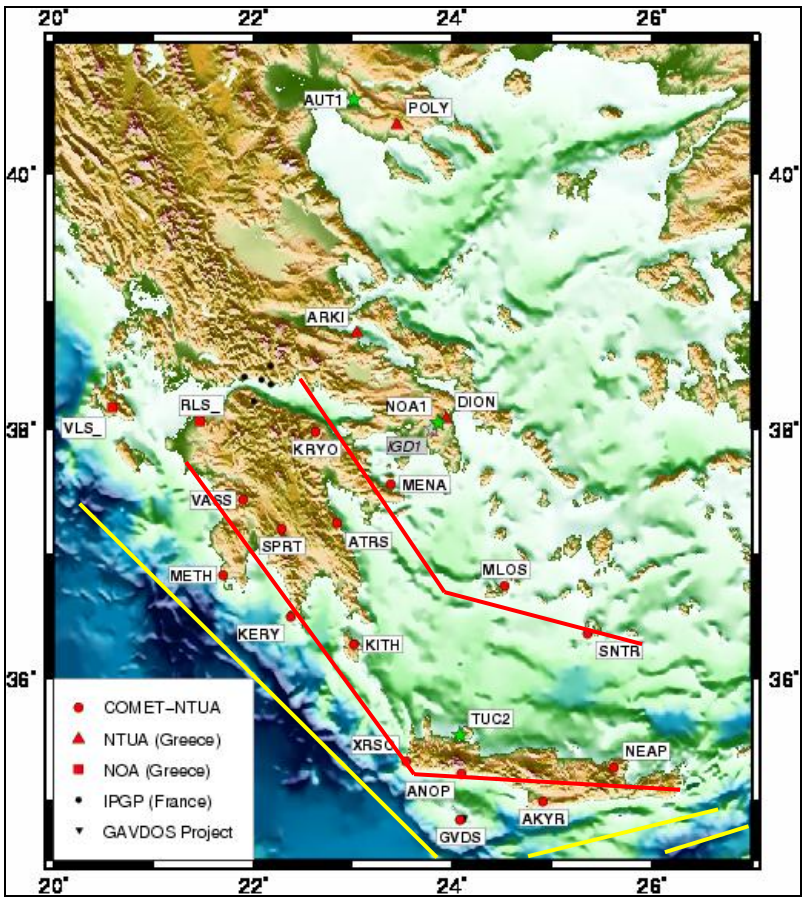

Figure 4.3: The current sites in the COMET network and additional relevant CORS.

The network was established in the Aegean with the potential discovery of transient slip events around the Hellenic arc in mind, as well as to observe the longer term strain rates across the region and potentially carry out the analysis of seismic events as well. These sites form two lines (red lines on figure 4.3) of stations installed approximately parallel to the trench (yellow lines on figure 4.3). Over the Peloponnese peninsula, the network was designed to realise an optimal geometry for measuring the elastic locking along the subduction interface and for slow slip events detection. In addition to the CGPS sites located in the Aegean area a range of IGS/EUREF sites from around the area were utilized. A list of the current IGS and EUREF sites in the area can be seen in figure 4.4.

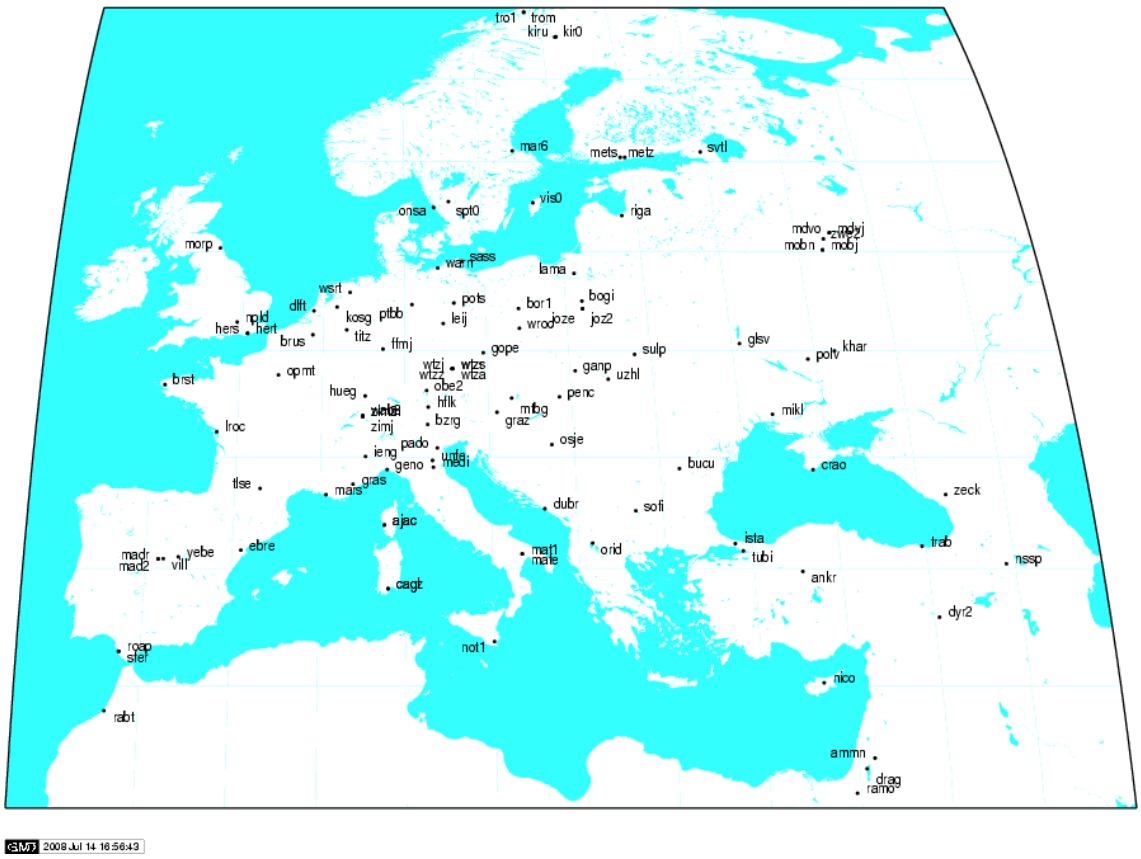

Figure 4.4: The current IGS and EUREF sites in the Aegean area (from the IGS http://igscb.jpl.nasa.gov. Accessed 14 July 2008)

4.2 Precise Point Positioning

In this study the principal GPS data processing technique used to determine station positions is PPP. This was chosen due to its practical applicatioin in processing large volumes of GPS data (*Zumberge et al. 1997*). A brief introduction to PPP was given in section 3.6.2. In this section the author covers the subject and principles behind the processing technique in a little more depth. Unlike in relative positioning common mode errors do not cancel in PPP, all errors that usually are expected to cancel in the double differencing process can cause problems in PPP therefore all possible corrections must be applied (*Witchayangkoon, 2000; Leick, 2004*). Satellite specific errors include satellite clock errors, satellites antenna phase center offset, group differential delay, relativity and satellite antenna windup error. On the receiver these errors include the receiver antenna phase center offset and the receiver antenna phase windup.

As a result of these error sources when using PPP all simplifying assumptions must be avoided i.e. all known corrections must be applied to the observations and the corrections must be consistent (Leick, 2004). This means that the simplified ionospheric-free combinations for a dual frequency GPS pseudorange and carrier-phase observations below (*Kouba and Heroux, 2000*) require some adjustment:

$$P_I = \rho + c(dt - dT) + T_r + \varepsilon_p \quad (4.1)$$

$$\phi_I = \rho + c(dt - dT) + T_r + N\lambda + \varepsilon_\phi \quad (4.2)$$

Where:

P_I = The ionosphere-free combination of L1 and L2 pseudoranges.

ϕ_I = The ionosphere-free combination of L1 and L2 carrier-phases.

dt = The station clock offset from GPS time.

dT = The satellite clock offset from GPS time.

T_r = The tropospheric delay.

λ = The carrier wavelength (Carrier combination).

N = The ambiguity of the ionosphere free carrier phase (non-integer).

$\varepsilon_p, \varepsilon_\phi$ = Relevant noise components such as multipath.

ρ = The geometrical range as a function of satellite (X_s, Y_s, Z_s), station (x, y, z) coordinates and respective phase centre offsets.

c = Speed of light (in a vacuum)

This is adjusted such that the troposhperic delay is a function of the zenith path delay (*zpd*) and a mapping function (M). In the case of GIPSY this is the Niell mapping function (*Webb et al 1993*). The satellite clocks are now known from a selection of approximately 40 globally distributed receivers (section 3.6.2) and so can also be removed from the model giving the following simplified mathematical models:

$$f_p = \rho + Cdt + Mzpd + \varepsilon_p - P_I = 0 \quad (4.3)$$

$$f_\phi = \rho + Cdt + Mzpd + N\lambda + \varepsilon_\phi - \phi_I = 0 \quad (4.4)$$

5.2.1 Precise Point Positioning Correction Models

The combination of precise GPS orbits and clocks (from JPL) combined with the development of research grade GPS software means that many of the corrections applied to pseudorange and carrier-phase observations to eliminate effects such as clock offsets, atmospheric delays or relativistic effects are standard procedures. Many of these errors are mentioned in section 3.4, the following additional error sources augment those as well as being directly relevant to PPP.

Satellite Attitude Effects

As mentioned in section 3.4.5 there is a separation between the GPS satellite centre of mass and the phase centre of the antenna. Force models for satellite orbit modelling, IGS precise satellite coordinates and clock products all refer to the satellite centre of mass, whilst measurements are made to the antenna phase centre. Therefore the antenna phase centre offsets (table 4.1) and the orientation of the offset vector in space must be modelled.

	X	**Y**	**Z**
Block II/IIA	0.279	0.000	1.023
Block IIR	0.000	0.000	0.000

Table 4.1: Antenna phase centre offsets in satellite fixed reference frame (meters)

It should be noted that these values were utilised in this study but there have been more recent studies that have shown that block specific phase centre variations are not sufficient as there are significant differences in the phase center variation between different sub groups or even individual satellites and receivers (*Schmid et al. 1995*). These values were determined as relative antenna phase center corrections. There are

now absolute phase center correction models for GPS receiver and satellite antennas (*Schmid et al. 2005; Schmid et al. 2007*).

Phase Wind-Up Correction

GPS satellites transmit right circularly polarised radio waves. The observed carrier phase therefore depends on the mutual orientation of the satellite and receiver antennas. A rotation of either the receiver or the satellite antenna around its bore axis will result in a change in the carrier-phase of up to one cycle (*Wu et al. 1993*).

Receiver antennas in CGPS studies such as this one are stable and oriented towards a reference direction (north) and do not therefore rotate. Satellite antennas do however slowly rotate as their solar panels are orientated towards the sun, this rotation can be far more rapid in eclipse seasons. In 1994 a yaw attitude bias was introduced (*Bar-Sever, 1995; 1996*) to constrain the yawing of satellites during the eclipse period to allow modelling of the effect. If discounted yawing can lead to errors of up to 10 cm in the antenna phase centre position and around the decimeter level due to the phase wind-up (*Wu et al. 1993*).

The phase wind-up correction has been discounted by most software where differential positioning removes most of the error through the double-differencing process. Wu et al report that errors of up to 4cm can still occur for long baselines (4000 km) but for shorter baselines the effect is negligible. Undifferenced point positioning such as PPP is a different matter and corrections need to be applied. Since 1994 the IGS analysis centers have applied a phase wind-up correction to the IGS orbit and clock products. GIPSY combines this with information about shadow periods and yaw attitude models to nullify the effect on PPP solutions.

Site Displacement Effects

Due to the independent nature of PPP all site displacement effects need to be included, in particularly the solid earth tides and ocean tides. All these corrections are discussed in section 3.2.

4.3 Ambiguity Resolution

The traditional method of resolving ambiguities is the double-differencing approach which cancels out the large receiver clock errors as well as cancelling the satellite clock errors (*Blewitt, 1989*). This study utilised the GIPSY – OASIS II processing software that estimates the clock parameters stochastically and therefore performs double-differencing on processed undifferenced data. The details of this process were shown in section 3.7.5.

4.4 Methodology

This section will introduce the concepts and methodologies applied by the author in the course of his research. It will investigate the processing and post-processing strategies used in order to arrive at improved coordinate time series.

The GPS data was processed using the GIPSY – OASIS II software. A precise point positioning strategy was applied using fiducial free daily precise orbits and clocks from JPL (Jet Propulsion Laboratory) (*Zumberge et al 1997*). Modeling of the troposphere total zenith delay used the Niell mapping function (*Webb et al 1993*), and also included estimation of horizontal troposphere gradients (*Bar-Sever et al 1998*). Neills mapping function was utilised as upposed to a more sophisticated function such as the Vienna mapping function or the Global mapping function as this was the only function available within the version of the GIPSY - OASIS II software used in this study. Ambiguity resolution (*Blewitt 1989*) was applied as described in section 3.7.5 and the daily station positions and corresponding covariance matrices determined in the ITRF 2000 (International Terrestrial Reference Frame), again using daily frame data products from JPL. GIPSY produces geocentric Cartesian coordinates which were converted to geodetic ellipsoidal coordinates (λ, φ and h). A full list of these calculations is located in Appendix B

The ellipsoidal parameters used in these coordinate transformations are continuously updated. The coordinates used in this study are those recommended by the IERS in Technical note no.32 (McCarthy and Petit, 2003).

This strategy was applied to all the COMET Aegean sites; Agios Kyrillos (AKYR), Anopoli (ANOP), Ano Tiros (ATRS), Gavdos (GVDS), Kerya (KERY), Kithira (KITH), Kryoneri (KRYO), Methana (MENA), Methoni (METH), Milos (MLOS), (NEAP), Santorini (SNTR), Sparti (SPRT), Vasses (VASS), Chrisoskalitissa (XRSO). In addition a number of IGS/EUREF stations were added; Matera (MATE), Nicosia-Athalassa (NICO), Ankara (ANKR), FOMI Satellite Geodetic Observatory (PENC), Dubrovnik (DUBR), Graz-Lustbuehel (GRAZ), Ohrid (ORID), Sophia (SOFI), Gebze (TUBI) and some additional sites from the National Technical University of Athens (NTU); (ARKI) (DION) (POLY). These site positions can be seen in figure 5.5.

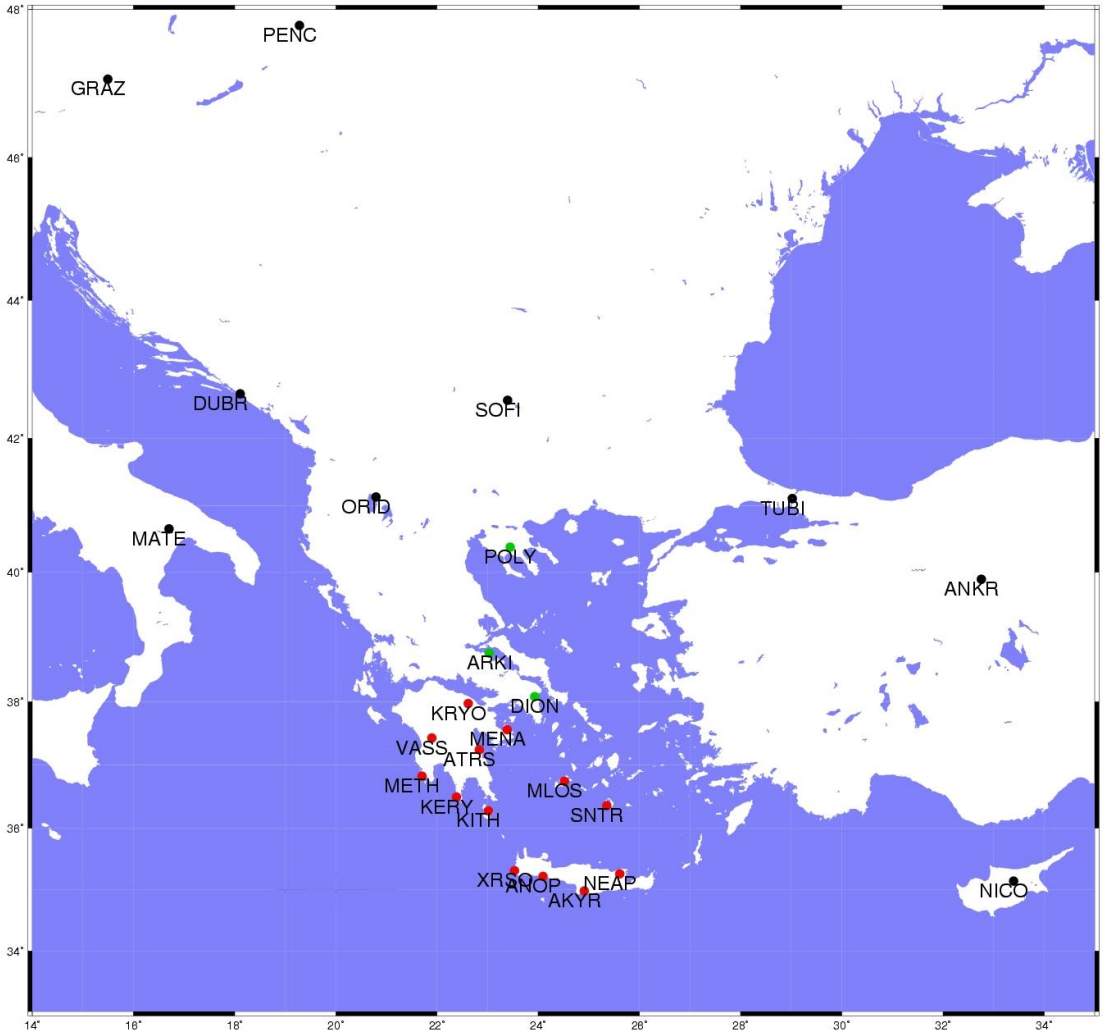

Figure 4.5: The ITRF (black), COMET (red) and NTU (green) CGPS sites used in the study

This daily GPS processing technique results in a series of loosely constrained daily GPS network solutions. This loosely constrained network was aligned with the ITRF2000 using the "x-files" provided by JPL (x-files available from sideshow.jpl.nasa.gov), resulting in ITRF coordinates for all the sites for the period 10th April 2002 until the 30th

September 2006. It should be noted at this stage that although this was the stated study period a complete network was only operating for approximately six months of this time. This was partly due to the gradual implementation of the COMET sites, but also due to some significant data losses which affected almost all sites at one time or another. For a list of some of the periods of lost data please see Appendix C. These data losses were a result of a wide range of problems however the predominant reasons were power losses, troubles with the phone lines and equipment failures. For example, all sites stopped returning data due to a problem with our software when a time server (used to synchronize the PCs over the network) was out of order. The problem was eventually solved but several failures of the computer attached to the receiver made the percentage of returned data of 40-50% for the Greek sites. Lightening strikes and the August 2006 wildfires also disrupted the data flow. Figures 4.6 – 4.11 show the sites used and the data availability at each site. It should be noted that although rinex files for each of the days listed in the figures were put into the processing strategy a lot of the rinex files were incomplete and did not show a full twenty four hours and therefore were rejected at a later processing stage.

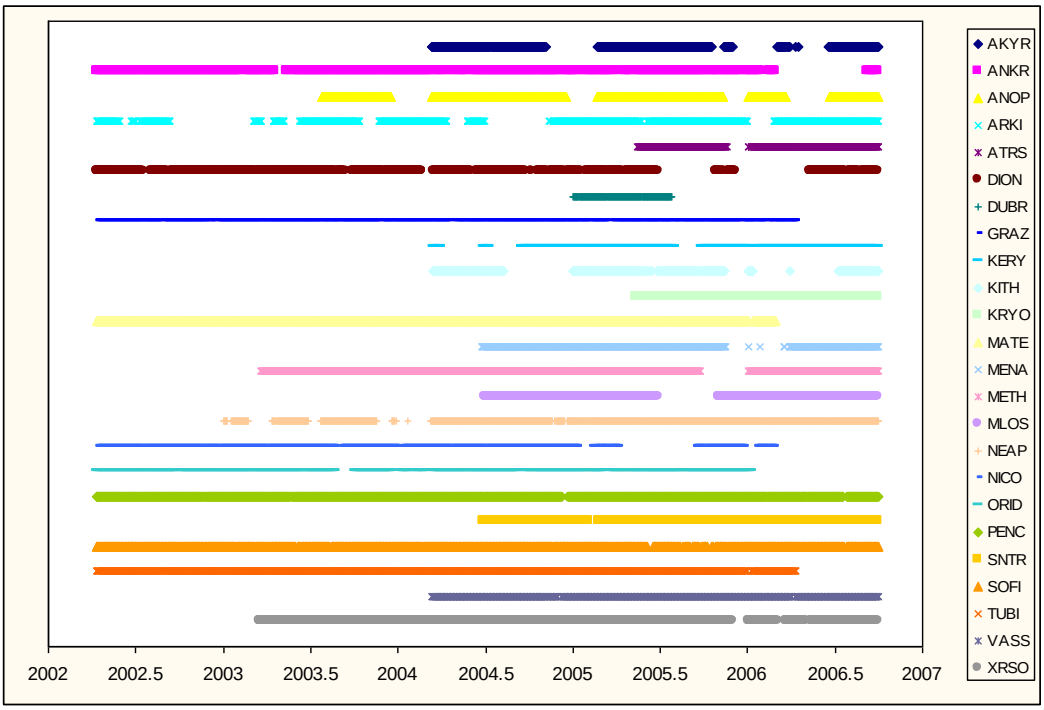

Figure 4.6: Data availability for sites utilized in the GPS processing, throughout the study period (10/04/02 – 30/09/06).

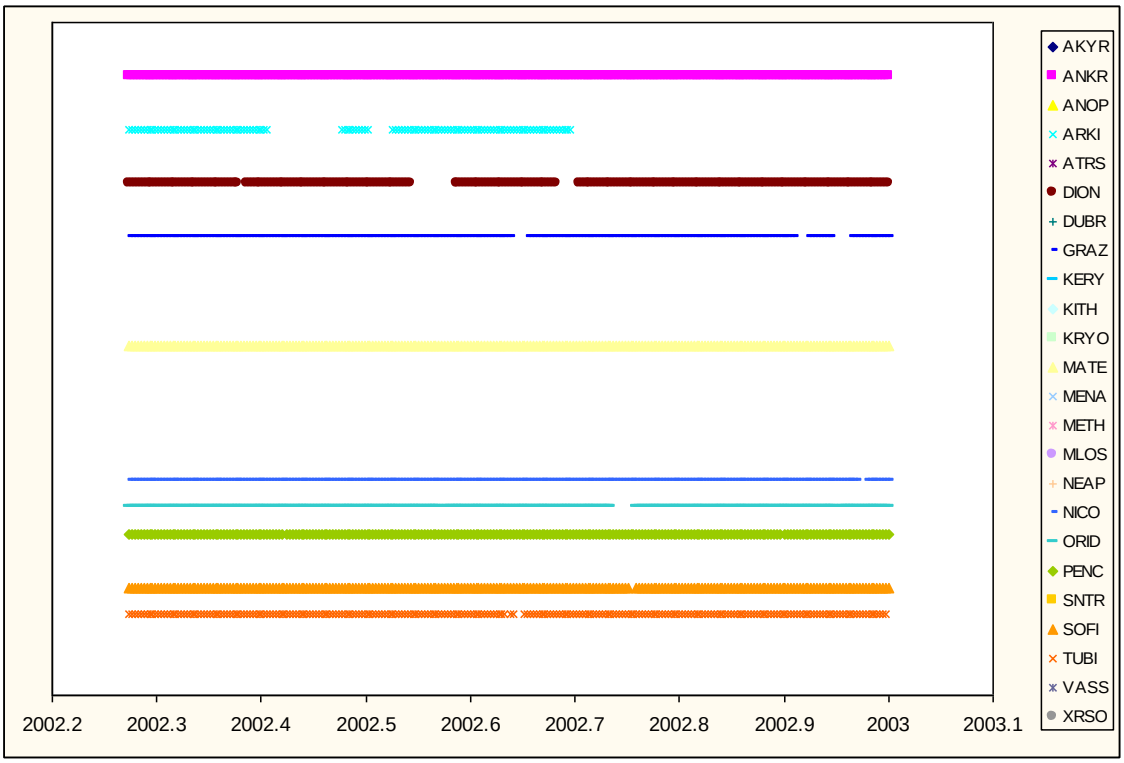

Figure 4.7: Data availability for sites utilized in the GPS processing during 2002

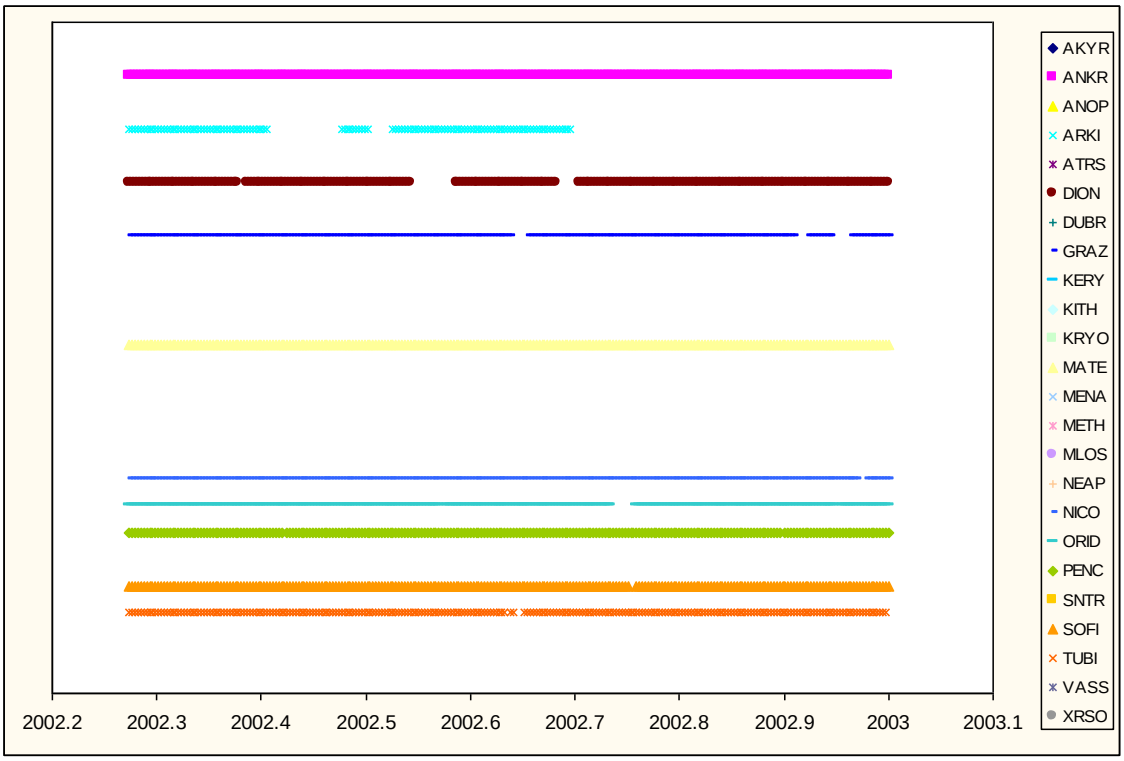

Figure 4.8: Data availability for sites utilized in the GPS processing during 2003.

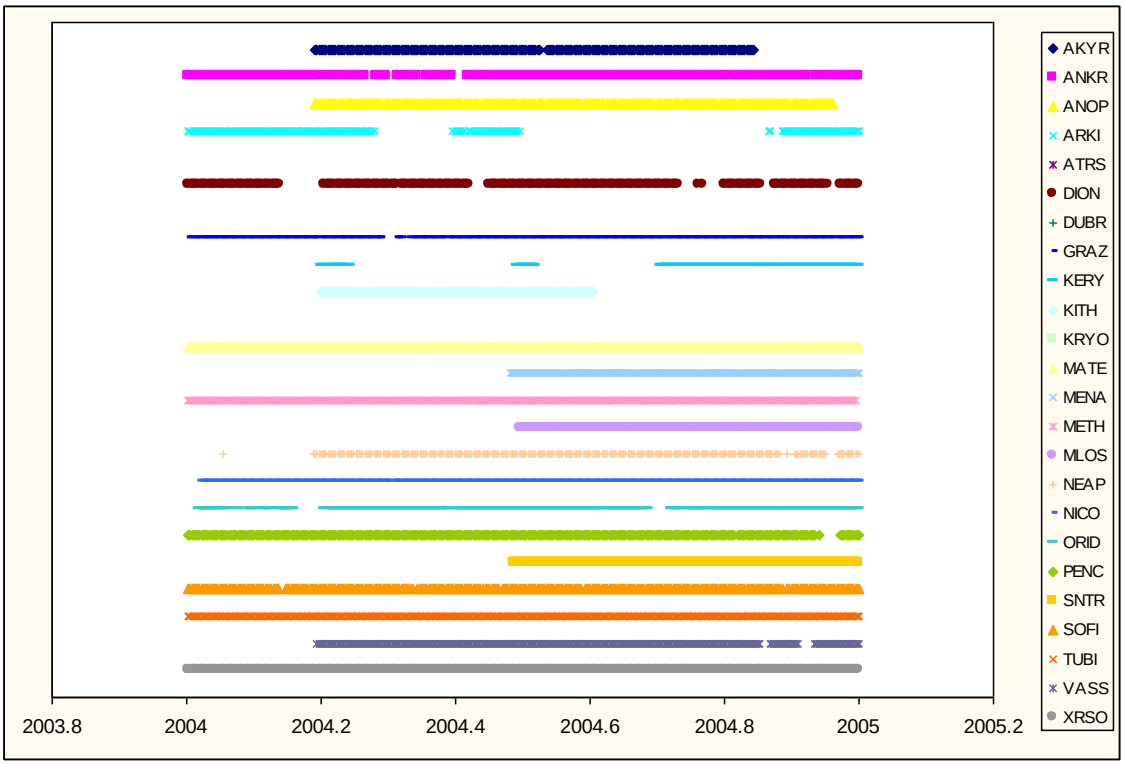

Figure 4.9: Data availability for sites utilized in the GPS processing during 2004.

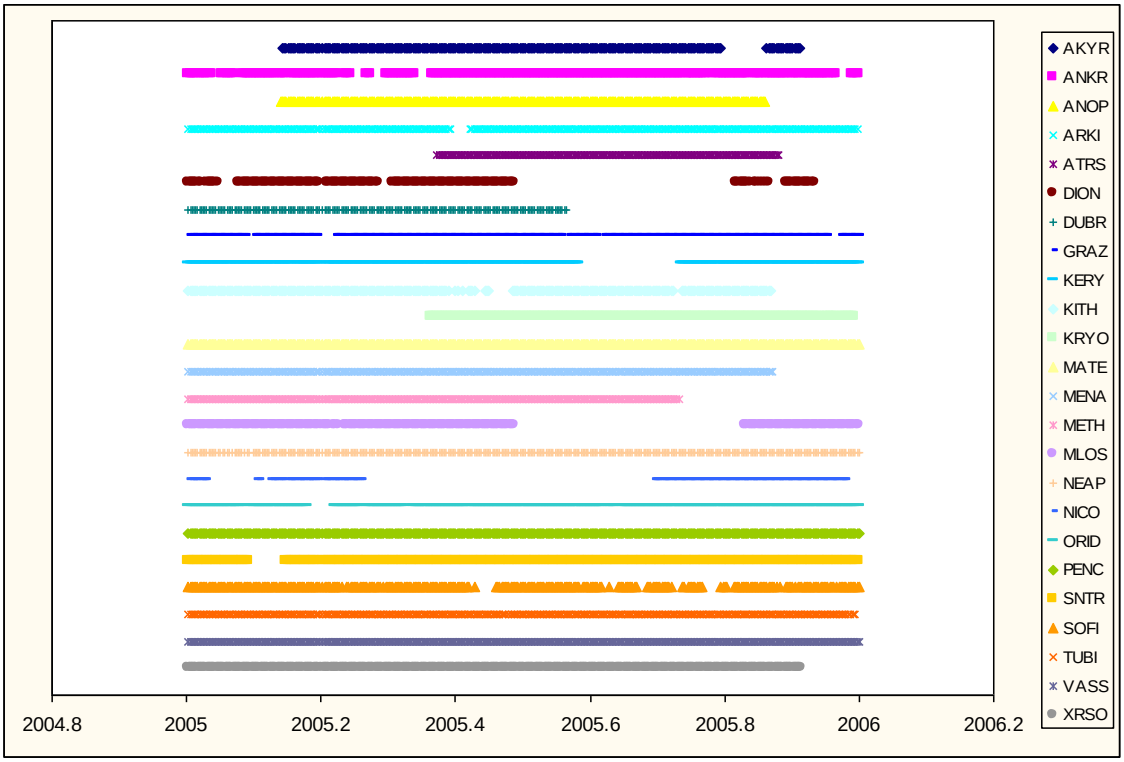

Figure 4.10: Data availability for sites utilized in the GPS processing during 2005.

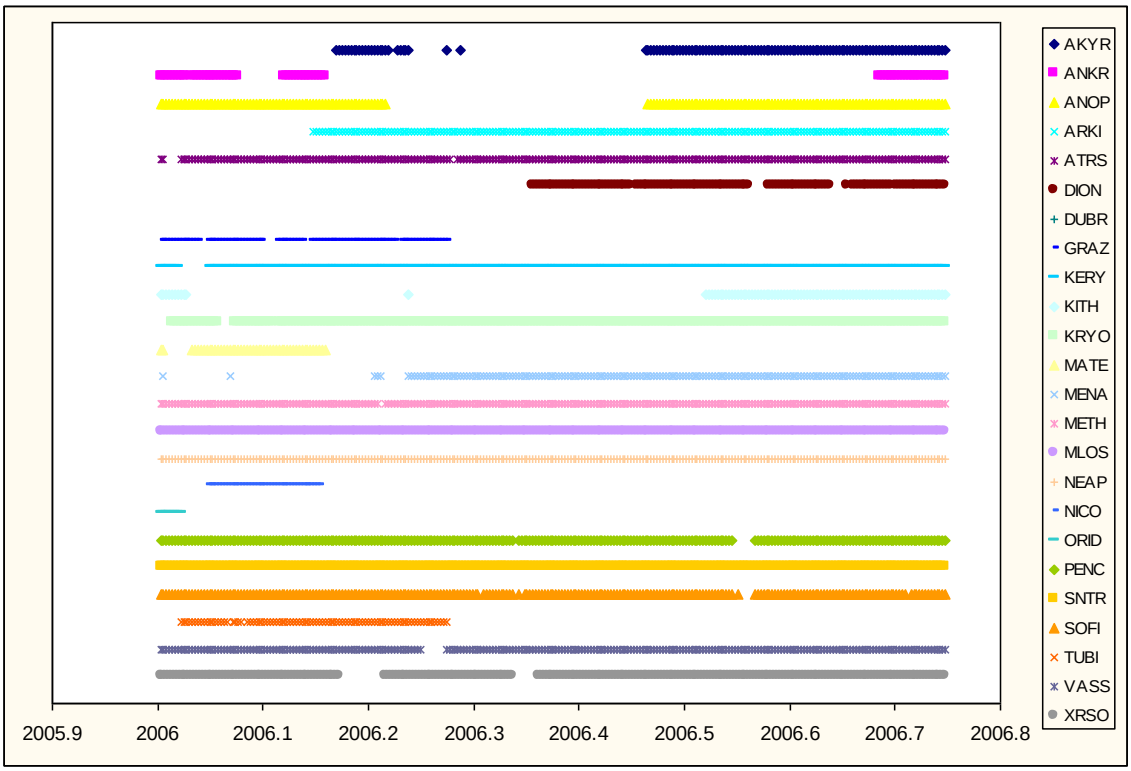

Figure 4.11: Data availability for sites utilized in the GPS processing during 2006.

At this stage a range of post-processing strategies were tested in order to determine which strategy was most applicable to the COMET network in the Aegean. A range of regional filters (*Wdowinski et al. 1997; Dong et al. 2006*) were applied to the resulting station time series using combinations of the more stable and longer standing sites within the network to remove common mode errors and to reduce the impact of noise on the estimated station motions. The variations in baseline components between various sites were then compared.

In addition, due to the immaturity of many of the network sites and an unclear picture of the exact stress fields across the region, common mode errors were also removed purely by differencing baseline components on a site by site basis, similar to the technique employed by Herb Dragert et al in their Cascadia work (*Dragert et al 2001)*.

In order to clarify that this technique could potentially reveal transient motion such as aseismic slip it was tested on a truth model. In this case that was the previous discovery of transient motion where the Juan de Fuca plate subducts beneath the North American plate along the Cascadia margin (*Dragert et al. 2001; Rogers and Dragert, 2003*). The results of this test can be seen in figure 4.12.

a

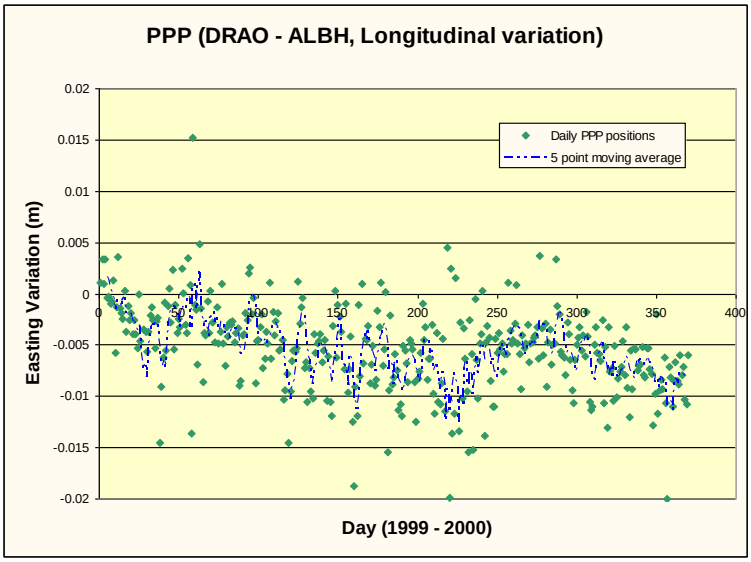

b

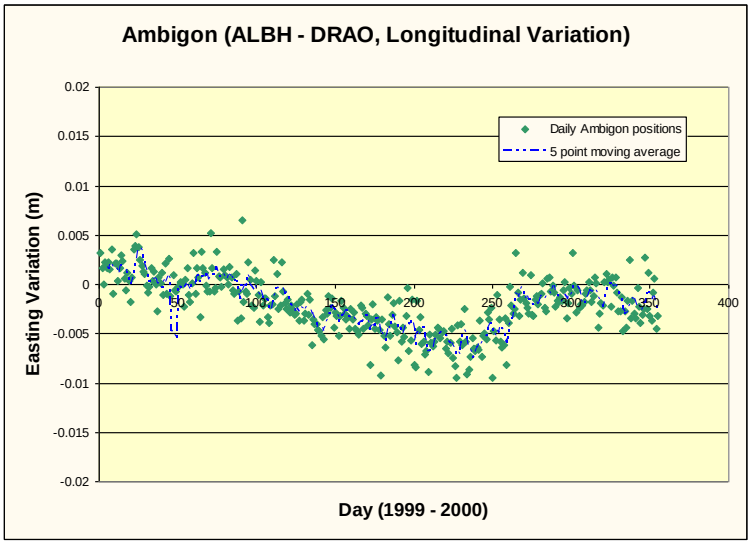

Figure 4.12: Examples of how the PPP and ambiguity resolution processing strategy reduced noise and improved the coordinate time series. The examples show, a) the longitudinal baseline variation between 2 sites in Cascadia (ALBH and DRAO) after PPP was applied. b) the longitudinal baseline variation between 2 sites in Cascadia (ALBH and DRAO) after ambiguity resolution (ambigon) was applied.

4.5 Further Processing

The initial processing steps of PPP followed by ambiguity resolution achieve good sub centimeter repeatabilities. This does not improve the positional estimates sufficiently to see subtle tectonic movements therefore a range of post processing techniques were applied to improve the coordinate time series.

4.5.1 Regional Filtering

The principles and mathematics behind regional filtering are explained in section 3.6.7. The exact methodology and filters applied in this study are now explained. When applying a regional filter it is important to remove all outliers from the data. These will inevitably add noise to the filtering process which in turn adds noise to any time series produced. An initial indication of problem data is accessed using a chi squared test looking for a normal distribution of data about a regression line. This gives an idea of the quality of the input data. A more comprehensive idea is obtained by calculating the standard deviation of the "X velocity" component for each individual site. That is the deviation from a best fit regression line fitted to the "X" component of the daily site positions in the Cartesian ITRF with an origin at the center of the Earth, the X component located along the Greenwich meridian, a Z component at the center of figure of polar motion for the period (1900-1905) and a Y component positive along the 270° meridian. Although the geographic position of the Aegean region is not exactly aligned with any of the cartesian components of the ITRF, the X velocity was used due to its relatively close proximity to the European study area and in particular its greater alignment with the height component of any geodetic ellipsoidal coordinates produced in the study. The equation for a straight line ($Y = MX + C$) had its components M (the gradient) and C (the intercept) calculated using a linear least squares method to determine the best fit regression line:

$$[A^T A][X] = [A^T b] \quad (4.5)$$

Where the **A** matrix is GPS time, **X** contains the components **M** and **C** and **b,** the observed values.

The following values shown in table 4.2 were determined for the sites in this study.

PENC	0.0500
TUBI	0.0616
GRAZ	0.0617
ANKR	0.0695
DION	0.0711
ARKI	0.0805
METH	0.0805
MATE	0.0814
XRSO	0.0818
NICO	0.0835
SOFI	0.0959
NEAP	0.0963
ORID	0.0985
AKYR	0.1416
KITH	0.1435
MLOS	0.1471
VASS	0.1472
SNTR	0.1507
MENA	0.1595
KERY	0.1617
DUBR	0.2163
KRYO	0.2890
ANOP	0.3345
ATRS	0.3598
GVDS	2.6334
IGD1	6.3593

Table 4.2: "X Velocity" standard deviations for all the COMET sites (blue) as well as additional EUREF / IGS sites (cm).

These standard deviations show great variation which largely reflects the age of the site in question. The sites ATRS and GVDS only have a few months of data and therefore any best fit regression line is not likely to reflect accurately the long term site motion. The results do give an idea which stations are most likely to have clean data with few errors. For example sites DUBR and IGD1 have long time series but still have relatively poor standard deviations and therefore may produce poor quality data.

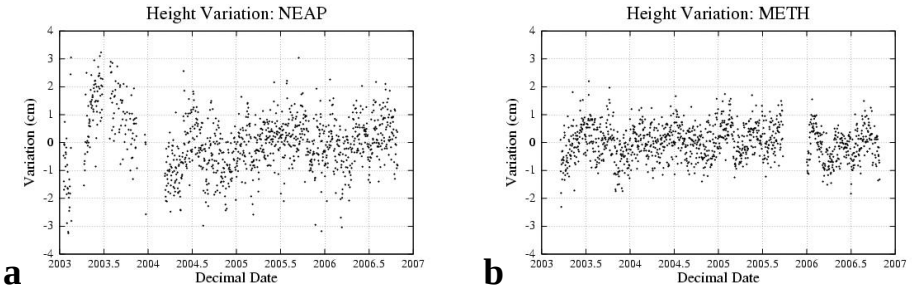

Figure 4.13: Examples of variation in data quality between (a) NEAP that shows considerably greater spread in its height variation than (b) METH. This is reflected in the σ of their "X" velocity (table 5.2) where METH is lower despite the similarity in the length of the time series.

The common approach with regional filtering is to select the sites with the more stable time series to reflect the common mode error within an area. In this respect the Aegean is not ideal for a number of reasons. Firstly the COMET sites (highlighted in blue in figure 4.2) all have relatively short observation periods of a few years, any average movement defined by short periods of data is susceptible to anomalous movements and outliers that could skew an average velocity. As mentioned before, Blewitt and Lavallee (2002) recommend at least 2.5 years of observations to mitigate the annual variations in a signal sufficiently for the regional filtering technique to be applicable. The COMET sites are therefore a little immature to define the common mode error within the Aegean, assuming that errors do conform to a common mode pattern. The other problem with the use of the COMET sites is that they are all located within an area of active tectonics, with seismic and potentially small aseismic movement. It is these subtle movements that the study and hence the regional filter is looking to highlight. These subtle shifts would be averaged out and lost if the sites concerned were used to define the common mode error. The seismicity map of Greece (figure 2.5) shows the extent of Greek seismicity, with the exception of the southern Aegean Sea the whole area is vulnerable to anomalous movements that would affect sites on an individual basis and lead to inaccuracy and noise in any regional filter produced. The technique if incorrectly applied could therefore either hide a real tectonic signal or, if a movement at one site was sufficiently large, give a false positive result at all the sites studied.

The other option is to define the common mode error using the longer standing sites. These in general have lower "X" velocity standard deviations (table 4.2) and could provide a filter that would cover the complete period of study. These also have some drawbacks. The EUREF/IGS sites within the Aegean (ANKR, DION, IGD1) would suffer some of the problems mentioned above, as they are located in tectonically active areas. The European sites such as PENC, GRAZ, SOFI, and MATE are all long standing sites in seismically inert areas but are located hundreds of miles away. This distance may well decorrelate the common mode errors from their locations to the location of the study area.

To deal with these problems a range of regional filters were applied to best determine which sites defined the Aegean common mode error. Before these were applied all the data was filtered to remove outliers. This was a two step process, firstly as a sigma test. The standard deviation was calculated by fitting a best fit regression line through the

respective topocentric coordinates (latitude, longitude and radial) for all available data and calculating the standard deviation from this line for each site and positional component. A threshold of 0.33 cm for latitude and longitude and 1.0 cm for radial variation was set and any site in excess of this on any component (northing, easting or vertical) had that particular day's solution removed. This was followed by a gross filter set at removing all stations that were 1.5 cm from the best fit position for latitude and longitude or 3.5 cm for radial position. Again any site that failed the test had that day removed. These threshold figures were utilised on the advice of Geoff Blewitt, who co-wrote much of the GIPSY - OASIS software, as a method of screening outliers. Testing of different threshold limits found that for both the gross and sigma tests an increase in the threshold tolerance (tolerance levels doubled in each case) had little effect on the number of site failures suggesting that the failures were in general significant outliers. Conversly reducing the threshold levels (0.25 cm for latitude and longitude, 0.6 cm for radial variation for the sigma test and 1.0 cm for latitude and longitude, 2.3 cm radial variation for the gross test) had the effect of screening out significant amounts of data (5+ sites per day). The adviced tolerance levels were therefore taken to be appropriate for the pupose of outlier detection without removing potentially important data.

The results of these filters can be seen in tables 4.3 and 4.4. The first column in each of these tables shows the date (year, month, day), the second column shows the number of parameters that failed. In all these cases only one parameter per site failed, the site or sites that failed are shown in the third column.

02-Apr-10	1	ANKR
02-Apr-23	1	MATE
02-May-14	1	MATE
02-Jun-02	2	NICO PENC
02-Jun-04	1	MATE
02-Jun-18	1	MATE
02-Jul-02	1	NICO
02-Jul-09	1	MATE
02-Jul-14	1	SOFI
02-Jul-15	1	SOFI
02-Jul-16	2	DION SOFI
02-Jul-17	1	SOFI
02-Jul-18	1	SOFI
02-Aug-10	1	ANKR
02-Oct-08	1	SOFI
02-Oct-10	1	SOFI
02-Oct-13	1	SOFI
02-Oct-14	1	SOFI
02-Oct-16	1	SOFI
02-Oct-17	1	SOFI
02-Dec-17	1	MATE
02-Dec-19	1	DUBR
03-Jan-02	1	GRAZ
03-Jan-13	1	DUBR
03-Jan-31	1	DUBR
03-Feb-14	2	DUBR NEAP
03-Feb-19	1	NEAP
03-Feb-20	1	NEAP
03-Feb-21	1	NEAP
03-Mar-04	1	SOFI
03-Mar-07	1	ANKR
03-Mar-31	2	ANKR SOFI
03-Apr-01	1	SOFI
03-Apr-02	1	SOFI
03-Apr-07	1	SOFI
03-Apr-19	1	ANKR
03-May-09	1	DION
03-May-16	1	DION
03-May-17	1	SOFI
03-May-21	1	DUBR
03-Jun-03	1	GRAZ
03-Jun-04	1	SOFI
03-Jun-09	1	ISTA
03-Jun-10	1	ISTA
03-Jun-11	1	ISTA
03-Jun-12	1	ISTA
03-Jun-16	1	DUBR
03-Jun-20	1	DUBR
03-Jun-23	2	DUBR SOFI
03-Jul-02	1	GRAZ
03-Jul-11	1	DION
03-Jul-12	1	DUBR
03-Jul-21	2	DUBR ORID
03-Aug-09	1	NEAP
03-Aug-19	1	ANKR
03-Sep-02	1	MATE
03-Sep-06	1	NEAP
03-Sep-22	1	ANKR
03-Sep-25	1	ANKR
03-Oct-04	1	NEAP
03-Oct-22	1	ANKR
03-Oct-23	1	ANKR
03-Nov-10	1	ORID
03-Nov-17	2	ANKR GRAZ
03-Nov-26	1	ORID
03-Nov-28	1	ORID
03-Dec-20	1	NEAP
03-Dec-21	1	DUBR
03-Dec-27	1	NEAP
03-Dec-30	1	ORID
04-Jan-01	1	SOFI
04-Jan-17	1	ORID
04-Jan-19	1	DION
04-Jan-22	1	ARKI
04-Jan-28	1	ANKR
04-Jan-29	1	ARKI
04-Feb-03	1	ORID
04-Feb-16	1	ORID
04-Feb-17	1	ORID
04-Feb-18	1	ARKI
04-Feb-22	1	DUBR
04-Feb-27	1	ARKI
04-Feb-29	1	ARKI
04-Mar-02	1	ORID
04-Mar-04	1	SOFI
04-Mar-05	2	ARKI ORID
04-Mar-06	1	ARKI
04-Mar-10	1	ARKI
04-Mar-11	1	ORID
04-Mar-12	1	ORID
04-Mar-15	1	ORID
04-Mar-16	1	ORID
04-Mar-19	1	ANKR
04-Mar-21	1	ANKR
04-Mar-25	1	ANKR
04-Mar-26	2	ANKR ARKI
04-Mar-27	1	ANKR
04-Mar-28	1	ANKR
04-Mar-30	1	ANKR
04-Mar-31	1	ANKR
04-Apr-02	1	ANKR
04-Apr-05	1	ANKR
04-Apr-06	1	ANKR
04-Apr-08	1	ANKR
04-Apr-09	2	ANKR ARKI
04-Apr-11	1	ARKI
04-Apr-12	1	ANKR
04-Apr-15	1	ANKR
04-Apr-17	1	ANKR
04-Apr-19	1	NICO
04-Apr-24	1	ANKR
04-May-05	1	ANKR
04-May-14	1	ANKR
04-May-16	1	ANKR
04-May-17	1	ANKR
04-May-18	1	ANKR
04-May-20	1	ANKR
04-May-21	1	ANKR
04-May-24	1	ANKR
04-Jun-02	1	ARKI
04-Jun-05	1	ANKR
04-Jun-06	1	ANKR
04-Jun-07	1	ANKR
04-Jun-15	1	ANKR

04-Jun-16	1	ANKR
04-Jun-19	1	ANKR
04-Jun-22	1	ANKR
04-Jun-25	2	ANKR DUBR
04-Jun-27	1	ANKR
04-Jun-28	1	ANKR
04-Jun-29	1	ANKR
04-Jul-02	1	ANKR
04-Jul-16	1	ANKR
04-Sep-02	1	PENC
04-Sep-04	1	ORID
04-Sep-05	1	ORID
04-Sep-28	1	ANKR
04-Oct-19	1	ORID
04-Oct-21	1	ORID
04-Oct-22	1	ORID
04-Oct-23	1	DION
04-Oct-24	1	ORID
04-Oct-28	1	ANKR
04-Nov-08	1	DION
04-Nov-19	1	ANKR
04-Dec-11	1	XRSO
04-Dec-14	1	DION
04-Dec-21	1	DION
04-Dec-22	1	DION
04-Dec-23	1	DION
04-Dec-24	1	DION
04-Dec-25	1	DION
04-Dec-26	1	DION
05-Jan-08	1	ANKR
05-Jan-11	1	ANKR
05-Jan-20	1	ANKR
05-Jan-22	1	ANKR
05-Jan-24	1	ANKR
05-Feb-05	1	ORID
05-Feb-06	1	NICO
05-Feb-14	1	NICO
05-Feb-15	1	NICO
05-Apr-07	1	NICO
05-May-23	1	ARKI
05-Jun-05	1	SOFI
05-Jun-10	1	ANKR
05-Jul-19	1	ORID
05-Sep-01	1	ANKR
05-Sep-14	1	ANKR
05-Nov-12	1	DION
05-Nov-22	1	MATE
05-Nov-23	1	ANKR
05-Dec-15	1	ANKR
06-Jan-13	1	ANKR
06-Jan-19	1	ANKR
06-Jan-27	1	ANKR
06-Jan-28	1	ANKR
06-Mar-03	1	AKYR
06-Mar-05	1	AKYR
06-Mar-06	1	AKYR
06-Mar-07	1	AKYR
06-Mar-09	1	AKYR
06-Mar-11	1	AKYR
06-Mar-12	1	AKYR
06-Mar-13	1	AKYR
06-Mar-14	1	AKYR
06-Mar-19	1	AKYR
06-Mar-21	1	AKYR
06-Mar-25	1	AKYR
06-Mar-28	1	AKYR
06-Mar-29	1	MENA
06-Apr-04	1	ARKI
06-Apr-15	1	AKYR
06-May-03	1	XRSO
06-Oct-20	1	ANKR
06-Oct-31	1	ANOP

Table 4.3: The stations removed from further processing due to failing the "sigma" test.

02-Jul-14	1	SOFI
02-Jul-15	1	SOFI
02-Jul-16	2	DION SOFI
02-Jul-17	1	SOFI
02-Jul-18	1	SOFI
02-Jul-30	1	MATE
02-Aug-10	1	ANKR
02-Oct-08	1	SOFI
02-Oct-10	1	SOFI
02-Oct-13	1	SOFI
02-Oct-14	1	SOFI
02-Oct-16	1	SOFI
02-Oct-17	1	SOFI
02-Oct-18	1	SOFI
02-Oct-23	1	SOFI
02-Dec-17	1	MATE
03-Jan-13	1	DUBR
03-Jan-31	1	DUBR
03-Feb-14	2	DUBR NEAP
03-Feb-19	1	NEAP
03-Feb-20	1	NEAP
03-Feb-21	1	NEAP
03-Mar-04	1	SOFI
03-Mar-31	2	ANKR SOFI
03-Apr-01	1	SOFI
03-Apr-02	1	SOFI
03-Apr-07	1	SOFI
03-Apr-21	1	PENC
03-May-13	1	PENC
03-May-17	1	SOFI
03-Jun-04	1	SOFI
03-Jun-09	1	ISTA
03-Jun-10	1	ISTA
03-Jun-11	1	ISTA
03-Jun-12	1	ISTA
03-Jun-23	1	SOFI
03-Jul-11	1	DION
03-Aug-09	1	NEAP
03-Sep-06	1	NEAP
03-Oct-04	1	NEAP
03-Oct-05	1	SOFI
03-Oct-20	1	SOFI
03-Oct-21	1	SOFI
03-Oct-22	2	ANKR SOFI
03-Oct-23	1	SOFI
03-Dec-20	1	NEAP
03-Dec-21	1	DUBR
03-Dec-27	1	NEAP
04-Jan-07	1	ARKI
04-Jan-13	1	PENC
04-Jan-19	1	SOFI
04-Jan-23	1	ARKI
04-Jan-24	1	ARKI
04-Jan-25	1	ARKI
04-Jan-26	1	ARKI
04-Jan-28	1	ARKI
04-Jan-29	1	ARKI
04-Jan-31	1	ARKI
04-Feb-09	1	ORID
04-Feb-17	1	ARKI
04-Feb-18	1	ARKI
04-Feb-21	1	ARKI
04-Feb-22	1	PENC
04-Feb-23	2	PENC SOFI
04-Feb-24	1	PENC
04-Feb-27	1	ARKI
04-Feb-28	1	ARKI
04-Feb-29	1	ARKI
04-Mar-04	1	ARKI
04-Mar-05	1	ARKI
04-Mar-06	1	ARKI
04-Mar-08	1	PENC
04-Mar-09	2	NEAP PENC
04-Mar-10	1	ARKI
04-Mar-24	1	ARKI
04-Mar-28	1	ANKR
04-Mar-31	1	ARKI
04-Apr-02	1	ARKI
04-Apr-07	1	SOFI
04-Apr-09	1	ARKI
04-Apr-10	1	ARKI
04-Apr-11	1	ARKI
04-May-07	1	ORID
04-May-26	1	ARKI
04-Jun-02	1	ARKI
04-Jul-16	1	ANKR
04-Sep-25	1	MENA
04-Oct-17	1	SOFI
04-Oct-19	1	ORID
04-Nov-08	1	DION
04-Dec-02	1	SOFI
04-Dec-03	1	SOFI
04-Dec-11	1	XRSO
04-Dec-14	1	DION
04-Dec-21	1	DION
04-Dec-22	1	DION
04-Dec-24	1	DION
04-Dec-26	1	DION
04-Dec-27	1	ARKI
05-Jan-17	1	KERY
05-Jan-31	1	DION
05-Feb-06	1	NICO
05-Feb-07	1	SOFI
05-Mar-13	1	SOFI
05-Jul-19	1	ORID
05-Sep-01	1	ANKR
05-Sep-04	1	ANOP
05-Nov-08	1	MATE
05-Nov-28	1	GRAZ
06-Jan-01	1	GRAZ
06-Jan-02	1	GRAZ
06-Jan-13	1	ANKR
06-Mar-03	1	AKYR
06-Oct-31	1	ANOP

Table 4.4: The stations removed from further processing due to failing the “gross” test.

Regional filters were then formed from these cleaned data series. Four filters were tested each with a different focus. Initially the traditional filters were formed using all sites that met a certain standard deviation on their "x velocity". These were as follows:

- **0.1 sigma filter** - PENC, TUBI, GRAZ, ANKR, DION, ARKI, METH, MATE, XRSO, NICO, SOFI, NEAP, ORID.
- **1.0 sigma filter** - PENC, TUBI, GRAZ, ANKR, DION, ARKI, METH, MATE, XRSO, NICO, SOFI, NEAP, ORID, AKYR, KITH, MLOS, VASS, SNTR, MENA, KERY, DUBR, KRYO, ANOP, ATRS.

The "sigmas" in these filters again refer to the "X" velocity figures detailed in table 4.2. In addition another two filters were formed based on spatial correlation, one using the Eurasian sites and another using the longest standing sites around the Aegean. The Eurasian sites were chosen initially for their stable and reliable time series as well as their relatively close proximity to the study area, when compared to sites located in England or Spain for example. The Aegean sites were all those with a time series longer than the COMET sites that were located away from the Hellenic arc:

- **Aegean filter** - ANKR, DION, NICO, ORID, TUBI.
- **Eurasian filter** - GRAZ, MATE, PENC, SOFI, DUBR

The filtering process then follows the procedure explained in section 3.6.7, the residual offsets for each positional component (easting, northing vertical), for each site within the filter are calculated on a day to day basis. The average residual on an epoch by epoch basis for all the sites forming the regional filter are then calculated and subtracted from all the sites being studied. The residuals in this case are given a weighting corresponding to their "x velocity" sigma (table 4.2) in order to avoid poor quality data from unpredictable sites skewing any result. An additional test of the data quality is added during this process, the WRMS values for each component (easting, northing, vertical) are calculated and any day with a value greater than 2.3mm for the easting or northing or 9mm for the vertical is deleted. To further test against biases from a limited number of sites any day where the regional filtering frame was formed from less than three of the sites is also deleted. This had no effect on the 0.1 sigma and 1.0 sigma filters which both contained 13 + sites but did have an effect on the Aegean and Eurasian filters which both had occasional days lost to insufficient frame information.

It should also be noted that this is an iterative process and best results are achieved by reprocessing the data, firstly by again applying the "sigma" and "gross" filter to remove outliers and then regionally filtering again.

A truth model to demonstrate the application of this technique and its validity in detecting subtle Earth movements was carried out on the Cascadia region (figure 4.14), replicating the evidence for silent earthquakes presented by Rogers and Dragert (2003).

4.5.2 Filtered Baseline Method

The method of baseline filtering applied in this study was initially similar to the regional filtering technique. The data was processed using precise point positioning followed by ambiguity resolution using GIPSY's ambigon function. The results were then filtered in the same manner as mentioned in section 4.3 in order to remove outliers. Firstly using a sigma test which was set as 0.33 cm for latitude and longitude, 1.0 cm for radial variation, this was followed by a gross filter set at removing all stations that were 1.5 cm from the best fit position for latitude and longitude or 3.5 cm for radial position.

All the the baselines between sites were then determined on a daily basis as were the variations in the baseline components (North, East and Radial).

In determining the northerly, easterly and vertical variations between sites the vectors in the geocentric Cartesian system have to be transformed to a topocentric Cartesian system by multiplying with the correct rotation matrix;

$$\begin{pmatrix} n \\ e \\ u \end{pmatrix} = \begin{pmatrix} -\sin\varphi\cos\lambda & -\sin\varphi\sin\lambda & \cos\varphi \\ -\sin\lambda & \cos\lambda & o \\ \cos\varphi\cos\lambda & \cos\varphi\sin\lambda & \sin\varphi \end{pmatrix} \cdot \begin{pmatrix} \Delta X \\ \Delta Y \\ \Delta Z \end{pmatrix} \tag{4.6}$$

n, e, u : Topocentric vector components

$\Delta X, \Delta Y, \Delta Z$: Geocentric vector components

φ, λ : Astronomical longitude and latitude of the topocenter

Once the vectors had been transformed they could be differenced on a site by site basis to remove common mode error and reveal any variations in the time series. Although this process was carried out for all sites more emphasis was put on the sites that had long, complete time series, that were in tectonically more inert settings and were located in close enough proximity such that any common mode errors should be well correlated.

The filtered baseline method of removing common mode errors has certain advantages but also a number of draw backs when comparing it to the regional filtering technique. The basic methodology assumes that the common mode errors at one site are the same as at another. This is accurate in principle as all errors with the exception of multipath and receiver noise should be the same provided the distance between two stations is less than $\approx$ 100km. Using this principle differencing the coordinates of one site from another, either in terms of the baseline length or the baseline components should remove all common mode errors and therefore reveal the underlying tectonic variations between the two sites.

In reality this method can have several draw backs. Firstly the common mode errors can vary from site to site especially in varied geographical settings where ocean loading and hydrological loading can vary over relatively short distances. Of more concern are receiver specific error sources such as multipath, receiver noise or equipment problems. These errors propagate directly into the results through the differencing process and due to the nature of a site by site comparison there is no additional data to average or mitigate the effects of such error sources. This can lead to false positive results whereby error sources are interpreted as real movement. To avoid this any results have be verified using a number of sites.

Other disadvantages include the time consuming process of having to compare the baselines between each and every site, especially compared to the regional filtering technique that provides site specific displacements rather than having to analyze baselines between pairs of stations. The technique leads to a lack of knowledge of exact site movements as you only determine the relative movements of one site to another, for example you can determine that the east-west component of a baseline between site 1 and site 2 is increasing but you have no way of knowing if site 1 is moving east or site 2 is moving west or alternatively they're both moving in the same direction at different

rates. This can lead to some confusion as to the exact location of an anomalous tectonic signal or movement, for example isobserved motion at site 1, site 2, or at both.

Despite the disadvantages and inherent dangers within the filtered baseline method mentioned above the technique still has some advantages over fiducial or regional filtering. The method does not involve any averaging as is prevalent in regional filtering. This means that any subtle signals will still be in the data rather than suppressed by the filtering technique. Baselines can be examined with optimal positions to highlight expected signals. For example in the Aegean the general movement of stations around the Hellenic arc is south southwest with reference to Eurasia. Baseline component motion should be orientation independent but reference sites should be chosen with some care as large relative movements can mask other more subtle signals.

5.6 Results

The initial processing stage of precise point positioning followed by ambiguity resolution using GIPSY's ambigon module gave site positions in the ITRF2000 reference frame. These time series were then filtered further to remove outliers and reduced in order to show the variation from the mean of the time series. This produced the graphs below.

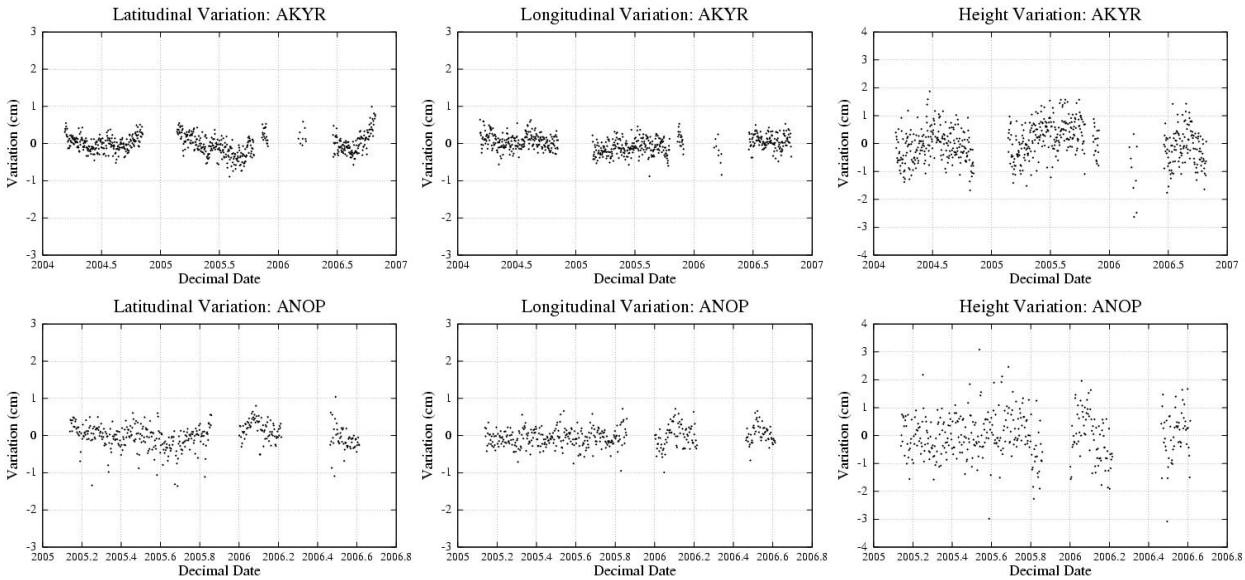

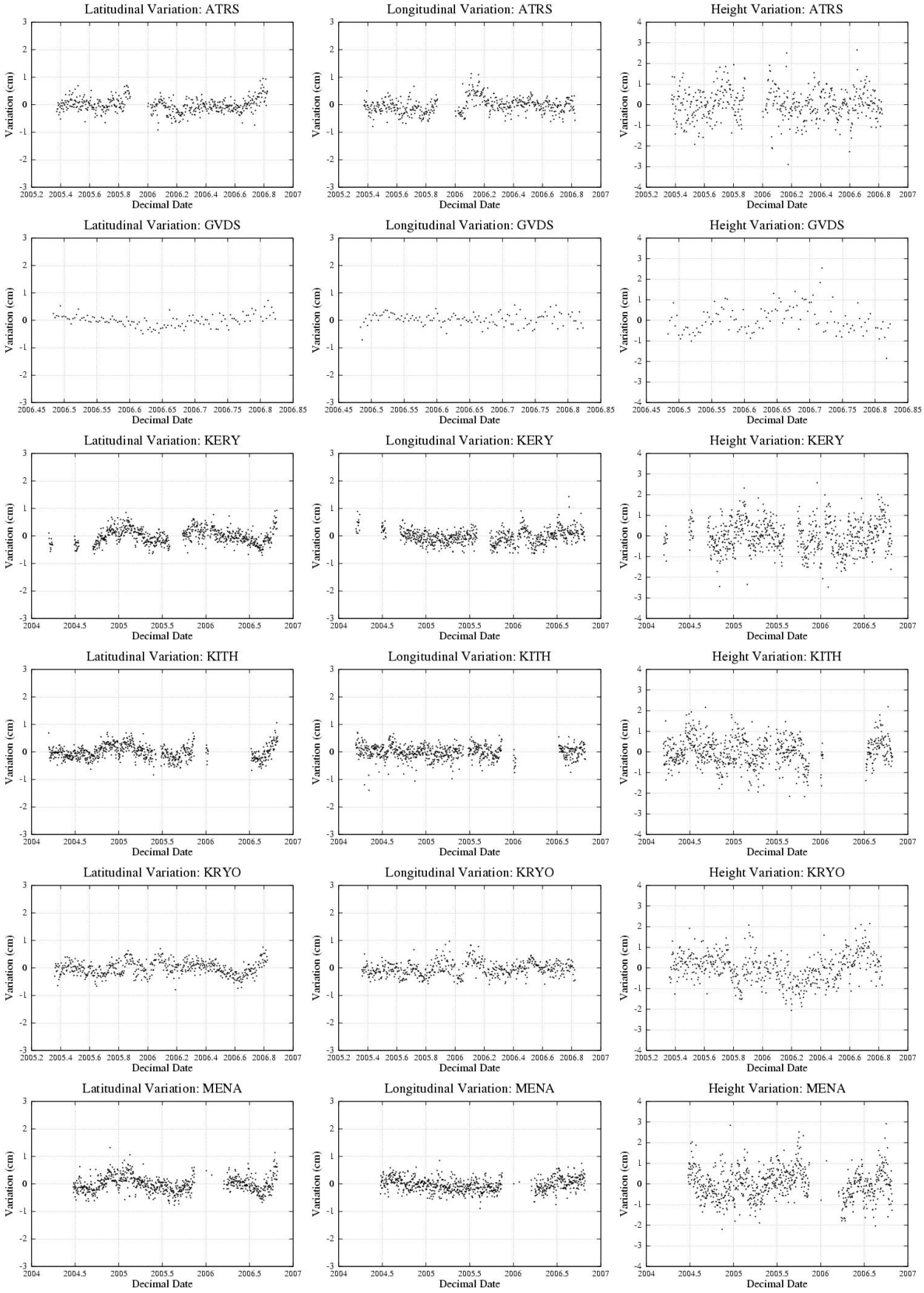
Latitudinal Variation: ATRS
Longitudinal Variation: ATRS
Height Variation: ATRS
Latitudinal Variation: GVDS
Longitudinal Variation: GVDS
Height Variation: GVDS
Latitudinal Variation: KERY
Longitudinal Variation: KERY
Height Variation: KERY
Latitudinal Variation: KITH
Longitudinal Variation: KITH
Height Variation: KITH
Latitudinal Variation: KRYO
Longitudinal Variation: KRYO
Height Variation: KRYO
Latitudinal Variation: MENA
Longitudinal Variation: MENA
Height Variation: MENA
Variation (cm)
Decimal Date

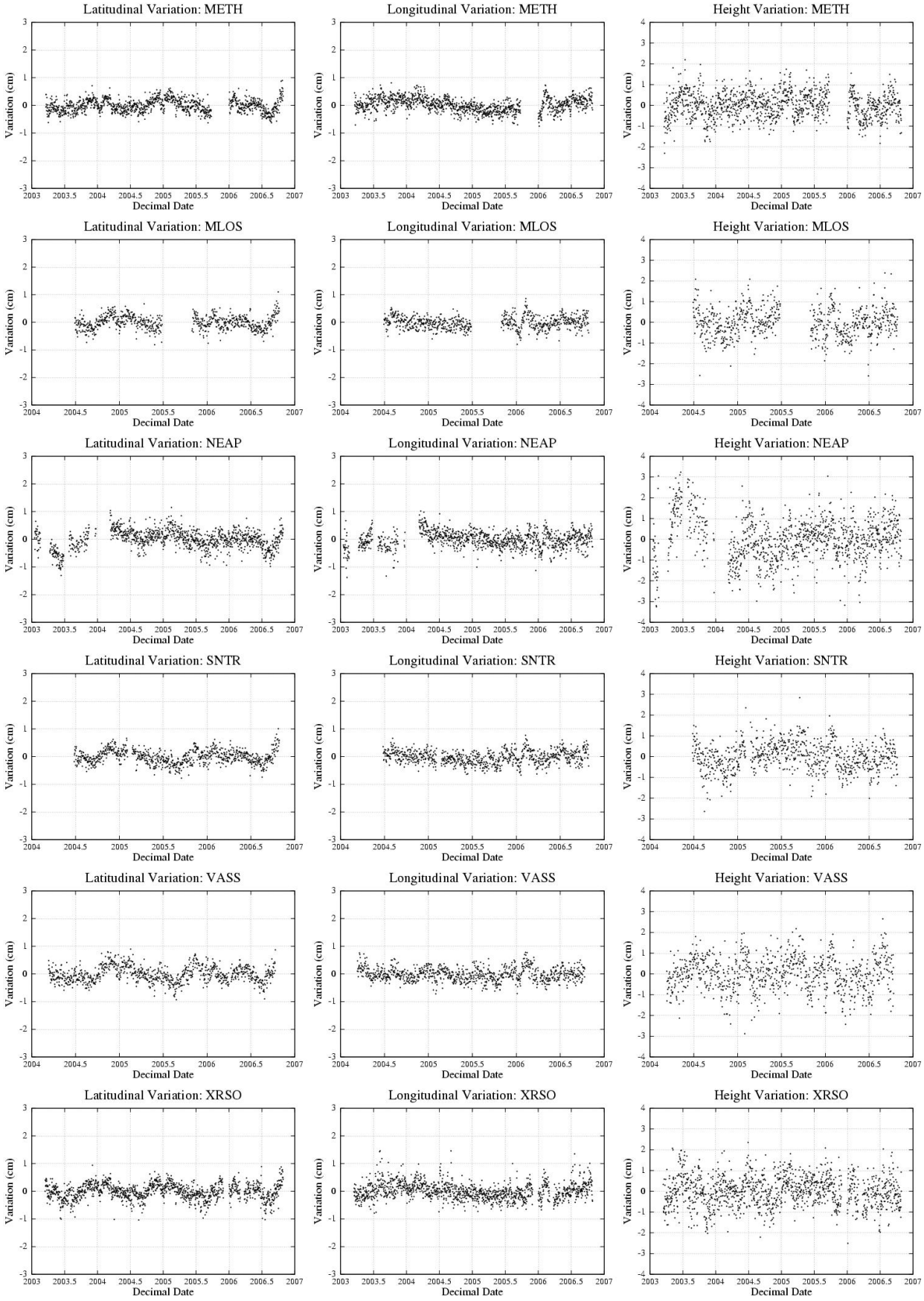
Latitudinal Variation: METH
Longitudinal Variation: METH
Height Variation: METH
Latitudinal Variation: MLOS
Longitudinal Variation: MLOS
Height Variation: MLOS
Latitudinal Variation: NEAP
Longitudinal Variation: NEAP
Height Variation: NEAP
Latitudinal Variation: SNTR
Longitudinal Variation: SNTR
Height Variation: SNTR
Latitudinal Variation: VASS
Longitudinal Variation: VASS
Height Variation: VASS
Latitudinal Variation: XRSO
Longitudinal Variation: XRSO
Height Variation: XRSO
Variation (cm)
Decimal Date

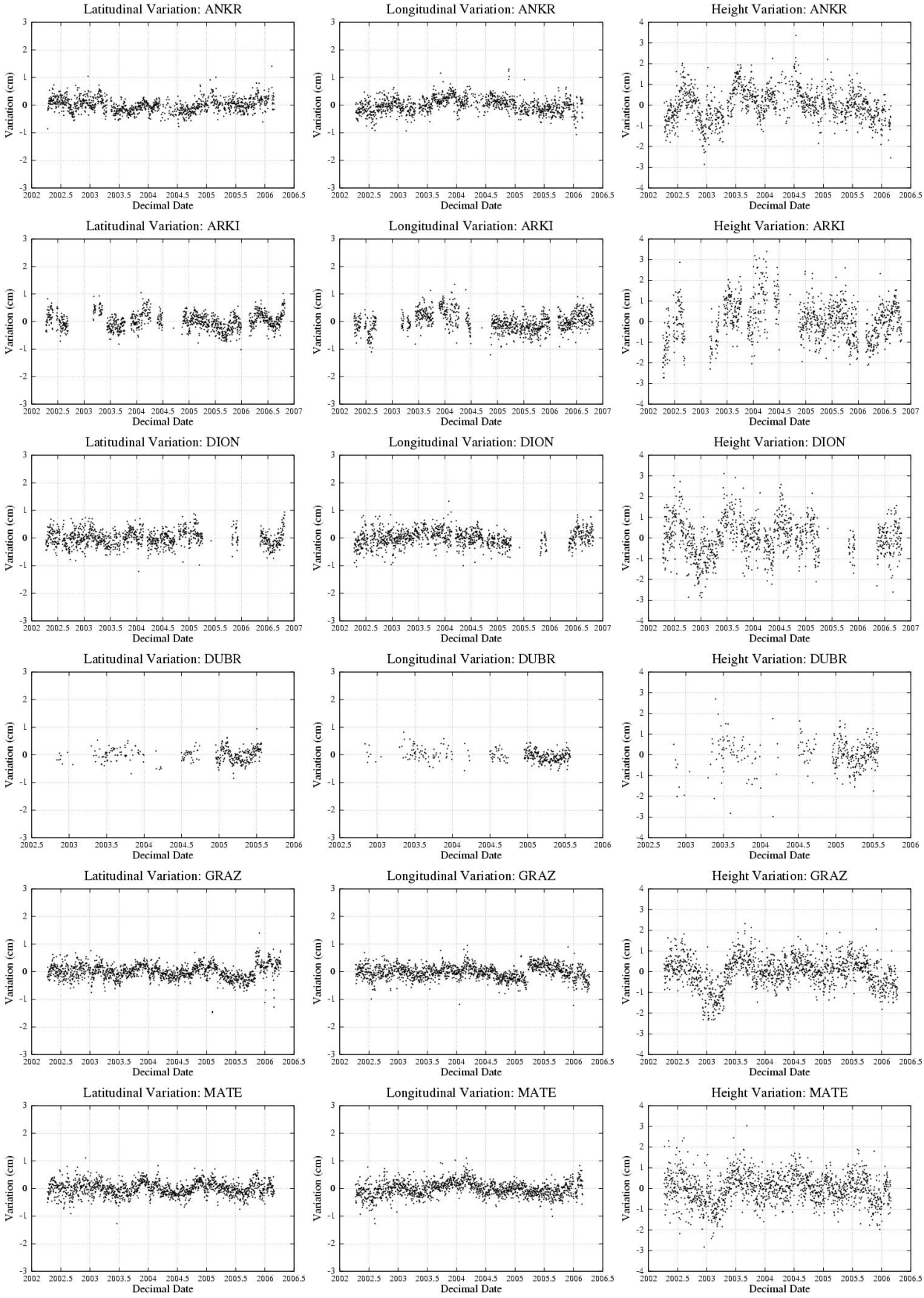
Latitudinal Variation: ANKR
Longitudinal Variation: ANKR
Height Variation: ANKR
Latitudinal Variation: ARKI
Longitudinal Variation: ARKI
Height Variation: ARKI
Latitudinal Variation: DION
Longitudinal Variation: DION
Height Variation: DION
Latitudinal Variation: DUBR
Longitudinal Variation: DUBR
Height Variation: DUBR
Latitudinal Variation: GRAZ
Longitudinal Variation: GRAZ
Height Variation: GRAZ
Latitudinal Variation: MATE
Longitudinal Variation: MATE
Height Variation: MATE
Variation (cm)
Decimal Date

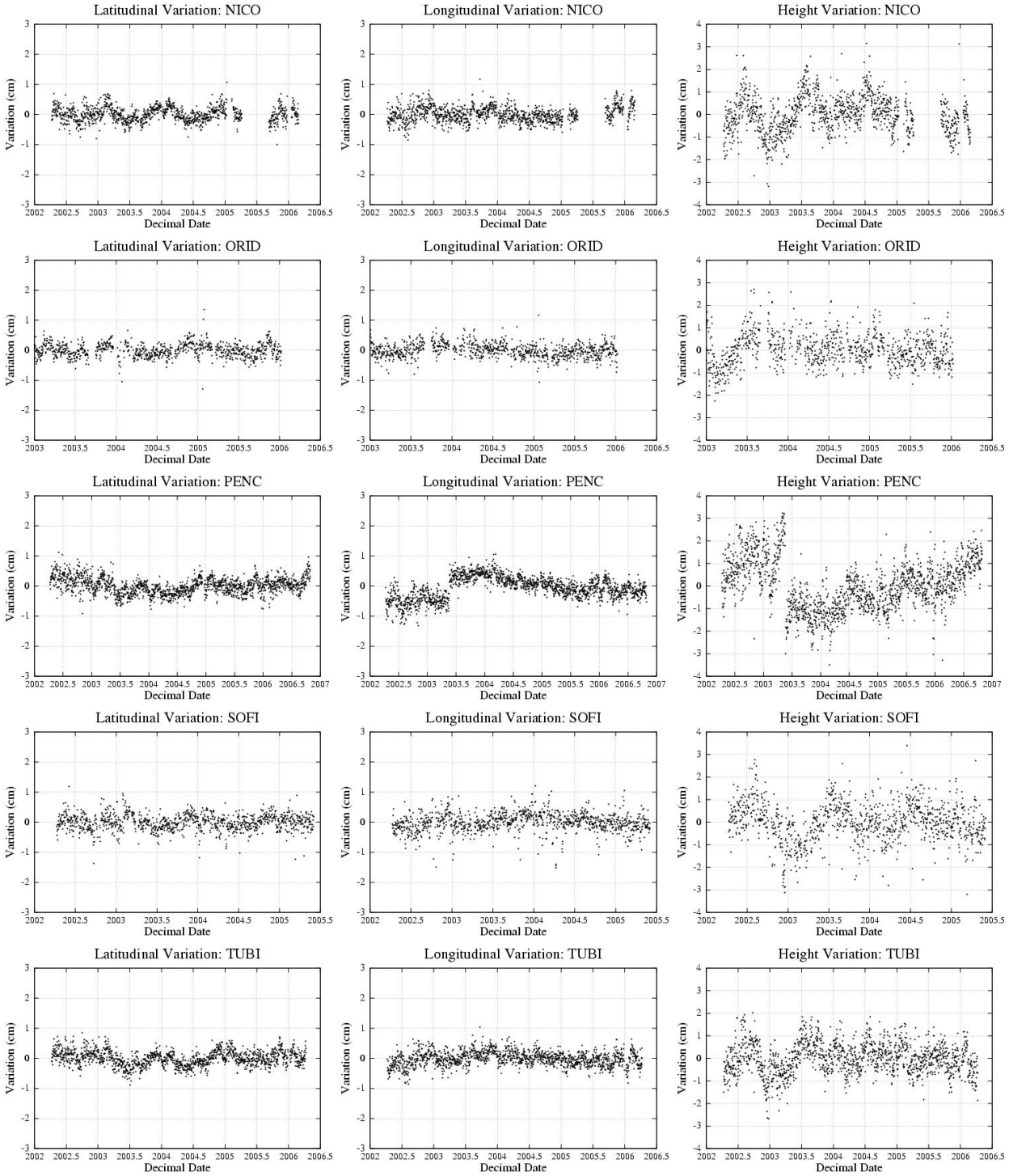

The graphs highlight a number of factors that have an impact on the methods used to further process this data. Firstly that the time series of the COMET sites are in general short (2 - 3 years of data) and that there are significant data losses throughout the study period. For this reason a number of sites were excluded from further processing as their data was seen as potentially detrimental, or of no benefit to the post processing strategies and results later in the research. These included IGD1, ISTA and TUC2.

The EUREF / IGS sites in general have data that cover the entire study period with few data outages (with the exception of DUBR and NICO). A couple of the sites exhibit small jumps in their time series these were both due to antenna and receiver changes (GRAZ on the 17th March 2005, PENC on the 22nd May 2003).

All the time series are coherent in the sense that the data displays distinct patterns to their time series with standard deviations all within the published limits for the processing techniques applied to this stage (≈ 1cm for PPP, improved with ambiguity resolution) (*Zumberge et al. 1997; Blewitt, 1989*). These standard deviations are shown in table 4.5

	Latitude	Longitude	Radial
AKYR	0.26	0.22	0.64
ANKR	0.24	0.27	0.73
ANOP	0.33	0.26	0.82
ARKI	0.29	0.32	0.89
ATRS	0.26	0.29	0.73
DION	0.28	0.29	0.9
DUBR	0.25	0.21	0.68
GRAZ	0.27	0.25	0.7
GVDS	0.22	0.22	0.66
KERY	0.28	0.27	0.75
KITH	0.26	0.25	0.67
KRYO	0.25	0.26	0.71
MATE	0.24	0.26	0.67
MENA	0.3	0.24	0.74
METH	0.23	0.25	0.62
MLOS	0.25	0.23	0.69
NEAP	0.34	0.3	1.03
NICO	0.24	0.25	0.81
ORID	0.23	0.23	0.69
PENC	0.27	0.34	1.09
SNTR	0.25	0.23	0.67
SOFI	0.26	0.31	0.84
TUBI	0.25	0.24	0.68
VASS	0.29	0.24	0.81
XRSO	0.29	0.31	0.73

Table 4.5: Standard deviations of the CGPS stations after PPP and ambiguity resolution (cm)

4.6.1 Results Regional Filtering

The regional filtering technique was first applied to the Cascadia region at a time shown by Dragert et al (2001) to exhibit a silent earthquake. The regional filter was applied using a range of North American CGPS stations to define the common mode error (will, wslr, drao and brew), and baseline components between a site in Penticton (DRAO) and sites in the Cascadia region were then plotted. Figure 4.14 shows these results and the gradual reduction in scatter achieved at each progressive step in the processing stage, from PPP to ambiguity resolution to a weekly averaged regional filter solution. A summary of the improved standard deviations at each stage can be seen in table 4.6. It should be noted that this standard deviation is based on a linear least squares regression line fitted through the data and not the five day moving average seen in the diagrams and therefore includes the notable kink in the time series caused by the silent earthquake

Processing technique	**Standard Deviation in meters (Easting component)**
PPP	0.0046
Ambiguity Resolution	0.0031
Weekly Regional Filter	0.0019

Table 4.6: Standard deviations of the CGPS baseline between ALBH and DRAO after PPP, ambiguity resolution and regional filtering (m)

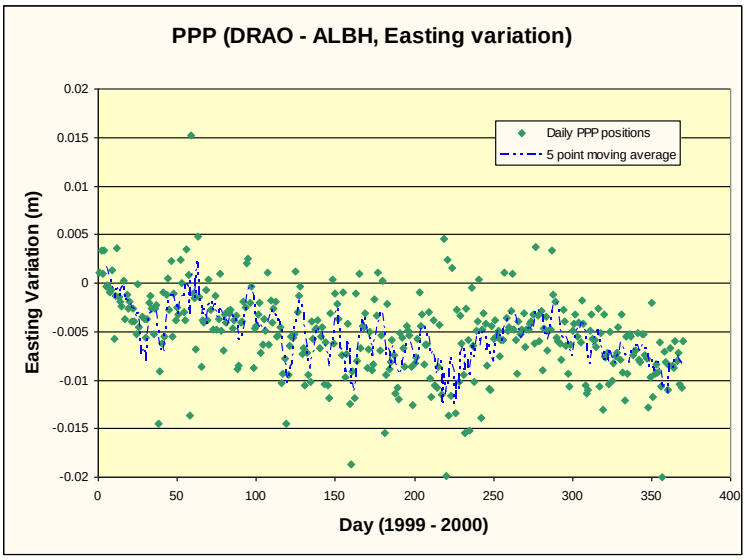

a

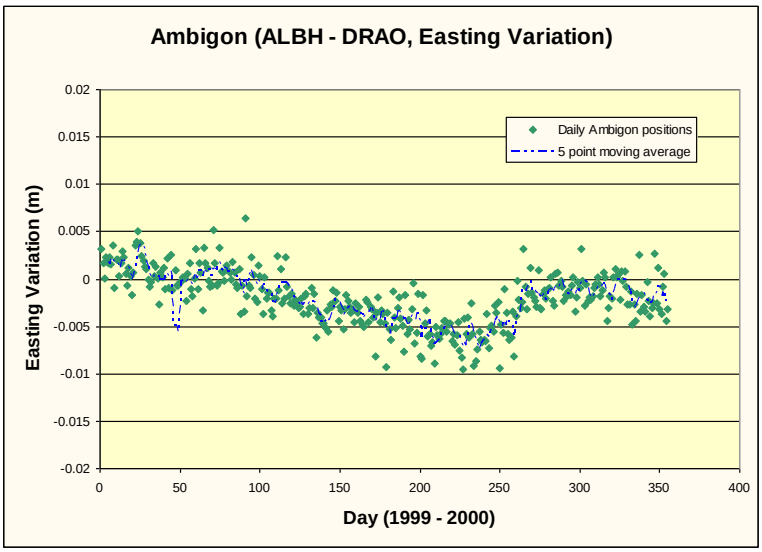

b

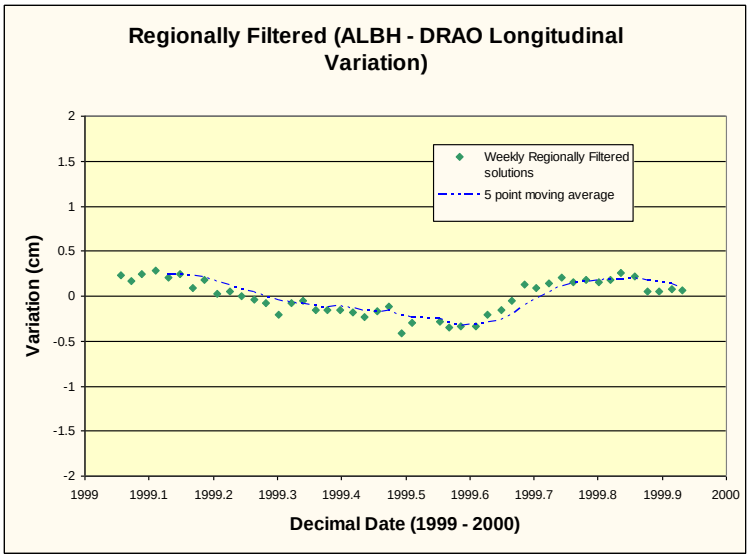

c

Figure 4.14: The variation in scatter achieved by various processing strategies applied to the 1999 Cascadia silent slip event. a) After Precise Point Positioning. b) After Ambiguity resolution. c) After regional filtering.

This initial test to determine the suitability of the processing technique demonstrated its effectiveness at highlighting transient tectonic events. The approach was therefore replicated in the Aegean study area.

The Aegean area is more complex than Cascadia, with a broad zone of continental deformation and therefore a poorer idea of which sites are susceptible to transient motion. Combined with this the seismicity of the area provides a poorer idea of which stations display sufficient stability to define the common mode errors of the region. As a result of this a range of regional filters were applied, the full results of which can be seen in appendix D. A number of characteristics were apparent from this processing, which are highlighted below.

Eurasian Frame

The Eurasian regional filter was formed using the sites GRAZ, MATE, PENC, SOFI, DUBR (figure 5.15). The frame did succeed in reducing the scatter and cleaning the data as can be seen in figure 5.16. This is particularly true for the Eurasian stations as can be seen below. GRAZ and ORID have both had the annual signals associated with their pre filtered time series removed which in the case of GRAZ clearly shows the hardware change it experienced towards the end of 2005.

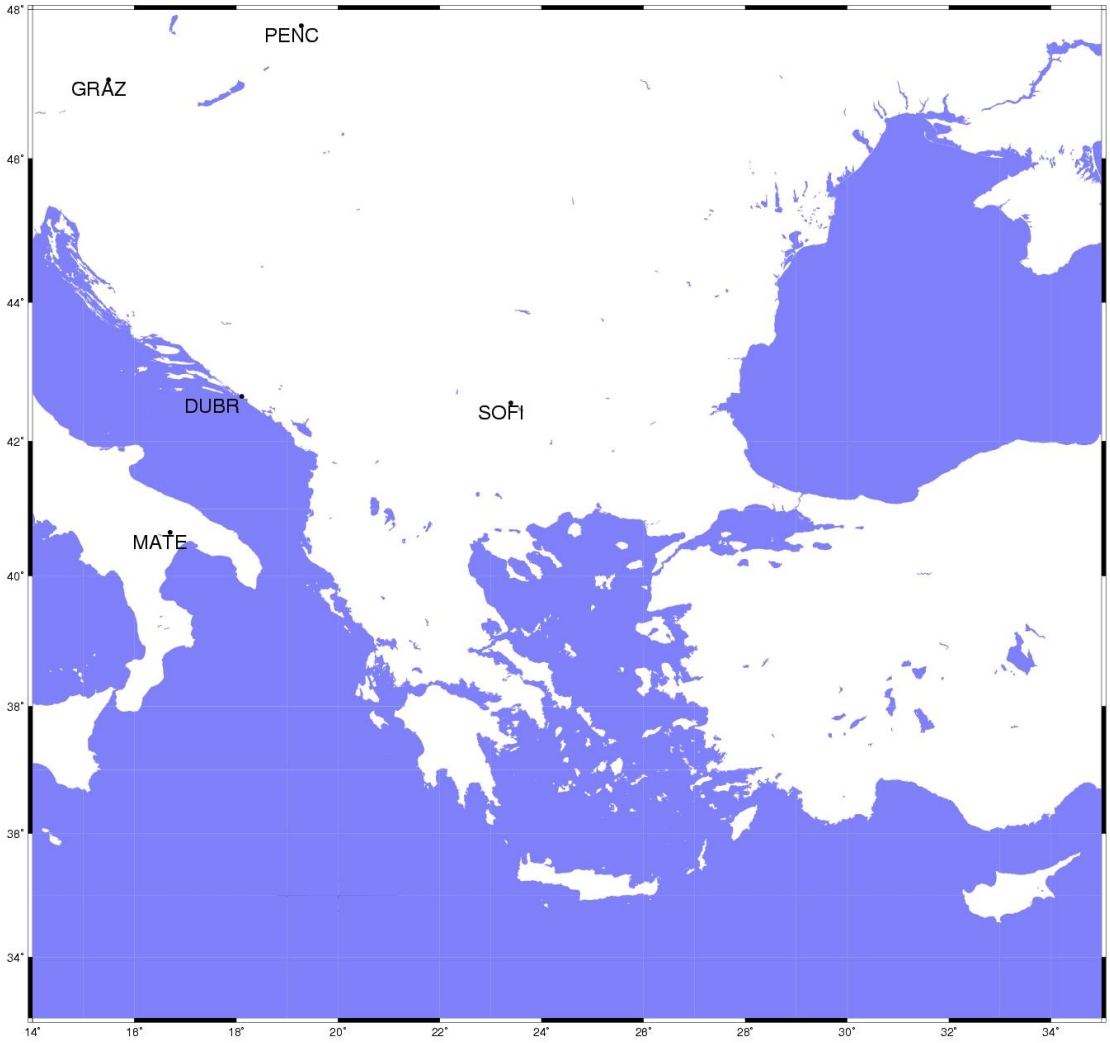

Figure 4.15: The stations used in the construction of the Eurasian regional filter.

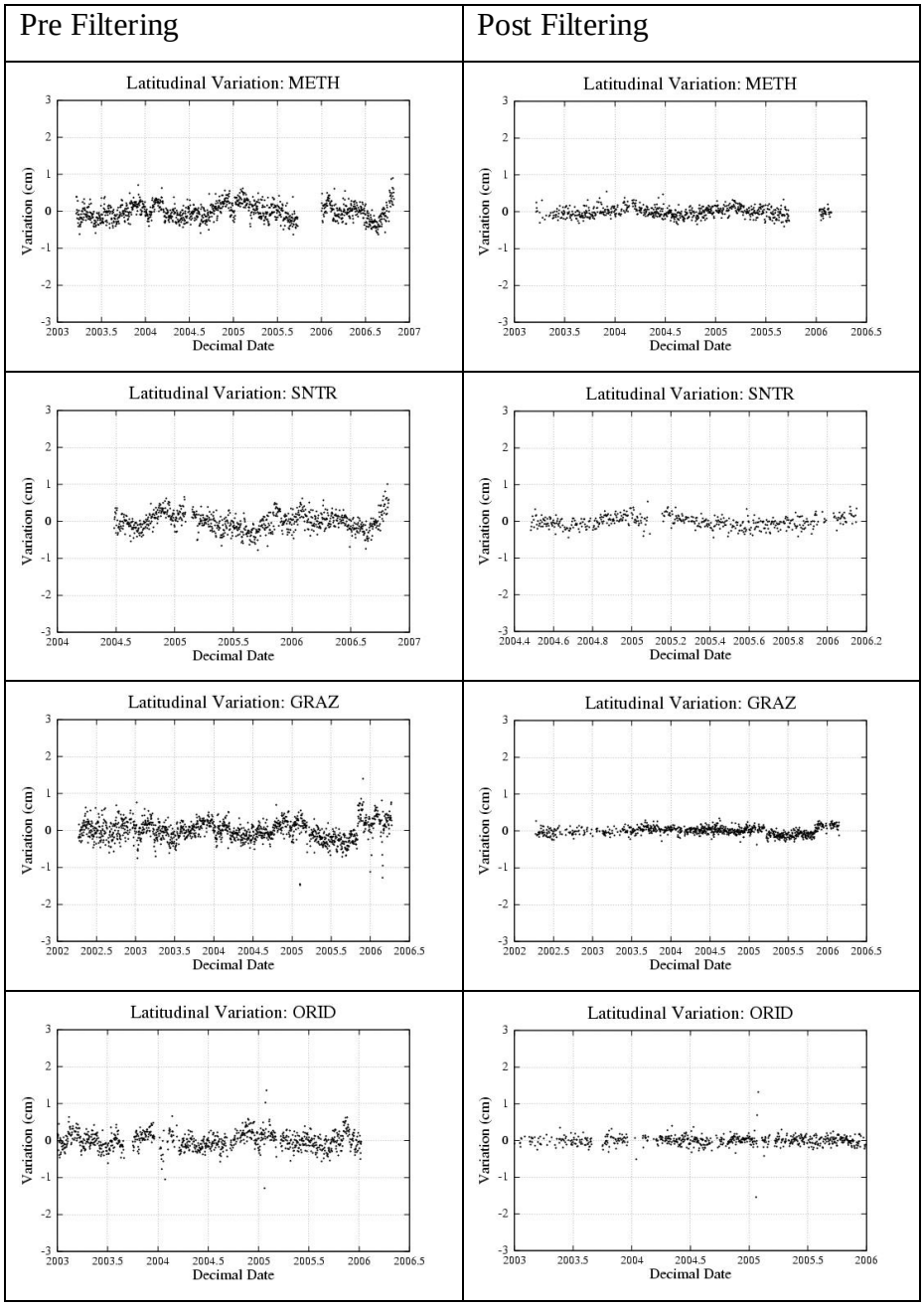

Figure 4.16: Pre and post filtered time series showing the effect of the Eurasian regional filter on a selection of CGPS stations.

The Aegean sites also show a significant reduction in scatter, but also still show strong annual signals suggesting a discrepancy between the common mode errors affecting the central European sites and those in the Aegean.

Aegean Frame

This frame consisted of the sites ANKR, DION, NICO, ORID, TUBI (figure 4.17). The Aegean regional filter had a varying affect across the area. As with the Eurasian filter all sites showed a marked improvement in their general scatter, particularly the sites in the Aegean area, for example METH in the figure below. Other Aegean sites still showed distinct annual signals, particularly in their longitudinal orientation (appendix D). The European sites showed a similar pattern to this. Some results showed distinct improvement, such as ORID, others maintained annual signals and other variations (figure 4.18).

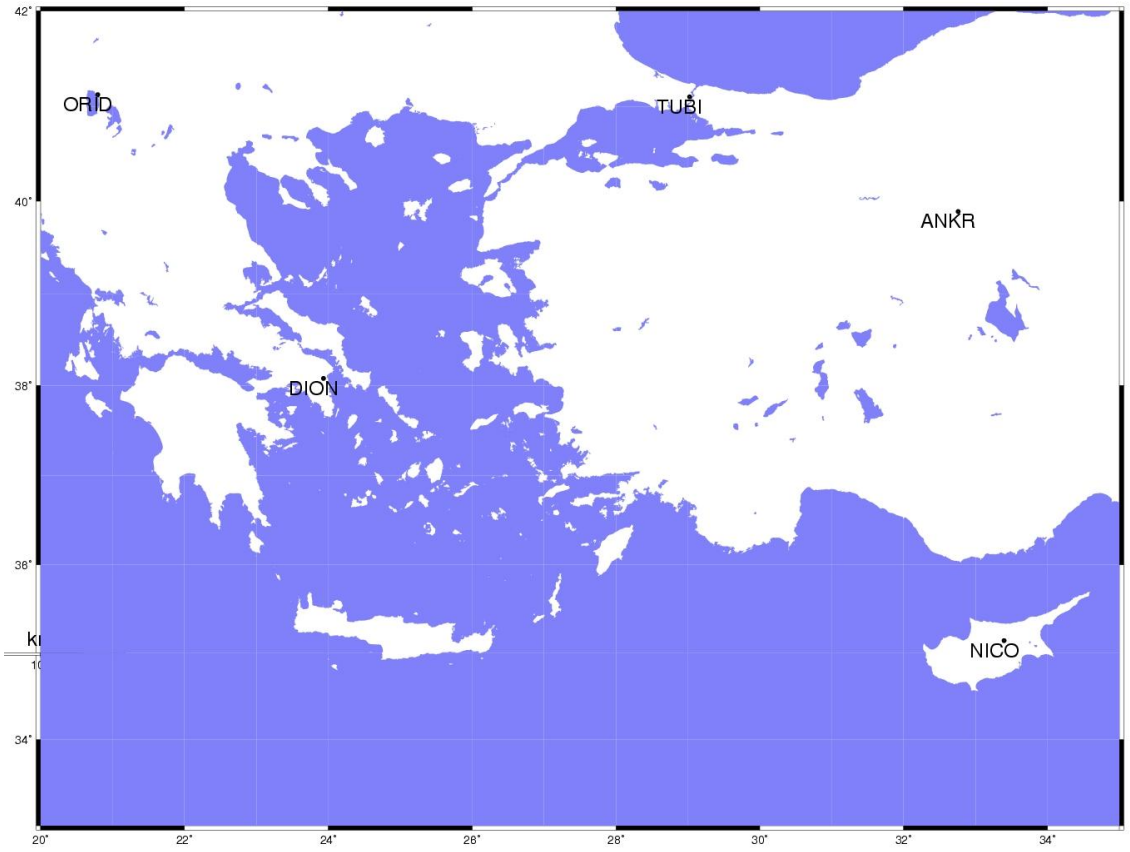

Figure 4.17: The stations used in the construction of the Aegean regional filter.

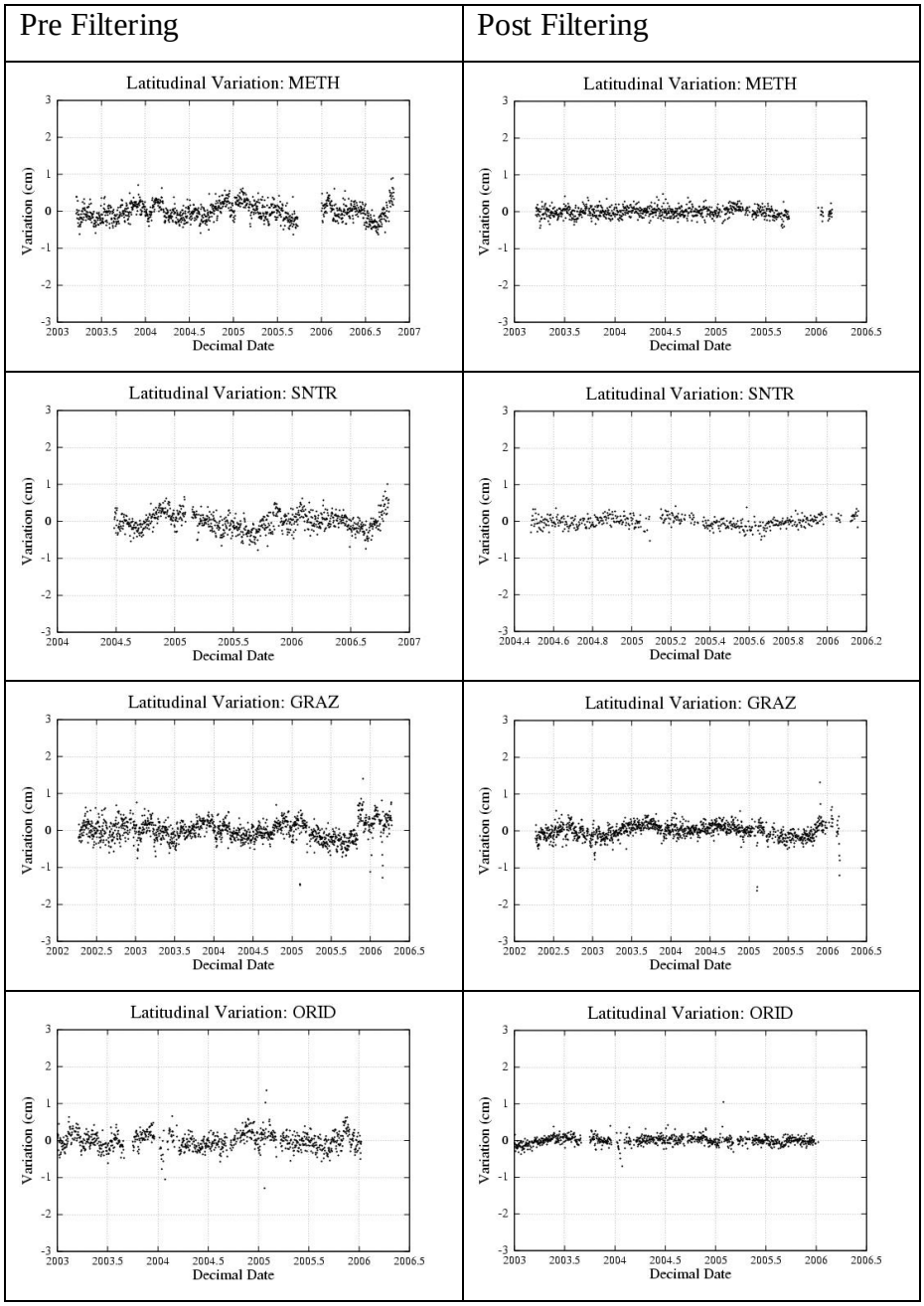

Figure 4.18: Pre and post filtered time series showing the effect of the Aegean regional filter on a selection of CGPS stations.

0.1 Sigma Frame

The result of the 0.1 sigma frame (see section 4.5.1 for sigma explanation) was a compromise between the Eurasian and Aegean frames as it was comprised of sites from across the region, namely PENC, TUBI, GRAZ, ANKR, DION, ARKI, METH, MATE, XRSO, NICO, SOFI, NEAP, ORID (figure 5.19). The filter showed a number of effects, all the time series were improved in terms of scatter but only served to reduce the effect of common mode errors at each site without removing them completely. The annual signals present before filtering were all still present afterwards (figure 4.20). These annual signals are examined in greater detail in section 4.7.

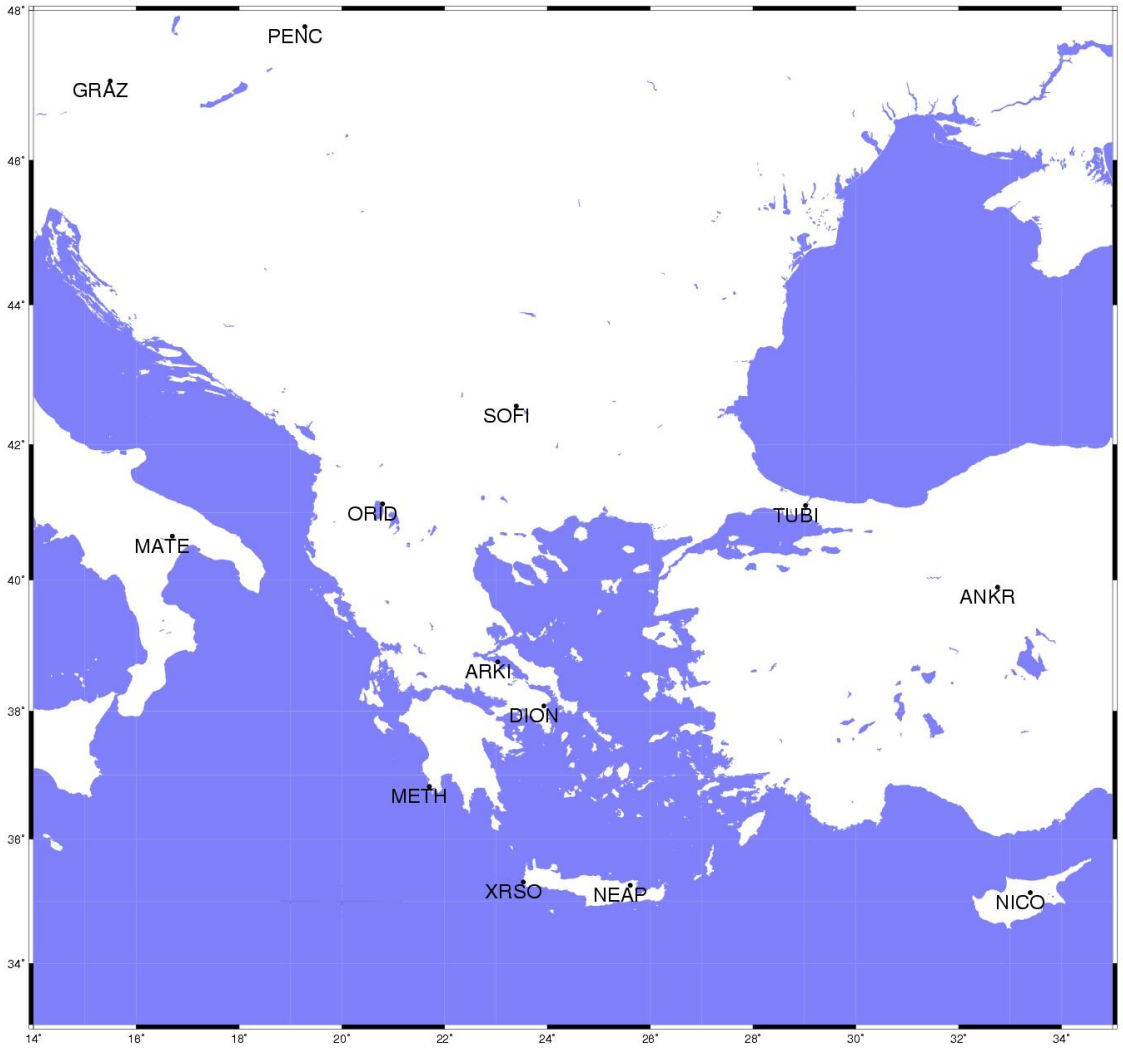

Figure 4.19: The stations used in the construction of the 0.1 sigma regional filter.

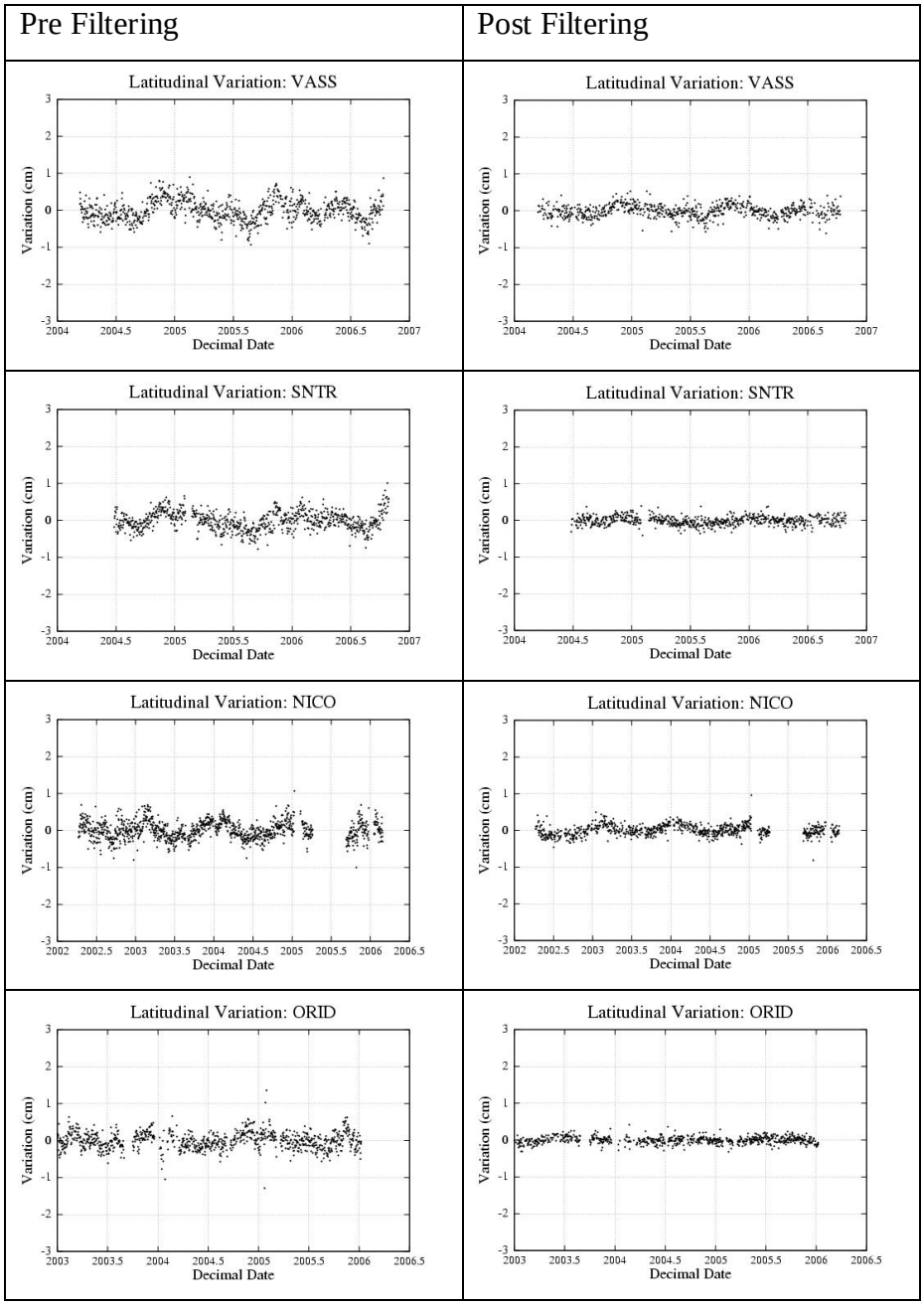

Figure 4.20: Pre and post filtered time series showing the effect of the 0.1 sigma regional filter on a selection of CGPS stations.

1.0 Sigma Frame

As would be expected the 1.0 sigma regional filter (see section 5.5.1 for sigma explanation) exhibited results almost identical to those produced by the 0.1sigma frame. Both the filters shared 13 sites (PENC, TUBI, GRAZ, ANKR, DION, ARKI, METH, MATE, XRSO, NICO, SOFI, NEAP, ORID) with an additional 11 sites forming the 1.0 sigma frame (AKYR, KITH, MLOS, VASS, SNTR, MENA, KERY, DUBR, KRYO, ANOP, ATRS), see figure 4.21. Due to their relatively high standard deviations these sites would have little overall affect on the filter due to the weighted nature of the root mean square method of determining the common mode error favoured in the algorithm.

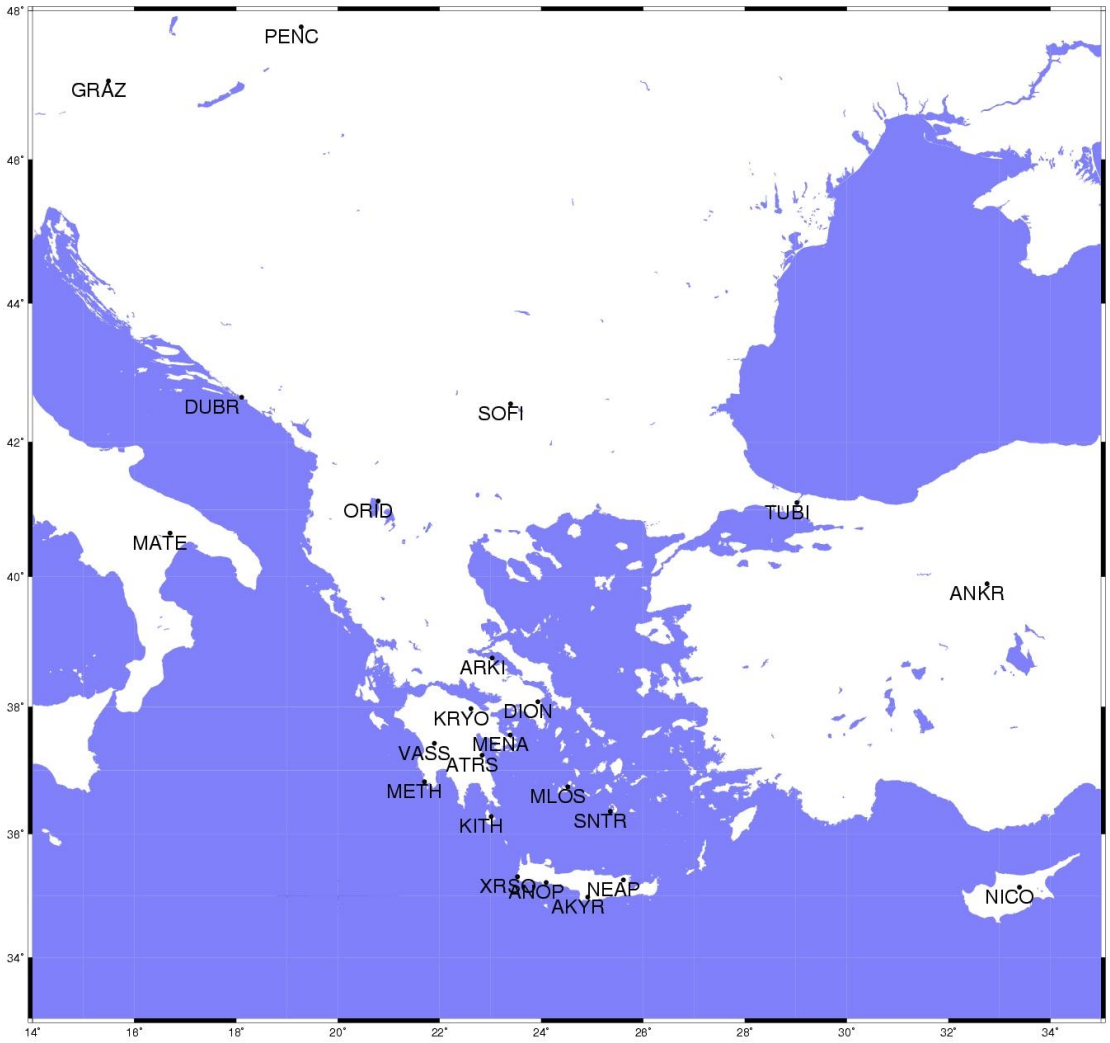

Figure 4.21: The stations used in the construction of the 1.0 sigma regional filter.

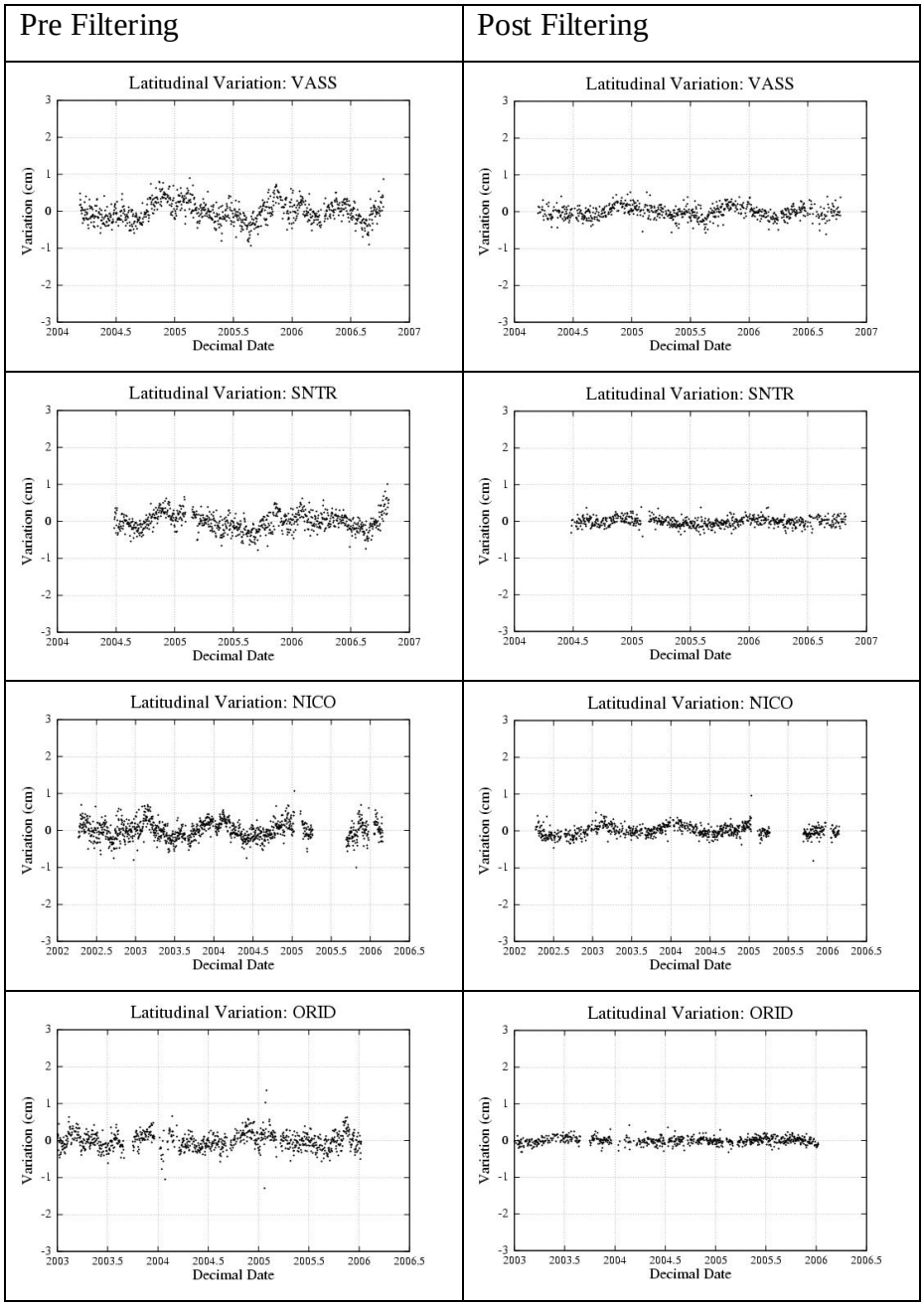

Figure 4.22: Pre and post filtered time series showing the effect of the 1.0 sigma regional filter on a selection of CGPS stations.

The results above (figure 4.22) demonstrated some of the benefits and drawbacks of both the regional filtering process and the area of study. The precision and standard deviation of many of the time series was improved by a factor of approximately 2. Despite this improvement several non-tectonic signals are still present, for example many of the graphs show annual signals with an amplitude of up to 3-4 mm remaining in the time series. The technique provided only a few time series with sufficient accuracy and precision to prove or disprove the presence of silent earthquakes. The lack

of confidence placed in these results due to the variation from one graph to another suggested that alternative post processing techniques should be explored.

4.6.2 Results: Filtered Baseline Method

The technique of differencing errors on a site by site basis has many inherent dangers as mentioned in the methodology, it does however reduce the effect of common mode errors by allowing the user to essentially differentiate stations on a site by site basis. The results of this technique are summarized below with a complete set of results in appendix E.

4.6.2.1 Northing, Easting and Vertical Components

In general the results showed a lot of noise as they suffered from similar decorrelation in their common mode errors on a site by site basis as were exhibited on the regional scales by the use of the regional filtering technique. The holes in the data also had more of an effect using this technique as any data outages at either site caused a null result in the subsequent time series. The regional filter only produced these “no results” when less than three stations were available to form the filter, giving a much higher data return to any time series. Despite this some of the sites did show good correlation and the time series were significantly improved with a great reduction in the scatter (figure 4.23)

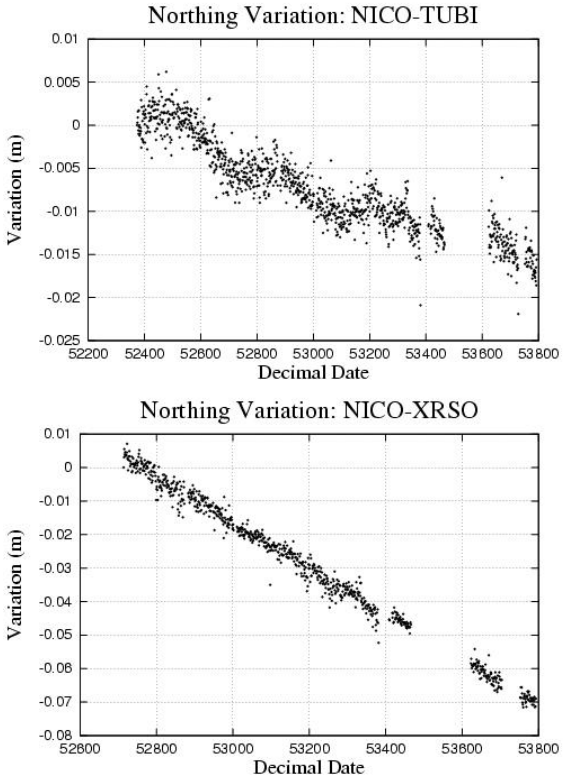

Figure 4.23: The varying results achieved using the filtered baseline method. The graphs both show the movement of sites with respect to NICO on Cyprus. Crete appears to be relatively well correlated whilst TUBI (near Istanbul) still exhibits strong annual signals.

With the number of sites in the COMET network combined with the additional IGS, EUREF and NTU sites the process of identifying which baselines and their components were relevant was potentially labour intensive, therefore initially the baseline analysis was focused on the COMET sites with reference to the longer standing IGS and EUREF sites. Within this a particular emphasis was placed on the nearer reference sites as they potentially would exhibit greater common mode error correlation. The application of the technique for each baseline component resulted in some interesting time series, particularly at the site VASS on the Peloponnese. Below are the time series showing the northerly variation between a number of sites used in the study and VASS (figure 4.24). The figures highlight a number of the problems encountered by the post processing technique, with insufficient data and decorrelated sites giving messy unclear results. The longer time series do however all show some anomalous features, firstly around mjd 53200 then around 53600.

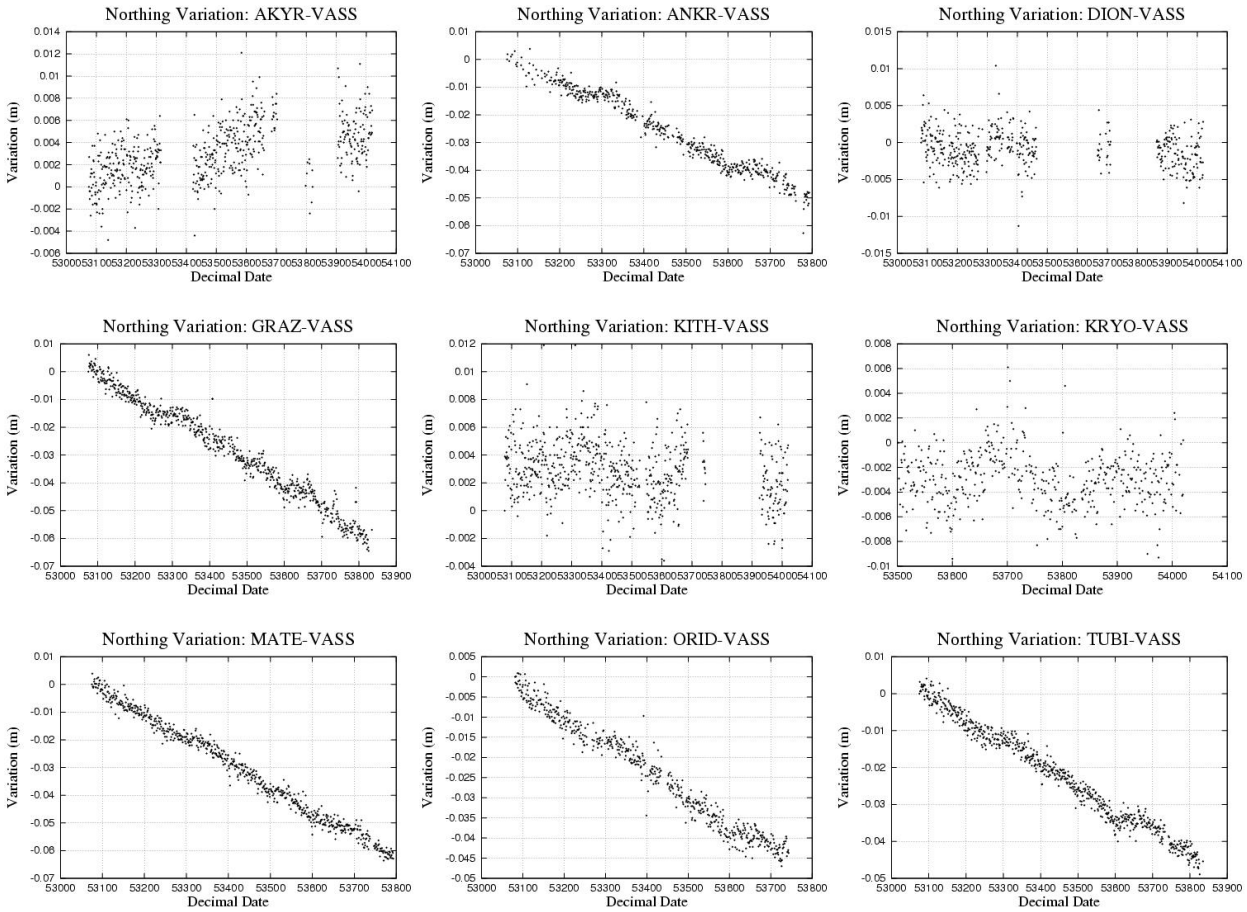

Figure 4.24: Timeseries of northerly variations between COMET, ITRF and EUREF CGPS stations and the COMET station VASS..

Having noted these anomalous northerly movements at VASS, other sites around that area of the Hellenic arc were examined at the same time. Although not as distinct some small but irregular shifts in the time series of a number of sites were observed. These are displayed below (figure 4.24), with details of the timing (mjd), and amount of movement experienced at each site over the stated time in both the north and east components in table 4.7. The values were calculated by fitting a regression line through the data with the start and end days judged by eye from the time series plot as change detection software proved too sensitive to isolate just those events that appear simultaneously at a number sites as well as struggling to define a start and end date for each event. The sigma values in table 4.7 are the standard deviations of the points from the fitted line and therefore give a measure of the data quality rather than a measure of the possible variation in the fitted line and hence velocity of the transient event.

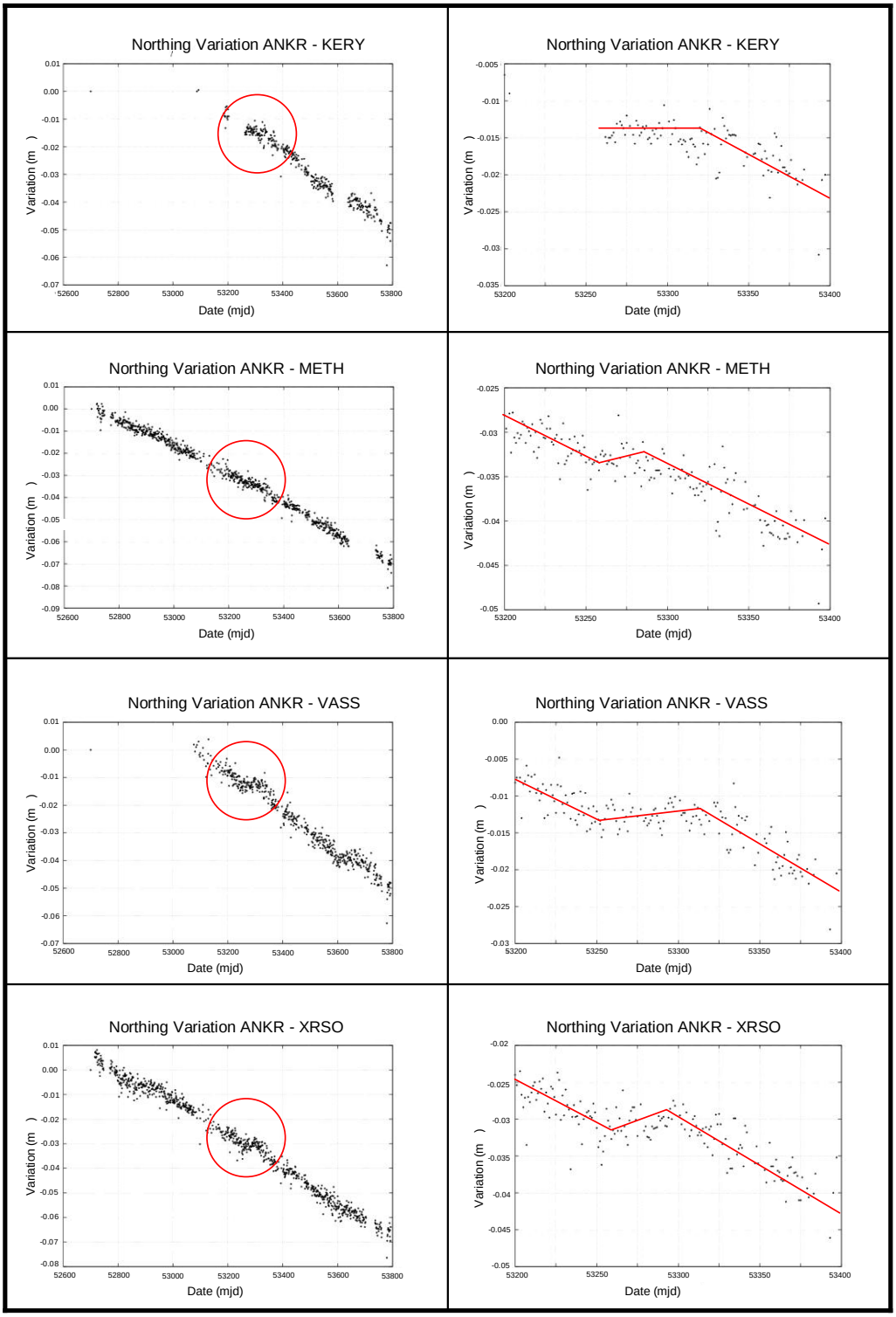

Figure 4.25: Irregularities in the time series of COMET sites around the Hellenic arc, noting that the plots have been stacked above each other to emphasise common events.

Site	Latitude (degrees)	Longitude (degrees)	Start (mjd)	End (mjd)	dN (mm)	Nσ (mm)	dE (mm)	Eσ (mm)
VASS	37.430	21.899	53250	53325	0.45	1.42	2.67	1.97
METH	36.825	21.705	53250	53285	0.82	1.56	0.05	1.75
KERY	36.493	22.384	53262	53300	1.01	1.11	0.48	1.68
XRSO	35.311	23.533	53250	53301	1.61	1.67	0.04	2.30

Table 4.7: Horizontal site displacements during transient events, relative to Ankara (ANKR).

There is also significant evidence to suggest that this was not an isolated event as other transient motion can be seen in the time-series. Figure 4.25 shows similar events occurring, at different times, at sites VASS and XRSO. Again an incomplete set of data for all the sites over the whole time period prevents us seeing if these events occurred throughout the region

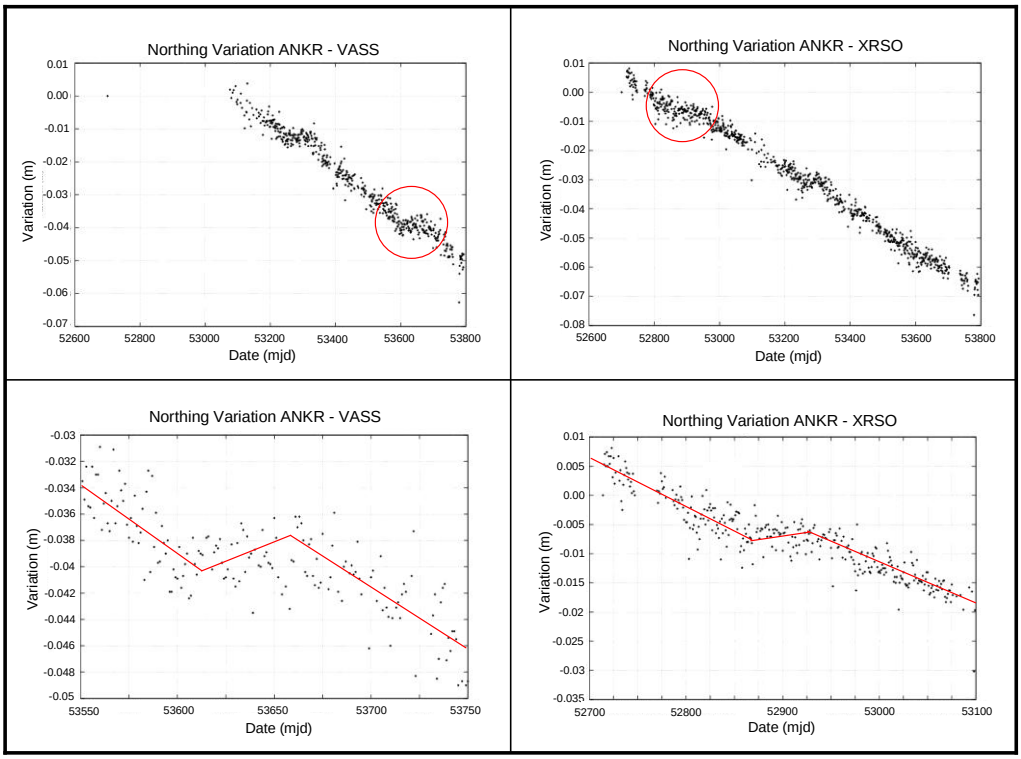

Figure 4.26: Anomalous movements observed in the north component of baselines between ANKR and the COMET network on the Peloponnese.

The extent and significance of these transient motions are looked at in more detail in section 4.7.2 and chapter 7

4.6.2.1 Baselines

As well as looking at the baseline components, the complete variation in the baseline length was examined and the yearly rates of change between each site were determined. This was again achieved by fitting a best fit regression line (using the least squares process, section 4.5.1) to the baseline variation time series between two sites and adjusting this rate to the 365.25 day period. This was performed to determine how the combined variations of all the positional components (east, north and vertical) varied over time, whether this exhibited any patterns at any temporal regime and also allowed the calculation of the strain rates for each baseline in the network. It is only with knowledge of strain in an area that an accurate picture of the seismic regime and hence risk can be compiled and assessed. The results of this can be seen in table 4.8 with a summary in figure 4.26.

BASELINE	Meters per year	Standard Deviation	BASELINE	Meters per year	Standard Deviation
AKYR - ATRS	-0.0022	0.00239	GVDS - METH	0.0011	0.00143
AKYR - KERY	0.0019	0.00217	GVDS - MLOS	-0.0025	0.00164
AKYR - KRYO	-0.0006	0.00185	GVDS - SNTR	-0.0019	0.00153
AKYR - MENA	0.0011	0.00214	GVDS - XRSO	0.0021	0.00287
AKYR - METH	0.0048	0.00205	KERY - KITH	-0.001	0.00258
AKYR - MLOS	0.0015	0.00169	KERY - KRYO	0.0021	0.00204
AKYR - NEAP	-0.002	0.00219	KERY - MENA	0.0004	0.00209
AKYR - SNTR	-0.0004	0.00171	KERY - METH	0.0027	0.00177
AKYR - XRSO	0.0017	0.00261	KERY - MLOS	0.0005	0.00192
ANOP - ATRS	-0.0062	0.00357	KERY - NEAP	0.0009	0.00253
ANOP - KERY	-0.0023	0.00262	KERY - SNTR	0.001	0.00195
ANOP - KRYO	-0.0024	0.00271	KERY - XRSO	-0.0007	0.00251
ANOP - MENA	-0.0017	0.00289	KERY - VASS	0.003	0.00216
ANOP - METH	0.0001	0.00252	KITH - KRYO	-0.0013	0.00173
ANOP - MLOS	-0.0012	0.0024	KITH -MENA	-0.0014	0.00244
ANOP - SNTR	-0.0004	0.00171	KITH -METH	0.0022	0.0022
ANOP - XRSO	-0.0013	0.00247	KITH -MLOS	0.0006	0.0022
ARKI - ATRS	0.0123	0.00251	KITH - SNTR	0.0013	0.00205
ARKI - KERY	0.0102	0.00277	KITH - XRSO	0.0007	0.002
ARKI - KRYO	0.01	0.00227	KRYO - MENA	-0.0007	0.00183
ARKI - MENA	0.0073	0.00229	KRYO - METH	0.0029	0.00157
ARKI - METH	0.0101	0.00252	KRYO - MLOS	-0.0015	0.0016
ARKI - MLOS	0.0032	0.00189	KRYO - NEAP	0.0006	0.00218
ARKI - SNTR	0.0034	0.00199	KRYO - SNTR	0.0001	0.00171
ARKI - XRSO	0.0053	0.00285	KRYO - VASS	0.0038	0.00198
ATRS - DION	0.0031	0.00231	KRYO - XRSO	-0.001	0.00223
ATRS - GVDS	-0.0041	0.00191	MENA - METH	0.0023	0.00198

ATRS - KERY	-0.0006	0.00224	MENA - MLOS	0.0006	0.00189
ATRS - KITH	-0.0037	0.00206	MENA - NEAP	0.0011	0.00237
ATRS - MENA	0.0009	0.00189	MENA - SNTR	0.001	0.00197
ATRS - METH	0.0023	0.00206	MENA - VASS	0.0026	0.00228
ATRS - MLOS	-0.0014	0.00232	MENA - XRSO	-0.0014	0.0025
ATRS - NEAP	-0.0015	0.00321	METH - MLOS	0.003	0.00146
ATRS - SNTR	-0.0011	0.00248	METH - NEAP	0.0044	0.00239
ATRS - VASS	0.005	0.00248	METH - SNTR	0.0039	0.00159
ATRS - XRSO	-0.0039	0.00307	METH - VASS	-0.0004	0.00179
DION - KERY	0.0024	0.00272	METH -XRSO	0.0025	0.00233
DION - KRYO	0.0021	0.00242	MLOS - NEAP	0.0017	0.00215
DION - MENA	0.0018	0.00284	MLOS - SNTR	0.0012	0.00161
DION - METH	0.0038	0.00249	MLOS - VASS	0.0022	0.00185
DION - MLOS	0.0002	0.00214	MLOS - XRSO	-0.0007	0.002
DION - SNTR	0.0017	0.00211	NEAP - SNTR	0.0004	0.00209
DION - XRSO	0.0005	0.00276	NEAP - XRSO	0.0008	0.003
GVDS - KERY	0.0021	0.00167	SNTR - VASS	0.0033	0.00197
GVDS - KRYO	-0.0018	0.0013	SNTR - XRSO	-0.0009	0.00213
GVDS - MENA	-0.0093	0.00229	VASS - XRSO	0.0007	0.00254

Table 4.8: Annual Baseline variations of the COMET sites.

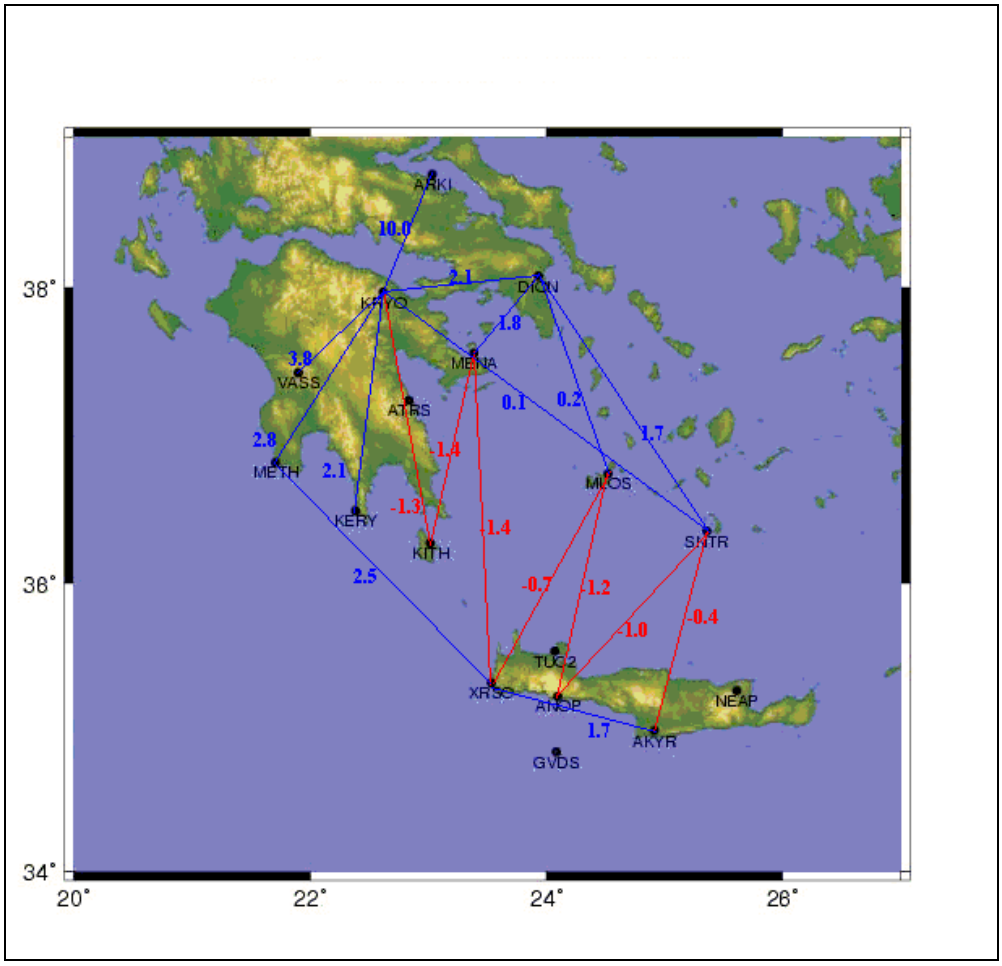

Figure 4.27: Selected Annual baseline variations (mm/yr) of the COMET network, showing the expansions (blue) and contractions (red) within the Aegean.

The results show small but significant variations in the southern Aegean with east – west arc parallel expansion and baseline shortening between Crete and Cyclades Islands.

4.7 Analysis

The initial results were very encouraging with the discovery of transient signals and baseline variations. However from the results of the general processing and the subsequent application of a range of filters, both regional and the filtered baseline method, it was clear that no single technique was cleaning all the data to the desired level as well as maintaining sufficient integrity that any observed signals were real events and not products of the post processing techniques applied.

The obvious reason for these discrepancies was initially presumed to be either the quality of the data, multipath or the decorrelation of the common mode errors on an area by area and site by site basis. To analyse this further a simple Fourier series was fitted to the data.

The technique applied looked to estimate the phase angle (φ) and amplitude (A) of a curve fitted by least squares to each of the latitudinal, longitudinal and radial time series of each site. The time series displayed in chapter 6 each often displayed a strong annual component which it was hoped could be defined and possibly removed in this manner.

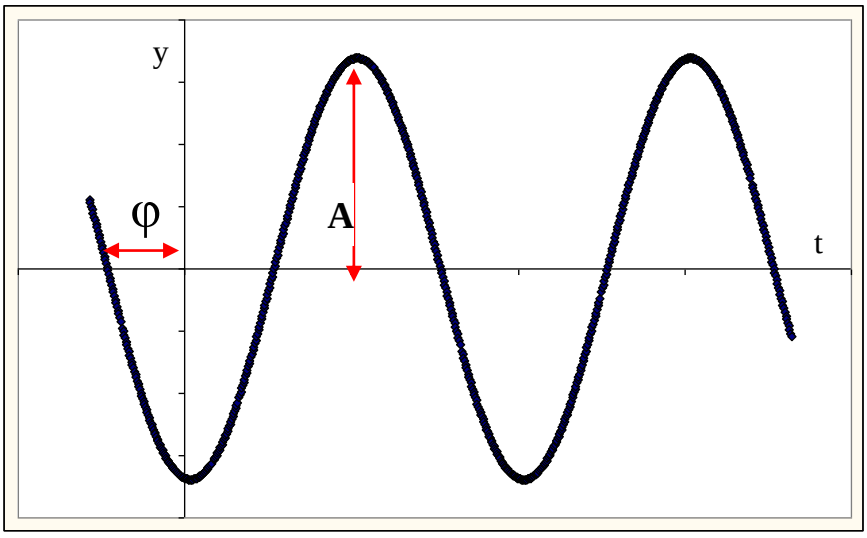

The line fitted followed the equation:

$$y = A\sin(\omega t + \varphi) \tag{4.7}$$

where

A = Amplitude

Φ = Phase offset (from nominal)

$$\omega = 2\pi f$$

$$f = \frac{1}{T}$$

These assumed that much of the common mode error was linked to the annual signals seen in the initially processed data (section 4.6). The nominal period (T) was therefore set at one year. This technique did on the whole closely mimic the changes in the annual signals observed at each site thereby reducing the standard deviation of each site (table 4.9)

	Latitude	Latitude Fourier curve	Longitude	Longitude Fourier curve	Radial	Radial Fourier curve
AKYR	0.26	0.23	0.22	0.24	0.64	0.62
ANKR	0.24	0.23	0.27	0.26	0.73	0.71
ANOP	0.33	0.30	0.26	0.26	0.82	0.82
DION	0.28	0.27	0.29	0.28	0.90	0.83
GRAZ	0.27	0.25	0.25	0.24	0.70	0.62
KERY	0.28	0.23	0.27	0.26	0.75	0.75
KITH	0.26	0.22	0.25	0.25	0.67	0.66
KRYO	0.25	0.24	0.26	0.25	0.71	0.63
MATE	02.4	0.23	0.26	0.25	0.67	0.66
MENA	0.3	0.25	0.24	0.24	0.74	0.72
METH	0.23	0.20	0.25	0.25	0.62	0.62
MLOS	0.25	0.23	0.23	0.22	0.69	0.69
NEAP	0.34	0.32	0.3	0.30	1.03	0.97
PENC	0.27	0.27	0.34	0.37	1.09	1.10
SNTR	0.25	0.22	0.23	0.23	0.67	0.67
VASS	0.29	0.25	0.24	0.24	0.81	0.78
XRSO	0.29	0.24	0.31	0.30	0.73	0.72

Table 4.9: The Standard deviations for each time series before and after reduction using a best fit first order Fourier curve.

This can be seen visually in the plots of these fits (figure 4.27). Although they are not perfect fits, being formed from first order terms, they do show the distinct annual variation that is present in much of the time series.

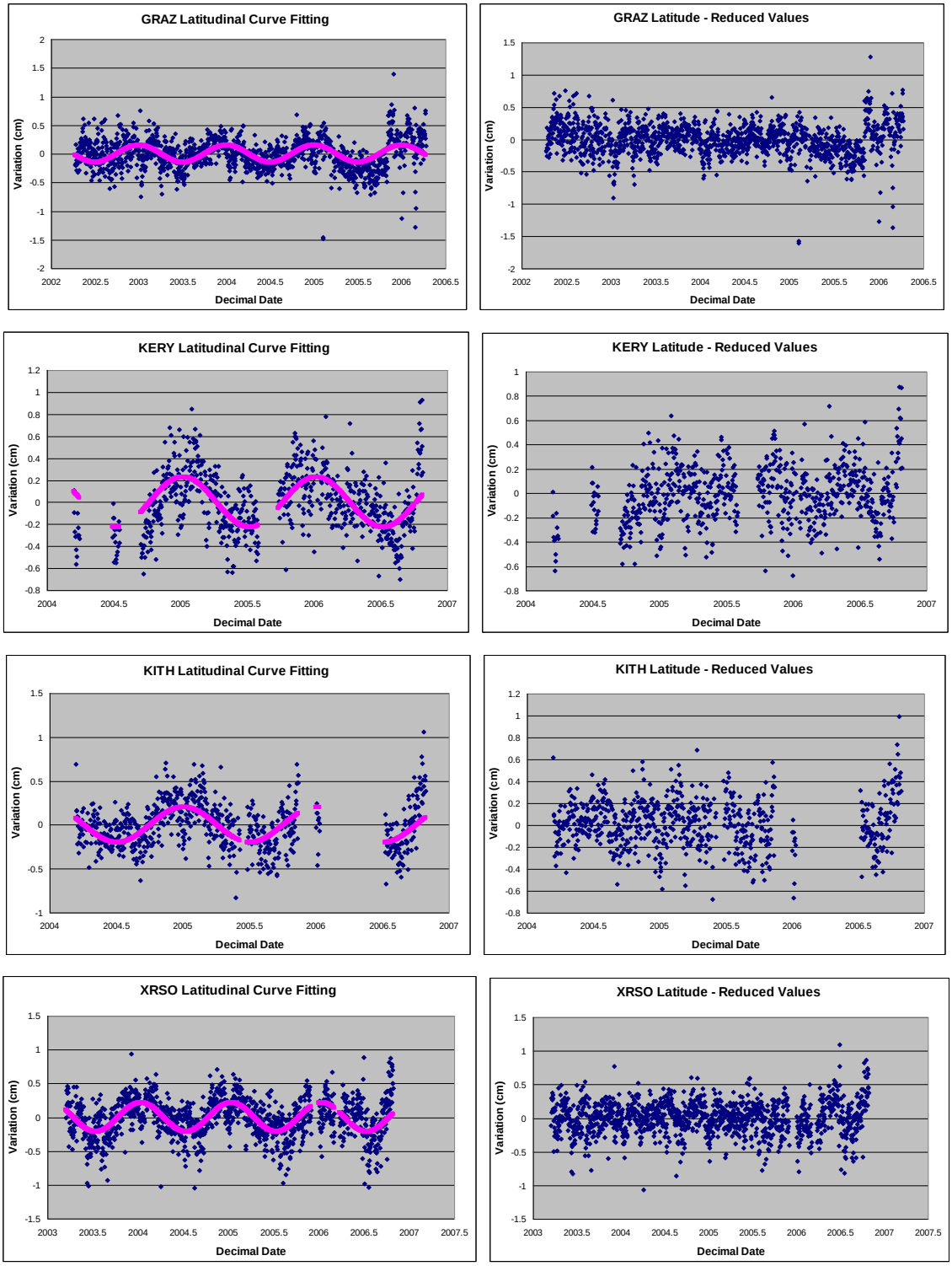

Figure 4.28: Examples of time series with first order Fourier curves fitted and the resulting time series of reduced values produced by differencing the raw data from the best fit curve.

Having established the presence of these annual variations the amplitudes and their phase offsets from the nominal time (the 1st of each year) can be compared (see table 4.10 and figure 4.28).

SITE	**latitude**		**longitude**		**radial**	
	Phase offset from nominal value (days)	Amplitude (cm)	Phase offset from nominal value (days)	Amplitude (cm)	Phase offset from nominal value (days)	Amplitude (cm)
AKYR	75.2	0.174	27.7	0.104	-121.0	0.247
ANKR	51.4	0.101	-30	0.111	-122.3	0.393
ANOP	52.3	0.166	-59.8	0.015	-164.0	0.129
DION	86.3	0.119	31.0	0.086	-117.8	0.489
GRAZ	90.4	0.149	-81.3	0.05	-119.3	0.513
KERY	83.9	0.228	50.0	0.091	-69.2	0.035
KITH	88.6	0.201	-87.1	0.042	-107.8	0.203
KRYO	53.2	0.118	67.5	0.063	-160.3	0.425
MATE	-90.6	0.132	78.9	0.08	-106.0	0.354
MENA	68.2	0.204	-1.6	0.064	-153.1	0.212
METH	81.0	0.153	2.5	0.043	-126.2	0.088
MLOS	88.0	0.127	11.7	0.061	-70.1	0.109
NEAP	60.0	0.178	-55.9	0.031	-114.8	0.496
PENC	-82.2	0.042	103.0	0.08	-119.1	0.269
SNTR	75.9	0.162	-43.3	0.031	-49.9	0.084
SOFI	-87.6	0.035	31.7	1.869	46.5	0.246
TUBI	-84.9	0.169	118.2	0.74	-153.2	0.318
VASS	89.9	0.191	53.5	0.064	-151.5	0.245
XRSO	78.7	0.215	-10.7	0.07	-75.7	0.113
mean	40.9	0.15	10.8	0.19	-108.1	0.26
σ	68.7	0.05	60.2	0.43	49.5	0.15

Table 4.10: The Amplitudes and phase offsets of each of the best fit Fourier curves.

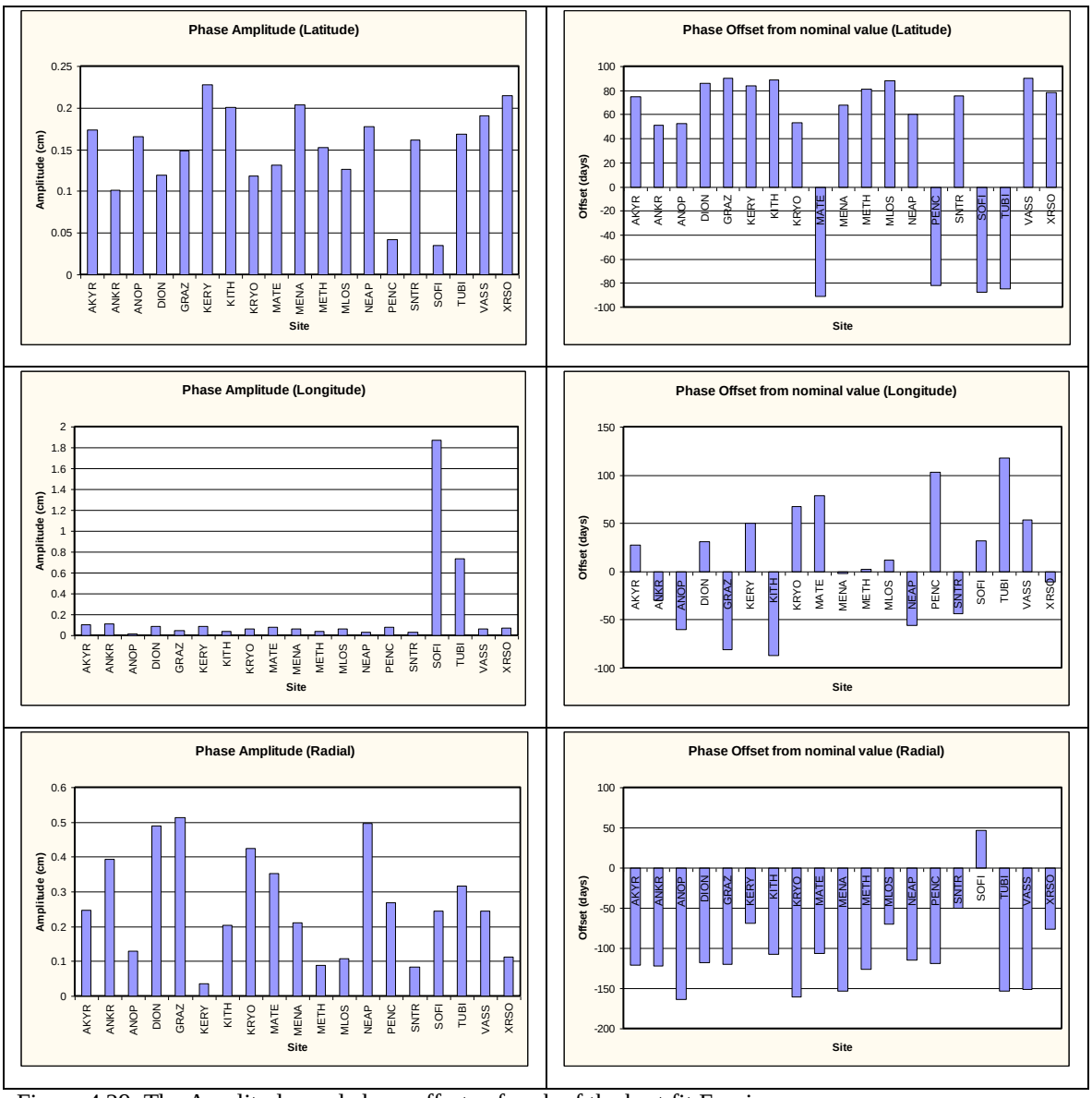

Figure 4.29: The Amplitudes and phase offsets of each of the best fit Fourier curves.

The results of this Fourier series analysis initially appear to have little coherence, the results do show a wide range of values both in terms of amplitude and phase offset. There are however a number of loosely constrained patterns within the data.

The phase offsets from the nominal date in the latitude show a distinct split between those sites in the Aegean area and those located on the Eurasian plate. The European sites (GRAZ, MATE, PENC, SOFI, and TUBI) with the exception of GRAZ all show negative phase offsets between 82.2 and 90.6 days. This is significantly different to that exhibited by the sites in the Aegean networks which all show positive phase offsets between 51.4 and 89.9. This phase offset between areas is only obvious and coherent in the latitudinal component but would give an initial indication as to the reason why the

European, the 1.0 sigma and the 0.1 sigma regional filters gave unreliable results for the Aegean sites. Offsets of this size (≈ 100 days), far from removing any annual signals could enhance the magnitude of any common mode errors when applied through the regional filtering process. This is illustrated by figure 4.29 which shows a comparison of the best fit curves fitted for NEAP and TUBI. The two sites display similar amplitudes but their phase offsets are significantly different. If we assume that the curve formed here by TUBI is representative of the European sites and that formed by NEAP is representative of the Aegean region. Applying the regional filtering technique whereby the mean offset for any given day (in the example in figure 4.29 the difference from zero on any day) is subtracted from all sites, the resulting offset defined by a filter comprised of NEAP would bear little resemblance to the annual signals at TUBI and would therefore add noise to this signal rather than remove it. The same would be true for a filter defined by NEAP, with the TUBI signal having noise added. If on the other hand a filter was defined using both these sites, the resulting mean offset value would be nearer to zero and would therefore remove no common mode error from any sites on which the filter was subsequently applied. This is obviously an extreme case using two sites with significantly different phase offsets which were estimated in a relatively crude fashion. The regional filtering technique takes the average of a number of sites which would average out extremes such as this. It does however demonstrate that great care should be taken when defining the regional filter as systematic differences such as the latitudinal variance between the Aegean and sites located on Eurasia will have an effect on results.

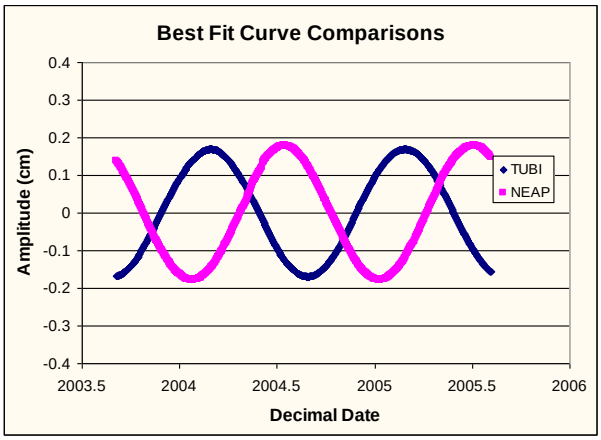

Figure 4.30: An example of sites with uncorrelated annual signals

4.7.1 Filtered Baseline Method: Analysis

As previously mentioned the filtered baseline method of error removal has a number of inherent dangers, it does however reduce the effect of common mode errors by allowing the user to essentially differentiate stations on a site by site basis. This advantage over other techniques such as the regional filtering method was reflected in the results achieved with the cleanest examples of baseline variation and the lowest standard deviations achieved using this method. This reduction of time series noise allowed the realization of the transient tectonic signals observed around the Hellenic arc.

The method is not with out inherent risk as any uncorrelated errors in the time series of either site will filter directly into the resulting baseline through the differencing process. This is clearly seen with the baseline time series involving the site NEAP (figure 4.30). Poor quality data collected by the receiver at NEAP in the first few months after installation (due to equipment error) translates directly into the subsequent baseline time series it forms with other sites around the Aegean using the filtered baseline method. Due to the nature of the technique there is no way of knowing whether the anomalous movements observed in the time series below are real movements or a result of error sources at either NEAP or METH or a combination of the two. For this reason when applying the technique great care and repeated evidence of any time series signal must be collected in order to verify it is a real signal and not the product of the filtering technique.

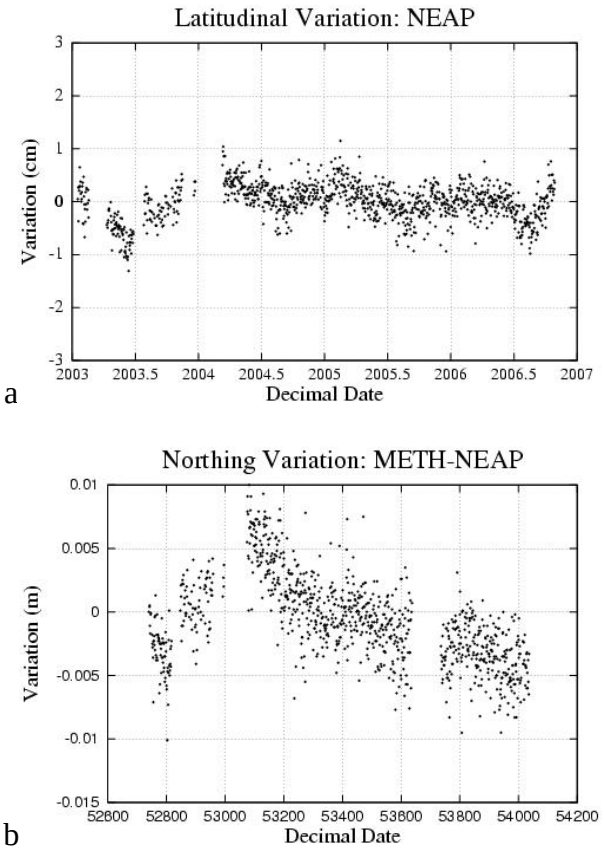

Figure 4.31: Example of poor quality data filtering (a) into site solutions (b) using the filtered baseline method

4.7.2 Aegean Results: Analysis

4.7.2.1 Transient Signals

The transient signals observed at VASS and subsequently observed as a periodically repeating signal at a number of sites around the Hellenic arc were initially thought to be the effect of common mode error variations between the initial baseline sites over which they were observed (ANKR and VASS), due to the approximately annual repeat period over which they occurred. It was the subsequent evidence that they appeared in the time series of a number of the baselines formed between VASS and other greatly varying localities i.e. GRAZ in Austria, ANKR in Turkey and MATE in Italy, that points to a real, observed tectonic movement. Common mode error sources are unlikely to be that well correlated across thousands of kilometers. The other option was that the observed movement was not a real movement at VASS but a product of site specific noise in that area. The discovery of similar but smaller signals in time series of sites around the

Hellenic arc demonstrates that this is not the case. This also makes it harder to compare the sites in close proximity to the Hellenic arc as the differencing process would remove not just the common mode error between the sites but also the transient signal. Comparing with sites in the back arc basin for example MENA and SNTR shows little evidence of the transient event but it may well be hidden by the annual variation that appears between these locations (figure 4.32)

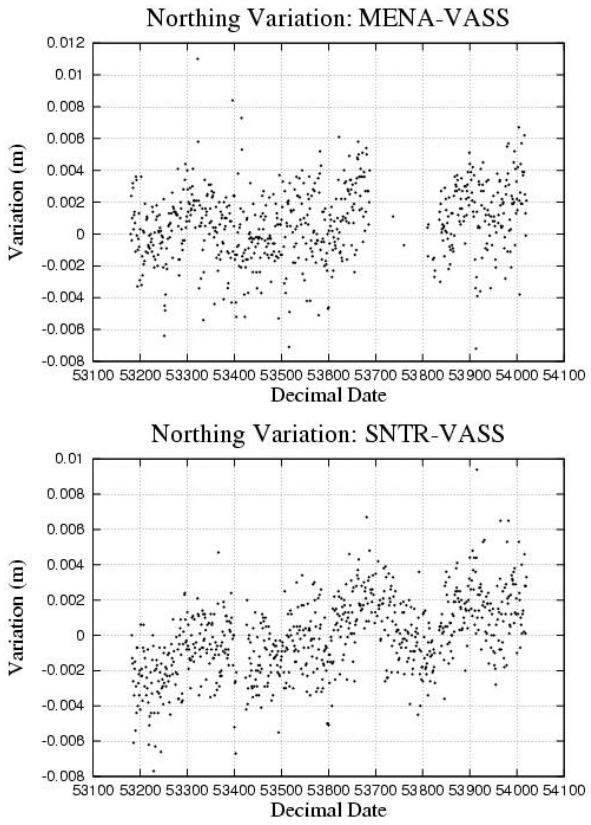

Figure 4.32: Comparisons of baselines formed between VASS and sites located back from the Hellenic arc (MENA, SNTR).

Offering a geological theory for the driving mechanisms behind the observed transient events is beyond the scope of this thesis, instead the author looks to highlight the facts as established in the study:

- The data shows that this motion has been detected approximately simultaneously at four sites that span a 400 km section of crust. This spatial coherence in turn suggests it is related to the Northward underthrusting of the African plate beneath the Aegean, rather than the normal faulting that affects sections of the Peloponnese

- The transient signals are not akin to the silent earthquakes that have been observed in Japan, Cascadia and Mexico. In each of those cases the silent slip event was a reversal of movement oriented towards the plate interface. In this case the transient motion is occurring on a plate that is already rapidly moving towards the subduction interface as the Aegean plate overrides the African lithosphere.
- In addition to this variation in tectonic setting the transients are not so much a reversal of tectonic motion as a pause in an otherwise stably moving part of lithosphere. This variation in motion can be seen in figure 4.33 and the events quantified in table 4.11.

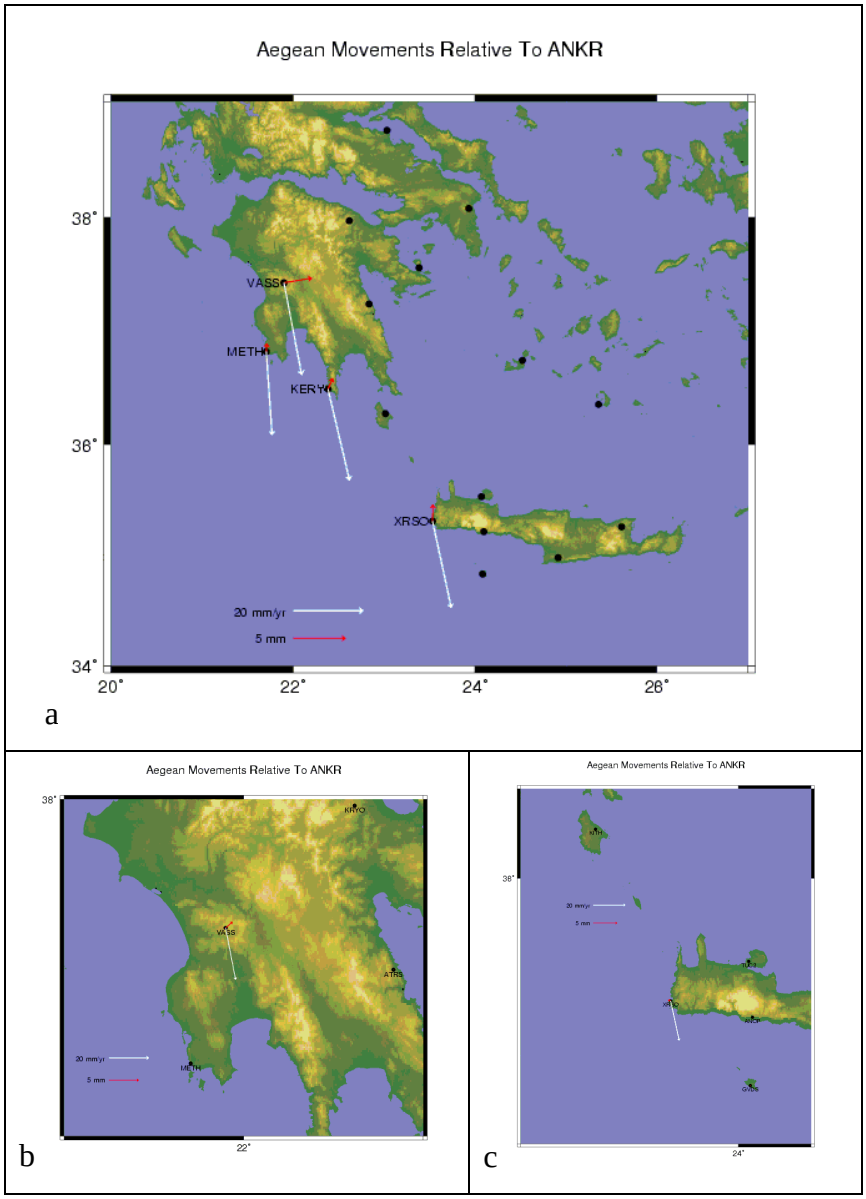

Figure 4.33: Comparison of normal site velocities and orientations (white) with site velocities and orientations during transient events (red). a) mjd 53250, b) mjd 53590, c) mjd 52850

Site	Latitude (degrees)	Longitude (degrees)	Start (mjd)	End (mjd)	dN (mm)	Nσ (mm)	dE (mm)	Eσ (mm)
XRSO	35.311	23.533	52850	52900	0.04	3.35	1.61	1.93
VASS	37.430	21.899	53250	53325	0.45	1.42	2.67	1.97
METH	36.825	21.705	53250	53285	0.82	1.56	0.05	1.75
KERY	36.493	22.384	53262	53300	1.01	1.11	0.48	1.68
XRSO	35.311	23.533	53250	53301	1.61	1.67	0.04	2.30
VASS	37.430	21.899	53590	53665	1.05	2.40	1.19	1.69

Table 4.11: Horizontal site displacements during transient events, relative to Ankara (ANKR).

The values were once again calculated by fitting a regression line through the data with the start and end days judged by eye from the time series plot. The sigma values in table 4.7 are the standard deviations of the points from the fitted line and therefore give a measure of the data quality rather than a measure of the possible variation the fitted line and hence velocity of the transient event.

5.7.2.2 Aegean Strain and Crustal Deformation

Despite the relatively short period of data collection at a number of the COMET sites, it was possible to calculate several of the annual baseline variations (figure 4.33a). These in general supported the findings of a number of the authors mentioned in section 2.6 who stated there was expansion across the Hellenic arc as well as in the Peloponnese and across the Gulf of Corinth. The strain rates were calculated using equation 4.8 (*Tarbuck and Lutgens, 1999*):

$$\varepsilon = \frac{\delta l}{l_0} = \frac{l - l_0}{l_0} \tag{4.8}$$

Where:

ε = the strain in the measured direction

δl = the change in length of a line

l_0 = the original length of the crust

l = the current length of the crust

The strain rates calculated are also comparable to previous studies with most strain being shown to occur across the arc and in the Peloponnese which in turn agrees with the strain and seismicity maps of the area. The small but consistent contraction behind the arc is hypothesized to be caused by the underthrusting of the African oceanic lithosphere beneath the Aegean microplate.

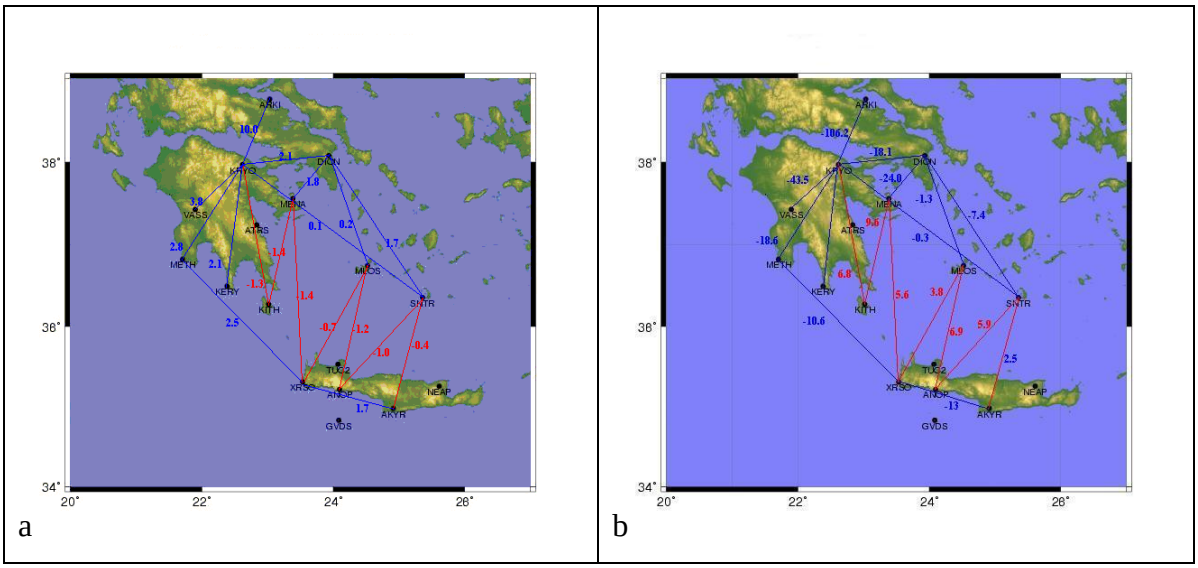

Figure 4.34: a) Annual site to site baseline variation (mm) All the standard deviations for these rates were +/- 0.1mm/yr. Baseline expansion (blue) and contraction (red). b) The corresponding strain (nstrain / yr). Expansive strain (blue) and contraction (red).

The results tend to confirm the findings of previous studies (*Kahle et al 1998; Hollenstein, 2007*) but it should be noted that with more time the study of the strain within the Aegean using the COMET network will improve. This study only looks at the mean deformation per unit time (nstrain / yr), an alternative is to look at the accumulated strain. That is the strain accumulated since a specific starting point. This allows the study of deviations from a uniform, time proportional increase in strain to non-linear or transient features such as seismic events or changes in the aseismic slip rates. In the future this may allow a better understanding of whether there are non-linear changes in the strain field prior to, or post a seismic event, how much strain must accumulate on a particular fault or baseline before an earthquake and is there an upper threshold to this strain accumulation.

It has not been possible to answer these questions using the GPS data collected to date. Although there was the Kythira fault earthquake on the 8th January 2006, there was no

obvious strain variation leading up to the earthquake and there have been no significant quakes on the fault since to enable an estimate of the strain threshold of the Kythira fault using the COMET network. Any strain detected by baselines in the area is hard to attribute to a single fault as the COMET sites are generally located at least 50 km apart and therefore any baseline variation would encompass the strain on all faults around those sites.

The Aegean has long been known to be moving at approximately 35mm yr SSW with respect to Eurasia. Variation in this movement on a site by site basis derived from numerous campaign and CGPS studies has lead to numerous kinematic models for Aegean tectonics (*Taymaz et al. 1991; Le Pichon et la, 1995; Armijo et al. 1996; McClusky et al. 2000; Goldsworthy et al. 2002; Nyst and Thatcher, 2004*). Each of these studies divided the area into a number of different microplates or zones which showed coherent movement. The most recent of these studies by Nyst and Thatcher (2004) hypothesized four microplates in the area with the Anatolian microplate, a Sea of Marmara block, Central Greece and a Southern Aegean plate (figure 4.35)

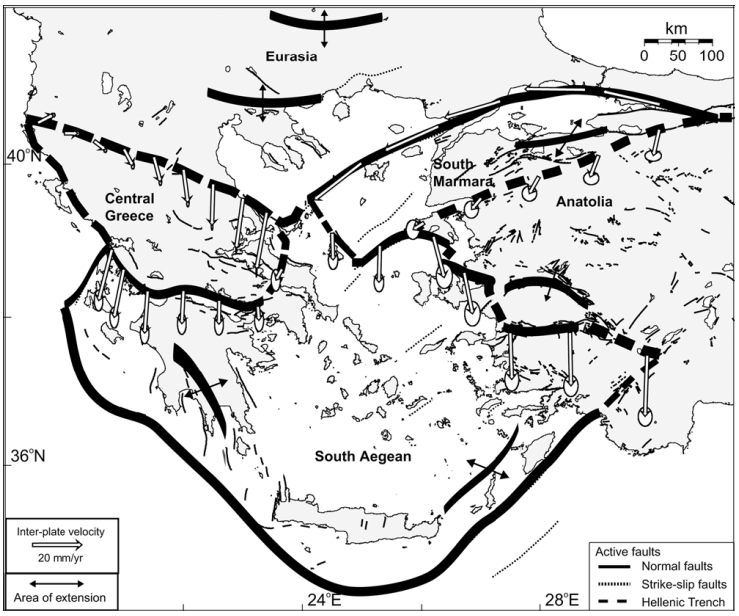

Figure 4.35: The Nyst and Thatcher 2004 model for block motions in Greece (2004)

The results of the site movements relative to Eurasia (GRAZ) determined by this study can be seen in figure 4.36 with a summary of these movements in tables 4.12 and 4.13. The results show a strong agreement with many of the studies. The whole of the southern part of the Aegean does appear to move as a coherent block with little variation in both the bearing and speed with which the sites move relative to Eurasia.

The exceptions to this are the sites ARKI, ATRS, DION and KRYO. ARKI and DION show different speeds, whilst ATRS and KRYO show significantly different bearings as they head in a more southerly direction relative to Eurasia. The different velocities of ARKI and DION are explained by the proximity of the normal faulting along the Gulf of Corinth which as seen from the baseline estimates is expanding at a rate of approximately 10 mm a year. This expansion lessens the further east you go which accounts for the greater velocity at DION. DION is located on the South Aegean block in Thatcher and Nyst's microplate model of the Aegean although this velocity difference combined with a slightly more southerly bearing (206.5º compared with 215.1º) may suggest it is on a different block or part of a broader band of deformation.

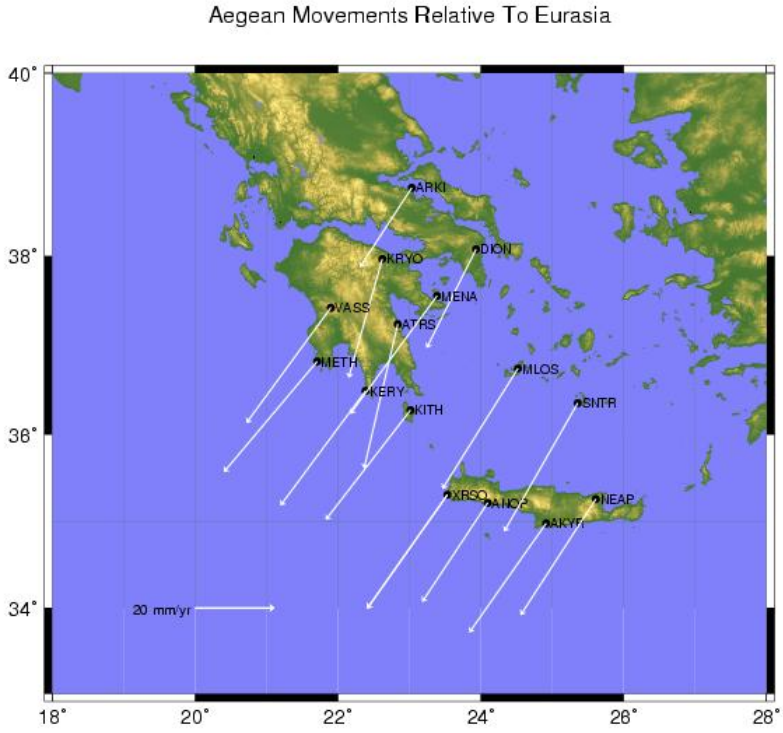

Figure 4.36: Annual movements of the COMET network relative to Eurasia

Aegean Site	Movement relative to Eurasia (m / yr)	Bearing of Movement	Time over which annual baseline velocities were calculated (days)
AKYR	0.0337	215.1355	747
ANOP	0.0299	213.4720	393
ARKI	0.0240	213.1701	1461
ATRS	0.0374	193.1416	328
DION	0.0279	206.5480	1337
KERY	0.0359	216.5797	757
KITH	0.0349	217.7051	668
KRYO	0.0312	195.8184	333
MENA	0.0369	216.3411	655
METH	0.0365	220.1259	1116
MLOS	0.0360	212.1250	650
NEAP	0.0349	212.9822	1179
SNTR	0.0374	209.8074	653
VASS	0.0361	216.2316	760
XRSO	0.0351	215.1988	1050

Table 4.12: Annual horizontal site displacement rates and bearings of the COMET sites and DION relative to Eurasia (GRAZ)..

Aegean Site	Easting variation relative to Eurasia		Northing variation relative to Eurasia		Time over which annual baseline velocities were calculated (days)
	M / yr	σ	(m/yr)	σ	
AKYR	-0.0194	0.0022	-0.0275	0.0022	747
ANKR	-0.0244	0.0029	0.0005	0.0030	1418
ANOP	-0.0165	0.0023	-0.0250	0.0027	393
ARKI	-0.0131	0.0031	-0.0201	0.0031	1461
ATRS	-0.0085	0.0024	-0.0364	0.0026	328
DION	-0.0125	0.0028	-0.0249	0.0027	1337
KERY	-0.0214	0.0033	-0.0289	0.0028	757
KITH	-0.0214	0.0029	-0.0276	0.0024	668
KRYO	-0.0085	0.0025	-0.03	0.0028	333
MENA	-0.0219	0.0031	-0.0297	0.0027	655
METH	-0.0235	0.0027	-0.0279	0.0022	1116
MLOS	-0.0191	0.0030	-0.0304	0.0026	650
NEAP	-0.019	0.0036	-0.0292	0.0045	1179
ORID	-0.0032	0.0026	-0.0039	0.0022	1103
SNTR	-0.0186	0.0031	-0.0324	0.0021	653
TUBI	-0.0052	0.0028	-0.0052	0.0022	1461
VASS	-0.0213	0.0032	-0.0291	0.003	760
XRSO	-0.0202	0.0031	-0.0287	0.0028	1050

Table 4.13: Annual horizontal site displacement rates of the COMET and EUREF sites in the Aegean relative to Eurasia (GRAZ).

The sites ATRS and KRYO showed a more southerly movement bearing relative to Eurasia. This was explained by the shorter study period at each of these sites (328 and 333 days respectively). Not having a full year's worth of data, let alone the 2.5 years minimum recommended by Blewitt and Lavallee (2002), left the calculation very open to the influence of annual variations. To test this all the site velocities and bearings were recalculated using the 328 day time period in which data was collected from ATRS (mjd 53507 – 53835). The results of this can be seen in figure 4.37.

The results highlight a number of features. Firstly the affect short time periods can have on the both the velocity and bearing of vectors describing tectonic motion. In addition to this the range of bearings formed by shorter data periods across the Aegean region again shows the variation in the annual signal across the area, for example many of the sites show a strong southerly motion compared with their previously calculated annual velocity and bearings whereas some sites such as KITH, DION and ANOP show little change.

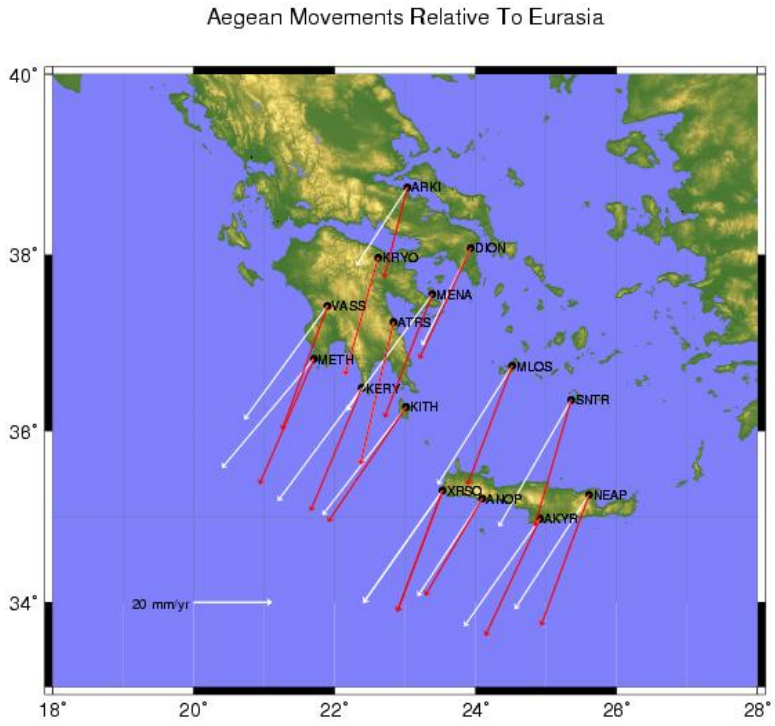

Figure 4.37: Annual movements of the COMET network relative to Eurasia determined from data collected between mjd 53507 and 53835. Movements calculated from all available data (white) and for the 328 day period in which ATRS was active (red).

Summary

This chapter has described the main techniques used to compute subtle tectonic movements in the Aegean using daily site positions. Methods tested for the elimination of common mode error included the regional filtering method and a technique described as the filtered baseline method. These techniques have revealed the presence of transient tectonic signals as well as subtle variations in the baselines and therefore strain rates around the Hellenic Arc. The methods for determining these geophysical signals are analysed and an overview of their benefits and drawbacks is presented.

Chapter 5

Sidereal Filtering

Firstly the chapter introduces sidereal filtering as a multipath mitigation technique, before explaining how this technique was applied in this study. Three case studies are then considered: the Aegean region around the time of the M_w 6.7 event on the 8th of January 2006, located near the island of Kithira and two examples near Macquarie Island, New Zealand which experienced a majoe seismic event during the study period (the M_w 8.1 event on the 23rd of December 2004 and the M_w 6.5 quake on the 10th of November 2007). The chapter is separated into the methods used, results achieved and some analysis and discussion of those results

5.1 Introduction

Most errors affecting short baselines in GPS can be removed or minimised by differencing techniques (*Leick, 2004*). Despite this, multipath and other geometry related error sources such as signal attenuation, signal diffraction, antenna phase center variations and diurnal monument variations remain due to the site-specific nature of CGPS stations and the reflection of the GPS signal off nearby surfaces (*Nikolaidis et al. 2001*).

The principal error source related to receiver - satellite geometry is multipath. This can be mitigated at the point of measurement by the choosing sites without multipath reflectors such as trees and buildings or with the use of choke-ring antennas, but also at the post processing stage for example Axelrad et al (1996) and later Lau and Mok (1999) weighted the data using the signal to noise ratio (SNR) as a measure of the

precision of carrier phase measurements. Satirapod and Rizos (2005) used wavelet decoupling which applied to GPS double difference residuals extracts the GPS carrier-phase multipath. This multipath signature can then be removed from subsequent days if the station environment remains the same.

A number of authors (Genrich and Bock, 1992; Nikolaidis et al. 2001; Choi et al. 2004) have used the sidereal filtering technique. Sidereal filtering is a method of improving the signal to noise ratio when determining geophysical signals over sub daily periods of time, for example volcanic deformation or seismic waves (*Ji et al. 2004*). This requires the removal of error sources normally mitigated by averaging over 12 hours or more of data, in particular those errors associated with site and satellite geometry such as multipath effects (*Bock, 1991; Bock et al. 2000; Choi et al. 2004*). Due to the sidereal repeatability of GPS orbits and hence their groundtracks these errors repeat over the same, approximately daily, basis.

The sidereal filtering is composed of the coordinate residuals to the long term position of a site's positions at a desired epoch rate (i.e., 1Hz). These residuals can be shifted by the nominal sidereal time period (23 hours, 56 minutes, 4 seconds) and subtracted from the site coordinates on a subsequent day to remove error such as multipath which is highly correlated over a number of days provided the same antenna is used in the same reflecting environment. To make this solution more robust the average coordinate residual of a number of days can be calculated by shifting days by the nominal sidereal time period and multiples of that period such that they are siderealy stacked. In this manner an average of the error associated with a particular satellite geometry, at a particular site can be built up and differenced from a period of interest to reduce the noise level inherent in the signal.

It should be noted that although ground tracks are designed to repeat exactly over a sidereal period, in reality satellite repeat periods are not sidereal and vary for different satellites and therefore sidereal filtering has to take this into account (*Choi et al. 2004*). Ragheb et al (2007) state that the optimum geometry repeat lag is 10 seconds faster than the nominal sidereal lag (23 hours, 55 minutes, 54 seconds). Choi et al (2004) state that the optimum geometry repeat lag is ≈ 8-9 seconds faster than the nominal sidereal lag. The optimum geometry is the satellite geometry that is closest to the satellite geometry and hence the ground tracks at a particular epoch the previous day. The orbital

precession of the GPS satellites means that to optimise this repeat of the ground track the orbital period has to be set roughly 4 seconds faster than half-sidereal which accounts for the ≈ 8 second variation noted by these authors.

5.2 Methodology

For the GPS data processing GIPSY was used in an epoch-by-epoch mode originally designed to study the kinematic movement of wave buoys. In this mode GIPSY treats each (30 second) epoch as an entirely independent measurement. For this study the IGS precise orbits and Earth orientation parameters (EOP) were used, in addition the high rate clock solutions (30 second) supplied by JPLwere utilised. The high rate clock solutions are necessary as the IGS and JPL rapid and final clock products traditionally include clock corrections at intervals of five minutes. This can lead to error interpolating the GPS clocks between these five minute points (*Kuang et al. 2006*). As such JPL has developed a technique whereby a range of globally distributed GPS receivers with precise time references (a hydrogenmaser or good rubidium or cesium clock) are able to estimate GPS clock parameters every thirty seconds (*Zumberge et al. 1997*). Using these precise GPS clock estimates far more accurate estimates can be made of site positions on an epoch by epoch basis. The IGS is taking this further by generating five second clock solutions using the same process but with IGS 1 Hz receivers (*Bock et al. 2008*)

GIPSY gives the options to either solve for site positions in a pure kinematic solution in which the coordinates of sites are calculated on an epoch by epoch basis or in a “fixed” base mode in which the coordinates of reference sites are specified *a priori*. The later of these solutions was employed by calculating the *a priori* positions using a precise point positioning solution and ambiguity resolution. The daily site coordinates of the reference stations estimated using PPP with ambiguity resolution were held fixed (constrained to 8 cm) to define a frame in which the variable sites could be observed. In addition one site was chosen to define the system clocks. This site GPS receiver was preferably attached to an atomic clock to enhance reliability (Matera in Italy). Using this method coordinates were determined for a number of sites every 30 seconds.

This process was undertaken for a day of interest, that is when there may be a transient or seismic signal present and for the three or four days preceding that event. Each of the

time signatures of the preceding days were adjusted by the correct nominal sidereal difference (for example 86164 seconds for the previous day, 172328 seconds for the day before that and so on) such that the coordinates could be stacked to determine a coordinate average, taken at each 30 second interval. This average coordinate was then differenced from the coordinates of the day of interest to give the final filtered time series.

This sidereal filter was applied to a number of sites. Firstly examining the site on Macquarie Island (MAC1) on the 23rd of December 2004 when there was the M_w 8.1 earthquake with an epicentre located 500km NNE of the site (50.145°S, 160.365°E). The fixed reference stations in this case were HOB2 (Hobart), OUS2 (Dunedin), MOB2 (Melbourne), STR1 (Stromolo) and SYDN (Sydney). This initial test was carried out in order to test the validity of the technique and whether it could detect significant co and post seismic movement at a major seismic event.

Secondly a number of COMET sites were tested around the M_w 6.7 event on the 8th of January 2006, located near the island of Kithira (see figure 6.1), in particular ANOP (Anapoli), KITH (Kithira), KERY (Kerya), KRYO (Kryoneri), METH (Methoni), MLOS (milos), VASS (Vasses) SNTR (Santorini) and XRSO (Chrisoskalitissa). In this case the reference stations utilised were GRAZ (Graz-Lustbuehel), MATE (Matera), PENC (FOMI Satellite Geodetic Observatory), POTS (Potsdam), RAMO (Mitzpe Ramon) and ZIMM (Zimmerwald)

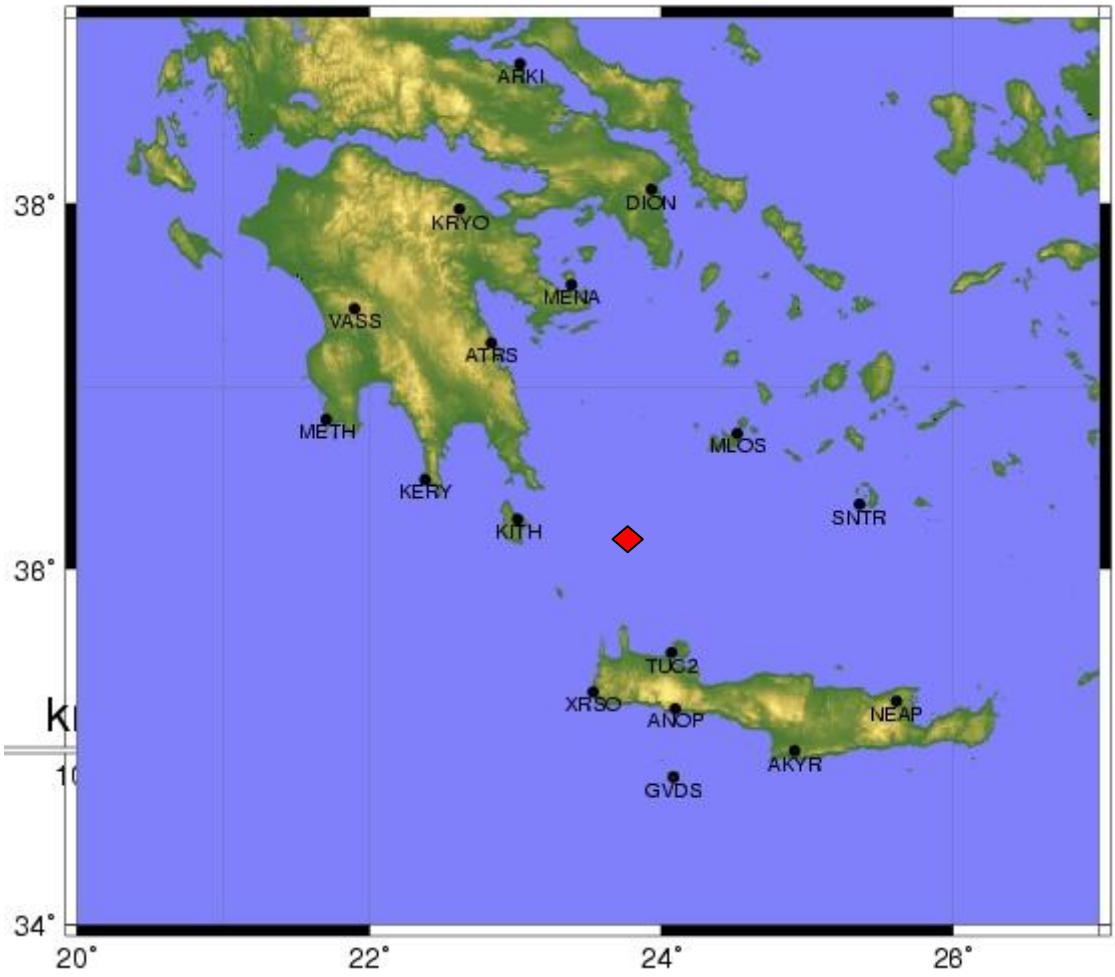

Figure 5.1: Position of the magnitude 6.7Aegean earthquake near Kithira (08, 01, 06).

Further testing was then carried out at another earthquake near Macquarie Island, the M_w 6.5 quake on the 10th of November 2007. This again used the reference sites HOB2 (Hobart), OUS2 (Dunedin), MOB2 (Melbourne), STR1 (Stromolo) and SYDN (Sydney) as the "fixed" points in the instantaneous processing strategy. This was done to compare the results of the southern Aegean event near Kithira with an event of a similar magnitude elsewhere. The positions of both the Macquarie Island quakes can be seen in figure 5.2

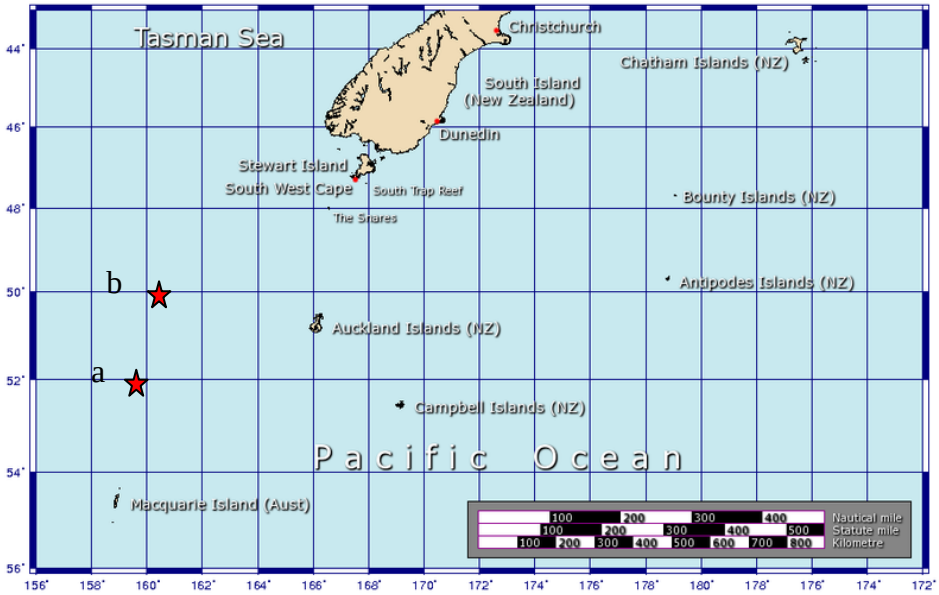

Figure 5.2: The Macquarie 6.5 M_w earthquake with an epicentre at 52.158°S, 159.527°E (a) and the Macquarie 8.1 M_w earthquake with an epicentre at 50.145°S, 160.365°E (b)

5.3 Results

As mentioned before the sidereal filtering technique was applied to a number of sites to determine what could be gained by the use of 1/30Hz data when studying tectonic events with durations of less than a sidereal day, in particular the M_w 8.1 and 6.5 earthquakes off Macquarie Island and the 6.7 earthquake near Kithira in the Aegean.

5.3.1 Macquarie Island (23/12/04)

This initial test was used to determine whether the processing technique achieved its goal of reducing 30 second time series scatter and thereby improving the overall precision of station coordinates by effectively reducing and removing GPS error sources associated with site and satellite geometry such as multipath effects. In addition the method looked to test whether the co and post seismic displacements of a large (M_w 8.1) earthquake could be picked up in the time series.

Figure 5.3 shows the siderealy adjusted time series of the site MAC1 in the days leading up to the quake. Although the figure demonstrates a significant number of outliers on a day to day basis there were also similar trends present. When this day to

day data is stacked, averaged and differenced these underlying trends are removed giving an improved coordinate time series. This improvement can be seen in figure 5.4 which shows the variation in the estimated coordinate time series on the 23rd of December 2004. The plot shows the time series before and after sidereal filtering was applied. From the plot two things are apparent, firstly that the overall scatter and variation of the coordinates was significantly reduced and also that the displacement caused by the earthquake is clearly visible. The standard deviation of each of the positional components (north, east and vertical) can be seen in table 5.1.

Date	North	East	Vertical
20,12,2004	0.011792	0.009436	0.017326
21,12,2004	0.013522	0.00673	0.024389
22,12,2004	0.012052	0.009756	0.019382
23,12,2004	0.013584	0.008698	0.013953
23,12,2004 - Filtered	0.009571	0.006523	0.014605

Table 5.1: Comparison of the Standard deviations (m) of unfiltered and Siderealy filtered time series for the 23, 12, 04 Macquarie Island earthquake.

The above table shows the significant improvement in the overall scatter of the plots after sidereal filtering

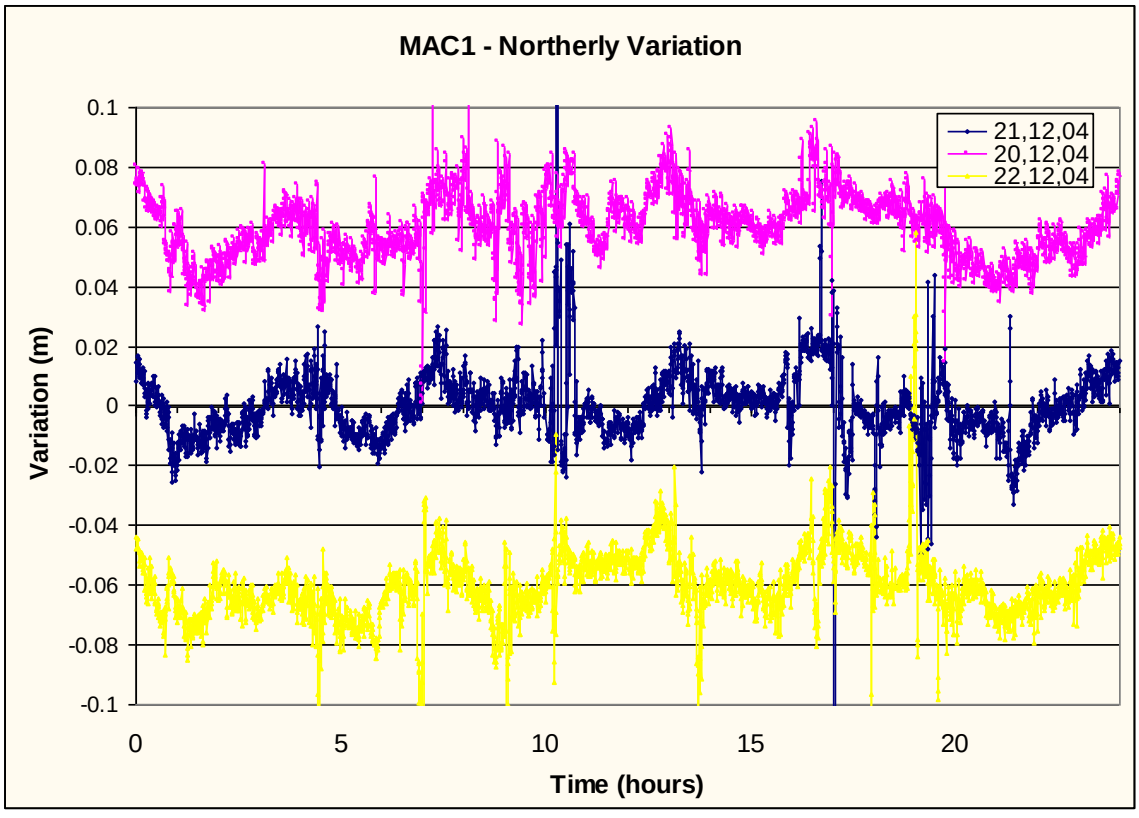

Figure 5.3: Coordinate time series of the days preceding the 23, 12, 04 Macquarie Island earthquake.

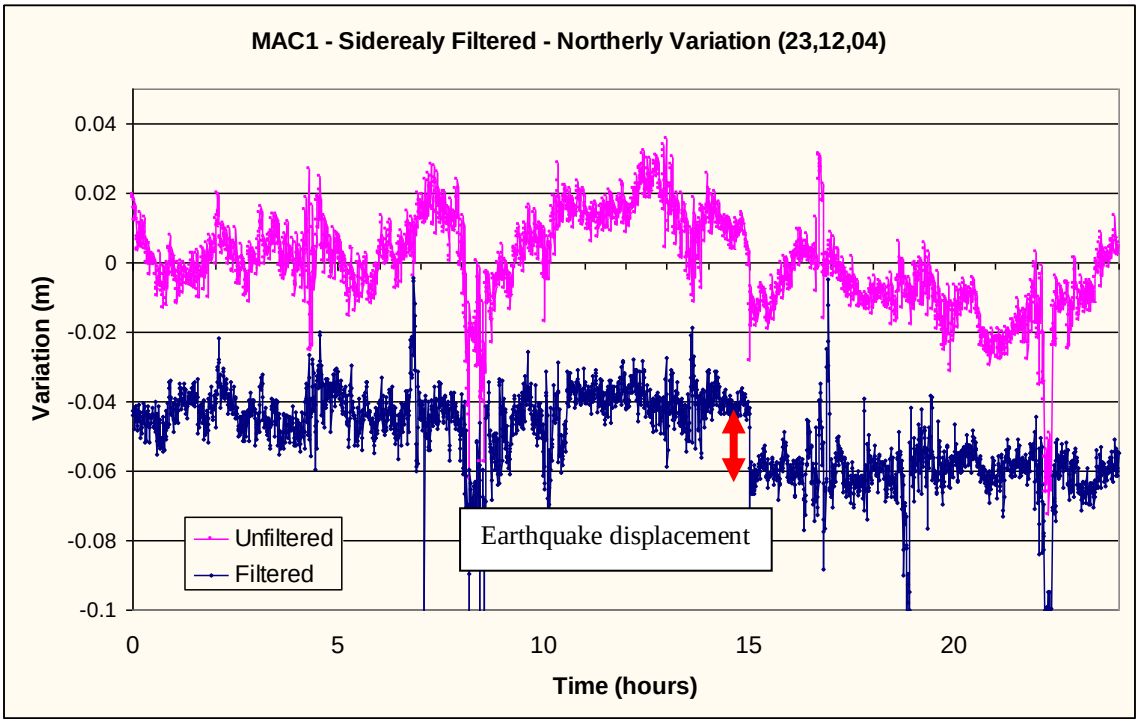

Figure 5.4: Siderealy filtered and unfiltered Coordinate time series of the 23, 13, 04 Macquarie Island earthquake.

5.3.2 Kithira (08/01/06)

With the success in reducing the standard deviation in the time series at Macquarie the same sidereal filtering technique was applied to the largest earthquake to affect the study area over the study period. The M_w 6.7 quake on the 8th of January occurred at 36.300° N, 23.358°E near the island of Kithira. The results can be seen in figures 5.5 and 5.6. Again the technique significantly reduced the residual scatter and hence the standard deviation of the time series (table 6.2), but on this occasion there is no obvious co or post seismic displacement of the earthquake that occurred at 11:34:55 UTC. This is despite witness reports that state that significant co seismic movement was felt as far away as Crete and Athens.

Date	North	East	Vertical
05,01,2006	0.00969	0.007886	0.015081
06,01,2006	0.009559	0.00913	0.016498
07,01,2006	0.009069	0.007253	0.014637
08,01,2006	0.008562	0.007085	0.01458
08,01,2006 Filtered	0.006183	0.005009	0.011744

Table 5.2: Comparison of the Standard deviations (m) of unfiltered and Siderealy filtered time series.

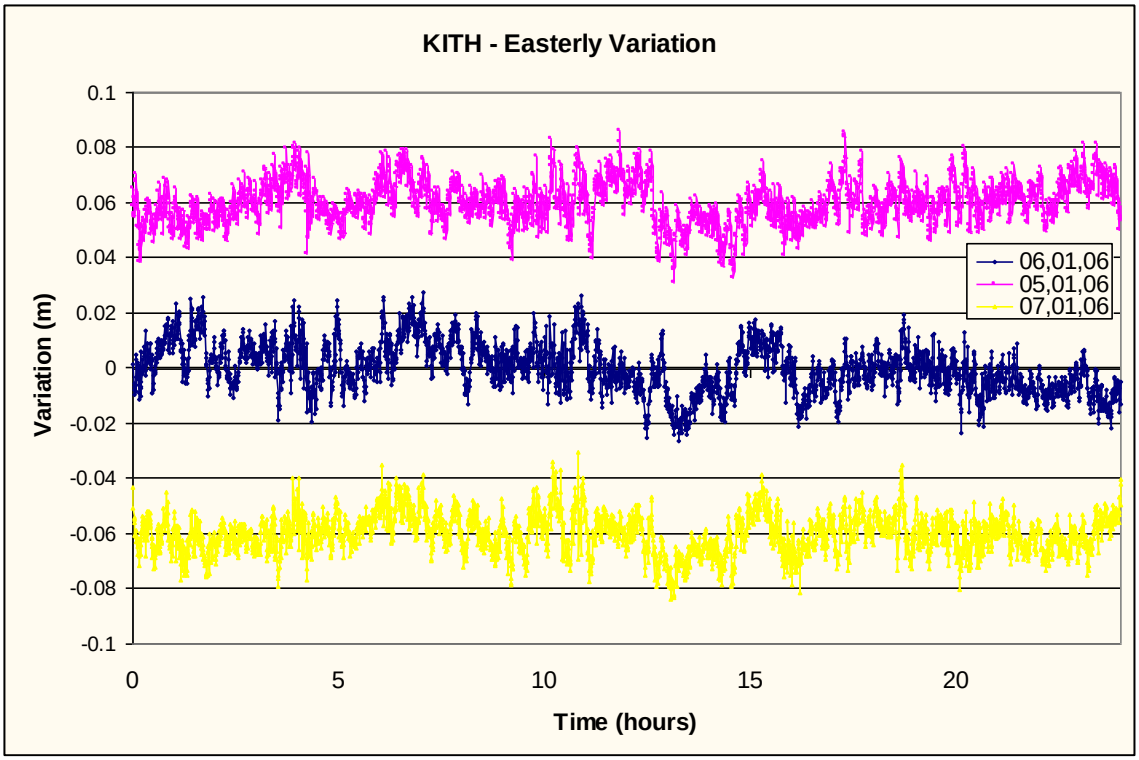

Figure 5.5: Coordinate time series of the days preceding the 08, 01, 06 Southern Aegean earthquake.

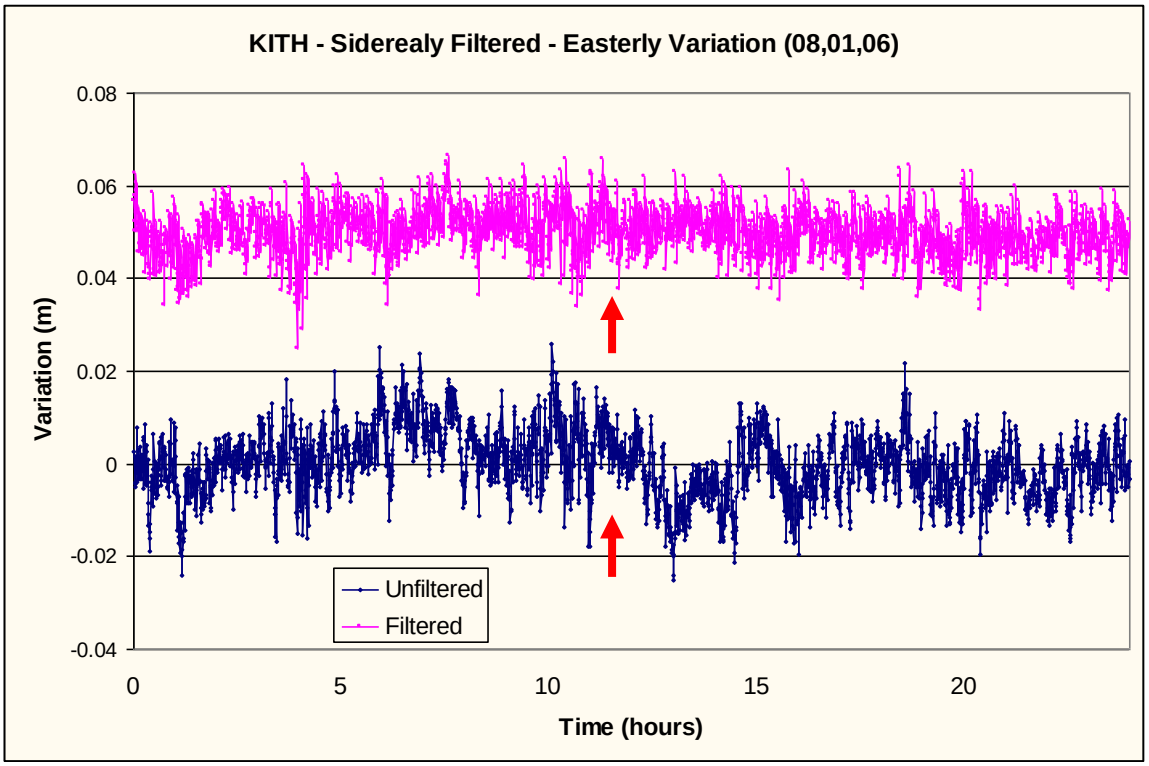

Figure 5.6: Siderealy filtered and unfiltered Coordinate time series of the 08, 01, 06 Southern Aegean earthquake. The time of the earthquake is highligted by the red arrows.

5.3.3 Macquarie Island (10/11/07)

To compare similar size earthquakes the same technique was applied to an M_w 6.5 earthquake, again near Macquarie Island. The time series of the days leading up to the quake are shown in figure 5.7 and the filtered and unfiltered time series of the 10th are displayed in figure 5.8. The standard deviations of each of these time series can be seen in table 5.3. These results vary slightly from the previous examples. Although the standard deviations of the days preceding the quake are comparable to the previous examples (around the 1cm in the horizontal components and 1.5 cm for the vertical), the day of the quake shows a different pattern. The standard deviation for the 10th is significantly higher than the days preceding the quake (table 5.3) with a coordinate scatter of over 10 centimeters in each positional component. This variation appears to be largely due to the last six hours of the time series and is therefore unlikely to be related to the earthquake itself which occurred at 01:13:34 UTC. The quake is not obvious as a co or post seismic signal.

Date	North	East	Vertical
07,11,2007	0.012787	0.009086	0.013373
08,11,2007	0.010615	0.010546	0.012806
09,11,2007	0.013421	0.009814	0.014299
10,11,2007	0.017157	0.018318	0.021624
10,11,2007 - Filtered	0.014544	0.015758	0.019619
11,11,2007	0.014285	0.00978	0.015141

Table 5.3: Comparison of the Standard deviations (m) of unfiltered and Siderealy filtered time series for the 10, 11, 07 Macquarie Island earthquake.

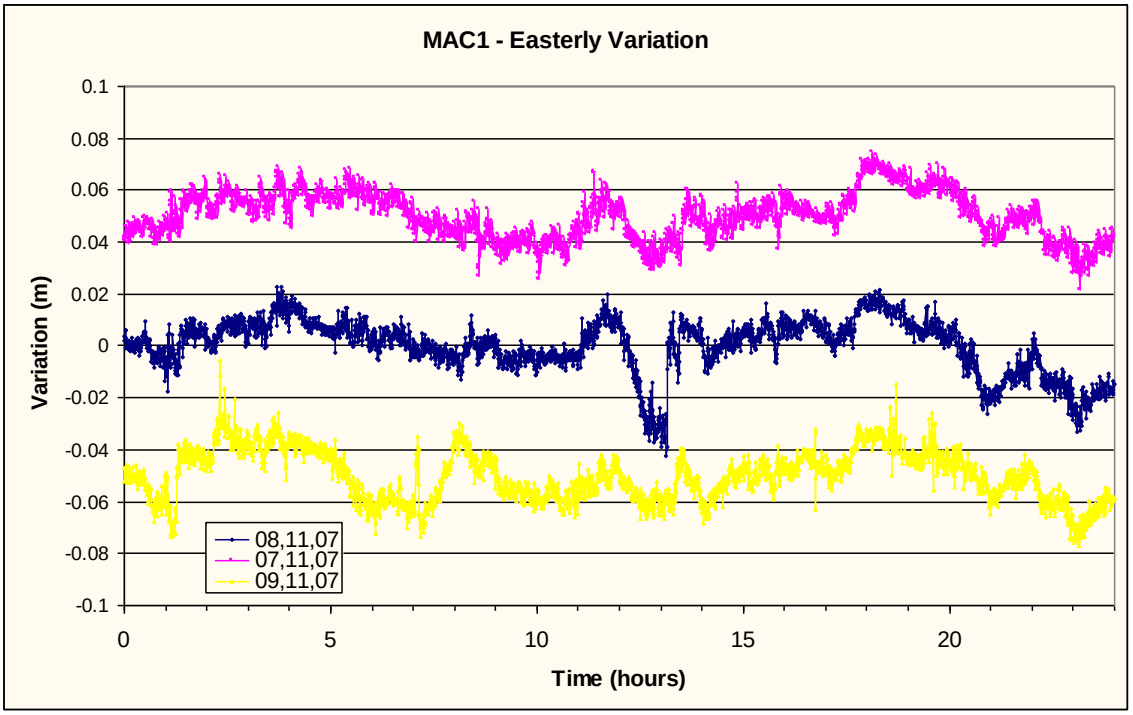

Figure 5.7: Coordinate time series of the days preceding the 10, 11, 07 Macquarie Island earthquake.

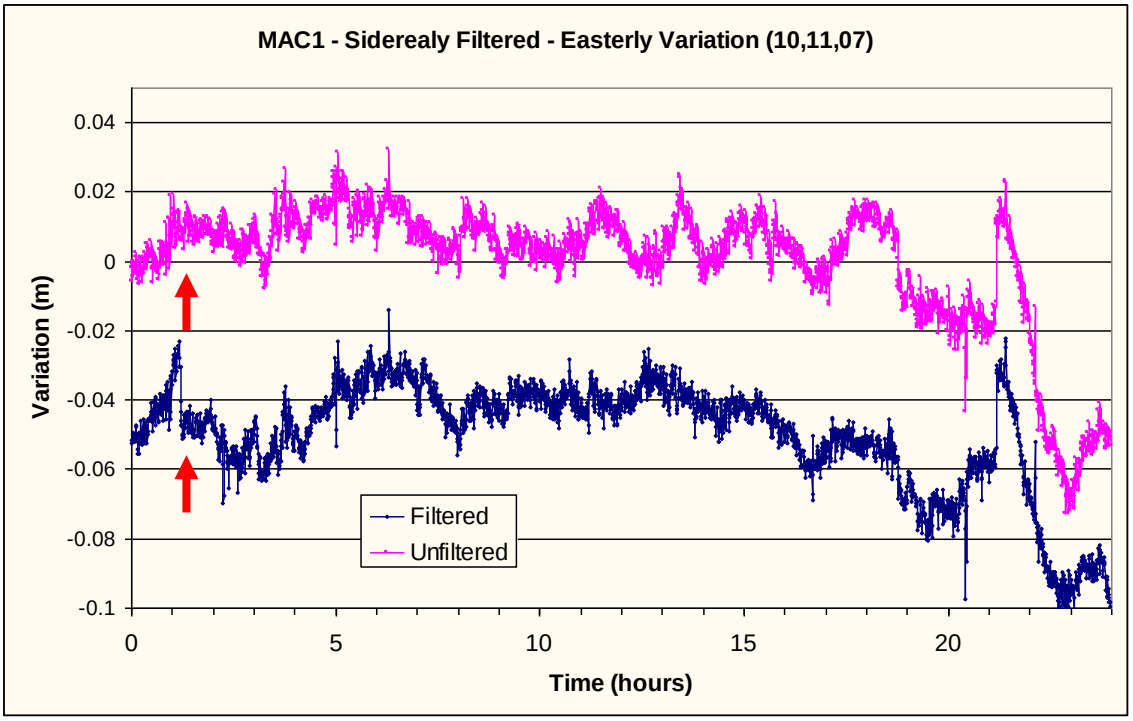

Figure 5.8: Siderealy filtered and unfiltered Coordinate time series of the 10, 11, 07 Macquarie Island earthquake. The time of the earthquake is highlighted by the red arrows.

Although the scatter and standard deviation of the siderealy filtered data for the 10,11,07 is worse than for the unfiltered data of the preceding days it is better than the

unfiltered coordinates of the 10th demonstrating the sidereal filter did have a positive impact reducing the scatter on this day.

The source or cause of the coordinate variation on the 10th is difficult to explain. The 11,11,07 shows a daily time series with a similar coordinate pattern to the days preceding the quake (figure 5.9), with similar variation and standard deviation, therefore any cause would be of a transient or temporary nature. Whether this is due to changing climatic conditions, variation in the geometry of features surrounding the antenna leading to a change in the multipath signal or real transient movement is impossible to say, but it does highlight the care with which this technique must be applied.

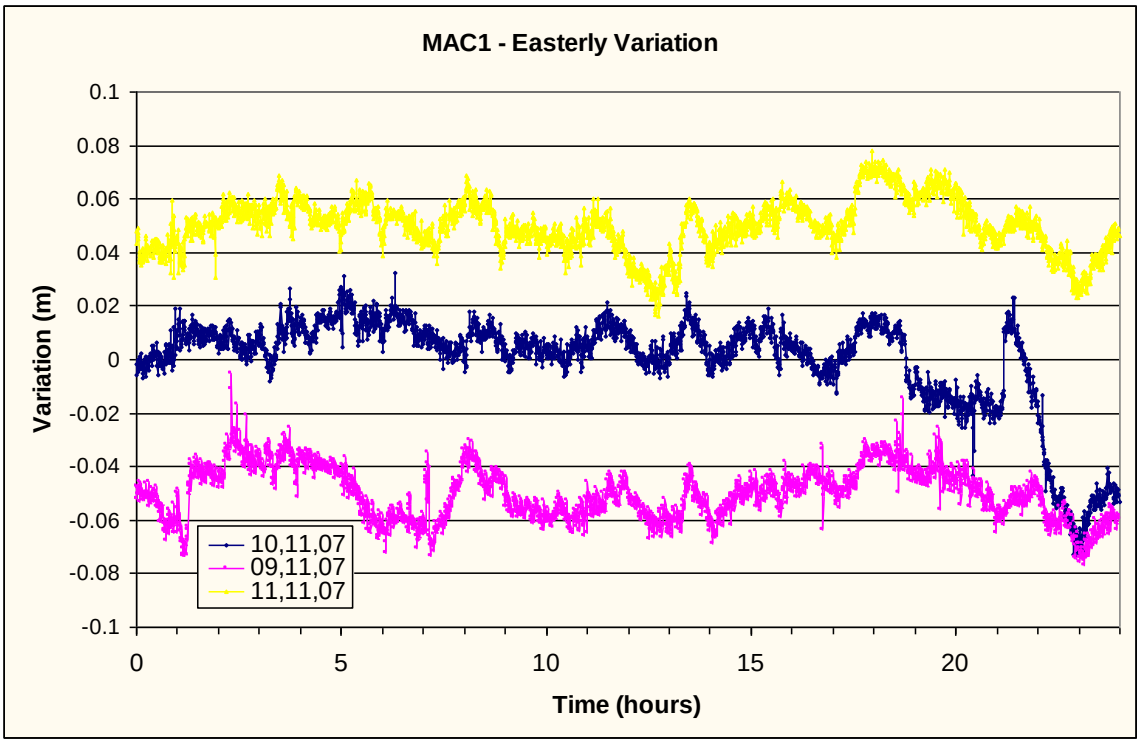

Figure 5.9: Coordinate time series of the day's pre and post the 10, 11, 07 Macquarie Island earthquake.

5.4 Analysis Sidereal Filtering

5.4.1 Orbit Repeatability

As mentioned in previous chapters the sidereal filtering technique relies on the sidereal repeat period of the GPS satellite orbits. This nominal repeat time (23h 56m 4s) ensures a repeat ground track and therefore a repeat of the satellite geometry around a receiver. A number of papers have discussed how this repeat period is not in fact the nominal value and due to variability in each satellite's repeat period an adjustment needs to be made to each orbit (*Choi et al. 2004; Ragheb et al. 2007*).

In order to clarify this Keplers third law, which states that the square of an orbital period is directly proportional to the cube of the semi-major axes of that orbit, was applied to the broadcast ephemeris files published by the IGS each day. The broadcast ephemeris files contain details of a range of clock and positional data including the square route of the semi major axis which can be used to determine the orbital period through equation 5.1.:

$$T = 2\pi\sqrt{\frac{a^3}{GM}} \tag{5.1}$$

Where **T** is the orbital period, **α** is the semi major axis of the orbit and **GM** is the gravitational coefficient of the earth in km^3/s^2 (398600.4415).

The results of plotting these orbital periods as a time series can be seen in figures 5.10 and 5.11. When looking at these figures a number of features are obvious. Firstly that the orbital periods of the satellites do vary with time and contain a number of oscillations and perturbations. The largest scale drift which occurs due to the variation in the gravitational attraction of the Sun appears to be the longest period event and requires a burn occasionally to keep the satellite in an appropriate orbit (figure 5.10). Superimposed on this long term drift are variations over periods of weeks due to the gravitational attraction of the moon (*Choi et al. 2004*).

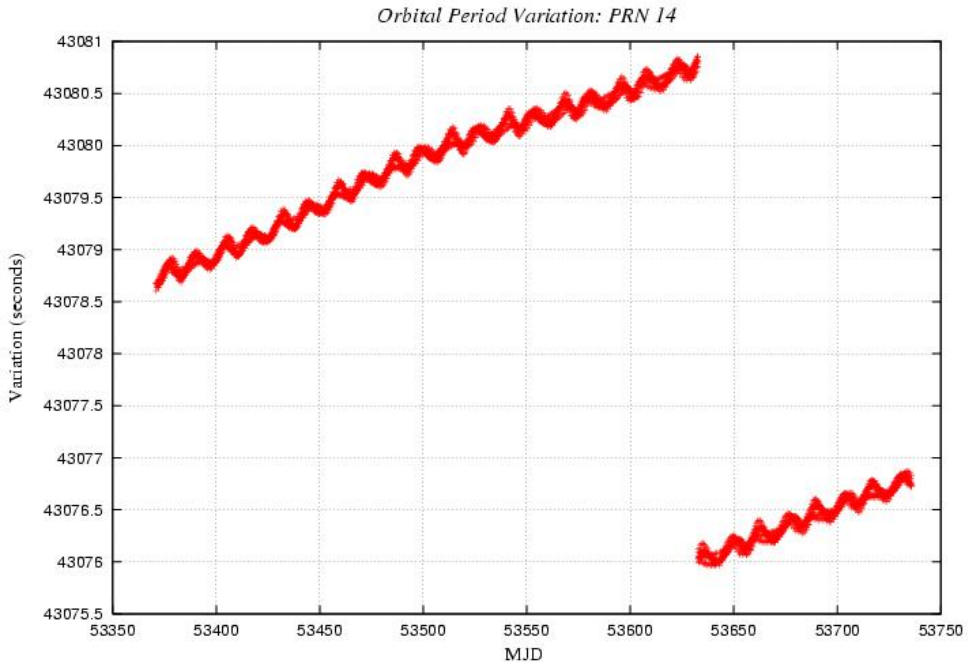

Figure 5.10: long term orbital period variations of a single GPS satellite. The break in the time series represents a burn to maintain its siderealy repeating groundtrack

Over an even shorter time scale day to day and orbit to orbit variations can be observed caused by a range of perturbing accelerations from the Earth. These variations do not however cause the orbital period to shift by more than 0.1 seconds on a day to day basis and are stable to 0.25 seconds over a five day period. As GPS satellites are traveling at approximately 4.5km a second these orbital period variations would have a minimal effect on the geometry of the satellites around a receiver on a day to day basis. This in turn would result in little or no variation in any multipath or other geometry based errors at a receiver as the angular difference would be around the five second level.

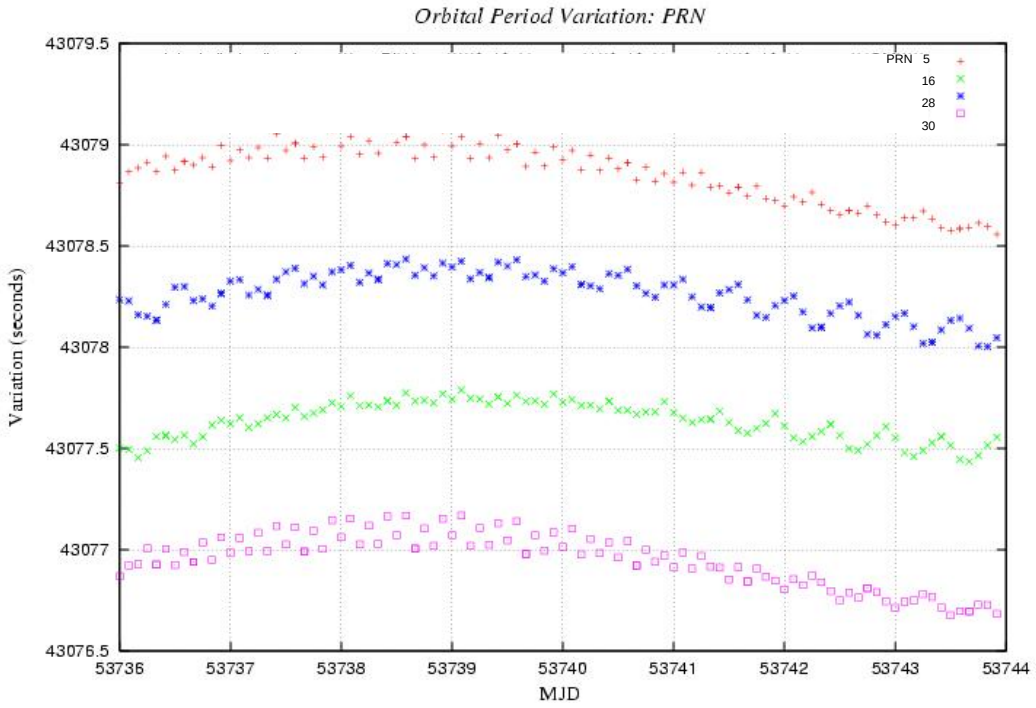

Figure 5.11: short term orbital period variations of a GPS satellite orbit

The results from the studies of earthquakes at Macquarie Island and in the Aegean demonstrated a number of the benefits and limitations of using the sidereal filtering technique on 1/30 Hz GPS data. Firstly the application of the technique does show a significant reduction in the overall scatter and hence standard deviation of a time series. This was true for all time series which showed a reduction in the scatter by a factor of 1.5 – 2. This in itself is a significant result allowing for analysis of the daily multipath sources at any given site and hence their mitigation. This also leads to a much clearer realization of sub-daily transient site movement as can be seen in figure 5.4 where the 2cm southerly shift of the site appears in significantly sharper contrast in the siderealy filtered time-series when compared to the unfiltered time series of the same day. This is true for the significant movement felt during an M_w 8.1 earthquake, but does not show up on either of the $<M_w$ 6.8 earthquakes near Macquarie Island or in the Southern Aegean. This suggests that either the noise levels are such that any displacement is not obvious in the time series, or that there was no site displacement during these events. The Macquarie Island M_w 6.8 event was located in a similar position and had similar moment tensor solutions (USGS) to the larger 8.1 event in that area which would suggest a similar, but smaller displacement could be expected, the lack of an obvious

signal therefore points toward a limitation in the technique rather than a lack of motion. This is also true for the southern Aegean event which does not show in the time series but which was reportedly felt as far away as Italy and Egypt.

The fact that the southern Aegean quake was felt but did not noticeably register as a co or post seismic event in the time series may just highlight the limitation of using 30 second data to study seismic events. Seismic events such as the M_w 6.8 event typically last under a minute and therefore would only register on one or two 30 second readings. Unless the epicenter of these events was very close to a permanent GPS site the chances of these readings being of sufficient magnitude to appear as a clear seismic marker on a time series are small, therefore it is more likely that they would show up as a displacement.

Recent studies looking at the Kithira event (*Karakostas et al. 2006; Konstantinos et al. 2006*) have stated that the earthquake was felt as far away as southern Italy, Cyprus, Egypt, Turkey, Syria and Jordan but caused minimal damage even in the local environment, most notably in the village of Mitata on Kithira. Here there was some structural damage to stone masonry buildings but the PGA (Peak Ground Accelerations) were measured at a_g = 0.12g which is relatively small especially for an event of magnitude 6.7 / 6.8. The earthquake was assigned to have occurred along the kythira seismic fault which is one of a number of fault zones running perpendicularly to the main Hellenic arc. The Kythira fault has experienced five similar magnitude events in the past century (1903: M7.5, 1910: M7.0, 1926: M7.2, 1932:6.3, 1937:M6.0). Figure 5.12 shows the location of this fault and epicenter and focal mechanism of the 8th January event.

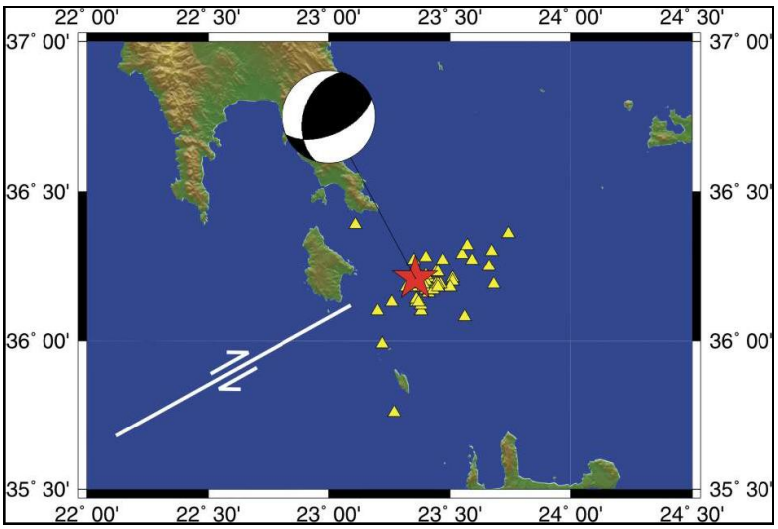

Figure 5.12: Epicenter (star) and mean mechanism of the 8th January 2006 earthquake as well as the seismic activity for the period 8-28 January (triangles) and the location of the Kythira fault (from Karakostas et al. 2006)

PGA results from corrected acceleration traces around the area showed a maximum of around 120cm /sec^2 (figure 5.13). The time over which this motion was felt was approximately 30 seconds which is characteristic of deep and intermediate focus depth events

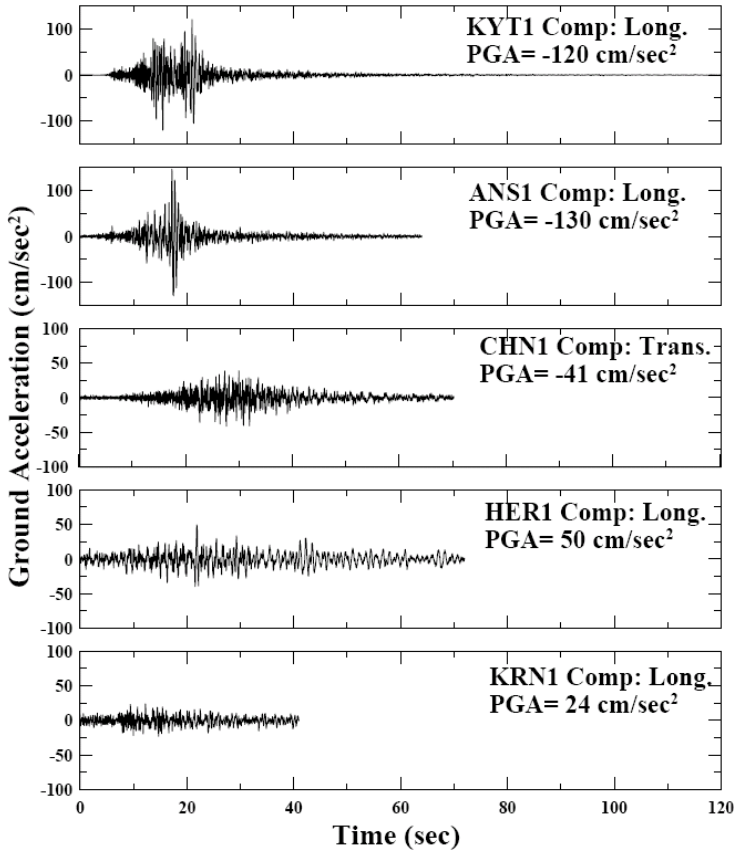

Figure 5.13: Horizontal components of accelerograms for the 8th January 2006 earthquake (from Karakostas et al. 2006)

These studies support the conclusions drawn from the sidereal GPS. Firstly although the Kythira earthquake was of a significant size it was at an intermediate depth (66 km) as such the seismic waves felt at the surface were reduced in scale and the PGA's were also less than expected. The GPS could therefore simply not have detected any co-seismic motion. There was little movement therefore no co and post seismic displacement to detect in the GPS time series. The duration of any co-seismic motion was also only a few seconds and therefore the use of 1/30 Hz GPS data was an inappropriate temporal resolution to detect any motion. The loss of the 1 Hz GPS data from the near field GPS receivers due to technical faults inhibited a more detailed study of this event and technique.

Summary

This chapter has described the technique used to reduce the error in a time series by reducing multipath and geometry related noise sources on sub daily positioning coordinates. This has been termed sidereal filtering as the processing technique takes advantage of the approximately half sidereal repeat period of the GPS satellite ground tracks. This technique revealed the presence of co seismic displacement at a major (M_w 8.1) earthquake but failed to detect smaller events ($\approx M_w$ 6.7). The technique was able to reduce the scale of noise in the time series by a factor of 1.5 – 2, it was therefore determined that there was either no displacement at these smaller earthquakes, or that any movement was of a magnitude indistinguishable from the noise inherent in instantaneous positioning. In addition the use of 30 second GPS data can prevent the detection of seismic motion from the time series, data with a higher temporal resolution (1Hz) would be more appropriate for the purpose of detecting these signals.

Chapter 6

GPS Visualisation Software

One of the aspects of characterising the motion of a CGPS network such as the COMET network in the Aegean is the ability to assess and visualise the network movements and variation as a whole. The traditional technique of looking at time series of either baseline components or relative movements within a defined reference frame allow the intricate and detailed examination of a site's variation without truly giving an overview of how this affects or fits into the overall movements of a region. As such I, in conjunction with a colleague, Anthony Sibthorpe, looked to develop a tool that allows a simultaneous view of the whole network in order to show the evolution of network velocity vectors in time and space.

6.1 Introduction – Ground Movement Visualisation

Our ability to determine the nature of any tectonic motion or deformation within an area is limited not just by the quality of the data collected and our ability to process that data to remove undesirable noise sources but also by our ability to visualise that information in a suitable fashion. The common remote sensing techniques used to study tectonic motion are GPS and Interferometric Synthetic Aperture Radar (InSAR). InSAR images (Interferograms) have the advantage that they display deformation with a high spatial resolution (tens of meters) continuously over a wide area, however the relatively small number of SAR satellites means that groundtracks are infrequently replicated (typically monthly) leading to a poor temporal resolution (*Burgmann et al. 2000; Wright, 2002*). In addition InSAR can experience a range of other error sources (mentioned in more detail in chapter 2.5) that can lead to the loss of more data. Some of the benefits and

drawbacks of interferograms are highlighted in figure 6.1. The image represents an area of roughly 100 km by 200 km and clearly shows the amount of ground movement over this whole area due to two earthquakes on the Denali fault at the end of 2002. Being a line of sight measurement means that SAR gives no clear idea of the exact direction of ground movement. All that can be concluded is that the difference in each pixel from one image to the next revealed certain changes along the line of sight, hypothetically the ground itself could have shifted by meters horizontally and this would not be distinguishable in the image. The large areas of unrecoverable data are highlighted by the grey areas in the image and the poor temporal resolution of the technique means there is no way of determining how much affect each of the two earthquakes had (one on 23/10/2002 the other on 03/11/2002).

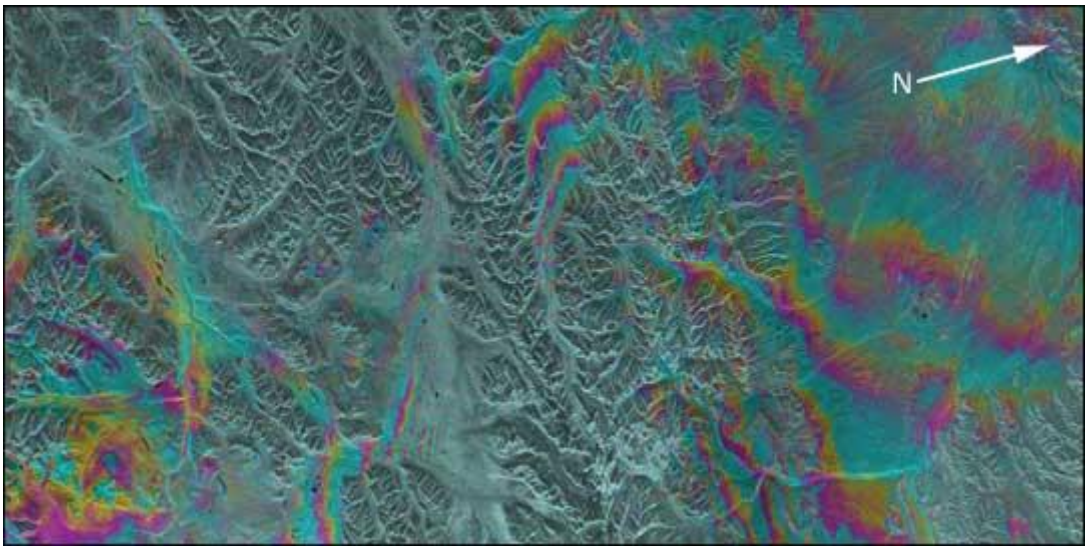

Figure 6.1: Interferogram of the October and November 2002 Denali fault earthquakes. Each colour cycle (blue to blue) represents 3 centimeters of ground motion. Grey represents areas where the data could not be collected or cleaned to a coherent level (image courtesy of the earth observatory, NASA).

The techniques employed to visualise GPS data also have positives and negatives. Traditionally GPS data is visualised using time series demonstrating either the variations in a site's north, east and vertical components within a defined reference frame, or its baseline variation relative to another site. Alternatively the velocity vectors of a site within a defined reference frame or relative to another site are calculated and overlain on a site map to give an overview of the ground motion of an area.

Time series give very detailed images of the movement of a site over practically any temporal regime, from seismic waves to annual signals and long term plate motion.

They do not however easily allow the visualisation of the motion of an area as a whole, particularly when studying positional components, such as easting or northing, individually. The motion of an area is much better represented by velocity vectors however, the vectors are normally plotted as an annual movement and therefore may lose subtle temporal variations.

6.2 GPS Visualisation software

The main motivation behind developing a different method of visualising GPS data was to combine the temporal benefits of the GPS time series with the spatial advantages of observing velocity vectors, thereby developing a tool that could be used to investigate and identify variations in ground motion as well as clearly displaying them.

The basic method was to plot the vector variations of the COMET sites relative to a reference site, either a separate IGS/EUREF site or another site within the network. These vector variations were derived from the baseline components between a reference site and every other site in the network and then plotted on a base map formed from SRTM data using GMT (Generic Mapping Tool). In order to introduce a way of visualising temporal variations a programme was developed that allows the user to compute vectors that best fit to data over a moving time window specified by the user. For example plotting a year's worth of data then shifting forward 50 days and plotting another year's worth of data and so on until the time evolution of an area at that resolution forms a short gif.

In this way gifs (graphic interchange format) can be produced to animate the simultaneous time evolution of the area at any temporal resolution. An example of this can be seen in figure 6.2. The sites that do not display velocity vectors in the images do so either because the site in question was not established at that time or because there was insufficient data to get a true reflection of the site's relative movements. The nominal value of data covering 50% of the days during a stated window was used as the minimum requirement to determine a velocity vector.

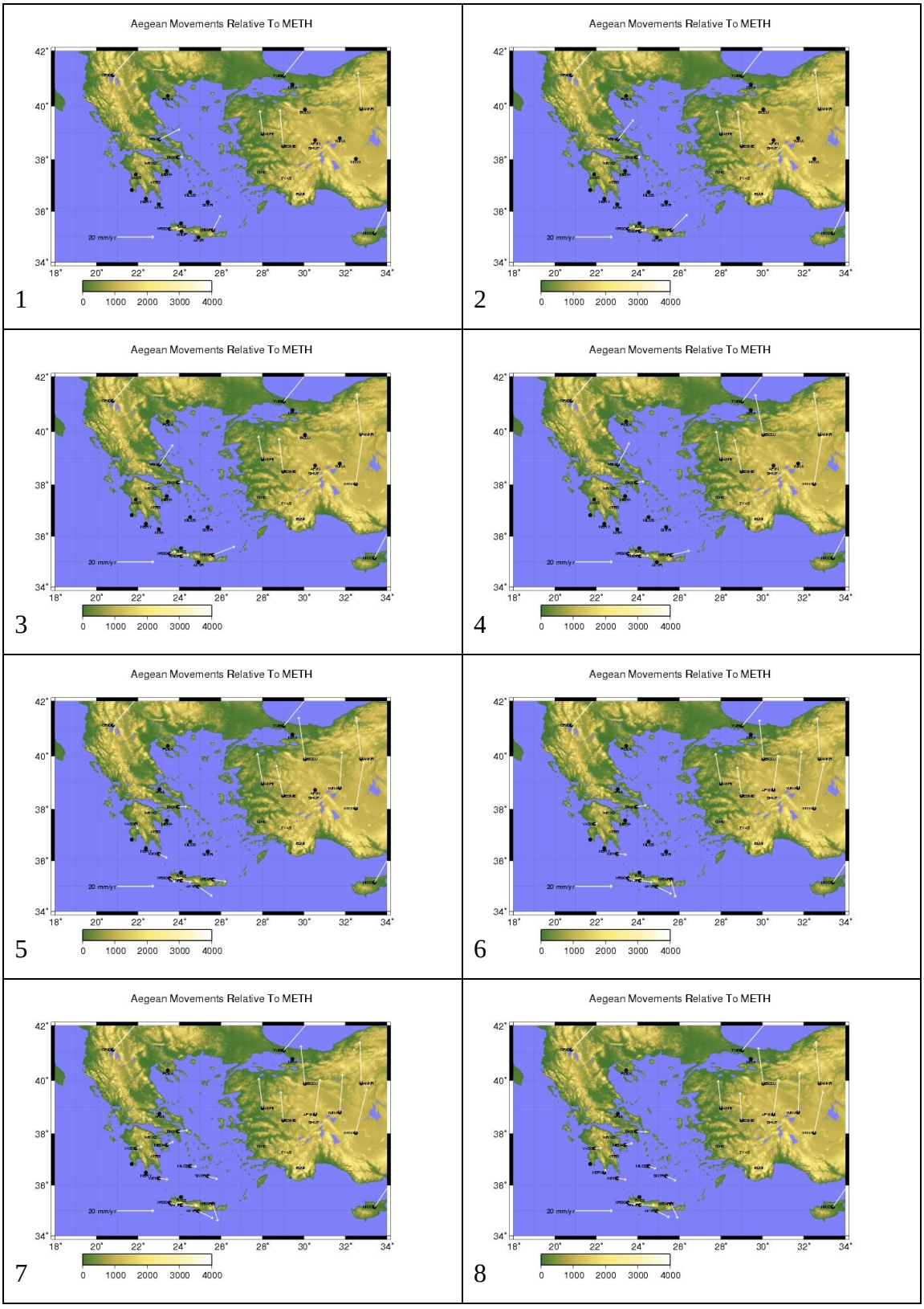
Aegean Movements Relative To METH
20 mm/yr
0 1000 2000 3000 4000
1
Aegean Movements Relative To METH
20 mm/yr
0 1000 2000 3000 4000
2
Aegean Movements Relative To METH
20 mm/yr
0 1000 2000 3000 4000
3
Aegean Movements Relative To METH
20 mm/yr
0 1000 2000 3000 4000
4
Aegean Movements Relative To METH
20 mm/yr
0 1000 2000 3000 4000
5
Aegean Movements Relative To METH
20 mm/yr
0 1000 2000 3000 4000
6
Aegean Movements Relative To METH
20 mm/yr
0 1000 2000 3000 4000
7
Aegean Movements Relative To METH
20 mm/yr
0 1000 2000 3000 4000
8

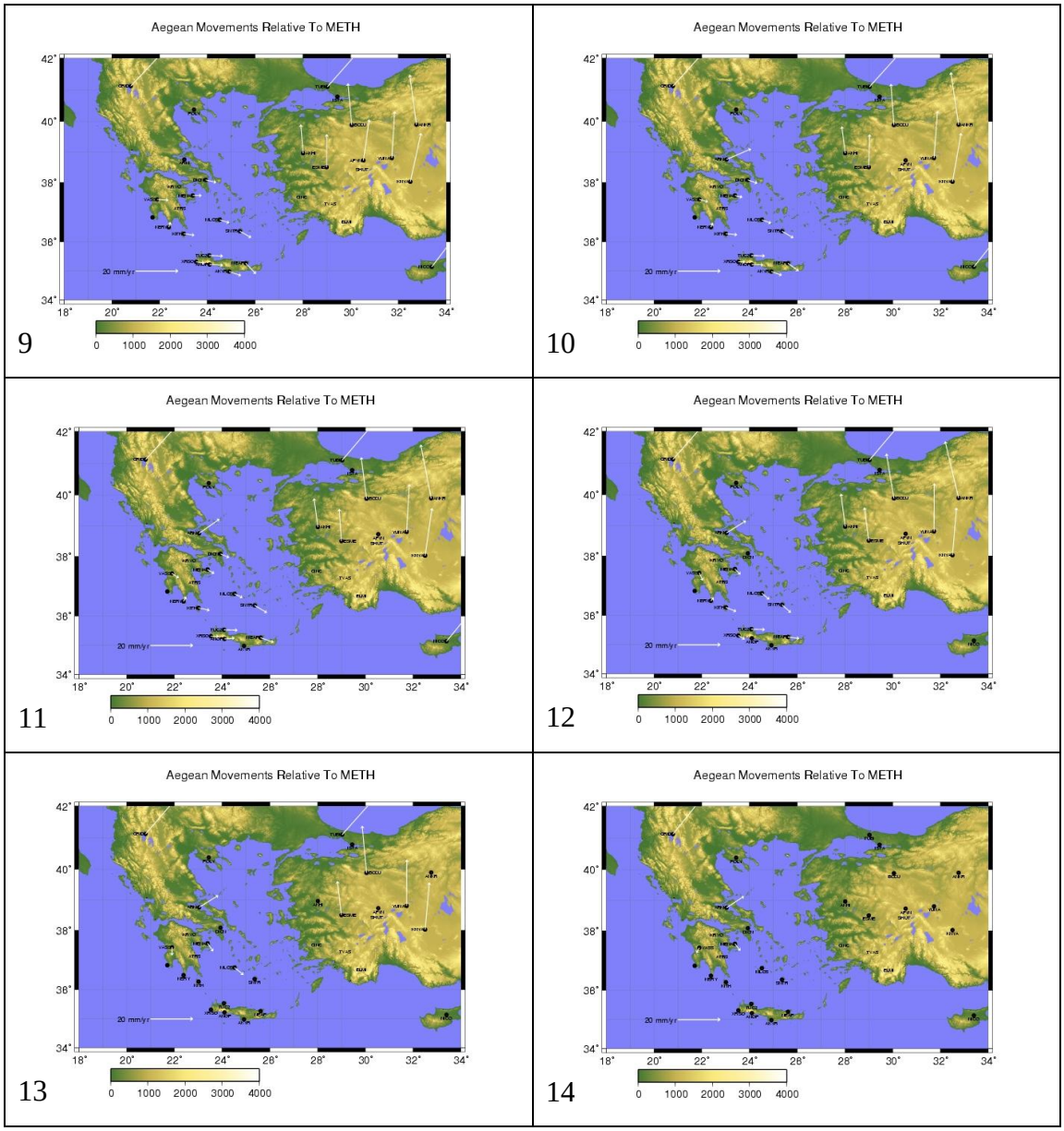

Figure 6.2: A selection of stills showing the time evolution of the Aegean relative to METH. Each plot represents a year of data and each plot is separated from the next by 50 days.

Figure 6.2 shows the time evolution of the Aegean relative to METH. Even this image series with a relatively short period of data (1 year per image) demonstrates a lot of the features of the Aegean that were derived from longer time series, such as the general east-west expansion across the Hellenic arc, the expansion across the gulf of Corinth and the rapid southward motion of the Aegean away from Eurasia and Anatolia. In addition to this it showed a number of other features that are not as clearly demonstrated when studying time series. Firstly the anomalous movements of site NEAP, on the eastern end of Crete. In image 1 and 2 of figure 6.2 NEAP's movement has a strong northerly component relative to METH. As you move through the images this orientation drifts round to the east before showing a strong southward relative motion in

images 6 and 7. Finally it drifts back round to the east. After this time there was insufficient data to define an orientation at NEAP (images 13 and 14, figure 6.2).

The reason for this variation in the movement of NEAP for the 400 days following the establishment of the site is not known. It is however worth noting that the visualization software was able to highlight this anomalous movement. After this initial period the annual velocity vector of NEAP show much greater coherence with the rest of the sites in Greece.

The example in figure 6.2 shows yearly velocity vectors with a separation of 50 days. The technique was also employed on much shorter time frames to illustrate shorter term tectonic events such as silent slip. Figure 6.3 shows the movements of a couple of sites in Cascadia relative to Penticton (DRAO). These images are generated with 60 day velocity vectors and a 40 day separation. They show the chronological development of these sites (ALBH and SEDR) with a small time overlap. The aim was to show the silent earthquake that occurred in the region around August 1999 (*Dragert et al. 2001*). The results highlighted some of the benefits and draw backs of the visualization software when examining tectonic events over these timescales.

The images do in general show a similar pattern to that seen in the time series, with the general easterly movement of the sites relative to DRAO, followed by a short reversal of this around August 1999 corresponding to the silent slip event that occurred at this time. The images are not however sufficiently coherent to suggest the technique would be a way of searching for such events. Images 1, 2, 3 and 4 do in general show an easterly movement but within this there is great variation in the north-south orientation and the size of any movement. This is just a reflection of the amount of data available in forming the velocity vectors. Forty days of data are particularly susceptible to outliers or short term errors such as seasonal variation that would be averaged out of longer time spans. The same process was attempted with even shorter data spans (20 and 30 days) but this led to even more random results with hardly any coherency in the velocity vectors at all. Longer time spans were also used but these tended to average out the slip events such that the complete reversal from easterly to westerly movement appeared more as a slowing down of the general drift.

Images 5 and 6 clearly show the westerly reversal during the slip event. Image 7 shows data on the cusp of the event with some data during the reversal but more during the period of normal easterly drift after it. As a result there appears to be very little easterly or westerly movement. Without prior knowledge of the slip event and its duration in this area it would be unlikely that the technique would highlight the exact nature of the tectonics occurring. Either there would be insufficient data to obtain accurate velocity vectors, too much data thereby hiding the anomalous movement through averaging or the duration between each image would fall at an inappropriate time to fully show and enhance the anomalous movement occurring, as is the case in image 7 of figure 6.3.

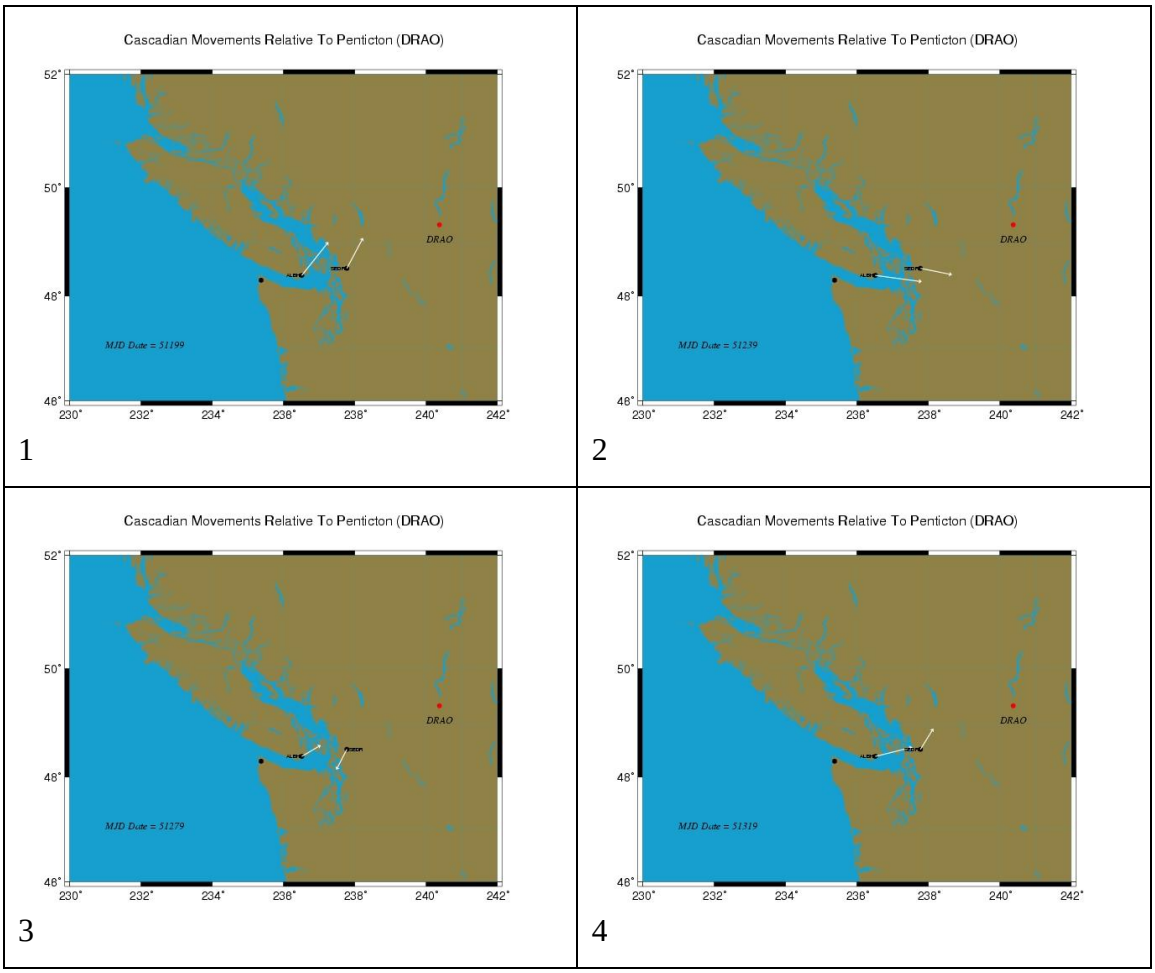

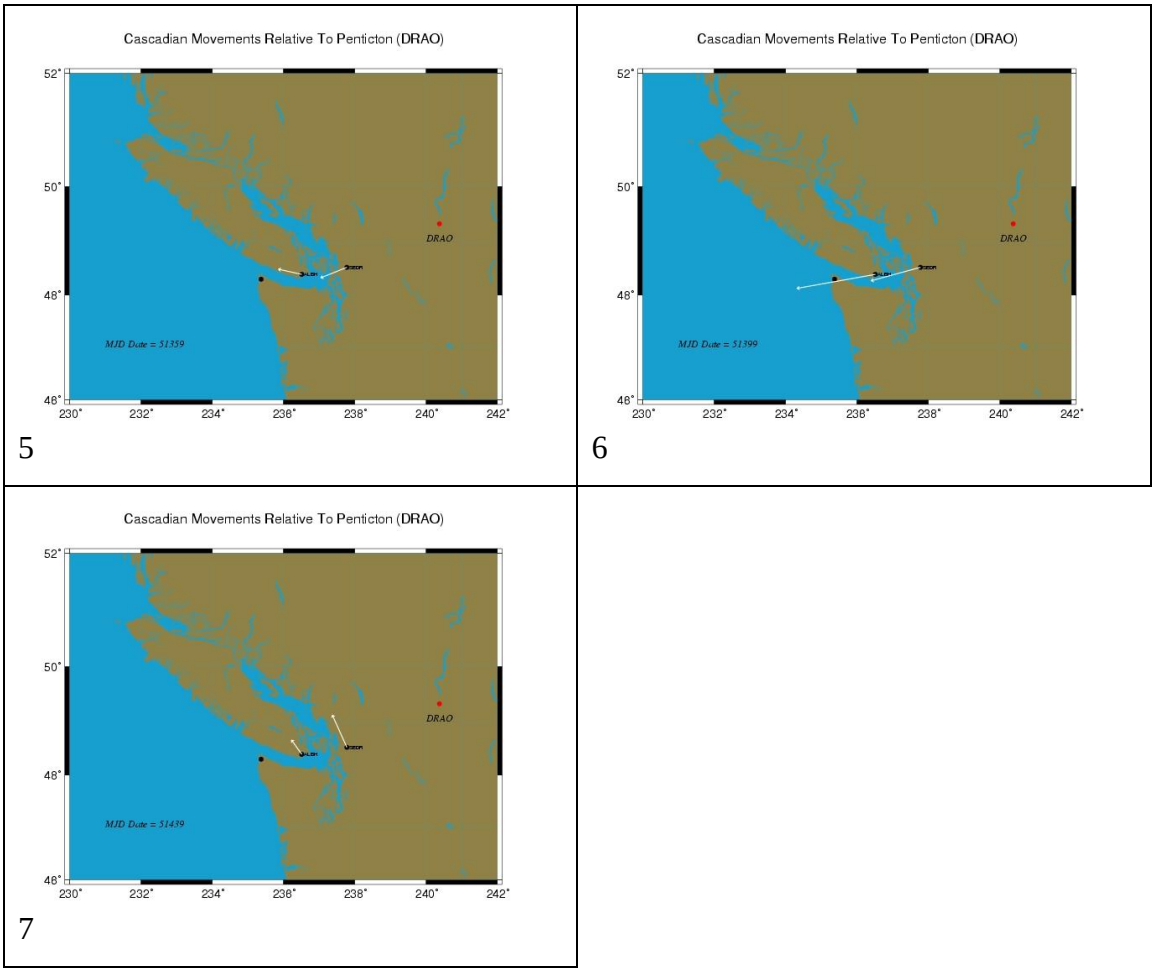

Figure 6.3: A selection of stills showing the time evolution of Cascadia relative to DRAO. Each plot represents 60 days of data and are separated by 40 days.

6.3 Analysis - GPS Visualisation software

The technique of showing ground motion as velocity vectors with optional variation in the duration of site movement and separation between movement estimates does add to the present methods of visualizing GPS site movement. Movement anomalies such as the changing orientation of the velocity vector at the site NEAP were obvious in this format whereas a single image would not identify this varying motion. Time series would highlight that there was irregular variation, but would not show how this related to the movement of other sites in the area. This is demonstrated in figure 6.4 which compares the time series of NEAP and XRSO relative to the reference site METH. There are striking differences between each of these time series but projecting how these motions vary across the Hellenic Arc is difficult.

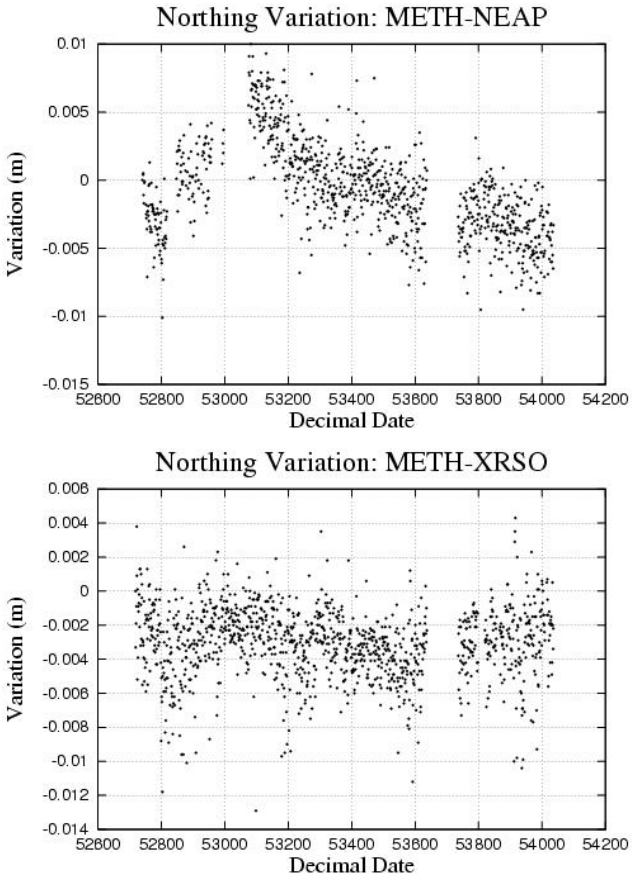

Figure 6.4: Time series showing the anomalous north-south movement of NEAP relative to METH and a comparative image of another site located on Crete, XRSO.

The technique does therefore have the capacity to highlight variations in ground movement, particularly significant changes in direction that occur over a reasonably long period. Shorter period variations are much harder to identify due to the greater inaccuracy associated with defining the relative velocity vectors from small amounts of data and an unclear picture when a shorter term tectonic motion may have occurred leading to the use of non event associated data in any velocity estimate, which adds noise to and masks the desired signal. In these cases the technique works better as a tool for demonstrating known anomalies rather than a method of identifying and defining events.

The time series show that the transient events detailed in chapter 4 are present in the baseline data between TUBI and VASS (figure 6.4). This information would therefore be present in the data used to form the images in figure 6.5.

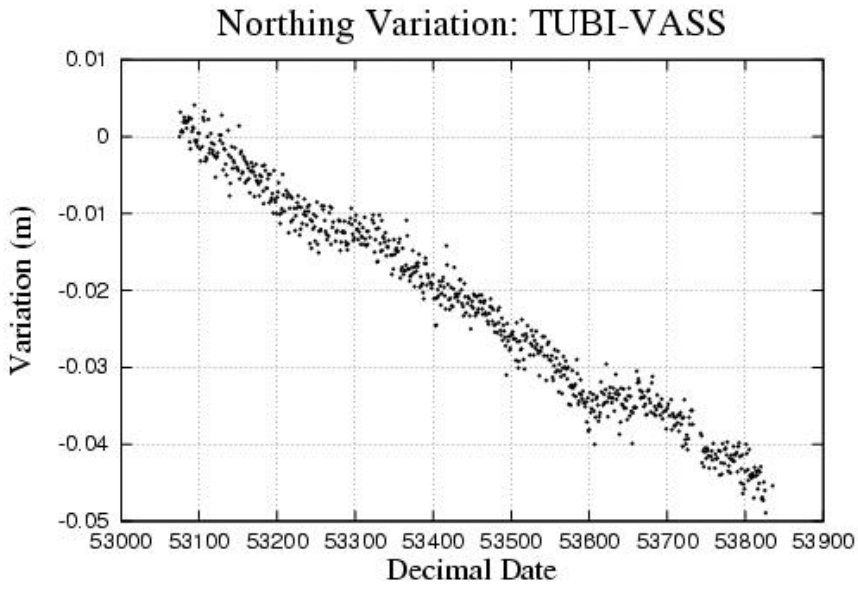

Figure 6.5: Time series showing the transient event identified at VASS using the filtered baseline method (reference station TUBI)

The choice of reference station can have the effect of visually masking this signal. This can be seen in figure 6.5 where a site located on the Eurasian plate is used as the reference station (TUBI). The velocity vectors displayed here are formed using a year's worth of data and are separated by 50 days. They show the significant movement (≈ 30 millimeters / yr) of the Aegean sites relative to Eurasia but subtle changes in these velocities are hard to distinguish. For example there are small changes in the northerly component of a number of sites around the Hellenic arc (particularly VASS) which may well relate to the transient events observed around the arc and described in chapter 4. From these images there is no way of telling the scale or duration of these events as the data is largely disguised by the general movement of the site.

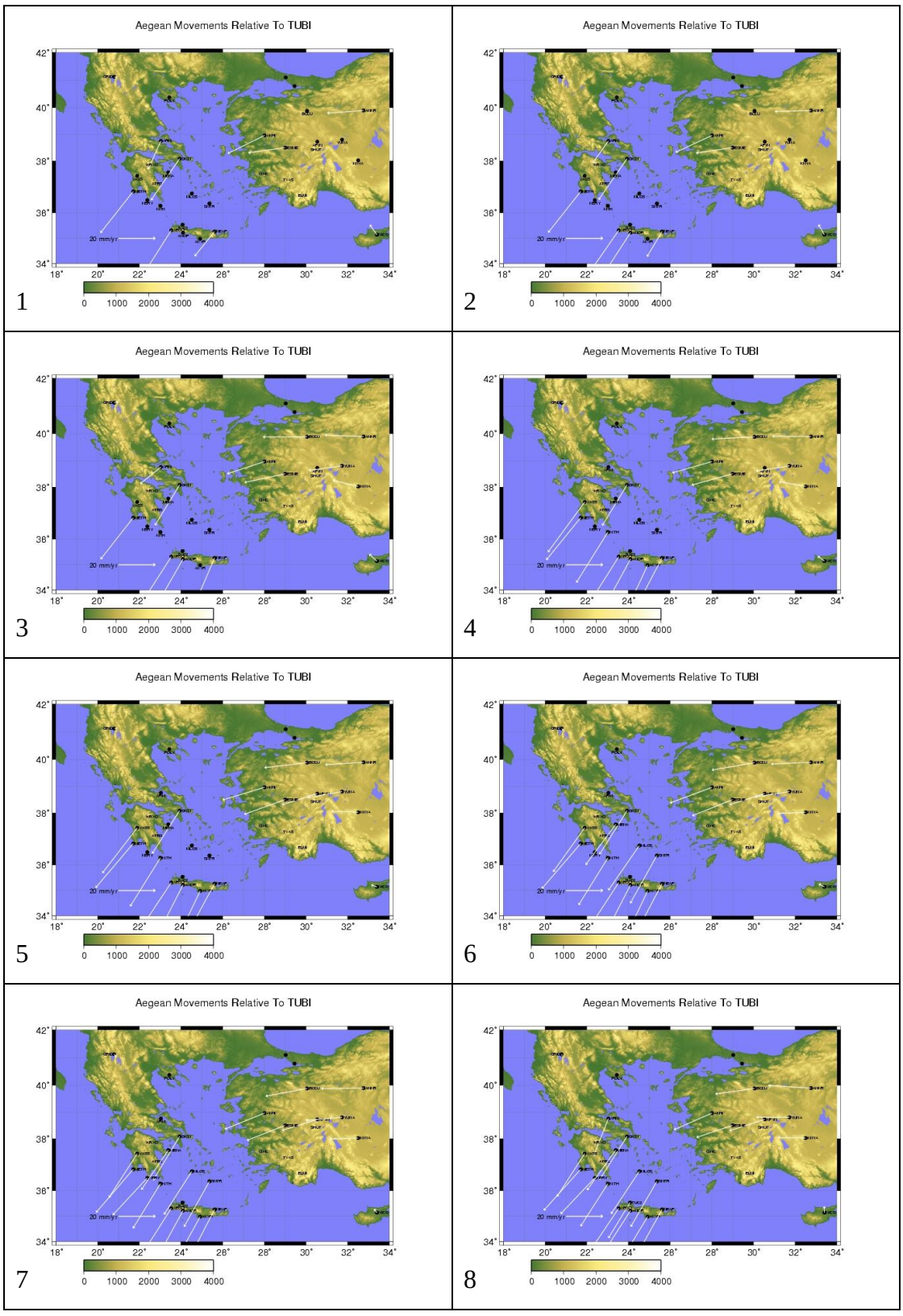
Aegean Movements Relative To TUBI
20 mm/yr
0 1000 2000 3000 4000
1
Aegean Movements Relative To TUBI
20 mm/yr
0 1000 2000 3000 4000
2
Aegean Movements Relative To TUBI
20 mm/yr
0 1000 2000 3000 4000
3
Aegean Movements Relative To TUBI
20 mm/yr
0 1000 2000 3000 4000
4
Aegean Movements Relative To TUBI
20 mm/yr
0 1000 2000 3000 4000
5
Aegean Movements Relative To TUBI
20 mm/yr
0 1000 2000 3000 4000
6
Aegean Movements Relative To TUBI
20 mm/yr
0 1000 2000 3000 4000
7
Aegean Movements Relative To TUBI
20 mm/yr
0 1000 2000 3000 4000
8

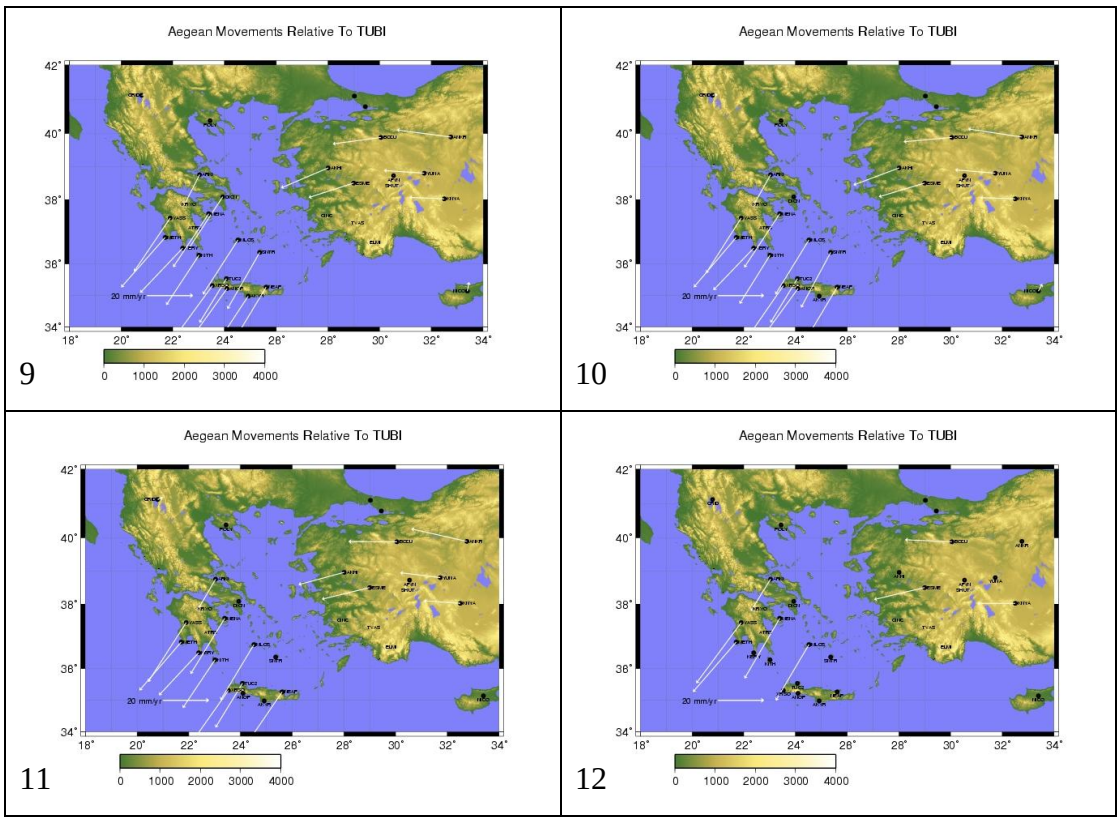

Figure 6.6: A selection of stills showing the time evolution of the Aegean relative to the Eurasian plate (TUBI). Each plot represents a year of data and each plot is separated from the next by 50 days

It is possible to refine the images by limiting the period over which the velocity vectors are defined and separating the images by a more appropriate period. For example figure 6.6 only includes 50 days worth of data and each image is separated from the next by 50 days. The transient event occurred at roughly mjd 53250 and lasted for between 50 and 75 days depending on the site. As such you would expect a number of the sites to show a noticeable reduction in their southerly movement (particularly VASS, METH, KERY, KITH and XRSO). There is a difference in a few of the sites in frames 2 and 3, when the transient event occurred however in general the short time period used to define the site movements results in a very unclear image of the general site movement and therefore makes it impossible to identify what would be anomalous movement.

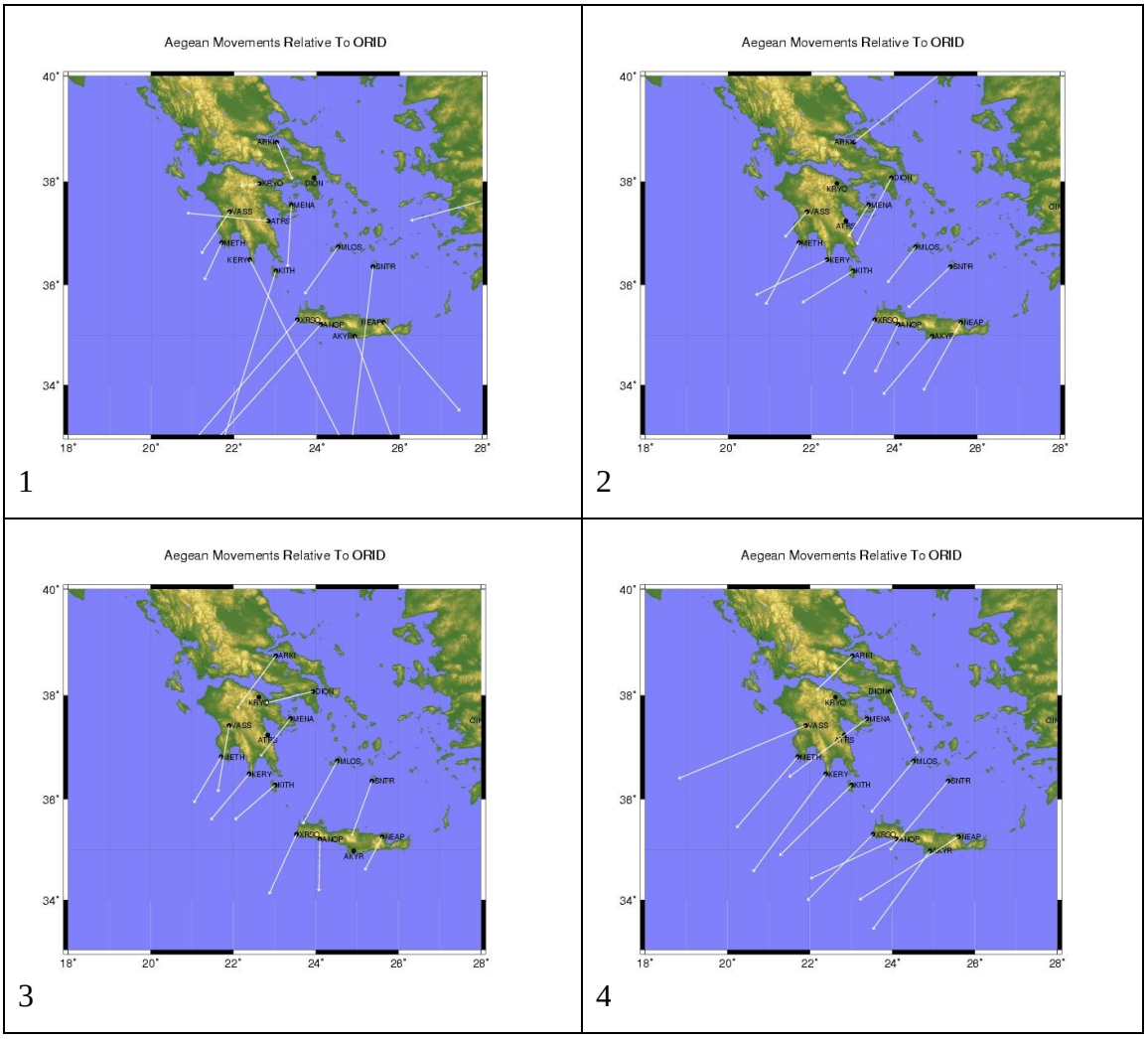

Figure 6.7: Stills showing the time evolution of the Aegean relative to the Eurasian plate (TUBI). Each plot represents 50days of data and is separated from the next by 50 days. Plot 1 started on mjd 53184. Plot 2 started on mjd 53234. Plot 3 started on mjd 53284. Plot 4 started on mjd 53334

6.4 Summary

A new method of visualizing ground movements derived from GPS data is presented and analysed. The technique appears to be a step forward when presenting the GPS time series of a network simultaneously, particularly when looking at long term variations in movement (>1 year). The visualization of shorter term movements requires a combination of clean data, sufficient time to accurately define a relative velocity vector and prior knowledge of when any anomalous movement has occurred. As such the technique is at present more suited to displaying ground movements than to investigating and defining them.

Chapter 7

Discussion

In the discussion chapter the wider context of the results and issues brought up in the studyis explored, which areas have been researched and the broader implications of any new knowledge. As with much of this thesis the study area is split into the daily CGPS studies involving the regional and baseline filtering and the sub daily results involving the sidereal filtering.

7.1 Daily CGPS Studies

The GPS data presented in chapter 4 in the form of time series, baseline variations and velocity vectors is in general insufficient to define definitively the kinematics and strain fields in the southern Aegean due to the limited data quantity (*Blewitt and Lavallee, 2002*). The results are however of sufficient accuracy to confirm the findings of several previous studies as well as to point towards some new features of the kinematics of the southern Aegean region.

The results of previous studies that were confirmed by the study included the rapid south south-westerly motion of the southern Aegean relative to the Eurasian plate, the apparent rigid block motion of the south Aegean with all sites south of the Gulf of Corinth moving in a coherent direction with a similar velocity (*Nyst and Thatcher, 2004*). The rapid extension across the Gulf of Corinth (*Armijo et al 1996*) was also highlighted as was the rapid southerly motion (relative to Eurasia) of the sites north of the Gulf.

In addition to these previously stated findings a number of new or undefined features were inferred, in particular the east – west arc parallel extension of the order of a few millimetres per year and the equally small north – south compression experienced between Crete and the volcanic islands of the Cyclades (figure 7.1). The discovery of transient variations in the motions of sites around the Hellenic arc also adds to the complex tectonic setting that characterises the Aegean region.

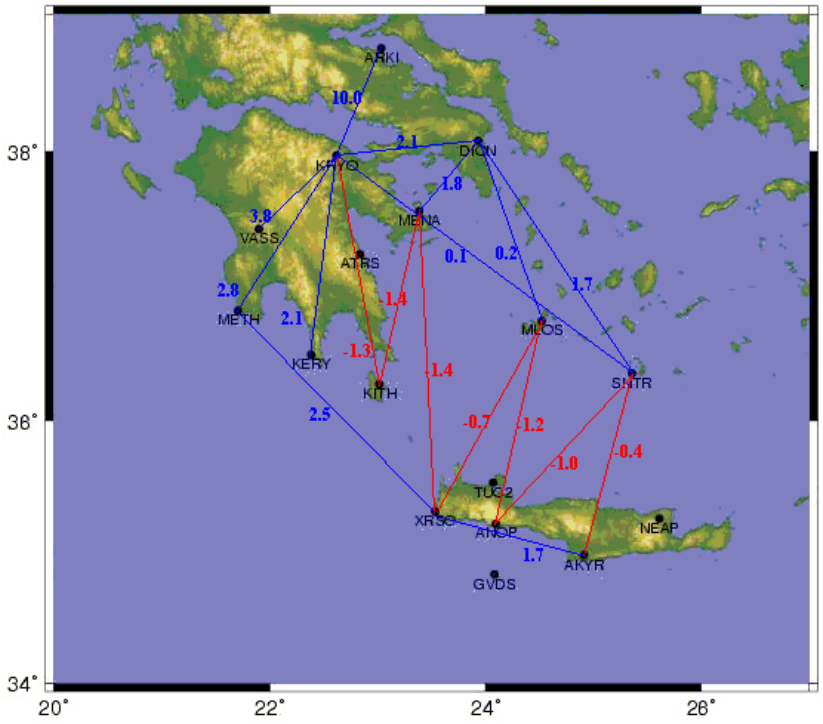

Figure 7.1: The extensional (blue) and compressional (red) baselines in the southern Aegean. All values are in mm/yr and had a standard deviation of 0.1 mm/yr

The east-west extension was originally inferred by Armijo et al (1992) and later confirmed in GPS studies such as that by Hollenstein (2007). In these studies it was stated that the Hellenic Arc extension was not distributed over the whole area, rather it is concentrated in the east (around Karpathos and Rhodes) and in the west (on the western Peloponnese). Hollenstein states a figure of arc-parallel extension of 16 ± 7 mm/yr with no significant deformation in the center of the arc. This study has no data from the east of the Arc around Karpathos and Rhodes but supports the idea of greater deformation in the western Peloponnese. A look at all the baselines from the site METH (the most western site in the network) shows a consistent extension of between 2.2 and 2.8 mm/yr to the other sites on the Peloponnese apart from VASS, suggesting that much of this extension is accommodated in the normal faulting around 22º longitude (figure

7.2). The next significant change in baseline length is to AKYR and NEAP on the eastern side of Crete where a further ≈ 2mm/yr of extension is added to the ≈ 2.5 mm/yr experienced across the Peloponnese. This is confirmed by the baseline between XRSO on the west of Crete and AKYR on the east which shows 1.7 mm/yr of extension (figure 7.1). These results agree with Hollenstein's idea that extension is concentrated in specific areas around the Arc (particularly in the western Peloponnese), but disagrees with her statement that there is no significant deformation around the central Arc (Crete). The rates calculated also disagree with her figures, the baselines suggest around 4 mm/yr of extension between the western Peloponnese and eastern Crete. To agree with Hollenstein's estimate of 16 mm/yr of overall extension there would need to be a further 12 mm/yr extension between eastern Crete and Rhodes which given the similar levels of seismicity across the Arc is unrealistic. The discrepancies between the studies may in part be due to the greater use of GPS campaign data in Hollenstein's study with the greater potential error sources associated with the campaign technique.

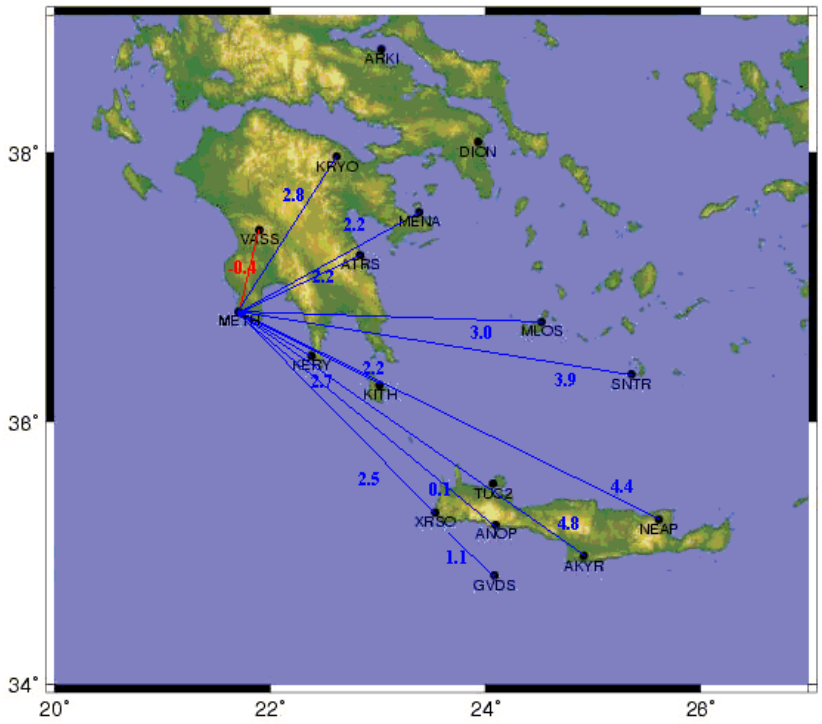

Figure 7.2: The extensional (blue) and compressional (red) baselines between METH and other COMET sites in the Aegean (mm/yr)

As the site motions confirm the findings of other studies so the strain rate results for Greece confirm previous findings. Again this is with the exception of the east – west

extension which most likely culminates in the seismicity experienced in the normal faulting across the arc but particularly in the Peloponnese where extension is at its greatest. The strain observed due to the north - south compression may result in the deeper thrust faulting around the Hellenic arc and could possibly be related to the major seismicity hypothesised by Pirazzoli (1982) and Pirazzoli et al (1996) who stated that around AD 365 there was a > M_w 8 earthquake that uplifted 100 km lithospheric block around Crete by up to 9 meters (*Stiros, 2001*, *Jackson, 2008*).

Harder to define or explain are the apparent transient variations in plate motion around the Hellenic arc. Transient motion has been observed in many parts of the Earth and been termed silent slip or silent earthquakes. In each of these examples the transient motion has occurred down dip of the seismogenic zone and been a simple reversal of the general plate motion which has led to the general hypothesis that transient motion could cause a build up of strain by pressuring the locked zone of a subduction zone (*Obara, 2002*). An example of this is the Cascadian example where the Juan de Fuca plate subducts beneath the North American plate (Figure 7.3)

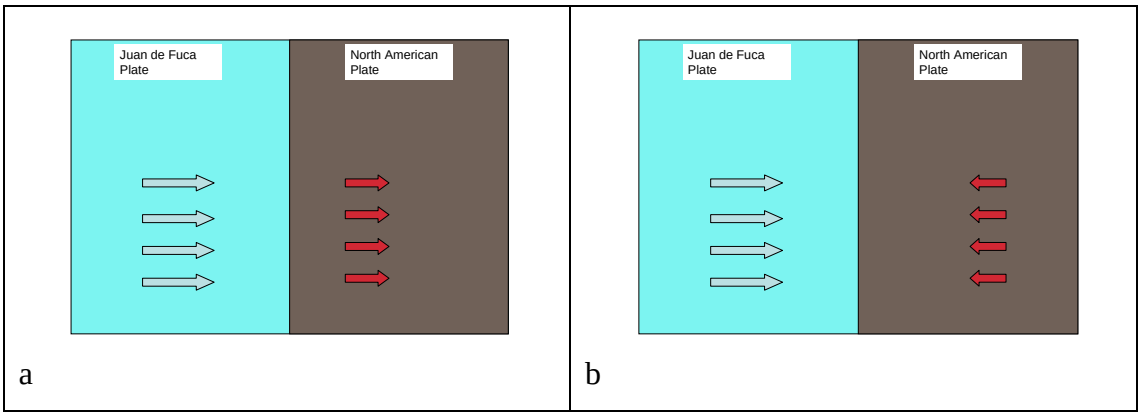

Figure 7.3: a) The general plate motion around Cascadia relative to Penticton (DRAO) b) the plate motion during a silent earthquake whereby the area down dip of the locked seismogenic zone reverses direction.

The Aegean shows a very different picture. Firstly the general motion of the Aegean plate relative to a stable reference site shows that the Hellenic arc does not move with the subducting African lithosphere in a compressional zone of thrust faulting. Instead the Aegean expands rapidly over the subducting African plate as it experiences slab roll back (figure 7.4). The transient tectonic motion presented in this thesis also differs from that seen in other examples. Rather than exhibiting a strong reversal of general motion the transient events appear more as a pause in the otherwise stable movement of the southern Aegean. What the cause of this pause is and how this affects the strain rates of

the area is debatable. It may demonstrate locking of the Aegean and the subducting African plate in what otherwise appears to be an area of stable slip but what causes or ends this hypothetical plate locking is not obvious. This is supported by the extent and locations of the sites exhibiting transient motion as they appear over a wide area ruling out any links with more localised faulting such as the normal faulting across the Peloponnese and are located only at the sites in close proximity to the Hellenic arc rather than the sites near the Gulf of Corinth or in the back arc area near the Cyclades. The location of any strain generated by these pauses is also debatable. If it is a locking of the subduction interface you would expect this to be the location of maximum strain build up as the African and Aegean plates converge on each other. If on the other hand the pause is unrelated to the subduction interface and is purely a feature associated with the southern Aegean microplate you would expect there to be a strain build up back from the Hellenic arc as the sites such as MENA and KRYO continue to move south relative to the paused sites on the arc (figure 7.4). This is not supported by the earthquake history, which shows normal, rather than thrust or reverse faulting across the Peloponnese. The pauses could be related to the compaction seen in the baselines between the Crete and the Cyclades although there is no evidence of transient motion at ANOP, AKYR or NEAP.

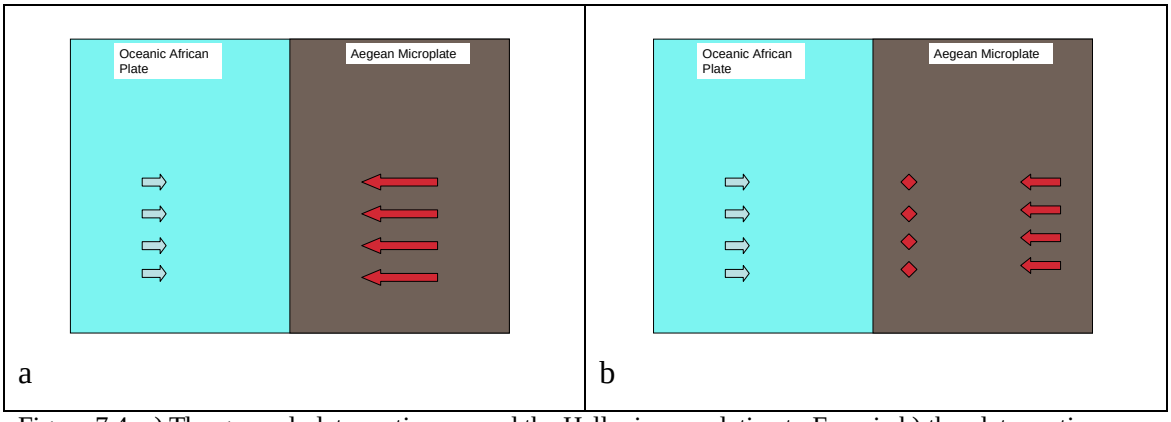

Figure 7.4: a) The general plate motion around the Hellenic arc relative to Eurasia b) the plate motion during a transient event whereby the area back from the arc pauses whilst the rest of the Aegean continues its southward movement.

To put these findings in the context of the seismic hazard assessment projects that have been undertaken on global and regional scales (*Jiminez et al. 2003*), at present the author does not feel there is sufficient data to accurately state the site movements and therefore the strain field in the region. This in turn means that an accurate image of the seismic hazard is beyond the scope of this project. The study has however demonstrated

that the techniques used do reduce noise levels in the time series to a level sufficient to highlight some of the subtler tectonic movements in the area and with greater time and therefore more data a more and more accurate image of these movements will be built up.

The use of the regional filter and the filtered baseline method highlighted the variation in common mode error across the Aegean and the European sites used. What is causing the variations in the phase and amplitude of the annual signals seen across the region is not definitively answered in this study but it is likely to be related to surface displacements due to long wavelength variations in water storage (*van Dam et al. 2007*). Some surface loads that contribute to annual signals are well modelled such as the atmosphere (*van Dam et al. 1994; Velicogna et al., 2001*) or non tidal oceanic loading (*Wahr et al. 1998*), the distribution of water on the continents in the form of soil moisture, groundwater, snow and ice is however poorly known. It can deform the Earth's surface at a scale large enough to contribute to the GPS signal (*van Dam et al. 2007*).

Variations in water mass distribution and hence surface load have been observed as a clear seasonal north/south hemispherical asymmetry in mass distribution over continents in rough accord with solar irradiance and temperature distribution (*Blewitt et al. 2001; Wu et al. 2006*). There is also variation within continents. This is particularly prevalent in Europe where a comparison of annual height signals detected by GPS and GRACE (Gravity Recovery and Climate Experiment) demonstrated that the annual signals detected by each technique do not agree in amplitude or phase and that the annual signal in the GPS heights are not coherent over the region, displaying significant variability from site to site (*van Dam et al. 2007*).

In this study van Dam et al suggest three reasons for the variation between GRACE and GPS (1) the predicted signal from GRACE does not represent the true environmental load signal, i.e., the GRACE observations are inaccurate; (2) the annual signal in the GPS heights is driven by shorter-wavelength environmental variability than is captured by GRACE gravity fields; or (3) in addition to the environment, other sources contribute to and dominate the annual signal in the GPS measurements. They conclude that the variation is due to site or network specific technique errors in the GPS observations. In particular they find a 25% improvement in agreement between the annual amplitudes

when they remove coastal sites from the comparison suggesting some mismodelling of semidiurnal ocean tide loading effects.

The variations in the amplitude and phase of annual signals observed in this study, particularly between the Aegean and Eurasian sites, supports the study by van Dam et al (2007). The coastal situation of many of the sites would be affected by any mismodelling in ocean tide loading effects which could contribute to the inconsistencies seen, however the tidal range across the meditteranean is very low (<10cm) (*Wells et al. 2005*). Although there is a micro tidal regime present in the Aegean it is not homogenous. Figure 7.5 highlights the longitudinal variation in the principal (M2) lunar tide across the region with the west of Greece experiencing 10cm of tidal variation compared with no movement around Crete. Any mismodelling of these effects would therefore lead to a small variation in the annual signal.

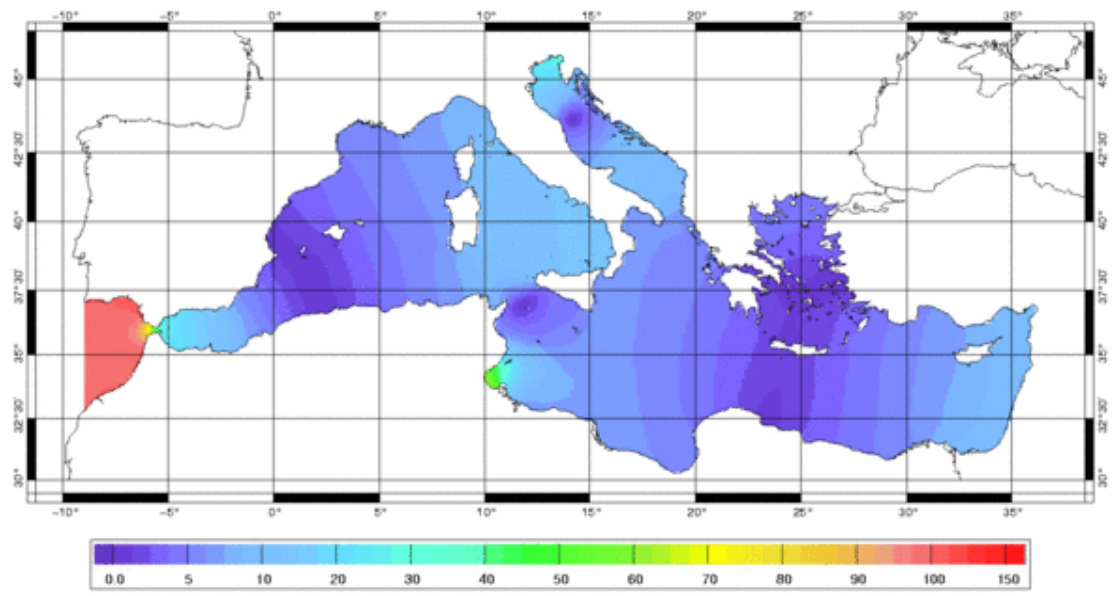

Figure 7.5: Amplitude (in cm) of the principal (M2) lunar tide in the Mediterranean predicted by the CEFMO model **(**from LEGOS http://www.legos.obs-mip.fr/).

In addition the Aegean sites are spatially located approximately 50 km apart. GRACE data looks for wavelengths in the order of 100s of kilometres and so would not detect localised changes in the COMET network. Whether these factors contribute to the annual signals is impossible to say especially as many factors can contribute to an erroneous annual signal in GPS height time series including zenith tropospheric delay, bedrock thermal expansion, monument thermal expansion, phase center modelling, orbital errors, mis-modelling of real periodic signals, etc. [Dong et al., 2002].

What the variations in common mode errors do show is the care with which regional filtering and baseline filtering need to be applied as many of the features such as atmospheric, non-tidal ocean and hydrological loading that they are intended to remove from a time series may well be less correlated than is assumed in some areas.

The spectral index of the noise in the time series produced in this study were not analysed in depth but they appear to support studies such as that by williams et al (2003) who stated that for regionally filtered time series the noise is significantly reduced. This could be due to the removal of coloureed noise from mis-modelled antenna phase center variations, mis-modelled atmospheric effects and reference frame effects (*Mao et al. 1999; Calais, 1999*), which are noise sources common to all sites. Williams et al state that the actual reduction in noise is dependant on the areal extent, between site distances and the number and quality of sites used to reduce the common mode noise. This explaions why a number of the regional filters utilised in this study did not remove all the common mode errors as many of the filters applied were formed using a limited number of sites spread over a wide area. In the same study Williams et al state that different noise sources may dominate at different sites and networks, in particular monument stability, localized dformation due to changes in groundwater and residual common mode noise may be prevalent. This would support the study of van Dam et al who stated that surface displacements due to long wavelength variations in water storage could lead to variation in the common mode error across a region and hence explain the annual signals and fluctuations across the Aegean.

7.2 Sidereal Filtering

The sidereal filtering in this thesis was performed on 30 second data. As such the instantaneous positions of the sites which were subsequently siderealy stacked and differenced from a time of interest were the product of that duration of data. It was noted by Seeber et al (1997) that the orbital periods of satellites were not in fact sidereal and varied for different satellites. The size of orbital variation could be up to 10s of seconds. This has little affect on 30 second data but for precise 1Hz applications such as the study of seismic signals the satellite geometry defined by the sidereal filter would not be optimum. As such there has been research into the formation of the optimal orbital repeat lag. Choi et al (2004) calculated the individual repeat times of each

satellite and took an average of these totals on any given day. They found that the sidereal repeat lag was generally ≈ 8 s less than the sidereal period of 23h 56m 4s due to the orbital precession of the GPS satellites. Ragheb et al (2007) autocorrelated the phase or coordinate residuals from one day to the next to best determine the optimum geometry and found that this equated to a reduction of ≈ 10 s than the nominal sidereal lag. Larson et al (2007) have taken this further still to look at the individual satellite orbits by their aspect repeat time such that their ground tracks match their previous day's topocentric position as closely as possible. Optimal shift periods are estimated from the position time series for each GPS site and are allowed to vary in time to accommodate changes in the multipath environment.

All these developments suggest that the phrase "sidereal filtering" to describe the process of shifting, averaging and differencing station positions in the coordinate domain is slightly misleading. The GPS orbits are not constrained by the US Department of Defense to be sidereal, they are set such that the ground tracks are fixed. A more apt term for the process is suggested by Larson et al (2007) who describe the process as aspect repeat time adjustment (ARTA), which better encapsulates the need to minimise the difference in ground tracks rather than the optimum difference from the nominal sidereal repeat period.

7.3 Current Developments in GPS Processing Strategies

Since the conception of the International GPS service in 1994 there has been a continuous range of improvements and corrections to the processing strategies and modelling of global GPS solutions. The period of this study has been no exception with several changes to the IGS processing taking place and with more developments under discussion. Of great significance within this is the simultaneous transition from relative phase center for receiver antennas to absolute phase center corrections for receiver and satellite antennas and the move from ITRF2000 (the reference frame used in this study) to ITRF2005. In addition there are developments in mapping functions and discussion over which function is most appropriate for GPS processing (*Steigenberger et al. 2006*).

7.3.1 Antenna Phase Center Models

The transition from relative phase center variations (mean offsets of the electrical antenna phase center compared to the physical antenna reference point), as well as phase center variations as a function of elevation angle (*Schmid et al. 2007*)) to absolute receiver antenna phase center variations (PCVs) determined by two independent approaches (calibration in a anechoic chamber and field calibration with a robot) (*Schmid et al. 2005*). This shift from relative to absolute PCVs should have the effect of avoiding systematic errors as well as allowing the use of GPS data below 10º elevation.

It was noted that there were scale differences between GPS and other techniques, in particular the global frame defined by VLBI and SLR compared to the global GPS frame which showed a terrestrial scale change of approximately 15 ppb. It was demonstrated that uncertainty in the satellite antenna phase center offset (PCO) in the z-direction was one of the major reasons for these scale differences (*Springer, 2000; Zhu et al 2003*). The gradual replacement of Block II and Block IIA GPS satellites with the introduction of more Block IIR satellites which have a larger uncertainty in the PCO in the z-direction was also causing the scale difference to drift. This has been largely solved by the generation of a consistent set of nadir-dependent PCVs. Rothacher and Schmid (2003) showed that the nadir- dependent PCVs could be solved by fixing the scale to that of the ITRF2000 and having absolute phase centers of the tracking antennas. The adoption of absolute PCVs in the ITRF2005 should result in a reduction in the previously observed scale drift and a reduction in the biases between different space geodetic techniques (*Steigenberger et al. 2006*).

All these factors improve GPS processing accuracy and would therefore improve the study of the COMET network in particular the removal of the scale drift which over time could bias strain rate estimation and therefore seismic risk assessment. Of more significance is the study by Steigenberger et al (2006a) who claim that reprocessing using absolute PCVs reduces the number and size of discontinuities, reduces the RMS of the coordinate time series and reduces annual signals. For the Aegean area the reduction and removal of annual signals would provide a powerful tool for the direct comparison of sites that display varying phase and amplitude in their annual signals.

7.3.2 ITRF2005

Unlike the past International Terrestrial Reference Frame (ITRF) versions, where global long-term solutions were combined, the ITRF2005 uses as input data time series of station positions and daily Earth Orientation Parameters (EOPs). The advantage of using time series of station positions is that it allows the monitoring of non-linear station motion and discontinuities and to examine the temporal behavior of the frame physical parameters, namely the origin and the scale (*Altimimi et al. 2007*). There are also many other developments that include a velocity field formed from 152 sites being used to estimate absolute rotation poles of 15 tectonic plates that are consistent with the ITRF2005 frame. This new absolute plate motion model supersedes and significantly improves that of the ITRF2000 which involved six major tectonic plates.

There are problems associated with the frame, for example the poor distribution and geometry of the SLR network used to define the frame's origin. Despite this the greater quantities of data and improved models used to define the frame mean that it is an advance on the ITRF2000. Any future processing of the COMET network should reflect this by homogenously reprocessing all data within the ITRF05 to avoid the discontinuities that exist between ITRF2000 and ITRF2005. This can be seen in figure 7.5 which shows a plot of the latitudinal variation of the European site PENC. The data is plotted using JPL's precise products which used the ITRF2000 frame until the 5th of November 2006 at which point they switched to ITRF2005. As can be seen there is a jump of approximately 1 cm in the latitudinal time series of this site which was purely due to this reference frame change rather than any other possible factors such as tectonic movement or equipment change.

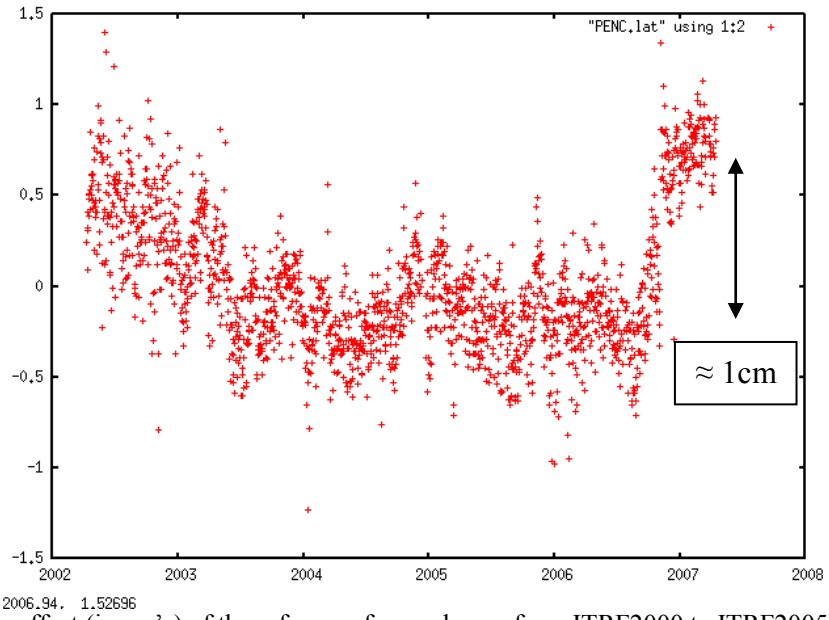

Figure 7.6: The effect (in cm's) of the reference frame change from ITRF2000 to ITRF2005 on the latitudinal position of the site PENC.

7.3.3 Mapping Functions

There has recently been the development of a range of tropospheric mapping functions these include the isobaric mapping function, IMF (*Niell, 2001*), the Vienna mapping functions (*Boehm and Schuh, 2004*) and VMF1 (*Boehm et al. 2006a*) formed using input data from numerical weather models and the Global mapping function (GMF) formed as a compromise between the IMF and VMF and Neill's mapping function (*Boehm et al. 2006b*).

The mapping function used in this study was Niell's mapping function (NMF) (*Niell, 1996*) which has been shown to produce greater scatter and significantly less reliable results than the functions mentioned above (see figure 8.3) (*Boehm et al. 2005*). This inaccuracy between the modelled troposphere and the actual tropospheric variation may in turn have contributed to the annual signals observed in much of the time series (*Boehm et al. 2006*).

At present there is still no common mapping function used by all the GPS ACs (Analysis Centers) although many still use NMF this will change in the near future, particularly given the greater accuracy of the Vienna mapping function (figure 8.6).

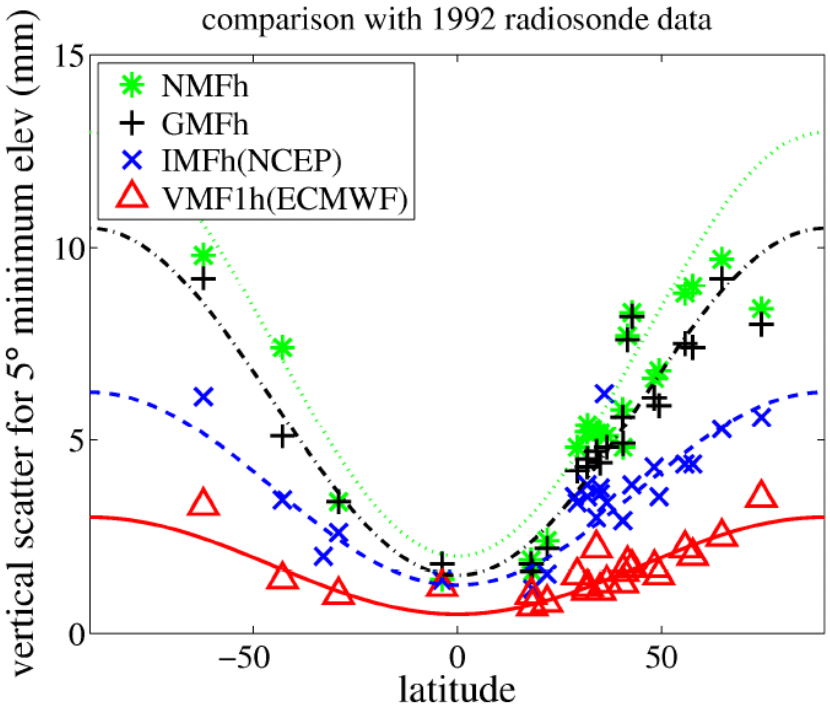

Figure 7.7: Hydrostatic height standard deviations showing the relatively higher scatter of NMF when compared to GMF, IMF and VMF1 (From Boehm et al. 2005).

7.3.4 Higher order ionospheric corrections

As mentioned in section 3.4.3, within the ionospheric delay to the GPS signal there are second-order term ionospheric terms (I_2), caused by the Faraday rotation effect induced by the Earth's magnetic field, which is about 1000 times smaller than the first order ionospheric effect and therefore usually ignored (*Kedar et al. 2003*). With increasing needs for improvements in precise GPS positioning the impact of the 2nd order term is becoming more relevant. Fritsche et al (2005) and Hernandez-Pajares et al (2007) have both shown deviations in receiver position of the order of several millimeters for sub-daily differential positioning. This was achieved using 5 days of data from four IGS stations during the time of solar maximum in an equatorial area firstly processing with out the I_2 correction and then processing with it. The two results were then compared to define the I_2 effect (*Hernandez-Pajares et al. 2007*).

The impact on daily positions has been shown to be less than a millimeter but with a latitudinal dependence. In addition, although the term has little effect on receiver parameters the satellite parameters can be affected, in particular the satellite clock which can show deviations in excess of 1cm. Satellite orbits have been shown to be

affected by a southward displacement of the orbits of several millimeters. There are now algorithms being developed to account for the I_2 using TEC maps (*Kedar et al. 2003; Fritsche et al. 2005*) or based on the GPS geometry free combinations in phase and code (*Hernandez-Pajares et al. 2007*).

In terms of this study the addition of a correction for the I_2 would have had little impact on the daily solutions due to the averaging affect of 24 hours of data, the higher latitude of the study area compared with that used in the studies by Kedar (2003), Fritsche et al (2005) and Hernandez-Pajares et al (2007), and the time of the study, which has moved away from the last solar maximum when the previous studies were investigated which would reduce the size of the I_2 error.

In contrast the sub daily solutions used in the study of sidereal filtering could have been affected. The technique of instantaneous positioning using some well constrained reference stations to determine the variations in a number of unconstrained receivers is very similar to the technique used by Hernandez-Pajares et al in their study (2007). Any significant deviations in the position estimate of a station at one time of day when compared with that same time on a subsequent sidereal day will feed into a sidereal filter. If the second order ionospheric effect can cause this deviation it is possible it could affect the results. This is not however obvious in the time series as noise levels are greater than the couple of millimeter variations mentioned in previous studies therefore further studies would be required to quantify its affect, if any.

All the developments in processing strategies mentioned in this section would have an impact on GPS positioning strategies, on this basis any reprocessing of the COMET network should take these into account and apply a homogenous processing strategy to all the available data.

Chapter 8

Conclusions

8.1 Overview of Study

This study's principal objective was to discern what could be gained from the use of CGPS for the purpose of understanding and characterising the tectonic signals in the Aegean region. For this reason a permanent GPS network was established by the COMET group across Greece and Turkey. The first sites were established in 2003 and the network has since expanded to19 continuously operating receivers when combined with the EUREF / IGS sites already in the region.

These CGPS sites were placed such that they could monitor the Hellenic arc in order to determine the apparent difference between the seismic energy released in the area and the seismic strain inferred from the Aegean microplate as it rapidly moves away from Eurasia, overriding the subducting African plate. This rapid movement is forced by the westward extrusion of the Anatolian plate in a broad zone of continental deformation where the Eurasian, African and Arabian plates interact in the eastern Mediterranean

In attempting to achieve the study's aims a range of GPS processing techniques, filters and visualisation tools were applied to the data collected in the COMET network using JPL's GIPSY – OASIS II processing software and a set of custom utilities and scripts developed by the author. In particular the GPS daily point positions were estimated using a precise point positioning strategy with ambiguity resolution. These daily positions were then filtered for outliers before regional filtering, baseline filtering and sidereal filtering were applied. In house visualisation software was used to view the

results over a range of temporal and spatial regimes. The project led to the principal conclusions, listed below.

8.2 Principal Conclusions

8.2.1 Regional Filtering

GPS daily point positions were estimated for all stations on all days of available data using a strategy of precise point positioning and ambiguity resolution in order to identify any anomalous long period or secular tectonic motion. A regional filtering technique was applied to identify and eliminate all common mode errors and error sources associated with reference frame noise that are commonly found in classical network based solutions used for tectonic studies.

The filtering process computes the daily common mode error by taking the average deviation from the positional component regression lines of a number of well established stations with clear coherent motions. That common mode error is then removed from all the sites in the study area with the aim of reducing the noise on any subsequently produced time series. In this thesis a range of regional filters were tested in an attempt to eliminate the common mode errors in the region without removing any subtle tectonic signals. A number of options were explored including using (1) a stable Eurasian based filter; (2) using only the IGS/EUREF sites within the region; (3) using only the longer standing sites (generally with the lowest σ value for their X velocity regression line due to its close orientation, 0º Longitude, to the study area in the ECEF reference frame) and (4) defining the common mode errors by the CORS located in the seismically most stable areas within the region.

Each filter worked with limited success. In general the filters would remove the common mode error and annual signals at only a limited number of sites which in turn reflected the individual characteristics exhibited at many of the COMET sites. Strong annual signals were prevalent at most locations but were out of phase by as much as 120 days, as well as exhibiting variation in their amplitudes.

These results suggested that although the technique is a well established and commonly used method of studying tectonic motion some care should be taken when defining the common mode error as networks where there is significant site by site variation in noise sources (common mode, tectonic and individual) that can effectively add ground motion signals and increase noise at other sites in the network.

8.2.2 Filtered Baseline Method

The lack of a coherent regional filter that would define and allow the removal of the common mode error from each site led to the development and application of the filtered baseline method whereby time series noise is reduced by differencing on a site by site basis to determine the baseline component variations. In principle the common mode errors at two sites, with close proximity, should be the same and therefore differencing their positional components should remove all coherent error sources. The method is not without inherent risk as any individual errors in the time series of either site will filter directly into the resulting baseline through the differencing process.

The advantage over other techniques such as the regional filtering method was reflected in the results achieved with the cleanest examples of time series variation and the lowest standard deviations achieved using this method. This reduction of time series noise allowed the detection of what appeared to be transient tectonic signals observed around the Hellenic arc.

This method highlighted a number of motions and stresses within the southern Aegean microplate. Firstly it confirmed the findings of many previous authors who have demonstrated movement at approximately 35 mm/yr SSW with respect to Eurasia. It did also demonstrate stresses within this microplate, with small amounts of compaction (≈ 5 nstrain / yr) north of Crete. At the same time the technique and data demonstrated east – west expansion along the Hellenic arc and more significant expansion throughout the Peloponnese.

8.2.3 Sidereal Filtering

Sidereal filtering was applied in order to reduce noise in sub-daily time series to the degree that seismic events and any potential seismic precursors could be observed. The technique involves the use of instantaneous positioning to obtain epoch by epoch positions at the 30 second data rate. The time series were then shifted by the sidereal period and stacked to obtain an average. This average is then differenced from a day of interest to remove geometry related noise, in particular multipath. Due to the sidereal repeatability of the of the GPS orbits and hence groundtracks these errors and noise sources also repeat on a day to day basis. The resulting time series were then studied visually at the epoch of a seismic event.

The technique was validated looking at the magnitude 8.1 earthquake north of Macquarie Island on December 23rd 2004. This showed a ≈3cm displacement at the site MAC1. The technique was then applied to the M_w 6.8 on the 8th of January 2006 earthquake near Kythira and a range of other M_w 4.5+ earthquakes around the Aegean but none of the events could be traced using the sidereal filtering technique despite many of them being felt by people tens of kilometres from the epicentre.

The filtering technique was able to reduce the scale of the noise in a time series by a factor of 1.5 – 2 which allowed a clear view of the co-seismic displacement experienced at MAC1 during the 8.1 earthquake north of Macquarie Island on December 23rd 2004. The lack of an obvious displacement or seismic signal during the weaker earthquakes is probably due to the loss of the 1 Hz CGPS data from this time due to errors in the phone line. The 30 second data was not of sufficient temporal resolution to pick out movement that only occurred for around 30 seconds. This combined with a lack of co-seismic movement showed no obvious displacement on the day of the quake when compared to other days around that time.

It is likely that the type of faulting (strike-slip near Macquarie and thrust faulting around the Hellenic Arc), may also play a significant role. A study of a similar sized earthquake at Macquarie Island (M_w 6.8) also revealed no obvious co or post seismic deformation so it may well be that the noise levels remaining in a time series after sidereal filtering are of sufficient magnitude to mask seismic signals when viewed at the 30 second rate,

especially when the receivers are a significant distance to the origin of a seismic disturbance (dependent on earthquake magnitude, depth and geological setting).

8.2.4 Observed Tectonic Signals

The study demonstrated a number of tectonic signals in the Aegean region, specifically the transient signals observed across the Hellenic arc and the pattern of strain across the region.

Transient signals

The processing filtered baseline technique revealed transient signals occurring every 12 months ±1.5 and lasting for 40 – 100 days. These signals were not so much a reversal of tectonic motion akin to the silent earthquakes observed in Cascadia, Japan and Mexico. Instead they appeared more as a pause in the otherwise consistent movement of the Aegean microplate overriding the subducting African lithosphere. The maximum horizontal movement in these events was approximately 1.5mm compared to an average annual movement of 25.5mm relative to the reference station at Ankara. This signal was noted simultaneously across approximately 400 km along the Hellenic arc suggesting it is related to the subduction process rather than the normal faulting found across the Peloponnese.

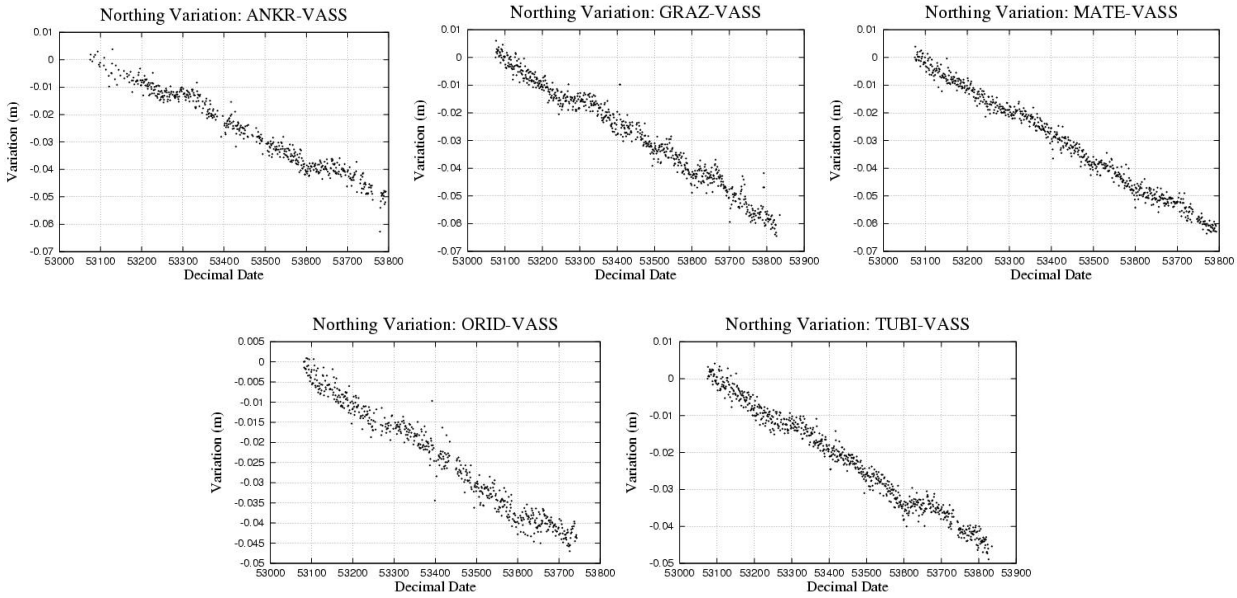

Figure 8.1: Irregularities in the time series of COMET site VASS seen from a number of seismically inert reference sites in Eurasia. (GRAZ, MATE and ORID) And from two sites in Anatolia (ANKR and TUBI)

Figure 8.1 highlights a number of the features of the transient motion. a) The events appear as distinct discontinuities, b) The events last for ≈ 60 days, c) The events are periodic occurring twice at site VASS during the period of study, d) The event occurs over a wide area across the Hellenic Arc (figure 8.2).

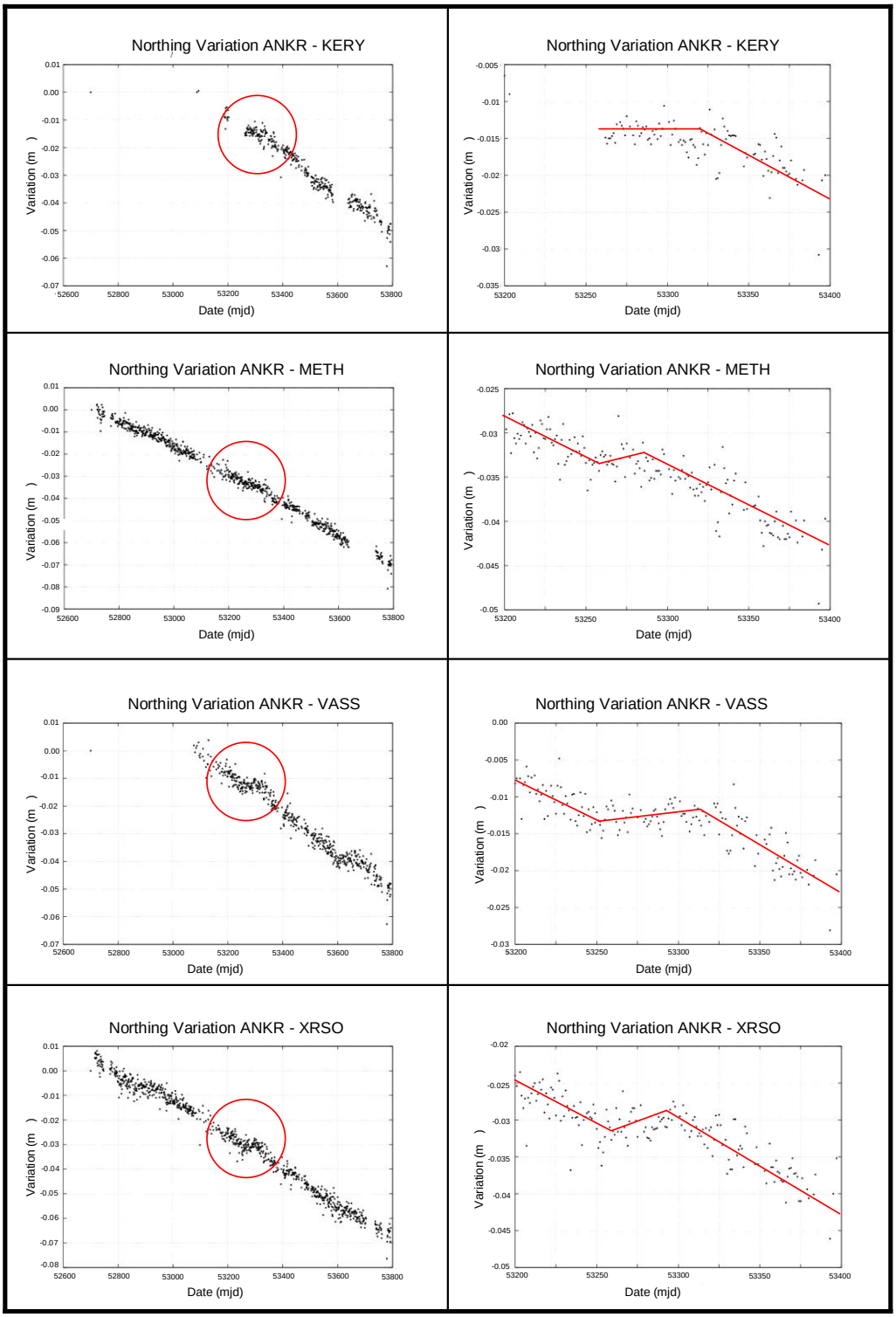

Figure 8.2: Irregularities in the time series of COMET sites around the Hellenic arc, noting that the plots have been stacked above each other to emphasise common events.

Aegean Strain and Crustal Deformation

Analysis of the annual baseline variations showed results comparable to numerous campaign GPS studies. These confirmed an east – west expansion along the Hellenic arc and expansion across the Peloponnese and Gulf of Corinth with similar annual rates of movement and hence strain levels to previous research. It also showed a small (≈ 1mm / yr) contraction between the Hellenic arc and the Cyclades islands.

These figures were in some cases calculated from less than a year of data and many baselines were calculated from less than the necessary 2.5 years needed to mitigate the effects of seasonal variations inherent in GPS time series. As such the accuracy and therefore the calculations of what seismic threat these strain build ups represent will become clearer as more data is available.

8.2.5 Visualisation Software

The traditional technique of studying time series in order to understand the temporal and spatial variations in the tectonics of an area seemed both inefficient and hard to visualise as individual site plots do not give an overview of the overall movements of a region. As such a tool was developed in collaboration with a colleague (Anthony Sibthorpe), that allows a simultaneous view of the whole network in order to show the evolution of network velocity vectors in time and space.

The method was to plot the vector variations of the COMET sites relative to a reference site. In order to introduce a way of visualising temporal variations a programme was developed that allows the user to compute vectors that best fit to data over a moving time window specified by the user.

The technique allowed the production of coherent plots that demonstrated the long term evolution of the Aegean area as well as identifying shorter term tectonic events such as the August 1999 silent earthquake event in Cascadia.

Although the technique was very good at identifying the long term tectonic motion it did prove to be an ineffective tool at identifying short term transient events. This was partly due an incomplete idea of the duration of a specific transient and therefore no idea what data span to vectorise but also due to a lack of knowledge of the start date of a transient event leading to an inappropriate temporal split between images. Both these factors essentially introduce non-transient data into the velocity vectors produced and therefore hide a transient signal to some degree. The technique can therefore be primarily used as tool for visualising tectonic motion across a region rather than a method of highlighting or discovering anomalous tectonic motion.

8.3 Future Research

The daily time series solutions presented in this thesis demonstrate the applicability of the precise point positioning strategy with post processing filters to obtain accurate network positions for the purpose of defining geophysical motion. There are areas where this work has provided partial or incomplete answers to the aims set out in the introduction. CGPS time series continuously get longer which will significantly improve the precision and reliability with which plate motions can be estimated. The majority of the post processing techniques described in this thesis would also benefit from longer time series. The COMET network was, as previously mentioned, established in 2004 with some sites having short or limited time to collect data to the degree that the techniques here require. In particular the regional filter would benefit by allowing better values for the standard deviations of the regression lines fitted to the X velocity used in defining the more stable sites (table 4.3). Extra data would also help many of the site to site baseline variation estimates calculated using the filtered baseline method. A number of these annual baseline variations were calculated from less than a year's worth of data and were therefore subject to annual signals and other noise sources that would alter both the annual variation and the bearings with which each site is moving relative to others. These baseline variations are used directly in any strain estimates of the area and therefore feed directly into the seismic risk assessment for the Aegean. In addition the more accurately the annual site movements are known the easier it is to identify confidently any anomalous or transient motion.

The investigation of vertical motion has been avoided in this work (apart from its inclusion in baseline estimates). The precision of height estimates is lower than that of horizontal motion. With increased amounts of data the vertical velocities should be investigated.

In addition to the collection of more data at the current sites care should be taken when positioning future CGPS stations. The current network was established with the aim to provide two arc parallel lines, one close to the subduction interface along the Hellenic arc and the other further back through the Peloponnese and the Cyclades islands. This network revealed the east – west expansion along the Hellenic arc and the contraction between the arc and the Cyclades demonstrated by this study. The extent of these stresses are not as yet fully defined, this would be helped by the presence of more receivers in the network particularly to the north and east of the region for example in the Dodecanese or the Sporades islands.

A feature of the study was the variation in the phase of the annual signals experienced throughout the study area but in particular between central Europe and the Aegean. The exact source of these signals and their variation is not investigated here but longer time series will enable more precise estimates of these signals and therefore a better idea of their origin. In particular an analysis of the structure of the noise content of the of these time series using maximum likelihood analysis (*Mao et al. 1999; Williams et al. 2003*) may give a better idea of whether white, flicker or random walk noise are prevalent and therefore whether monument stability, groundwater variation, etc are the source of the fluctuations in seasonal variation.

The ground motion visualisation technique developed in the study is a useful method of viewing the regions movements over a range of temporal regimes. The limit of those temporal regimes was not explored in this study as all data applied was processed as daily solutions. Further studies could attempt to see if sub 24 hour processing can also be studied for example looking at seismic events by plotting the variations in siderealy filtered time series. In addition to this the technique could be used to plot the strain developed over a given baseline and time period, particularly when looking at cumulated strain before a seismic event.

References

Agnew, D. C. (1992). The time-domain behaviour of power-law noises, *Geophysical Research Letters* 19, 333-336.

Aksu, A. E., Hall, J., Yaltirak, C. (2005). "Miocene to recent evolution of the eastern Mediterranean: New pieces of the old Mediterranean puzzle." *Marine Geology* 221: 1-13.

Allen, C. R. (1976). Responsibilities in earthquake prediction. *Bulletin of the Seismological Society of America*. 66, 2069-2074.

Altamimi, Z., Sillard, P., Boucher, C. (2002). "ITRF2000: A new release of the International Terrestrial Reference Frame for earth science applications." *Journal of Geophysical Research* 107(B10): 2214.

Altamimi, Z., Sillard, P., Boucher, C. (2003). "The impact of a No-Net-Rotation Condition on ITRF2000." *Geophysical Research Letters* 30(2).

Altamimi, Z., Collilieux, X., Legrand, J., Garayt, B., Boucher, C. (2007). "ITRF2005: A new release of the International Terrestrial Reference Frame based on time series of station positions and Earth Orientation Parameters." *Journal of Geophysical Research* 112(B09401).

Angermann, D., Drewes, H., Gerstl, M., Kaniuth, K., Kelm, R., Muller, H., Seemuller, W., Tesmer, V. (2001). Realisation of the International Terrestrial Reference Frame by DGFI Analysis center. EOS Transactions, *American Geophysical Union* 82, 47.

Angermann, D., Kaniuth, K., Muller, H., Tesmer, V., (2002). Contributions of individual space techniques to the realisation of vertical reference systems. Vertical

Reference Systems. International Association of Geodesy Symposia, vol 124. Springer-Verlag Heidelberg. 91-96

Angermann, D., Drewes, H., Gerstl, M., Kelm, R., Krugel, M., Meisel, B., (2006). ITRF Combination – Status and Recommendations for the Future. A window on the future of Geodesy. International Association of Geodesy Symposia, vol 128. Springer-Verlag Heidelberg. 3-8.

Argus, D. F., Gordon, R. G.,(1991). No-Net Rotation model of current plate velocities incorporating plate model NUVEL-1. *Geophysical Research Letters* 18 (11), 2039-2042.

Armijo, R., Lyon-Caen, H., Papanastassiou, D (1992). "East-west extension and Holocene normal-fault scarps in the Hellenic Arc." *Geology* 20(6): 491-494.

Armijo, R., Meyer, B., King, G. C. P., Rigo, A., Papanastassiou, D (1996). "Quaternary evolution of the Corinth Rift and its implications for the Late Cenozoic evolution of the Aegean." *Geophysical Journal International* 126(1): 11-53.

Ayhan, M. E., Demir, C., Lenk, O., Kilicoglu, A., Altiner, Y., Barka, A. A., Ergintav, S., Ozener, H (2002). "Interseismic strain accumulation in the Marmara Sea region." *Bulletin of the Seismological Society of America* 92(1): 216-229.

Axelrad, P., Comp, C. J., Macdoran, P.F. (1996). "SNR-Based Multipath Error Correction for GPS Differential Phase." *IEEE Transactions on Aerospace and Electronic Systems* 32: 650-660.

Baker, T. F., Curtis, D. J., Dobson, A. H., (1995). Ocean Tide Loading and GPS. *GPS World* 6 (3), 54-59.

Banitsiotou, I. D., Tsapanos, T. M., Margaris, V. N., Hatzidimitriou, P. M., (2004). Estimation of the seismic hazard parameters for various sites in Greece using a probabilistic approach. *Natural Hazards and Earth System Sciences* 4, 399-405.

Bar-Sever, Y. E. (1995). "A New Model for Yaw Attitude of Global Positioning System Satellites." *TDA Progress Report* 42-123.

Bar-Sever, Y. E. (1996). "A new model for GPS yaw attitude." *Journal of Geodesy* 70: 714-723.

Bar-Sever, Y., Kroger, P. M., Borjesson, J. A. (1998). "Estimating Horizontal gradients of tropospheric delay with a single receiver." *Journal of Geophysical Research* 103(B3): 5019-5035.

Bierman, G. J.,(1977). Factorization Methods for Discrete Sequential Estimation. Academic Press, Inc., New York.

Benetatos, C., Kiratzi, A., Papazachos, C., Karakaisis, G. (2004). "Focal mechanisms of shallow and intermediate depth earthquakes along the Hellenic Arc." *Journal of Geodynamics* 37: 253-296.

Bernard, P., Boudin, F., Sacks, S., Linde, A., Blum, P., Courteille, C., Esnoult, M., Castarede, H., Felekis, S., Billiris, H. (2004). "Continuous strain and tilt monitoring on the Trizonia Island, Rift of Corinth, Greece." C. R. *Geoscience* (336): 313-323.

Blewitt, G. (1989). "Carrier Phase Ambiguity Resolution for the Global Positioning System Applied to Geodetic Baselines up to 2000 km." *Journal of Geophysical Research* 94 (B8): 10,187-10,203.

Blewitt, G. (1990). "An automatic editing algorithm for GPS data." *Geophysical Research Letters* 17(3): 199-202.

Blewitt, G., Heflin, M. B., Webb, F. H., Lindqwister, U. J., Malla, R, P (1992). "Global Coordinates with Centimeter Accuracy in the International Terrestrial Reference Frame using GPS." *Geophysical Research Letters* 19(9): 853-856.

Blewitt, G. (1993). Advances in global positioning system technology for geodynamic investigations: 1978-1992, in Contributions of Space Geodesy to Geodynamics: *Technology*, 25, 195-213.

Blewitt, G. (1998). GPS for Geodesy, chapter 6 - GPS data processing methodology: From theory to applications. Eds. P.J.G. Teunissen and A. Kleusberg. Berlin, Springer-Verlag. ISBN 3-540-63661-7

Blewitt, G., Lavallee, D., Clarke, P., Nurutdinov, K (2001). "A new global mode of Earth deformation: Seasonal cycle detected." *Science* 294: 2342-2345.

Blewitt, G., Lavallee, D. (2002). "Effect of annual signals on geodetic velocity." *Journal of Geophysical Research* 107(B7).

Bock, H., Dach, R., Schaer, S., Meindl, M., Beutler, G (2008). CODE's New High-Rate GPS Clock Product. Analysis Center Workshop 2008, Miami Beach, Florida.

Bock, Y., Abbot, R. I., Councelman, C. C., King, R. W. (1986). "A demonstration of 1–2 parts in 107 accuracy using GPS." *Journal of Geodesy* 60(3): 241-254.

Bock, Y. (1991). "Continuous monitoring of crustal deformation." *GPS World* 2(6): 40-47.

Bock, Y., (1996). Reference systems . In :Teunissen, P. J. G., Kleusberg, A. (Eds), GPS for Geodesy, 2nd Edition. Springer-Verlag, Berlin. 1-41. ISBN 3-540-63661-7

Bock, Y., Nikolaidis, R. M., de Jonge, P.J. (2000). "Instantaneous geodetic positioning at medium distances with the Global Positioning System." *Journal of Geophysical Research* 105(B12): 28223-28253.

Bock, Y., Prawirodirdjo, L., Melbourne, T. I. (2004). "Detection of arbitrarily large dynamic ground motions with a dense high-rate GPS network." *Geophysical Research Letters* 31(L06604).

Boehm, J., Schuh, H (2004). "Vienna mapping functions in VLBI analyses." *Geophysical Research Letters* 31(L01603).

Boehm, J., Weber,R., Schuh, H., Tregoning, P., Niell, A (2005). Atmospheric delay modelling in GPS Analysis using mapping functions based on data from numerical weather models. COMET 2005. UCL London.

Boehm, J., Niell, A., Tregoning, P., Schuh, H. (2006a). "Global Mapping Function (GMF): A new emphirical mapping function based on numerical weather model data." *Geophysical Research Letters* 33(L07304).

Boehm, J., Werl, B., Schuh, H (2006b). "Troposphere mapping functions for GPS and very long baseline interferometry from European Centre for Medium-Range Weather Forecasts operational analysis data." *Journal of Geophysical Research* 111(B02406).

Boucher, C., Altamimi, Z., Feissl, M., Sillard, P. (1994). Results and analysis of the ITRF94. *IERS Technical note 18*, International Earth Rotation Service, Paris.

Boucher, C., Altamimi, Z., Feissl, M., Sillard, P. (1996). Results and analysis of the ITRF96. *IERS Technical note 20*, International Earth Rotation Service, Paris.

Boucher, C., Altamimi, Z., Sillard, P. (1999). The 1997 International Terrestrial Reference Frame, *IERS Technical note 27*, International Earth Rotation Service, Paris, 1999.

Burgmann, R., Rosen, P. A., Fielding, E. J. (2000). Synthetic Aperture Radar Interferometry to Measure Earth's Surface Topography and its Deformation. *Annual Review of Earth and Planetary Sciences*. 28, 169-209.

Calais, E. (1999). "Continuous GPS measurements across the Western Alps, 1996-1998." Geophysical Journal International 138(1): 221-230.

Carlson, R. L., Hilde, T. W. C., Uyeda, S. (1983). The driving mechanism of plate tectonics: Relation to age of the lithosphere at trench, *Geophysical Research Letters* 10, pp. 297–300.

Cerveilli, P., Segall, P., Johnson, K., Lisowski, M., Miklius, A (2002). "Sudden aseismic fault slip on the south flank of Kilauea volcano." *Nature* 415: 1014-1018.

Chapman. C. (2004). Fundamentals of Seismic Wave Propogation. Cambridge Press 2004. ISBN 0-521-81538

Choi. K, B. A., Larson. K.M, Axelrad (2004). "Modified siderial filtering: Implications for high-rate GPS positioning." *Geophysical Research Letters* 31(L22608).

Clarke, P. J., Davies, R.R., England, P.C., Parsons, B., Billiris, H., Paradissis, D., Veis, G., Cross, P.A., Denys, P.H., Ashkenazi, V., Bingley, R., Kahle, H.G., Muller, M.V., Briole, P (1998). "Crustal strain in central Greece from repeated GPS measurements in the interval 1989-1997." *Geophysical Journal International* 135: 195-214.

Clews, J. E. (1989). Structural controls on basin evolution: Neogene to Quaternary of the Ionian zone, Western Greece. *Journal of the Geological Society* . 146 (3). 447-457.

Clift, P. (1992). The collision tectonics of the southern Greek Neotethys. *Geologishe Rundschau* 81/3, 669-679.

Cocard, M., Kahle, H. G., Peter, Y., Geiger, A., Veis, G., Felekis, S., Paradissis, D., Billiris, H (1999). "New constraints on the rapid crustal motion of the Aegean region: recent results inferred from GPS measurements (1993-1998) across the West Hellenic Arc, Greece." *Earth and Planetary Science Letters* 172: 39-47.

Cross, P. (2004). MSc Surveying, Positioning lecture. Dept Geomatic Engineering, University College London.

Czopek, F., Mader, G. (2002). "Calibrating antenna phase centers." *GPS World* (May 1).

Davies, R., England, P., Parsons, B., Billiris, H., Paradissis, D., Veis, G (1997). "Geodetic strain of Greece in the interval 1892–1992." *Journal of Geophysical Research* 102(B11): 24571-24588.

DeMets, C., Gordon, R., Argus, D., (1990). Current plate motions. *Geophysics Journal International*. 101, 425-478.

DeMets, C., Gordon, R., Argus, D., Stein, S., (1994). Effect of recent revisions to the geomagnetic reversal time scale on estimates of current plate motions. *Geophysical Research Letters* 21, 2191-2194.

Dewey, J. F., Hempton, M. R., Kidd, W. S. F., Saroglu, F., Sengor, A. M. C.(1986). Shortening of continental lithosphere: the neotectonicsof eastern Anatolia – a young collision zone. *Collision Tectonics*, vol 19, 3-36.

Dobson, A. H., Shardlow, P. J., Hubbard, L. C. M., Elgered, G., Jarlemark, P. O. J. (1996). Wet tropospheric effects on precise relative GPS height determination. *Journal of Geodesy*, 70 (4), 188-202.

Dong, D., Fang, P., Bock, Y., Cheng, M. K., Miyazaki, S. (2002a). "Anatomy of apparent seasonal variations from GPS-derived site position time series." *Journal of Geophysical Research* 107 (B4): 2075.

Dong, X., Woodworth, P., Moore, P., Bingley, R., (2002). Absolute Calibration of the TOPEX/POSEIDON Altimeters using UK Tide Gauges, GPS, and Precise, Local Geoid-Differences. *Marine Geodesy*, 25, 189-204.

Dong, D., Fang, P., Bock, Y., Webb, F., Prawirodirdjo, L., Kedar, S., Jamason, P. (2006). "Spatiotemporal filtering using principal component analysis and Karhunen-Loeve expansion approaches for regional GPS network analysis." *Journal of Geophysical Research* 111(B03405).

Dragert, H., Wang, K., James, T. S. (2001). "A Silent Slip Event on the Deeper Cascadia Subduction Interface." *Science* 292: 1525-1528.

Ernst, W.G., (1990), The Dynamic Planet: Columbia University Press, New York

Evans, A. G., Hill, R. W., Blewitt, G., Swift, E. R., Yunck, T. P., Hatch, R., Lichten, S. M., Malys, S., Bossler, J., Cunningham, J. P. (2002). "The Global Positioning System Geodesy Odyssey." *Journal of the Institute of Navigation* 49(1).

Franco, S. I., Kostoglodov, V., Larson, K. M., Manea, V. C., Manea, M., Santiago, J. A. (2005). "Propogation of the 2001-2002 silent earthquake and interpolate coupling in the Oaxaca subduction zone, Mexico." *Earth Planets Space*, 57, 973-985.

Ferretti, A., Novali, F., Burgmann, R., Hilley, G., Prati, C (2004). "InSAR Permanent Scatterer Analysis Reveals Ups and Downs in San Francisco Bay Area." *Transactions American Geophysical Union* 85 (34).

Fritsche, M., Dietrich, R., Knofel, C., Rulke, A., Vey, S., Rothacher, M., Steigenberger, P (2005). "Impact of high-order ionospheric terms on GPS estimates." *Geophysical Research Letters* 32(L23311).

Gautier, P., Brun, J. P. (1994). Ductile crust exhumation and extensional detachments in the central Aegean (Cyclades and Evvia islands). *Geodinamica Acta*, 7 (2), 57-85.

Geller, R. J. (1997). Earthquake prediction: a critical review. *Geophysical Journal International*, 131, 425-450.

Genrich, J. F., Bock, Y (1992). "Rapid Resolution of Crustal Motion at Short Ranges With the Global Positioning System." *Journal of Geophysical Research* 97(B3): 3261-3269.

Giardini, D., (1999). The Global Seismic Hazard Assessment Program 1992-1999. *Special Issue. Annalis Geofis*. 42 (6)

Giardini, D., Jimenez, M.–J., Grunthal, G., (2000). European-Mediterranean Seismic Hazard Map. European Seismological Commission. UNESCO-IUGS International Geological Correlation Program Project no. 382 SESAME.

GIPSY-OASIS homepage
Available at < https://gipsy-oasis.jpl.nasa.gov >
[Accessed 15 January 2008]

Goldsworthy, M., Jackson, J., Haines, J. (2002). "The continuity of active fault systems in Greece." *Geophysical Journal International* 148: 596 - 618.

Goscombe, B. D., Everard, J. L. (2001). “Tectonic evolution of Macquarie Island: extensional structures and block rotations in oceanic crust.” *Journal of Structural Geology* 23, 639-673.

Gregorius, T. (1996). GIPSY-OASIS II, How it Works. Department of Geomatics, University of Newcastle upon Tyne.

Grunthal, G., Bosse, C., Sellami, S., Mayer-Rosa, D., Giardini, D., (1999). Compilation of the GSHAP regional seismic hazard for Europe, Africa and the Middle East. Special Issue. *Annalis Geofis*. 42, 1215-1223.

Gupta,H., Chadha, R.K., Srinagash, D. (Editors) (2001). Special Issue. The Nature of Seismic Sources and the Prediction of Earthquakes, Proceedings of the IASPEI Symposium held during the 22nd IUGG General Assembly in Birmingham, UK, *Tectonophysics*, v. 338.

Gurtner, W., Estey, L. (2007). RINEX: The Reciever Independent Exchange Format – Version 3.00.
Available at < http://www.aiub-download.unibe.ch/rinex/rinex300.pdf >
[Accessed 23 August 2007]

Hamilton, S., Shennan, I., (2005a). Late Holocene great earthquakes and relative sea level change at Kenai, southern Alaska. *Journal of Quarternary Science Review*. 20, 95-111.

Hamilton, S., Shennan, I., (2005b). Late Holocene relative sea level changes and the earthquake deformation cycle around upper Cook inlet, Alaska. *Journal of Quarternary Science Review*. 24, 1479-1498.

Heflin, M., Bertiger, W., Blewitt, G., Freedman, A., Hurst, K., Lichten, S., Lindqwister, U., Vigue, Y. Webb, F., Yunck, T., Zumberge, J (1992). "Global geodesy using GPS without fiducial sites." *Geophysical Research Letters* 19(2): 131-134.

Hernandez-Pajares, M., Juan, J. M., Sanz, J., Orus, R (2007). "Second-order ionospheric term in GPS: Implementation and impact on geodetic estimates." *Journal of Geophysical Research* 112(B08417).

Heuret, A., Lallemand, S. (2005). Plate motions, slab dynamics and back-arc deformation. *Physics of the Earth and Planetary interiors* 149 31-51.

Hollenstein, C. H., Geiger, A., Kahle, H., Veis G. (2006). "CGPS time-series and trajectories of crustal motionalong the West Hellenic Arc." *Geophysical Journal International* 164: 182 - 191.

Hollenstein, C. (2007). GPS Deformation Field and Geodynamic Implications for the Hellenic Plate Boundary Region. Institut fur Geodasie und Photogrammetrie. Zurich, Swiss Federal Institute of Technology. PhD.

Hopfield, H. S. (1969). Two-quatic tropospheric refractivity profile for correcting satellite data. *Journal of Geophysical Researc*h, 74, (18), 4487-4499.

Huang, C., Hu, X., Chen, Z (2002). "Solution of Regional GPS Network Using Presice Point Positioning with Undifferenced data." *Chinese Astronomy and Astrophysics* 26: 69-80.

IERS
Available at < http://hpiers.obspm.fr >
[Accessed 13 August 2007]

IERS Conventions 2000 (2003).
Available at < http://maia.usno.navy.mil/conv2003.html >
[Accessed 02 August 2006]

Current IGS/EUREF CGPS sites.
Available at < http://igscb.jpl.nasa.gov >
[Accessed 14 July 2008]

Jackson, J., and McKenzie, D., (1988). The relationship between plate motions and seismic moment tensors and the rates of active deformation in the Mediterranean and Middle East., *Geophysical Journal*., 93, pp. 45-73.

Jackson, J., McKenzie, D (1988). "Rates of active deformation in the Aegean Sea and Surrounding regions." *Basin Research* 1: 121-128.

Jackson, J., Haines, J., Holt, W (1992). "The Horizontal Velocity Field in the Deforming Aegean Sea Region Determined From the Moment Tensors of Earthquakes." *Journal of Geophysical Research* 97(B12): 17657-17684.

Jackson, J. (1994). "Active tectonics of the Aegean region." *Annual Review Earth and Planetary Science* 22: 239-271.

Jackson, J., (2008). The AD 365 earthquake and the tectonics of the Hellenic Trench. COMET meeting, Dept of Earth Sciences, University of Oxford, 8th January 2008.

Janssen, V. GPS on the Web: GPS Volcano Deformation Monitoring.
Available at < http://www.gmat.unsw.edu.au/snap/publications/janssen_2002.pdf >
[Accessed 22 July 2007]

Jenny, S., Goes, S., Giardini, D., Kahle, H (2004). "Earthquake recurrence parameters from seismic and geodetic strain rates in the eastern mediterranean." *Geophysical Journal International* 157: 1331-1347.

Ji, C., Larson, K. M., Tan, Y., Hudnut, K. W., Choi, K. (2004). "Slip history of the 2003 San Simeon earthquake constrained by combining 1-Hz GPS, strong motion, and teleseismic data." *Geophysical Research Letters* 31(L17608).

Jiminez, M.-J., Giardini, D., Grunthal, G., (2001). Unified seismic hazard modelling throughout the Mediterranean region. *Bollettino di Geofisica Teorica ed Applicata*. 42 (1-2), 3-18.

Jiminez, M.-J., Giardini, D., Grunthal, G. (2003). The ESC-SESAME Unified Hazard Model for the European-Mediterranean region. *CSEM-EMSC newsletter*,19.

Jin, S., Zhu, W., (1994). A revision of the parameters of the NNR-NUVEL-1A plate velocity model. *Journal of Geodynamics* 38 (2004) 85-92.

Jolivet, L., Faccenna, C., Goffe, B., Mattei, M., Rossetti, F., Brunet, C., Storti, F., Funiciello, R., Cadet, J. P., d'Aostino, N., Parra, T. (1998). "Midcrustal shear zones in postorogenic extension: Example from the northern Tyrrhenian Sea." *Journal of Geophysical Research* 103(B6): 12,123 - 12,160.

Jolivet, L. (2001). "Acomparison of geodetic and finite strain pattern in the Aegean, geodynamic implications." *Earth and Planetary Science Letters* 187: 95-104.

Kahle, H. G., Straub, C., Reilinger, R., McClusky, S., King, R., Hurst, K., Veis, G., Kastens, K., Cross, P (1998). "The strain rate field in the eastern Mediterranean region, estimated by repeated GPS measurements." *Tectonophysics* 294: 237-252.

Kahle, H. G., Cocard, M., Peter. Y., Geiger, A., Reilinger, R., McClusky, S., King, R., Barka, A., Veis, G (1999). "The GPS strain feild in the Aegean Sea and Western Anatolia." *Geophysical Research Letters* 26(16): 2513-2516.

Kahle, H.-G., Cocard, M., Peter, Y., Geiger, A., Reilinger, R., Barka, A., Veis, G (2000). "GPS-derived strain rate field within the boundary zones of the Eurasian, African and Arabian Plates." *Journal of Geophysical Research* 105(B10): 23,353-23,370.

Kanamori, H., Brodsky, E. E (2001). "The Physics of Earthquakes" *Physics Today* 54(6): 34.

Kaplan, E. D., Hegarty, C. J (2006). Understanding GPS Principles and Applications. Norwood, Artech House inc. ISBN 1-58053-894-0

Karagianni, E. E., Papazachos, C. B., Panagiotopolous, D. G., Suhadolic, P., Vuan, A., Panza, G. F. (2005). "Shear velocity structure in the Aegean area obtained by inversion of Rayleigh waves." *Geophysical Journal International* 160(1): 127-143.

Karakostas, C., Makarios, T., Lekidis, V., Salonikios, T., Sous, S., Makra, K., Anastasiadis, A., Klimis, N., Dimitriou, P., Margaris, B., Papaioannou, C., Theodulidis, N., Savvaidis, A (2006). "The Kythira (Greece) earthquake of January 8, 2006: Preliminary report on strong motion data, geotechnical and structural damage."
Available from: Earthquake Engineering Research Institute
Available at < www.eeri.org/lfe/pdf/greece_kythira_ITSAK.pdf >
[Accessed 08 May 2008]

Katsumata, A., Kamaya, N. (2003). "Low-frequency continuous tremor around the Moho discontinuity away from volcanoes in the southwest Japan" *Geophysical Research Letters* 30(1): 1020.

Kedar, S., Hajj, G. A., Wilson, B. D., Heflin, M. B. (2003). "The effect of the second order GPS ionospheric correction on reciever positions." *Geophysical Research Letters* 30(16): 1829.

Keilis-Borok, V., Ismail-Zadeh, A., Kossobokov, V., Shebalin, P. (2001). Non-linear dynamics of the lithosphere and intermediate-term earthquake prediction. *Tectonophysics*, 338, 247-260.

Kelley, M. C., Heelis, R. A. (1989). In "The Earth's Ionosphere: Plasma Physics and Electrodynamics". Academic Press, San Diego, CA.

Kim, D., Langley, R. B (2000). GPS Ambiguity Resolution and Validation: Methodologies, Trends and Issues. *Proceedings of the 7th GNSS Workshop - International Symposium on GPS/GNSS*. Seoul, Korea.

King, M., Edwards, S., Clarke, P. J (2002). "Precise Point Positioning: Breaking the monopoly of relative GPS processing." *Engineering Showcase*: 40-41.

Kissel, C., Laj, C. (1988). The Tertiary geodynamical evolution of the Aegean arc: a paleomagnetic reconstruction. *Tectonophysics* 146, 183-201.

Kobayashi, A., Manago, N., Yoshida, A (2002). "Sea level change at Uragami just before the 1946 Nankai earthquake." *Journal of the Geodetic Society of Japan* 48(1): 1-12.

Kodaira, S., Iidaka, T., Kato, A., Park, J., Iwasaki, T., Kaneda, Y (2004). "High Pore Fluid Pressure May Cause Silent Slip in the Nankai Trough." *Science* 304(5675): 1295-1298.

Konstantinou, K. I., Kalogeras, I. S., Melis, N. S., Kourouzidis, M. C., Stavrakakis, G. N (2006). "The 8 January Earthquake (Mw 6.7) Offshore Kythira Island, Southern Greece: Seismologica, Strong-motion and Macroseismic Observations of an Intermediate-depth Event." *Seismological Research Letters* 77(5): 544-553.

Koravos, G., Main, I. G., Tsapanos, T. M., Musson, R. W. M (2003). "Maximum earthquake magnitudes in the Aegean area constrained by tectonic moment release rates." *Geophysical Journal International* 152: 94 - 112.

Kostoglodov, V., Singh, S.K., Santiago, J. A., Franco, S. I., Larson, K. M., Lowry, A. R., Bilham, R (2003). "A large silent earthquake in the Guerrero seismic gap, Mexico." *Geophysical Research Letters* 30(15): 1807-1810.

Kouba, J., Heroux, P (2001). "GPS Precise Point Positioning Using IGS Orbit Products." *Physics and Chemistry of the Earth*, Part A: Solid Earth and Geodesy 26(6-8): 573-578.

Kreemer, C., Chamot-Rooke, N. (2004) Contemporary kinematics of the southern Aegean and the Mediterranean Ridge. *Geophysical Journal International* 157:3, 1377–1392

Kuang, D., Bertiger, W., Byun, S., Zumberge, J (2006). Extending GPS Orbit and Clock Products to High Rate GPS Satellite Clock Solutions. JPL Plans 2006, San Diego, JPL (Jet Propulsion Laboratory).

Kunches, J. M., Klobuchar, J. A. (2000). Some aspects of the variability of geomagnetic storms. *GPS solutions*, 4, 1, 77-78.

Langley, R. B. (1996). Propogation of GPS signals. In: Teunissen, P. J. G., Kleusberg, A. (Eds), GPS for Geodesy, 2nd Edition Springer-Verlag, Berlin Heidelberg, 111-150. ISBN 3-540-63661-7.

Larson, K. M., Bodin, P., Gomberg, J (2003). "Using 1-Hz GPS Data to Measure Deformations Caused by the Denali Fault Earthquake." *Science* 300: 1421 - 1424.

Larson, K. M., Bilich, A., Axelrad, P (2007). "Improving the precision of high-rate GPS." *Journal of Geophysical Research* 112(B05422).

Larson, K. M., Kostoglodov, V., Miyazaki, S., Santiago, J. A. (2007). "The 2006 aseismic slow slip event in Guerrero, Mexico: New results from GPS." *Geophysical Research Letters,* 23, L13309.

Lau, L., Mok, E (1999). "Improvementof GPS Relative Positioning Accuracy by using SNR." *Journal of Surveying Engineering* 125(4): 185-202.

Lavallee, D. A. (2000). Tectonic plate motions from global GPS measurements. Ph.d. thesis, University of Newcastle upon Tyne.

Leick, A.2004. GPS Satellite Surveying.(3rd ed.), John Wiley and Sons., Hoboken, New Jersey. ISBN 0-471-05930-7.

Le Pichon, X., Chamot-Rooke, N., Lallemant, S., Noomen, R., Veis, G. (1995). "Geodetic determination of the kinematics of central greece with respect to Europe." *Journal of Geophysical Research* 100: 12675-12690.

Le Pichon, X., Chamot-Rooke, N., Rangin, C., Sengor, A. M. C. (2003). "The North Anatolian fault in the Sea of Marmara." *Journal of Geophysical Research* 108(B4): 2179.

Linde, A. T., Gladwin, M. T., Johnston, M. J. S., Gwyther, R. L., Bilham, R. G. (1996). "A slow earthquake sequence on the San Andreas fault." *Nature* 383: 65-68.

Linde, A. T., Sacks, I. S., (2002). Slow earthquakes and great earthquakes along the Nankai trough. *Earth and Planetary Science Letters* 203, 265-275.

Macelwane, J. B. (1997). Forecasting earthquakes. *Geophysical Journal International*. 131, 421-422.

Mader, G. L. (1999). "GPS antenna calibration at the National Geodetic Survey." *GPS Solutions* 3(1): 50-58.

Main, I. G., Burton, P. W (1989). "Seismotectonics and the earthquake frequency magnitude distribution in the Aegean area." *Geophysical Journal Internationa*l 98(3): 575-586.

Mao, A., Harrisson, C. G. A., Dixon, T. H. (1999). Noise in GPS coordinate time series. *Journal of Geophysical Research* 104(B2): 2797-2818.

Marone, F., van der Meijde, M., van der Lee, S., Giardini, D. (2003). "Joint inversion of local, regional; and teleseismic data for crustal thickness in the Eurasia-Africa plate boundary region." *Geophysical Journal International* 154: 499-514.

Marquez-Azua, B., DeMets, C (2003). "Crustal velocity field of Mexico from continuous GPS measurements, 1993 to June 2001: Implications for the neotectonics of Mexico." *Journal of Geophysical Research* 108(B9): 2450.

Masson, F., Chery, J., Hatzfeld, D., Martinod, J., Vernant, P., Tavakoli, F., Ghafory-Ashtiani, M (2005). "Seismic versus aseismic deformation in Iran inferred from earthquakes and geodetic data." *Geophysical Journal International* 160: 217-226.

Massonnet, D., Fiegl, K. L (1998). "Radar Interferometry and its application to changes in the Earth's surface." *Reviews of Geophysics* 36(4): 441-500.

McCarthy, D. D., 1996. IERS Conventions (1996). *IERS Technical Note 21*, Central Bureau of IERS, Observatoire de Paris.

McCarthy, D. D., Petit, G., (2003). IERS Conventions (2003). *IERS Technical Note 32*, Central Bureau of IERS, Observatoire de Paris.

McClusky, S., Balassanian, s., Barka, A., Demir, C., Ergintav, S. Georgiev, I., Gurkan, O., Hamburger, M., Hurst, K., Kahle, H., Kastens, K., Kekelidze, G., King, R., Kotzev, V., Lenk, O., Mahmoud, S., Mishin, A., Nadariya, M., Ouzounis, A., Paradissis, D., Peter, Y., Prilepin, M., Reilinger, R., Sanli, I., Seeger, H., Tealeb, A., Toksov, M. N., Veis, G. (2000). "Global Positioning System constraints on plate kinematics and dynamics in the eastern Mediterranean and Caucasus." *Journal of Geophysical Research* 105(B3): 5695-5719.

McClusky, S. C., Reilinger, R. E., Mahmoud, S., Ben Sari, D., Tealeb, A. (2003). GPS constraints on Africa (Nubia) and Arabian plate motions. *Geophysical Journal International* 155:1, 126 –138.

McGuire, R. K. (2001). "Deterministic vs. probabilistic earthquake hazards and risks." *Soil Dynamics and Earthquake Engineering* 21(5): 377-384.

McKenzie, D. (1978). "Active tectonics of the Alpine—Himalayan belt: the Aegean Sea and surrounding regions." *Geophysical Journal International* 55(1): 217-254.

McKenzie, D., Jackson, J (1983). "The relationship between strain rates, crustal thickening, palaeomagnetism, finite strain and fault movements within a deforming zone." *Earth and Planetary Science Letters* 65: 182-202.

Meade, B. J., Hager, B. H., McClusky, S. C., Reilinger, R., Ergintav, S., Lenk, O., Barka, A., Ozener, H. (2002). "Estimates of seismic potential in the Marmara sea region from block models of secular deformation constrained by Global Positioning System measurements." *Bulletin of the Seismological Society of America* 92: 208-215.

Meehan, T. K., Young, L. E. (1992). On-reciever Signal Processing for GPS Multipath Reduction. Proceedings of the 6th International Symposium on Satellite Positioning, 200-208, DMA.

Melbourne, T. E., Webb, F. H (2002). "Precursory transient slip during the 2001 Mw = 8.4 Peru earthquake sequencefrom continuous GPS." *Geophysical Research Letters* 29(21): 1-28.

Mendes, V. B., Langley, R. B. (1999). Tropospheric zenith delay prediction accuracy for high precision GPS Positioning and Navigation. *Navigation*, 46, 25-34.

Miller, M. M., Johnson, D. J., Dixon, T. H., Dokka, R. K (2001). "Refined kinematics of the Eastern California shear zone from GPS observations, 1993-1998." Journal of Geophysical Research 106(B2): 2245-2263.

Milly, P. C. D., Shmakin, A. B., Dunne, K. A. (2002). Global modelling of Land Water Balances: The Land Dynamics Model (LaD), *Journal of Hydrometerology*, 3, 283-299.

Mitrovica, J. X., Milne, G. A., Davies, J. L., (2001). Glacial isostatic adjustment on a rotating earth. *Geophysical Journal International* 147, (3), 562-578.

Mitrovica, J. X., Wahr, J., Matsuyama, I., Paulson, A., (2005). The rotational stability of an ice-age earth. *Geophysical Journal International* 161 (2), 491-506.

Miyazaki, S., Larson, K, M., Choi, K., Hikima, K., Koketsu, K., Bodin, P., Haase, J., Emore, G., Yamagiwa, A (2004). "Modeling the rupture process of the 2003 September 25 Tokachi-Oki (Hokkaido) earthquake using 1-Hz GPS data." *Geophysical Research Letters* 31(L21603).

Mogi, K. (1985). "Precursors of the 1983 Japan Sea earthquake." *Earthquake Prediction Research* 3: 493-517.

Nadeau, R. M., Dolenc, D (2005). "Nonvolcanic Tremors Deep Beneath the San Andreas Fault." *Science* 307: 389.

Neill, A. E. (1996). Global mapping functions for the atmosphere delay at radio wavelengths. *Journal of Geophysical Research*, 101, B2, 3227-3246.

Niell, A. E. (2001). "Preliminary evaluation of atmospheric mapping functions based on numerical weather models." *Physics and Chemistry of the Earth* 26(6-8): 475-480.

Nikolaidis, R., Bock, Y., de Jonge, P. J., Shearer, P., Agnew, D. C., Domselaar, M (2001). "Seismic wave observations with the Global Positioning System." *Journal of Geophysical Research* 106(B10): 21,897-21,916.

Nikolaidis, R. (2002). Observation of Geodetic and Seismic Deformation with the Global Positioning System. Department of Earth Sciences. San Diego, University of California. PhD.

Nolet, G. (1990). Partitioned waveform inversion and two-dimensional structure under the Network of Autonomous Recording Seismographs, *Journal of Geophysical Research*. 95, B6, 8499–8512.

Nocquet, J.-M., Calais, E (2004). "Geodetic Measurements of Crustal Deformation in the Western Mediterranean and Europe." *Pure and Applied Geophysics* 161: 661 - 681.

Nyst, M., Thatcher, W. (2004). "New constraints on the active deformation of the Aegean." *Journal of Geophysical Research* 109(B11406).

Obara, K. (2002). "Nonvolcanic Deep Tremor Associated with Subduction in Southwest Japan." *Science* 296: 1679-1681.

Oreskes, N. (2003). Plate Tectonics: An insiders history of the Modern Theory of the Earth. Westview press. ISBN 0-8133-4132-9.

Ozawa, S., Murakami, M., Kaidzu, M., Tada, T., Sagiya, T., Hatanaka, Y., Yarai, H., Nishimura, T. (2002). "Detection and monitoring of ongoing aseismic slip in the Tokai region, Central Japan." *Science* 298: 1009-1012.

Ozawa S., H. Y., Kaidzu, M., Murakami, M., Imakiire, T., Ishigaki, Y (2004). "Aseismic slip and low-frequency earthquakes in the Bungo channel, southwestern Japan." *Geophysical Research Letters* 31(L07609).

Papazachos, C., Nolet, G. (1997). "P and S deep velocity structure of the Hellenic area obtained by robust nonlinear inversion of travel times." *Journal of Geophysical Research* 102(B4): 8349-8367.

Park, Y. J., Ang, A. H-S., Wen, Y. K (1987). "Damage-Limiting Aseismic Design of Buildings." *Earthquake Spectra* 3(1).

Parry, S., Campbell, S. D. G. (2007). Deformation associated with a slow moving landslide, Tuen Mun, Hong Kong, China. *Bulletin of Engineering Geology and the Environment*. 66, 135-141.

Payero, J. S., Kostoglodov, V., Shapiro, N., Mikumo, T., Iglesias, A., Perez-Campos, X., Clayton, R. W. (2008). "Nonvolcanic tremor observed in the Mexican subduction zone." *Geophysical Research Letters* 35(L07305).

Pirazzoli, P. A., Thommeret, J., Thommeret, Y., Laborel, J., Montaggioni, L. F (1982). "Crustal block movements from Holocene shorelines: Crete and Antikythira (Greece)." *Tectonophysics* 86: 27-43.

Pirazzoli, P. A., Laborel, J., Stiros, S. C (1996). "Earthquake clustering in the Eastern Mediterranean during historical times." *Journal of Geophysical Research* 101(B3): 6083-6097.

Poulimenos, G., Doutsos, T. (1996). "Barriers on seismogenic faults in central Greece." *Journal of Geodynamics* 22(1/2): 119-135.

Poutanen, M., Vermeer, M., Makinen, J., (1996). The permanent tide in GPS positioning. *Journal of Geodesy* 70 (8), 499-504.

Rabbel, W., Schuh, H., (1985). Static deformations and gravity changes at the Earth's surface due to atmosphere loading. *Journal of Geophysics* 56, 81-99.

Rabbel, W., Schuh, H.,(1986). The influence of atmospheric loading on VLBI experiments. *Journal of Geophysics* 59, 164-170.

Ragheb, A. E., Clarke, P. J., Edwards, S. J. (2007). "GPS Sidereal filtering: coordinate and carrierphase level strategies." *Journal of Geodesy* 81: 325-335.

Reilinger, R. E., McClusky, S. C., Oral, M. B., King, R. W., Toksoz, M. N., Barka, A. A., Kinik, I., Lenk, O., Sanli, I. (1997). "Global Positioning System measurements of present-day crustal movements in the Arabia-Africa-Eurasia plate collision zone." *Journal of Geophysical Research* 102(B5): 9983-9999.

Rius, A., Juan, J. M., Hernandez-Pajares, M., Madrigal, A. M (1995). "Measuring geocentric radial coordinates with a non-fiducial GPS network." *Bulletin Geodesique* 69: 320-328.

Rizos, C. (1999). Principles and Practice of GPS Surveying.
Available at < http://www.gmat.unsw.edu.au/snap/gps/gps_survey/principles_gps.htm > [Accessed 22 September 2007]

Roeloffs, E. A., Quilty, E (1997). "Water level and strain changes preceeding and following the August4, 1985 Kettleman Hills, Califronia, earthquake." *Pure and Applied Geophysics* 149: 21-60.

Roeloffs, E. A., (2006). Evidence for Aseismic Deformation Rate Changes Prior to Earthquakes. The *Annual Review of Earth and Planetary Science* 2006, 34, 591-627.

Rogers, G., Dragert, H. (2003). "Episodic Tremor and Slip on the Cascadia Subduction Zone: The Chatter of Silent Slip." *Science* 300: 1886-7.

Rothacher, M., Schaer, S., Mervart, L., Beutler, G. (1995). "Determination of antenna phase center variation using GPS data." *Proceedings of 1995 IGS Workshop*: Special Topics and New Directions: 205-220.

Sagiya, T., (1998). Crustal movements as earthquake precursors – Levelling anomally before the 1944 Tonankai earthquakerevisited. *Bull, Geographical, surv*. Inst 44, 23-36.

Sagiya, T. (2004). "Interplate Coupling in the Kanto District, Central Japan, and the Boso Peninsula Silent Earthquake in May 1996." *Pure and Applied Geophysics* 161: 2327-2342.

Santerre, R. (1991). Impact of GPS satellite sky distribution. *Manuscripta geodetica*, 16, 28-53.

Saastamoinen, J. (1972). Atmospheric correction for the troposphere and stratosphere in radio ranging of satellites. *Geophysical Monograph 15*, Use of Artificial Satellites for Geodesy, 247-251. American Geophysical Union.

Satirapod, C., Rizos, C (2005). "Multipath mitigation by wavelet analysis for GPS base station applications." *Surveying Review* 38(23): 2184.

Schmid, R., Rothacher, M (2003). "Estimation of elevation-dependant satellite antenna phase center variations of GPS satellites." *Journal of Geodesy* 77(7-8): 440-446.

Schmid, R., Rothacher, M., Thaller, D., Steigenberger, P. (2005). "Absolute phase center corrections of satellite and reciver antennas." *GPS Solutions* 9: 283-293.

Schmid, R., Steigenberger, P., Gendt, G., Ge, M., Rothacher, M (2007). "Generation of a consistent absolute phase center correction model GPS receiver and satellite antennas." *Journal of Geodesy* 81: 781-798.

Schubert, G, Turcotte, D. L., Olson, P. (2001). Mantle Convection in the Earth and Planets. Cambridge University Press, Cambridge.

Schuh, H., Estermann, G., Cretaux, J. F., Berge-Nguyen, M., van Dam, T. (2003). Investigation of Hydrological and Atmospheric Loading by Space Geodetic Techniques. *International Association of Geodesy Symposia*, (126), 123-132.

Scoppola, B., Boccaletti, D., Bevis, M., Carminati, E., Doglioni, C (2006). "The westward drift of the lithosphere: A rotational drag?" *Bulletin Geological Society of America* 118(1/2): 199-209.

Seeber, G., Menge, F., Volksen, C., Wubbena, G., Schmitz, M (1997). Precise GPS positioning improvements by reducing antenna and site dependant effects. *IAG Symposium 115*. Rio de Janeiro.

Segall, P., Desmarais, E. k., Miklius, A., Okubo, P (2005). (Nearly) Silent Earthquakes on Volcanoes. *Transcript AGU Fall Meeting*, 86 (52), G43A-01.

Segall, P., Desmarais, E. k., Shelley, D., Miklius, A., Cervelli, P (2006). "Earthquakes triggered by silent slip events on Kilauea volcano, Hawaii." *Nature* 442(7098): 71-74.

Sengor, A. M. C., Tuysuz, O., Imren, C., Sakinc, M., Eyidogan, H., Gorur, N., Le Pichon, X., Rangin, C (2005). "The North Anatolian Fault: A New Look." *Annual Review Earth and Planetary Science* 33: 37-112.

Severs, J. O., Faneslow, J. L., Jacobs, C. S., (1995). Theoretical modelling in Very Long Baseline Interferometry. JPL, Calafornia Institute of Technology (November 20, 1995)

Shelley, D. R., Beroza, G. C., Ide, S., Nakamula, S (2006). "Low-frequency earthquakes in Shikoku, Japan, and their relationship to episodic tremor and slip." *Nature* 442: 188-191.

Shennan, I., Long, A. J., Rutherford, M. M., Innes, J. B. Green, F. M., Walker, K. J., (1998). Tidal marsh stratigraphy, sea-level change and large earthquakes :Submergence events during the last 3500 years at NewartsBay, Oregon, USA. *Journal of Quarternary Science* Review. 17, 365-394.

Smith, D. E., Kolenkiewicz, R., Robbins, J. W., Dunn, P. J., Torrence, M. H., Klosko, S. M., Williamson, R. G., Pavlis, E. C., Douglas, N. B., Fricke, S. K., (1990). Tectonic motion and deformation from satellite laser ranging to LAGEOS. *Journal of Geophysical Research*, 95, 22013-22041.

Smith, K. D., Seggern, D., Blewitt, G., Preston, L., Anderson, J. G., Wernicke, B. P., Davis, J. L (2004). "Evidence for deep magma injection beneath lake Tahoe, Nevada-California." Science 305: 1277-1280.

Sodoudi, F., Kind, R., Hatzfeld, D., Priestley, K., Hanka, W., Wylegella, K., Stavrakakis, G., Vafidis, A., Harjes, H.-P., Bohnhoff, M (2006). "Lithospheric structure of the Aegean obtained from P and S reciever functions." *Journal of Geophysical Research* 111(B12307).

Soicher, H. (1988). Traveling ionospheric disturbances (TIDs) at mid-latitudes: solar cycle phase dependence. *Radio Science*, 23, 283-291.

Song, T. (2008). NASA tsunami research makes waves in the science community. Available at <http://www.nasa.gov/topics/earth/features/tsunami-20080117.html> [Accessed 12 February 2008]

Spence, W.,, Sipkin, S. A., Choy, G. L., (1989). Measuring the size of an earthquake. *Earthquakes and Volcanoes*, 21 (1).

Springer, T. A. (2000). Common Interests of the IGS and the IVS. Proceedings IVS 2000 General Meeting. Kotzting.

Stavrakakis, G. N., Drakopolous, J. (1995). "Bayesian probabilities o fearthquake occurences in Greece and surrounding areas." *Pure and Applied Geophysics* 144(2).

Steigenberger, P., Schmid, R., Rothacher, M (2004). "Consistent Long Time series of GPS satellite antenna phase center corrections." *American Geophysical Union*, Fall Meeting 2004.

Steigenberger, P., Romero, I., Fang, P (2006). Reprocessing Issues, Standardization, New models. *IGS Workshop 2006*. Darmstadt.

Steigenberger, P., Rothacher, M., Schmid, R., Dietrich, R., Fritsche, M., Rulke, A., Tesmer, V (2006a). Effects of Different Antenna Phase Center Models on GPS-derived Reference Frames. *Geodetic Reference Frames* 2006. Munich.

Stewart, R. R. (1991). Exploration Seismic Tomography: Fundamentals. In: *Course Notes Series* vol. 3, Society of Exploration Geophysicists, Tulsa.

Stiros, S. C. (2001). "The AD 365 Crete earthquake and possible seismic clustering during the fourth to sixth centuries AD in the Eastern Mediterranean: a review of historical and archaeological data." *Journal of Structural Geology* 23(2-3): 545-562.

Tarbuck, E. J., Lutgens, F. K (1999). Earth: An Introduction to Physical Geology. New Jersey, Prentice Hall Inc. ISBN 0131447297.

Taymaz, T., Jackson, J, A., McKenzie, D (1991). "Active tectonics of the north and central Aegean Sea." *Geophysical Journal International* 106: 433-490.

Teferle, F. N. (1996). Strategies for long-term monitoring of tide gauges using GPS. Institute of Engineering Surveying and Space Geodesy. Nottingham, University of Nottingham. PhD.

Teunissen, P. J. G. (2005). "Integer aperture bootstrapping: a new GNSS ambiguity estimator with controllable fail-rate." *Journal of Geodesy* 79(6-7): 389-397.

Tiberi, C., Lyon-Caen, H., Hatzfeld, D., Achauer, U., Karagianni, E., Kiratzi, A., Louvari, E., Panagiotopoulos, D., Kassaras, I., Kaviris, G., Makropolous, K., Papadimitriou, P. (2000). "Crustal and upper mantle structure beneath the Corinth rift (Greece) from a teleseismic tomography study." *Journal of Geophysical Research* 105(B12): 28159-28171.

Tushingham, A. M., Peltier, R. W., (1991). ICE-3G: A New Global Model of late Pleistocene Deglaciation based upon Geophysical Predictions of Post Glacial Relative Sea Level Change. *Journal of Geophysical Research* 96: 4497-4523.

Underhill, J. R. (1989). Late Cenzoic deformation of the Hellenide Foreland, Western Greece. *Bulletin of the Geological Society of America* 101, 613-634.

Earthquake information services
Available at: < http://www.usgs.gov/ >
< http://earthquake.usgs.gov/regional/world.php >
[Accessed 03 December 2007]

Van Dam, T. M., Plag, H. P., Francis, O., Gegout, P., (2002). GGFC Special Beaureau for Loading: Current Status and Plans.
Available at : < http://www.sbl.statkart.no/aboutloading >
[Accessed 01 August 2006]

Van Dam, T. M., Blewitt, G., Heflin, M.B., (1994) Atmospheric pressure loading effects on Global Positioning System coordinate determinations. *Journal of Geophysical Research* 99 (B12) 23939-23950.

Van Dam, T. M., Wahr, J., Milly, P. C. D., Shmakin, A. B., Blewitt, G., Lavallee, D., Larson, K. M. (2001). Crustal displacements due to continental water loading. *Geophysical Research Letters* 28 (4), 651-654.

Van Dam, T., Wahr, J., Lavallee, D (2007). "A comparison of annual vertical crustal displacements from GPS and Gravity Recovery and Climate Experiment (GRACE) over Europe." *Journal of Geophysical Research* 112(B03404).

Van der Hilst, R., Engdahl, R., Spakman, W., Nolet, G. (1991). Tomographic imaging of subducted lithosphere below northwest Pacific island arcs. *Nature* 353, 37 – 43.

Velicogna, I., Wahr, J (2001). "Can surface pressure be used to remove atmospheric contributions from GRACE data with sufficient accuracy to recover hydrological signals." *Journal of Geophysical Research* 106(B8): 16,415-16,434.

Vermeersen, L. L.A., (2002). The potential of GOCE in constraining the structure of the crust and Lithosphere from post-glacial rebound. *Space Science Reviews* 108, 105-113.

Wahr, J., (1985). Deformation induced by polar motion. *Journal of Geophysical Research*, 90, 9363.

Wahr, J., Molenaar, M., Bryan, F (1998). "Time variability of the Earth's gravity field: Hydrological and oceanic effects and their possible detection using GRACE." *Journal of Geophysical Research* 103(B12): 30,205-30,299.

Warnant, R., Pottiaux, E. (2000). "The increase of the ionospheric activity as measured by GPS." *Earth Planets Space* 52: 1055-1060.

Warren, D. L. M., Raquet, J. F (2003). "Broadcast vs. precise GPS ephemerides: a historical perspective." *GPS Solutions* 7: 151-156.

Wdowinski, S., Bock, Y., Zhang, J., Feng, P., Genrich, J. (1997). "Southern California Permenant GPS Geodetic Array: Spatial filtering of daily positions for estimating co-seismic and postseismic displacements induced by the 1992 Landers earthquake." *Journal of Geophysical Research* 102(B8): 18,057-18,070.

Wdowinski, S., Bock, Y., Baer, G., Prawirodirdjo, L., Bechor, N., Naaman, S., Knafo, R., Forrai, Y., elzer, Y (2004). "GPS measurements of current crustal movements along the Dead Sea Fault." *Journal of Geophysical Research* 109(B05403).

Webb, F. H., Zumberge, J. F. (1993). An Introduction to GIPSY OASIS II. *JPL Publ D-11088*, Jet Propulsion Laboratory, Pasadena.

Wells, D. (1987). Guide to GPS Positioning. Fredericton, University of New Brunswick Graphic Services.

Wells, M. R., Allison, P. A., Piggott, M. D., Pain, C. C., Hampson, G. J., Olivera, C. (2005). "Large Sea, Small Tides: the Late Carboniferous Seaway of NW Europe." *Journal of the Geological Society* 162 (3): 417-420.

Widiyantoro, S., van der Hilst, R. D., Wenzel, F. (2004). "Deformation of the Aegean Slab in the Mantel Transition Zone." *International Journal of Tomography and Statistics* D04: 1-14.

Williams , S. D. P., Bock, Y., Fang, P., Jamason, P., Nikolaidis, R. M., Prawirodirdjo, L., Miller, M., Johnson, D. J. (2003). "Error analysis of continuous GPS position time series." *Journal of Geophysical Research* 109(B03412).

Witchayangkoon, B. (2000). Elements of GPS Precise Point Positioning. Spatial Information Science and Engineering, The University of Maine: 286.

Wortel, M. J. R., Goes, S. D. B., Spakman, W. (1990). Structure and seismicity of the Aegean subduction zone. *Terra Nova*, 2, 554-562.

Wortel, M. J. R., Spakman, W. (2000). "Subduction and Slab Detachment in the Mediterranean-Carpathian Region." *Science* 290: 1910-1917.

Wright, T. J. (2002). "Remote monitoring of the earthquake cycle using satellite radar interferometry." *Phil. Trans. R. Soc. Lond* 360: 2873-2888.

Wu, J. T., Wu, S. C., Hajj, G. A., Bertiger, W. I., Lichten, S. M (1993). "Effects of antenna orientation on GPS carrier phase." *Manuscripta Geodetica* 18: 91-98.

Wu, X., Heflin, M. B., Ivins, E. R., Fukumori, I (2006). "Seasonal and interannual global surface mass variations from multisatellite geodetic data." *Journal of Geophysical Research* 111(B09401).

Wyss, M., Booth, D. C. (1996). The IASPEI procedure for the evaluation of earthquake precursors. *Geophysical Journal International* 131, 423-424.

Wyss, M. (2001). Why is earthquake prediction research not progressing faster. *Tectonophysics*, 338, 217-223.

Xu, C., Wang, H., Ge, L., Yonezawa, C., Cheng, P (2006). "InSAR tropospheric delay mitigation by GPS observations: A case study in Tokyo area." *Journal of Atmospheric and Solar-Terrestrial Physics* 68: 629-638.

Zhang, J., Bock, Y. Johnson, H., Fang, P., Williams, S., Genrich, J., Wdowinski, S., Behr J (1997). "Southern California Permenant Geodetic Array: Error analysis of daily position estimates and site velocities." *Journal of Geophysical Research* 102(B8): 18,035-18,055.

Zhang, F., Dong, D., Cheng, Z., Cheng, M., Huang, C. (2002). Seasonal vertical crustal motions in China detected by GPS and their geophysical explanation. *APSG-IRKUTSK* 2002. Irkutsk, Russia.

Zhdanov, A. V., Zhodzishsky, M. I., Veitsel, V. A., Ashjaee, J. (2001). Evolution of Multipath Error Reduction with GPS Signal Processing. *GPS Solutions*, 5, 1, 19-28

Zhu, S. Y., Massmann, F.-H., Yu, Y., Reigber, Ch (2003). "Satellite antenna phase center offsets and scale errors in GPS solutions." *Journal of Geodesy* 76: 668-672.

Zhu, L., Mitchell, B.J., Akyol, N., Cemen, I., Kekovali, K. (2006). "Crustal thickness variations in the Aegean region and its implications for the extension of continental crust." *Journal of Geophysical Research* 111.

Zong, Y., Shennan, I., Combellick, R. A., Hamilton, S. L., Rutherford, M. M., (2003). Microfossil evidence for land movements associated with the AD 1964 Alaska earthquake. *Holocene* 13, 7-20.

Zumberge, J. F., Watkins, M. M., Webb, F. H. (1997). "Characteristics and applications of precise GPS clock solutions every 30 seconds." Beacon eSpace.
Available at: < http://hdl.handle.net/2014/22369 >
[Accessed 15 July 2008]

Appendix A

COMET Site Information

COMET CGPS (Greece): AKYR (Agios Kyrillos)

Location Summary

WGS84 ellipsoid		ECEF cartesian co-ordinates	
Longitude:	24° 56' 45.39" E	*X*:	4745189.1 m
Latitude:	34° 58' 50.99" N	*Y*:	2203912.7 m
Height:	458.2 m	*Z*:	3636387.4 m

Occupation Summary

Installation date: 10 March 2004 (070 2004)

First full UTC day of data: 11 March 2004 (071 2004)

Current Equipment Summary

Receiver		Antenna		Computer	
IGS code:	TRIMBLE 5700	*IGS code:*	TRM41249.00	*Computer type:*	Fairchild (RedHat 7.3)
Firmware version:	NP 1.23 / SP 0.00	*Radome:*	TZGD	*COMET software:*	1.7.2
Serial number:	0220301071	*Serial number*	12399618		

COMET CGPS (Greece): ANOP (Anopoli)

Location Summary

ECEF cartesian co-ordinates		WGS84 ellipsoid	
X:	4762453.8 m	*Longitude:*	24° 05' 45.57699" E
Y:	2129948.9 m	*Latitude:*	35° 13' 04.67588" N
Z:	3658026.2 m	*Height:*	654.1976 m

Occupation Summary

Installation date: 25 July 2003 (206 2003)

First full UTC day of data: 26 July 2003 (207 2003)

Current Equipment Summary

Receiver		Antenna		Computer	
IGS code:	TRIMBLE 5700	*IGS code:*	TRM41249.00	*Computer type:*	MPL PIP-6 (Debian "Sarge")
Firmware version:	NP 1.23 / SP 0.00	*Radome:*	NONE	*COMET software:*	1.8
Serial number:	0220298312	*Serial number*	12399061		

COMET CGPS (Greece): ARKI (Arkitsa)

Location Summary

ECEF cartesian co-ordinates		WGS84 ellipsoid	
X:	4583365.6 m	*Longitude:*	23º 2’ 0.9” E
Y:	1948697.0 m	*Latitude:*	38º 45’ 18.2” N
Z:	3971175.0 m	*Height:*	42.6007 m

Occupation Summary

Installation date: 10 March 2004 (070 2004)

Decommission date: (075 2007)

First full UTC day of data: 11 March 2004 (207 2004)

Known periods of missing data:

2004:	001–069
	354–355
	357–366
2005:	001–050

COMET CGPS (Greece): ATRS (Ano Tiros)

Location Summary

ECEF cartesian co-ordinates		WGS84 ellipsoid	
X:	4685505.7 m	*Longitude:*	22° 50' 05.57" E
Y:	1972962.6 m	*Latitude:*	37° 14' 39.70" N
Z:	3839262.7 m	*Height:*	406.5 m

Occupation Summary

Installation date: 16 May 2005 (136 2005)

First full UTC day of data: 17 May 2005 (137 2005)

Current Equipment Summary

Receiver		Antenna		Computer	
IGS code:	TRIMBLE 5700	*IGS code:*	TRM41249.00	*Computer type:*	Fairchild (RedHat 7.3)
Firmware version:	NP 1.23 / SP 0.00	*Radome:*	NONE	*COMET software:*	1.7.2
Serial number:	0220297100	*Serial number*	12368942		

COMET CGPS (Greece): DION (Dionysos)

Location Summary

ECEF cartesian co-ordinates		WGS84 ellipsoid	
X:	4595216.4 m	*Longitude:*	23º 55’ 57.53” E
Y:	2039453.0 m	*Latitude:*	38º 04’ 42.72” N
Z:	3912626.7 m	*Height:*	514.5352 m

Occupation Summary

Installation date: 10 March 2004 (070 2004)

First full UTC day of data: 11 March 2004 (207 2004)

Current Equipment Summary

Receiver		Antenna		Computer	
IGS code:	TRIMBLE 4000SSI	*IGS code:*	TRM29659.00	*Computer type:*	Fairchild (RedHat 7.3)
Firmware version:	NP 7.32 / SP 3.08	*Radome:*	NONE	*COMET software:*	20060622
Serial number:	...16442	*Serial number*	0220067535		

COMET CGPS (Greece): GVDS (Gavdos)

Location Summary

ECEF cartesian co-ordinates		WGS84 ellipsoid	
X:	4785203.7 m	*Longitude:*	24° 04' 52.34" E
Y:	2138641.6 m	*Latitude:*	34° 49' 53.30" N
Z:	3622704.5 m	*Height:*	295.0 m

Occupation Summary

Installation date: 26 June 2006 (177 2006)

First full UTC day of data: 27 June 2006 (178 2006)

Current Equipment Summary

Receiver		Antenna		Computer	
IGS code:	TRIMBLE 5700	*IGS code:*	TRM41249.00	*Computer type:*	MPL PIP-6 (Debian "Sarge")
Firmware version:	NP 1.24 / SP 0.00	*Radome:*	NONE	*COMET software:*	1.8
Serial number:	0220298303	*Serial number*	12399557		

COMET CGPS (Greece): KERY (Kerya)

Location Summary

ECEF cartesian co-ordinates		WGS84 ellipsoid	
X:	4746993.4 m	*Longitude:*	22° 23' 00.65" E
Y:	1954971.7 m	*Latitude:*	36° 29' 35.77" N
Z:	3772452.5 m	*Height:*	198.8

Occupation Summary

Installation date: 13 March 2004 (073 2004)

First full UTC day of data: 14 March 2004 (074 2004)

Current Equipment Summary

Receiver		Antenna		Computer	
IGS code:	TRIMBLE 5700	*IGS code:*	TRM41249.00	*Computer type:*	Fairchild (RedHat 7.3)
Firmware version:	NP 1.23 / SP 0.00	*Radome:*	NONE	*COMET software:*	1.7.2
Serial number:	0220298304	*Serial number*	12378164		

COMET CGPS (Greece): KITH (Kithira)

Location Summary

ECEF cartesian co-ordinates		WGS84 ellipsoid	
X:	4738508.9 m	*Longitude:*	23° 00' 54.59" E
Y:	2012857.9 m	*Latitude:*	36° 16' 28.29" N
Z:	3752992.2 m	*Height:*	337.3 m

Occupation Summary

Installation date: 13 March 2004 (073 2004)

First full UTC day of data: 14 March 2004 (074 2004)

Current Equipment Summary

Receiver		Antenna		Computer	
IGS code:	TRIMBLE 5700	*IGS code:*	TRM41249.00	*Computer type:*	MPL PIP-6 (Debian "Sarge")
Firmware version:	NP 2.01 / SP 0.00	*Radome:*	NONE	*COMET software:*	20060622
Serial number:	0220301080	*Serial number*	12399600		

COMET CGPS (Greece): KRYO (Kryoneri)

Location Summary

ECEF cartesian co-ordinates		WGS84 ellipsoid	
X:	4647807.3 m	*Longitude:*	22° 37' 04.37" E
Y:	1936397.5 m	*Latitude:*	37° 58' 20.30" N
Z:	3903591.5 m	*Height:*	926.9 m

Occupation Summary

Installation date: 12 May 2005 (132 2005)

First full UTC day of data: 13 May 2005 (133 2005)

Current Equipment Summary

Receiver		Antenna		Computer	
IGS code:	TRIMBLE 5700	*IGS code:*	TRM41249.00	*Computer type:*	Fairchild (RedHat 7.3)
Firmware version:	NP 1.23 / SP 0.00	*Radome:*	TZGD	*COMET software:*	20070109
Serial number:	0220297115	*Serial number*	12378153		

COMET CGPS (Greece): MENA (Methana)

Location Summary

ECEF cartesian co-ordinates		WGS84 ellipsoid	
X:	4646460.0 m	*Longitude:*	23° 23' 09.78" E
Y:	2009359.8 m	*Latitude:*	37° 33' 39.74" N
Z:	3866971.7 m	*Height:*	57.5 m

Occupation Summary

Installation date: 22 June 2004 (174 2004)

First full UTC day of data: 23 June 2004 (175 2004)

Current Equipment Summary

Receiver		Antenna		Computer	
IGS code:	TRIMBLE 5700	*IGS code:*	TRM41249.00	*Computer type:*	MPL PIP-6 (Debian "Sarge")
Firmware version:	NP 1.23 / SP 0.00	*Radome:*	NONE	*COMET software:*	20060622
Serial number:	0220298307	*Serial number*	12399180		

COMET CGPS (Greece): METH (Methoni)

Location Summary

ECEF cartesian co-ordinates		WGS84 ellipsoid	
X:	4749280.4 m	*Longitude:*	21° 42' 16.45" E
Y:	1890407.1 m	*Latitude:*	36° 49' 31.85" N
Z:	3801955.9 m	*Height:*	75.1 m

Occupation Summary

Installation date: 20 March 2003 (079 2003)

First full UTC day of data: 20 March 2003 (080 2003)

Current Equipment Summary

Receiver		Antenna		Computer	
IGS code:	TRIMBLE 5700	*IGS code:*	TRM41249.00	*Computer type:*	Fairchild (RedHat 7.3)
Firmware version:	NP 1.23 / SP 0.00	*Radome:*	NONE	*COMET software:*	
Serial number:	0220301077	*Serial number*	12377818		

COMET CGPS (Greece): MLOS (Milos)

Location Summary

ECEF cartesian co-ordinates		WGS84 ellipsoid	
X:	4655589.1 m	*Longitude:*	24° 31' 08.85" E
Y:	2123551.3 m	*Latitude:*	36° 44' 48.50" N
Z:	3795046.3 m	*Height:*	218.4 m

Occupation Summary

Installation date: 28 June 2004 (180 2004)

First full UTC day of data: 29 June 2004 (181 2004)

Current Equipment Summary

Receiver		Antenna		Computer	
IGS code:	TRIMBLE 5700	*IGS code:*	TRM41249.00	*Computer type:*	Fairchild (RedHat 7.3)
Firmware version:	NP 1.23 / SP 0.00	*Radome:*	NONE	*COMET software:*	1.7.1
Serial number:	0220297116	*Serial number*	12377755		

COMET CGPS (Greece): NEAP

Location Summary

ECEF cartesian co-ordinates		WGS84 ellipsoid	
X:	4701748.1 m	*Longitude:*	25° 36' 37.33" E
Y:	2253746.6 m	*Latitude:*	35° 15' 40.88" N
Z:	3661764.3 m	*Height:*	318.1522 m

Occupation Summary

Installation date: 31 December 2002 (365 2002)

First full UTC day of data: 01 January 2003 (001 2003)

Current Equipment Summary

Receiver		Antenna		Computer	
IGS code:	TRIMBLE 5700	*IGS code:*	TRM41249.00	*Computer type:*	Fairchild (RedHat 7.3)
Firmware version:	NP 1.23 / SP 0.00	*Radome:*	NONE	*COMET software:*	1.2
Serial number:		*Serial number*			

COMET CGPS (Greece): SNTR (Santorini)

Location Summary

ECEF cartesian co-ordinates		WGS84 ellipsoid	
X:	4647218.3 m	*Longitude:*	25° 21' 25.48" E
Y:	2202396.6 m	*Latitude:*	36° 21' 27.54" N
Z:	3760306.9 m	*Height:*	137.9 m

Occupation Summary

Installation date: 26 June 2004 (178 2004)

First full UTC day of data: 27 June 2004 (179 2004)

Current Equipment Summary

Receiver		Antenna		Computer	
IGS code:	TRIMBLE 5700	*IGS code:*	TRM41249.00	*Computer type:*	Fairchild (RedHat 7.3)
Firmware version:	NP 1.23 / SP 0.00	*Radome:*	NONE	*COMET software:*	1.7.2
Serial number:	0220296463	*Serial number*	12399047		

COMET CGPS (Greece): SPRT (Sparti)

Location Summary

ECEF cartesian co-ordinates		WGS84 ellipsoid	
X:	4713881.6 m	*Longitude:*	22° 22' 19.55" E
Y:	1940236.7 m	*Latitude:*	37° 02' 45.66" N
Z:	3821960.7 m	*Height:*	814.0 m

Occupation Summary

Installation date: 20 July 2006 (201 2006)

First full UTC day of data: 21 July 2006 (202 2006)

Current Equipment Summary

Receiver		Antenna		Computer	
IGS code:	TRIMBLE 5700	*IGS code:*	TRM41249.00	*Computer type:*	Fairchild (RedHat 7.3)
Firmware version:	NP 1.23 / SP 0.00	*Radome:*	TZGD	*COMET software:*	20061009
Serial number:	0220297108	*Serial number*	12399241		

COMET CGPS (Greece): VASS (Vasses)

Location Summary

ECEF cartesian co-ordinates		WGS84 ellipsoid	
X:	4706041.4 m	*Longitude:*	21° 53' 57.34" E
Y:	1891746.0 m	*Latitude:*	37° 25' 49.60" N
Z:	3856151.3 m	*Height:*	1175.5 m

Occupation Summary

Installation date: 10 March 2004 (070 2004)

First full UTC day of data: 11 March 2004 (071 2004)

Current Equipment Summary

Receiver		Antenna		Computer	
IGS code:	TRIMBLE 5700	*IGS code:*	TRM41249.00	*Computer type:*	Fairchild (RedHat 7.3)
Firmware version:	NP 1.23 / SP 0.00	*Radome:*	TZGD	*COMET software:*	1.7.2
Serial number:	0220298316	*Serial number*	12399150		

COMET CGPS (Greece): XRSO (Chrisoskalitissa)

Location Summary

ECEF cartesian co-ordinates		WGS84 ellipsoid	
X:	4777260.3 m	*Longitude:*	23° 31' 57.71" E
Y:	2080454.5 m	*Latitude:*	35° 18' 37.96" N
Z:	3666053.4 m	*Height:*	31.4 m

Occupation Summary

Installation date: 16 March 2003 (075 2003)

First full UTC day of data: 17 March 2003 (076 2003)

Current Equipment Summary

Receiver		Antenna		Computer	
IGS code:	TRIMBLE 5700	*IGS code:*	TRM41249.00	*Computer type:*	Fairchild (RedHat 7.3)
Firmware version:	NP 1.23 / SP 0.00	*Radome:*	NONE	*COMET software:*	1.2
Serial number:	0220301082	*Serial number*	12399258		

Appendix B

The conversion of geocentric Cartesian coordinates to geodetic ellipsoidal coordinates

This is calculated as:

$$X = (N + h)\cos\varphi\cos\lambda$$
$$Y = (N + h)\cos\varphi\sin\lambda$$
$$Z = \left(N\left(1 - e^2\right) + h\right)\sin\varphi$$

Where

λ, φ, h : Geodetic ellipsoidal Longitude and Latitude and ellipsoidal height

N : Transverse radius of curvature

The auxiliary quantities N and e are:

$$N = \frac{a}{\sqrt{1 - e^2 \sin^2 \varphi}}$$
$$e^2 = 2f - f^2$$

These equations can be inverted to determine the geodetic ellipsoidal coordinates (λ, φ, h);

$$\lambda = \arctan\left(\frac{Y}{X}\right)$$

$$\varphi = \arctan\left(\frac{Z}{\sqrt{X^2+Y^2}} \cdot \frac{1}{1-\frac{N}{N+h}e^2}\right)$$

$$h = \frac{\sqrt{X^2+Y^2}}{\cos\varphi} - N$$

Appendix C

COMET Site Logs

Available data per station and day

x : data available

- : no data available

The numbers in the heading lines represent the day of year.

2002

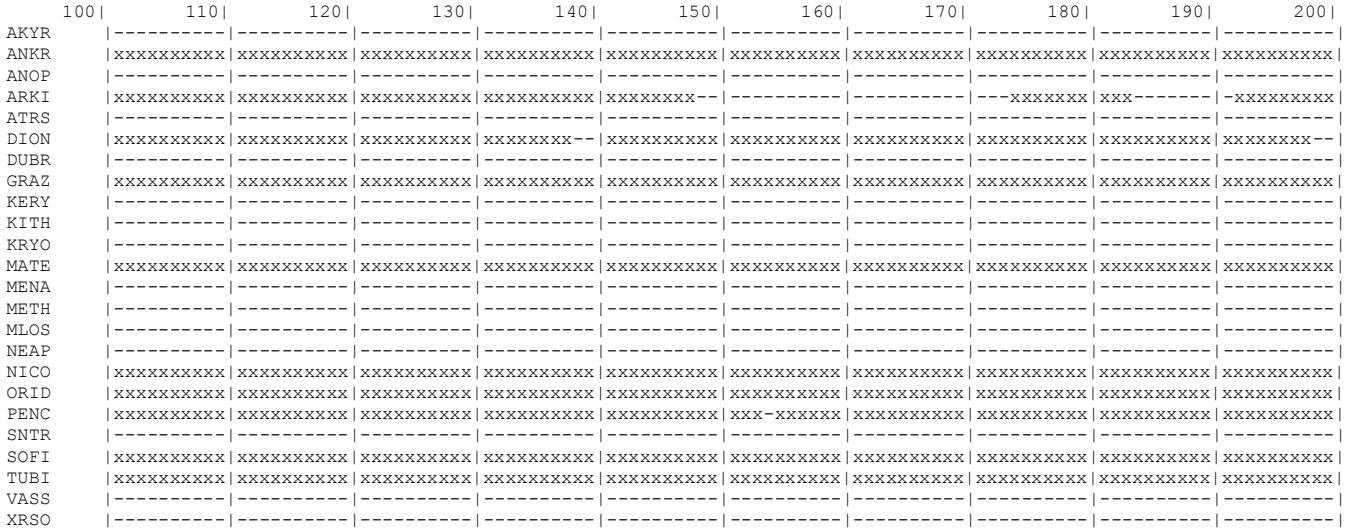

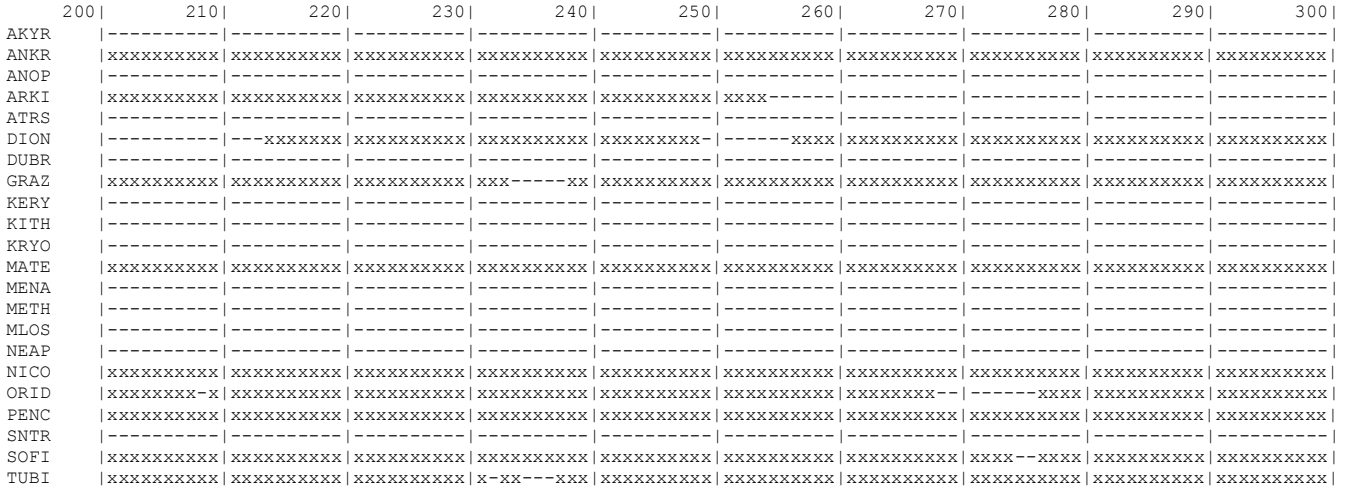

```
VASS    |----------|----------|----------|----------|----------|----------|----------|----------|----------|----------|
XRSO    |----------|----------|----------|----------|----------|----------|----------|----------|----------|----------|
```

```
     300|       310|       320|       330|       340|       350|       360|
AKYR    |----------|----------|----------|----------|----------|----------|-----
ANKR    |xxxxxxxxxx|xxxxxxxxxx|xxxxxxxxxx|xxxxxxxxxx|xxxxxxxxxx|xxxxxxxxxx|xxxxx
ANOP    |----------|----------|----------|----------|----------|----------|-----
ARKI    |----------|----------|----------|----------|----------|----------|-----
ATRS    |----------|----------|----------|----------|----------|----------|-----
DION    |xxxxxxxxxx|xxxxxxxxxx|xxxxxxxxxx|xxxxxxxxxx|xxxxxxxxxx|xxxxxxxxxx|xxxxx
DUBR    |----------|----------|----------|----------|----------|----------|-----
GRAZ    |xxxxxxxxxx|xxxxxxxxxx|xxxxxxxxxx|xx----xxxx|xxxxx-----|-xxxxxxxxx|xxxxx
KERY    |----------|----------|----------|----------|----------|----------|-----
KITH    |----------|----------|----------|----------|----------|----------|-----
KRYO    |----------|----------|----------|----------|----------|----------|-----
MATE    |xxxxxxxxxx|xxxxxxxxxx|xxxxxxxxxx|xxxxxxxxxx|xxxxxxxxxx|xxxxxxxxxx|xxxxx
MENA    |----------|----------|----------|----------|----------|----------|-----
METH    |----------|----------|----------|----------|----------|----------|-----
MLOS    |----------|----------|----------|----------|----------|----------|-----
NEAP    |----------|----------|----------|----------|----------|----------|-----
NICO    |xxxxxxxxxx|xxxxxxxxxx|xxxxxxxxxx|xxxxxxxxxx|xxxxxxxxxx|xxxx--xxxx|xxxxx
ORID    |xxxxxxxxxx|xxxxxxxxxx|xxxxxxxxxx|xxxxxxxxxx|xxxxxx-xxx|xxxxxxxxxx|xxxxx
PENC    |xxxxxxxxxx|xxxxxxxxxx|xxxxxxx-xx|xxxxxxxxxx|xxxxxxxxxx|xxxxxxxxxx|xxxxx
SNTR    |----------|----------|----------|----------|----------|----------|-----
SOFI    |xxxxxxxxxx|xxxxxxxxxx|xxxxxxxxxx|xxxxxxxxxx|xxxxxxxxxx|xxxxxxxxxx|xxxxx
TUBI    |xxxxxxxxxx|xxxxxxxxxx|xxxxxxxxxx|xxxxxxxxxx|xxxxxxxxxx|xxxxxxxxxx|xxxx-
VASS    |----------|----------|----------|----------|----------|----------|-----
XRSO    |----------|----------|----------|----------|----------|----------|-----
```

2003

```
      0|        10|        20|        30|        40|        50|        60|        70|        80|        90|       100|
AKYR    |----------|----------|----------|----------|----------|----------|----------|----------|----------|----------|
ANKR    |xxxxxxxxxx|xxxxxxxxxx|xxxxxxxxxx|xxxxxxxx--|-------xxx|xxxxxxxxxx|xxxxxxxxx|xxxxxxxx-x|xxxxxxxxxx|
ANOP    |----------|----------|----------|----------|----------|----------|----------|----------|----------|----------|
ARKI    |----------|----------|----------|----------|----------|----------|---xxxxxxx|xxxxxxxxx|----------|----------|
ATRS    |----------|----------|----------|----------|----------|----------|----------|----------|----------|----------|
DION    |xxxxxxxxxx|xxxxxxxxxx|xxxxxxxxxx|xxxxxxxxxx|xxxxxxxxxx|xxxxxxxxx|xxxxxxxx-|--xxxxxxxx|xxxxxxx-xx|xxxxxxxxxx|
DUBR    |----------|----------|----------|----------|----------|----------|----------|----------|----------|----------|
GRAZ    |xxxxxxxxxx|xxxxxxxxxx|xxxxxxxxxx|xxxxxxxxxx|xxxxxxxxxx|xxxxxxxxx|xxxxxxxxx|xxxxxxx-x|xxxxxxxxxx|xxxxxxxxxx|
KERY    |----------|----------|----------|----------|----------|----------|----------|----------|----------|----------|
KITH    |----------|----------|----------|----------|----------|----------|----------|----------|----------|----------|
KRYO    |----------|----------|----------|----------|----------|----------|----------|----------|----------|----------|
MATE    |xxxxxxxxxx|xxxxxxxxxx|xxxxxxxxxx|xxxxxxxxxx|xxxxxxxxxx|xxxxxxxxx|xxxxxxxxx|xxxxxxxxx|xxxxxxxxx|xxxxxxxxxx|
MENA    |----------|----------|----------|----------|----------|----------|----------|----------|----------|----------|
METH    |----------|----------|----------|----------|----------|----------|----------|--------xx|xxxxxxxxx|xxxxxxxxx|
MLOS    |----------|----------|----------|----------|----------|----------|----------|----------|----------|----------|
NEAP    |xxxxxxxx--|------xxxx|xxxxxxxxx|xxxxxxxxx|xxxxxxxxx|xx--------|----------|----------|----------|----------|
NICO    |xxxxxxxxx|xxxxxxxxx|xxxxxxxxx|xxxxxxxxx|xxxxxxxxx|xxxxxxxxx|xxxxxxxxx|xxxxxxxxx|xxxxxxxxx|xxxxxxxxx|
ORID    |xxxxxxxxx|xxxxxxxxx|xxxxxxxxx|xxxxxxxxx|xxxxxxxxx|xxxxxxxxx-|-xxxxxxxxx|xxxxxxxxx|xxxxxxxxx|xxxxxxxxx|
PENC    |xxxxxxxxx|xxxxxxxxx|xxxxxxxxx|xx-xxxxxxx|xxxxxxxxx|xxxxxxxxx|xxxxxxxxx|xxxxxxxxx|xxxxxxxxx|xxxxxxxxx|
SNTR    |----------|----------|----------|----------|----------|----------|----------|----------|----------|----------|
SOFI    |xxxxxxxxx|xxxxxxxxx|xxxx---xxx|xxxxxxxxx|xxxxxxxxx|xxxxxxxxx|xxxxx---x|xxxxxxxxx|xxxxxxx-x|xxxx-xxxxx|
TUBI    |xxxxxxxxx|xxxxxxxxx|xxxxxxxxx|xxxxxxxxx|xxxxxxxxx|xxxxxxxxx|xxxxxxxxx|xxxxxxxxx|xxxxxxxxx|xxxxxxxxx|
VASS    |----------|----------|----------|----------|----------|----------|----------|----------|----------|----------|
XRSO    |----------|----------|----------|----------|----------|----------|----------|----xxxxxx|xxxxxxxxx|xxxxxxxxx|
```

```
      100|       110|       120|       130|       140|       150|       160|       170|       180|       190|       200|
AKYR    |----------|----------|----------|----------|----------|----------|----------|----------|----------|----------|
ANKR    |xxxxxxxxx-|----------|----------|xxxxxxxxx|------xxxx|xxxxxxxx-|xxxxxxxxx|xxxxxxxxx|xxxxxxxxx|xxxxxxxxx|
ANOP    |----------|----------|----------|----------|----------|----------|----------|----------|----------|----------|
ARKI    |---xxxxxxx|xxxxxxxxx|xxxxxxx---|----------|----------|--------x|xxxxxxxxx|xxxxxxxxx|xxxxxxxxx|xxxxxxxxx|
ATRS    |----------|----------|----------|----------|----------|----------|----------|----------|----------|----------|
DION    |xxxxxxxxx|xxxxxxxxx|xxxxxxxxx|xxxxxxxxx|xxxxxxxxx|xxxxxxxxx|xxxxxxxxx|xxxxxxxxx|xxxxxxxx-|-xxxxxxxxx|
DUBR    |----------|----------|----------|----------|----------|----------|----------|----------|----------|----------|
GRAZ    |xxxxxxxxx|xxxxxxxxx|xxxxxxxxx|xxxxxxxxx|xxxxxxxxx|xxxxxxxxx|xxxxxxxxx|xxxxxxxxx|xxxxxxxxx|xxxxxxxxx|
KERY    |----------|----------|----------|----------|----------|----------|----------|----------|----------|----------|
KITH    |----------|----------|----------|----------|----------|----------|----------|----------|----------|----------|
KRYO    |----------|----------|----------|----------|----------|----------|----------|----------|----------|----------|
MATE    |xxxxxxxxx|xxxxxxxxx|xxxxxxxxx|xxxxxxxxx|xxxxxxxxx|xxxxxxxxx|xxxxxxxxx|xxxxxxxxx|xxxxxxxxx|xxxxxxxxx|
MENA    |----------|----------|----------|----------|----------|----------|----------|----------|----------|----------|
METH    |xxxxxxxxx|xxxxxxxxx|xxxxxxxxx|xxxxxxxxx|xxxxxxxxx|xxxxxxxxx|xxxxxxxxx|xxxxxxxxx|xxxxxxxxx|xxxxxxxxx|
MLOS    |----------|----------|----------|----------|----------|----------|----------|----------|----------|----------|
NEAP    |xxxxxxxx--|-xxxxxxxxx|xxxxxxxxx|xxxxxxxxx|xxxxxxxxx|xxxxxxxxx|xxxxxxxxx|xxxxxxxx--|----------|----------|
NICO    |xxxxxxxxx|xxxxxxxxx|xxxxxxxxx|xxxxxxxxx|xxxxxxxxx|xxxxxxxxx|xxxxxxxxx|xxxxxxxxx|xxxxxxxxx|xxxxxxxxx|
ORID    |xxxxxxxxx|xxxxxxxxx|xxxxxxxxx|xxxxxxxxx|xxxxxxxxx|xxxxxxxxx|xxxxxxxxx|---xxxxxxx|xxxxxxxxx|xxxxxxxxx|
PENC    |xxxxxxxxx|xxxxxx-xxx|xxxxxxxxx|xxxxxxxx-|-xxxxxxxxx|xxxxxxxxx|xxxxxxxxx|xxxxxxxxx|xxxxxxxxx|xxxxxxxxx|
SNTR    |----------|----------|----------|----------|----------|----------|----------|----------|----------|----------|
SOFI    |xxxxxxxxx|xxxxxxxxx|xxxxxxxxx|xxxxxxxxx|xxxxxxxxx|-----xxxxx|xx--xxxxxx|xxxxxxxxx|xxxxxxxxx|xxxxxxxxx|
TUBI    |xxxxxxxxx|xxxxxxxxx|xxxxxxxxx|xxxxxxxxx|xxxxxxxxx|xxxxxxxxx|xxxxxxxxx|xxxxxxxxx|xxxxxxxxx|xx-xxxxxxx|
VASS    |----------|----------|----------|----------|----------|----------|----------|----------|----------|----------|
XRSO    |xxxxxxxxx|xxxxxxxxx|xxxxxxxxx|xxxxxxxxx|xxxxxxxxx|xxxxxxxxx|xxxxxxxxx|xxxxxxxxx|xxxxxxxxx|xxxxxxxxx|
```

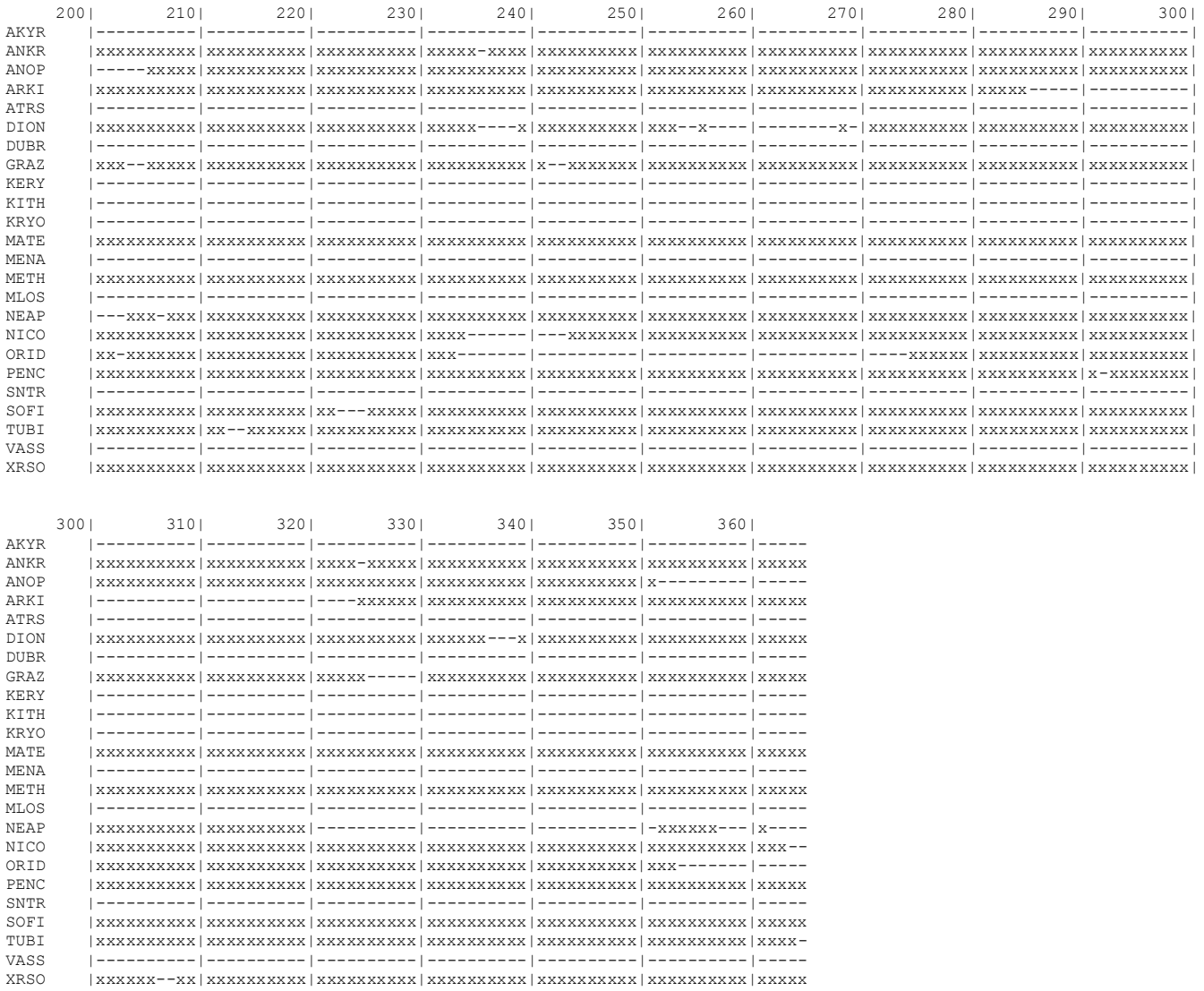
200 210 220 230 240 250 260 270 280 290 300
AKYR
ANKR
ANOP
ARKI
ATRS
DION
DUBR
GRAZ
KERY
KITH
KRYO
MATE
MENA
METH
MLOS
NEAP
NICO
ORID
PENC
SNTR
SOFI
TUBI
VASS
XRSO
300 310 320 330 340 350 360
AKYR
ANKR
ANOP
ARKI
ATRS
DION
DUBR
GRAZ
KERY
KITH
KRYO
MATE
MENA
METH
MLOS
NEAP
NICO
ORID
PENC
SNTR
SOFI
TUBI
VASS
XRSO

2004

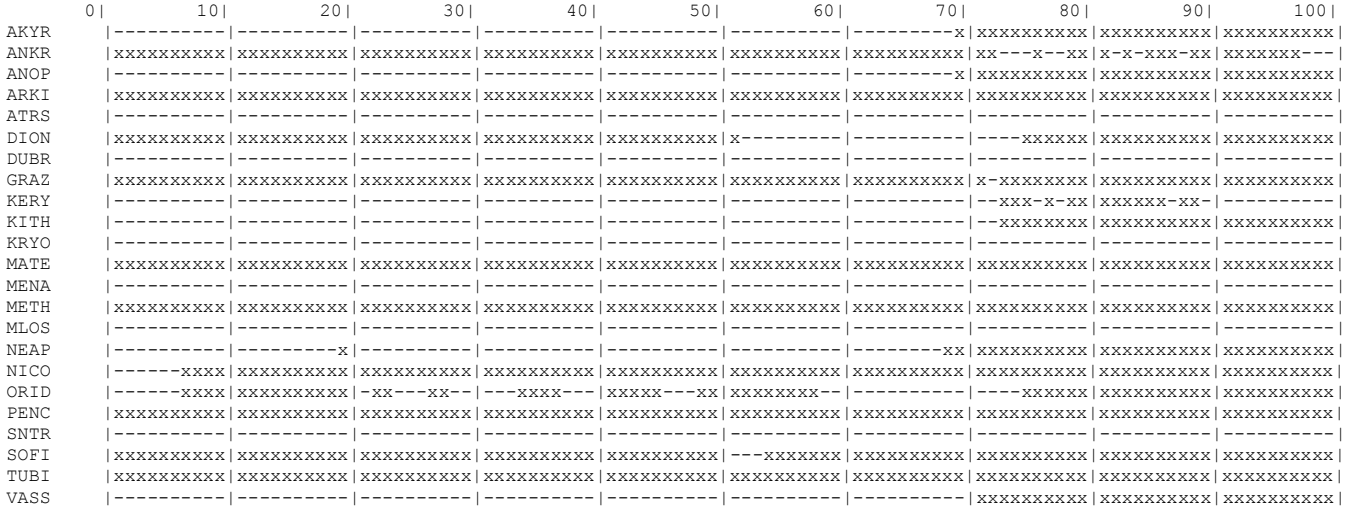
0 10 20 30 40 50 60 70 80 90 100
AKYR
ANKR
ANOP
ARKI
ATRS
DION
DUBR
GRAZ
KERY
KITH
KRYO
MATE
MENA
METH
MLOS
NEAP
NICO
ORID
PENC
SNTR
SOFI
TUBI
VASS
XRSO

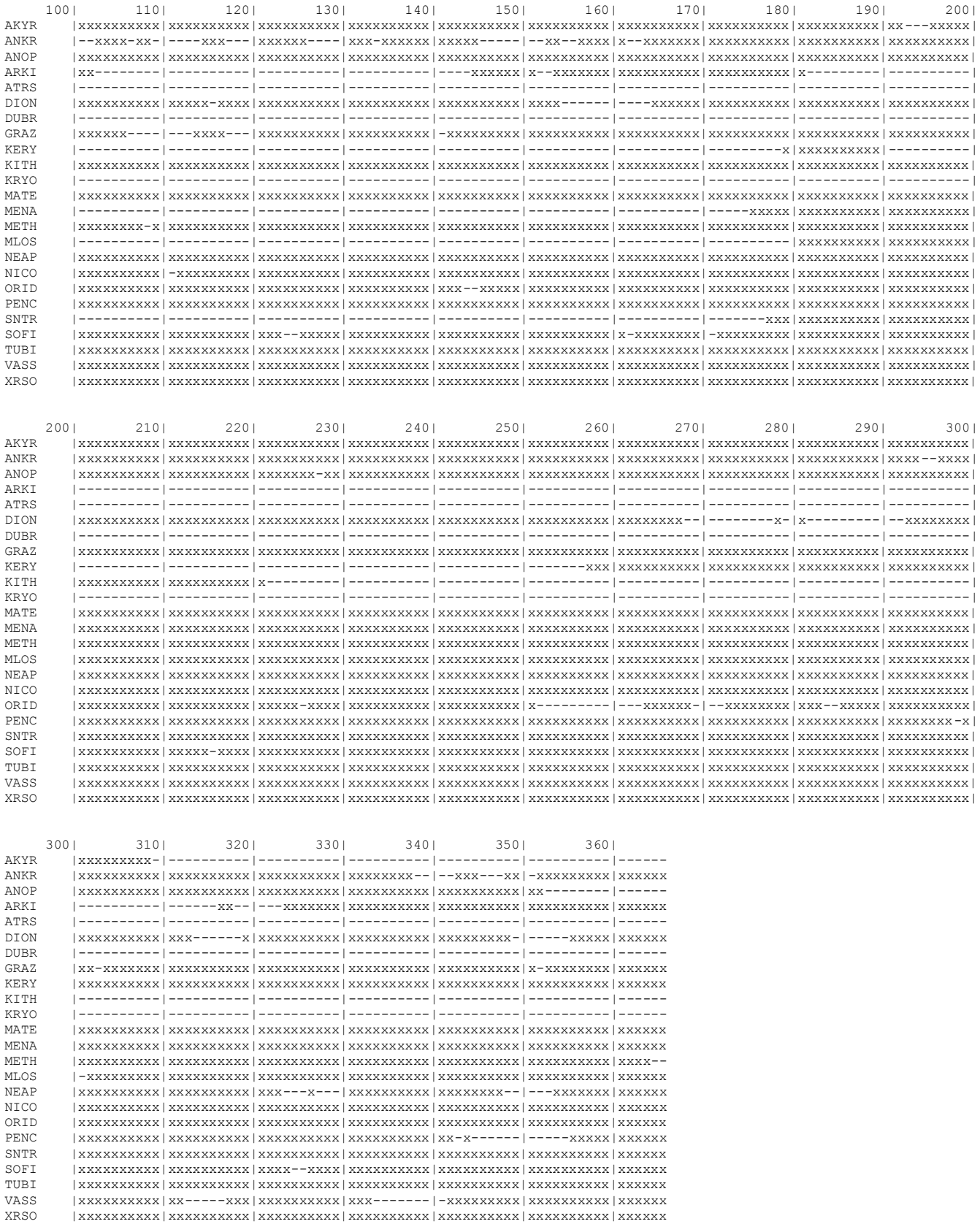
100 110 120 130 140 150 160 170 180 190 200
AKYR
ANKR
ANOP
ARKI
ATRS
DION
DUBR
GRAZ
KERY
KITH
KRYO
MATE
MENA
METH
MLOS
NEAP
NICO
ORID
PENC
SNTR
SOFI
TUBI
VASS
XRSO
200 210 220 230 240 250 260 270 280 290 300
AKYR
ANKR
ANOP
ARKI
ATRS
DION
DUBR
GRAZ
KERY
KITH
KRYO
MATE
MENA
METH
MLOS
NEAP
NICO
ORID
PENC
SNTR
SOFI
TUBI
VASS
XRSO
300 310 320 330 340 350 360
AKYR
ANKR
ANOP
ARKI
ATRS
DION
DUBR
GRAZ
KERY
KITH
KRYO
MATE
MENA
METH
MLOS
NEAP
NICO
ORID
PENC
SNTR
SOFI
TUBI
VASS
XRSO

2005

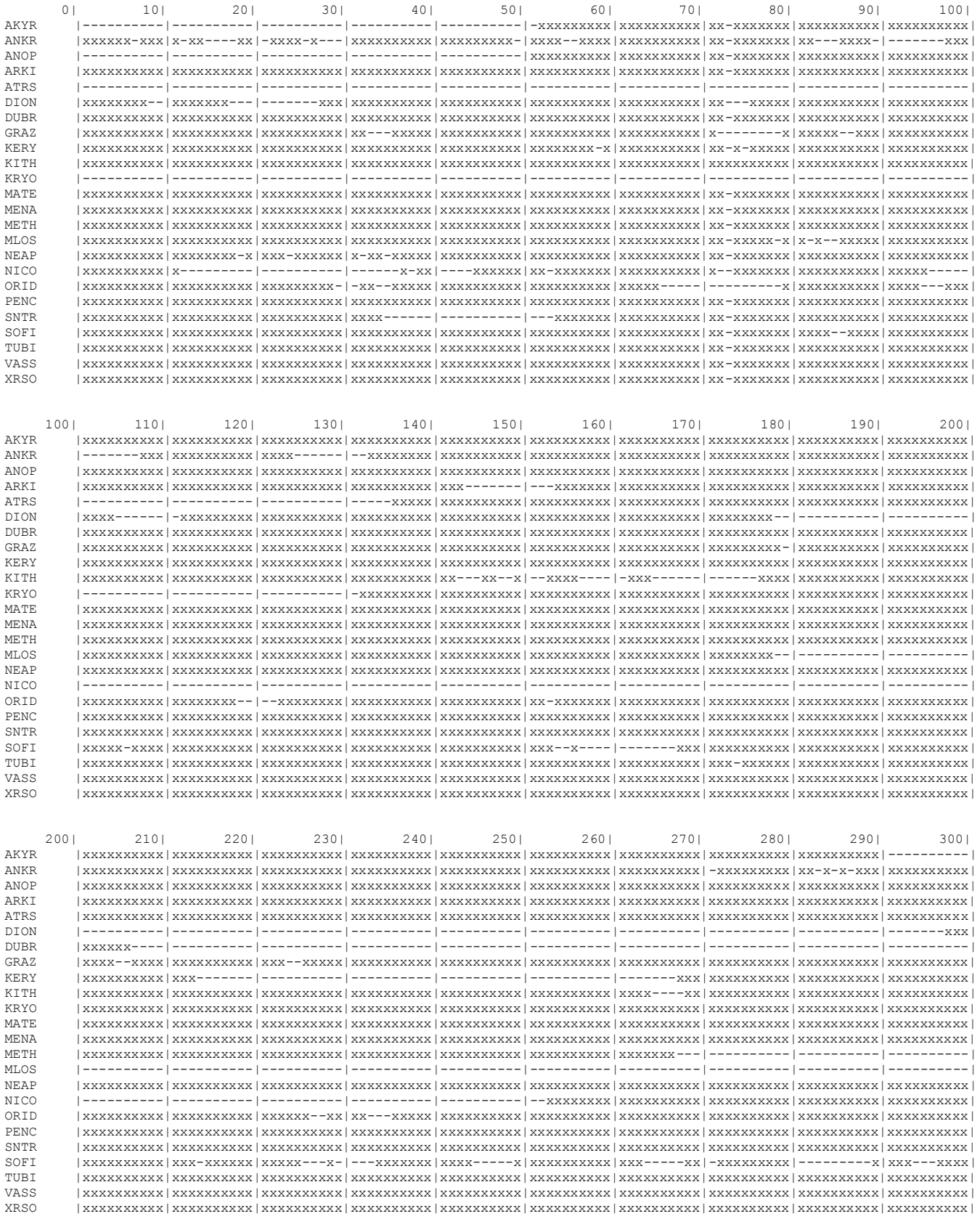
0 10 20 30 40 50 60 70 80 90 100
100 110 120 130 140 150 160 170 180 190 200
200 210 220 230 240 250 260 270 280 290 300
AKYR ANKR ANOP ARKI ATRS DION DUBR GRAZ KERY KITH KRYO MATE MENA METH MLOS NEAP NICO ORID PENC SNTR SOFI TUBI VASS XRSO

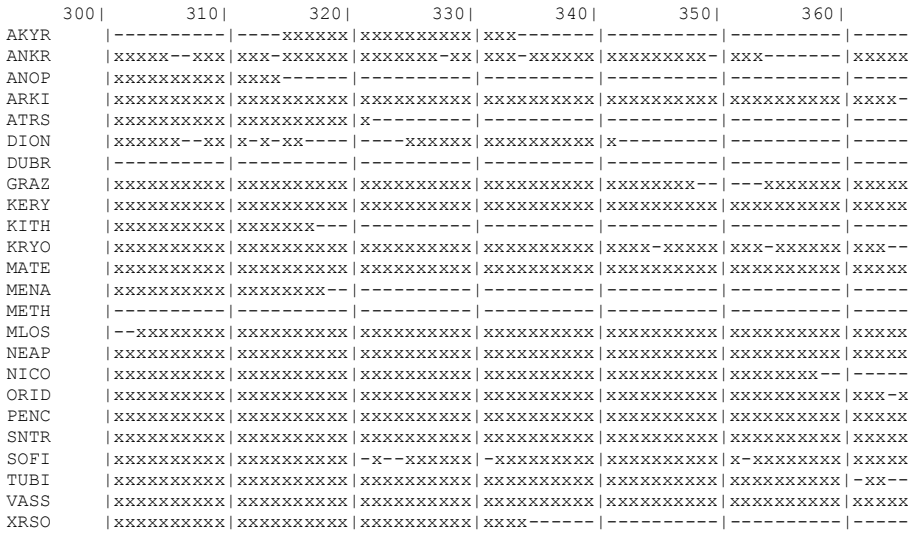
300| 310| 320| 330| 340| 350| 360|
AKYR |----------|----xxxxxx|xxxxxxxxxx|xxx-------|----------|----------|-----
ANKR |xxxxx--xxx|xxx-xxxxxx|xxxxxxx-xx|xxx-xxxxxx|xxxxxxxxx-|xxx-------|xxxxx
ANOP |xxxxxxxxxx|xxxx------|----------|----------|----------|----------|-----
ARKI |xxxxxxxxxx|xxxxxxxxxx|xxxxxxxxxx|xxxxxxxxxx|xxxxxxxxxx|xxxxxxxxxx|xxxx-
ATRS |xxxxxxxxxx|xxxxxxxxxx|x---------|----------|----------|----------|-----
DION |xxxxxx--xx|x-x-xx----|----xxxxxx|xxxxxxxxxx|x---------|----------|-----
DUBR |----------|----------|----------|----------|----------|----------|-----
GRAZ |xxxxxxxxxx|xxxxxxxxxx|xxxxxxxxxx|xxxxxxxxxx|xxxxxxxx--|---xxxxxxx|xxxxx
KERY |xxxxxxxxxx|xxxxxxxxxx|xxxxxxxxxx|xxxxxxxxxx|xxxxxxxxxx|xxxxxxxxxx|xxxxx
KITH |xxxxxxxxxx|xxxxxxx---|----------|----------|----------|----------|-----
KRYO |xxxxxxxxxx|xxxxxxxxxx|xxxxxxxxxx|xxxxxxxxxx|xxxx-xxxxx|xxx-xxxxxx|xxx--
MATE |xxxxxxxxxx|xxxxxxxxxx|xxxxxxxxxx|xxxxxxxxxx|xxxxxxxxxx|xxxxxxxxxx|xxxxx
MENA |xxxxxxxxxx|xxxxxxxx--|----------|----------|----------|----------|-----
METH |----------|----------|----------|----------|----------|----------|-----
MLOS |--xxxxxxxx|xxxxxxxxxx|xxxxxxxxxx|xxxxxxxxxx|xxxxxxxxxx|xxxxxxxxxx|xxxxx
NEAP |xxxxxxxxxx|xxxxxxxxxx|xxxxxxxxxx|xxxxxxxxxx|xxxxxxxxxx|xxxxxxxxxx|xxxxx
NICO |xxxxxxxxxx|xxxxxxxxxx|xxxxxxxxxx|xxxxxxxxxx|xxxxxxxxxx|xxxxxxxx--|-----
ORID |xxxxxxxxxx|xxxxxxxxxx|xxxxxxxxxx|xxxxxxxxxx|xxxxxxxxxx|xxxxxxxxxx|xxx-x
PENC |xxxxxxxxxx|xxxxxxxxxx|xxxxxxxxxx|xxxxxxxxxx|xxxxxxxxxx|xxxxxxxxxx|xxxxx
SNTR |xxxxxxxxxx|xxxxxxxxxx|xxxxxxxxxx|xxxxxxxxxx|xxxxxxxxxx|xxxxxxxxxx|xxxxx
SOFI |xxxxxxxxxx|xxxxxxxxxx|-x--xxxxxx|-xxxxxxxxx|xxxxxxxxxx|x-xxxxxxx|xxxxx
TUBI |xxxxxxxxxx|xxxxxxxxxx|xxxxxxxxxx|xxxxxxxxxx|xxxxxxxxxx|xxxxxxxxx|-xx--
VASS |xxxxxxxxxx|xxxxxxxxxx|xxxxxxxxxx|xxxxxxxxxx|xxxxxxxxxx|xxxxxxxxxx|xxxxx
XRSO |xxxxxxxxxx|xxxxxxxxxx|xxxxxxxxxx|xxxx------|----------|----------|-----

2006

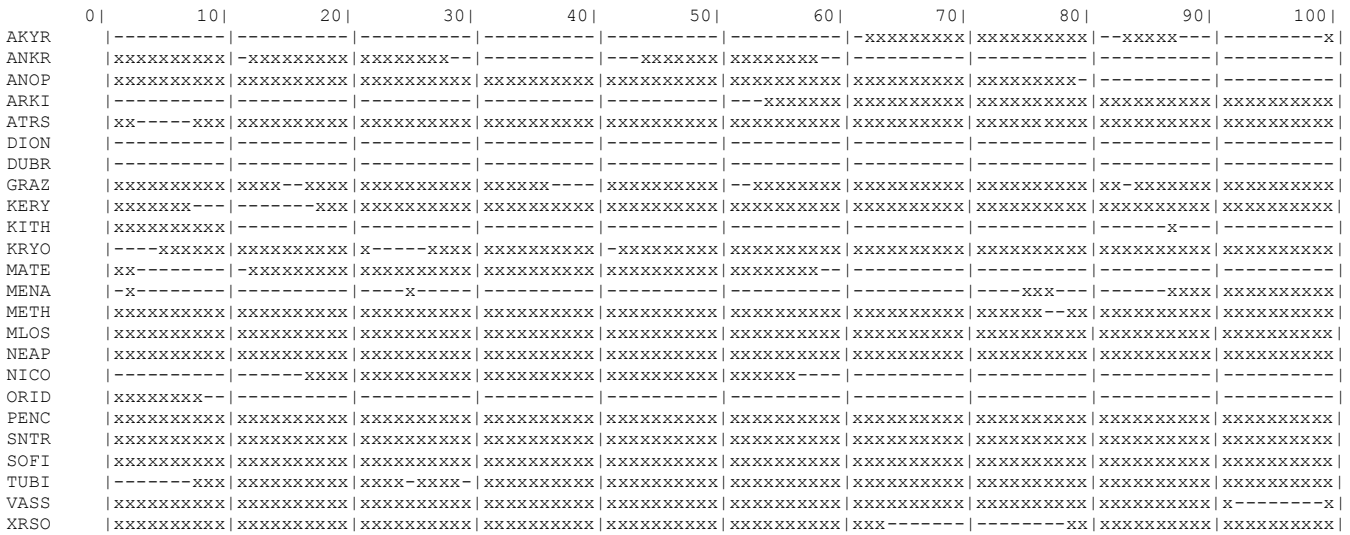
0| 10| 20| 30| 40| 50| 60| 70| 80| 90| 100|
AKYR |----------|----------|----------|----------|----------|----------|-xxxxxxxxx|xxxxxxxxxx|--xxxxx---|---------x|
ANKR |xxxxxxxxxx|-xxxxxxxxx|xxxxxxx--|----------|---xxxxxxx|xxxxxxxx--|----------|----------|----------|----------|
ANOP |xxxxxxxxxx|xxxxxxxxxx|xxxxxxxxxx|xxxxxxxxxx|xxxxxxxxxx|xxxxxxxxxx|xxxxxxxxx-|----------|----------|
ARKI |----------|----------|----------|----------|----------|---xxxxxxx|xxxxxxxxxx|xxxxxxxxxx|xxxxxxxxxx|xxxxxxxxxx|
ATRS |xx-----xxx|xxxxxxxxxx|xxxxxxxxxx|xxxxxxxxxx|xxxxxxxxxx|xxxxxxxxxx|xxxxxxxxxx|xxxxxxxxxx|xxxxxxxxxx|xxxxxxxxxx|
DION |----------|----------|----------|----------|----------|----------|----------|----------|----------|----------|
DUBR |----------|----------|----------|----------|----------|----------|----------|----------|----------|----------|
GRAZ |xxxxxxxxxx|xxxx--xxxx|xxxxxxxxxx|xxxxx----|xxxxxxxxxx|--xxxxxxxx|xxxxxxxxxx|xxxxxxxxxx|xx-xxxxxxx|xxxxxxxxxx|
KERY |xxxxxxx---|-------xxx|xxxxxxxxxx|xxxxxxxxxx|xxxxxxxxxx|xxxxxxxxxx|xxxxxxxxxx|xxxxxxxxxx|xxxxxxxxxx|xxxxxxxxxx|
KITH |xxxxxxxxxx|----------|----------|----------|----------|----------|----------|----------|------x---|----------|
KRYO |----xxxxxx|xxxxxxxxxx|x-----xxxx|xxxxxxxxxx|-xxxxxxxxx|xxxxxxxxxx|xxxxxxxxxx|xxxxxxxxxx|xxxxxxxxxx|xxxxxxxxxx|
MATE |xx--------|-xxxxxxxxx|xxxxxxxxxx|xxxxxxxxxx|xxxxxxxxxx|xxxxxxxx--|----------|----------|----------|----------|
MENA |-x--------|----------|----x-----|----------|----------|----------|----------|----xxx---|-----xxxx|xxxxxxxxxx|
METH |xxxxxxxxxx|xxxxxxxxxx|xxxxxxxxxx|xxxxxxxxxx|xxxxxxxxxx|xxxxxxxxxx|xxxxxxxxxx|xxxxxx--xx|xxxxxxxxxx|xxxxxxxxxx|
MLOS |xxxxxxxxxx|xxxxxxxxxx|xxxxxxxxxx|xxxxxxxxxx|xxxxxxxxxx|xxxxxxxxxx|xxxxxxxxxx|xxxxxxxxxx|xxxxxxxxxx|xxxxxxxxxx|
NEAP |xxxxxxxxxx|xxxxxxxxxx|xxxxxxxxxx|xxxxxxxxxx|xxxxxxxxxx|xxxxxxxxxx|xxxxxxxxxx|xxxxxxxxxx|xxxxxxxxxx|xxxxxxxxxx|
NICO |----------|------xxxx|xxxxxxxxxx|xxxxxxxxxx|xxxxxxxxxx|xxxxxx----|----------|----------|----------|----------|
ORID |xxxxxxxx--|----------|----------|----------|----------|----------|----------|----------|----------|----------|
PENC |xxxxxxxxxx|xxxxxxxxxx|xxxxxxxxxx|xxxxxxxxxx|xxxxxxxxxx|xxxxxxxxxx|xxxxxxxxxx|xxxxxxxxxx|xxxxxxxxxx|xxxxxxxxxx|
SNTR |xxxxxxxxxx|xxxxxxxxxx|xxxxxxxxxx|xxxxxxxxxx|xxxxxxxxxx|xxxxxxxxxx|xxxxxxxxxx|xxxxxxxxxx|xxxxxxxxxx|xxxxxxxxxx|
SOFI |xxxxxxxxxx|xxxxxxxxxx|xxxxxxxxxx|xxxxxxxxxx|xxxxxxxxxx|xxxxxxxxxx|xxxxxxxxxx|xxxxxxxxxx|xxxxxxxxxx|xxxxxxxxxx|
TUBI |-------xxx|xxxxxxxxxx|xxxx-xxxx-|xxxxxxxxxx|xxxxxxxxxx|xxxxxxxxxx|xxxxxxxxxx|xxxxxxxxxx|xxxxxxxxxx|xxxxxxxxxx|
VASS |xxxxxxxxxx|xxxxxxxxxx|xxxxxxxxxx|xxxxxxxxxx|xxxxxxxxxx|xxxxxxxxxx|xxxxxxxxxx|xxxxxxxxxx|xxxxxxxxxx|x--------x|
XRSO |xxxxxxxxxx|xxxxxxxxxx|xxxxxxxxxx|xxxxxxxxxx|xxxxxxxxxx|xxxxxxxxxx|xxx-------|--------xx|xxxxxxxxxx|xxxxxxxxxx|

100| 110| 120| 130| 140| 150| 160| 170| 180| 190| 200|
AKYR |----x-----|----------|----------|----------|----------|----------|-------xx|xxxxxxxxxx|xxxxxxxxxx|xxxxxxxxxx|
ANKR |----------|----------|----------|----------|----------|----------|----------|----------|----------|----------|
ANOP |----------|----------|----------|----------|----------|----------|---------x|xxxxxxxxxx|xxxxxxxxxx|xxxxxxxxxx|
ARKI |xxxxxxxxxx|xxxxxxxxxx|xxxxxxxxxx|xxxxxxxxxx|xxxxxxxxxx|xxxxxxxxxx|xxxxxxxxxx|xxxxxxxxxx|xxxxxxxxxx|xxxxxxxxxx|
ATRS |x--xxxxxxx|xxxxxxxxxx|xxxxxxxxxx|xxxxxxxxxx|xxxxxxxxxx|xxxxxxxxxx|xxxxxxxxxx|xxxxxxxxxx|xxxxxxxxxx|xxxxxxxxxx|
DION |----------|----------|---------x|xxxxxxxxxx|xxxxxxxxxx|xxxxxxxxxx|xxxx-xxxxx|xxxxxxxxxx|xxxxxxxxxx|xxxxxxxxxx|
DUBR |----------|----------|----------|----------|----------|----------|----------|----------|----------|----------|
GRAZ |----------|----------|----------|----------|----------|----------|----------|----------|----------|----------|
KERY |xxxxxxxxxx|xxxxxxxxxx|xxxxxxxxxx|xxxxxxxxxx|xxxxxxxxxx|xxxxxxxxxx|xxxxxxxxxx|xxxxxxxxxx|xxxxxxxxxx|xxxxxxxxxx|
KITH |----------|----------|----------|----------|----------|----------|----------|----------|---------x|xxxxxxxxxx|
KRYO |xxxxxxxxxx|xxxxxxxxxx|xxxxxxxxxx|xxxxxxxxxx|xxxxxxxxxx|xxxxxxxxxx|xxxxxxxxxx|xxxxxxxxxx|xxxxxxxxxx|xxxxxxxxxx|
MATE |----------|----------|----------|----------|----------|----------|----------|----------|----------|----------|
MENA |xxxxxxxxxx|xxxxxxxxxx|xxxxxxxxxx|xxxxxxxxxx|xxxxxxxxxx|xxxxxxxxxx|xxxxxxxxxx|xxxxxxxxxx|xxxxxxxxxx|xxxxxxxxxx|
METH |xxxxxxxxxx|xxxxxxxxxx|xxxxxxxxxx|xxxxxxxxxx|xxxxxxxxxx|xxxxxxxxxx|xxxxxxxxxx|xxxxxxxxxx|xxxxxxxxxx|xxxxxxxxxx|
MLOS |xxxxxxxxxx|xxxxxxxxxx|xxxxxxxxxx|xxxxxxxxxx|xxxxxxxxxx|xxxxxxxxxx|xxxxxxxxxx|xxxxxxxxxx|xxxxxxxxxx|xxxxxxxxxx|
NEAP |xxxxxxxxxx|xxxxxxxxxx|xxxxxxxxxx|xxxxxxxxxx|xxxxxxxxxx|xxxxxxxxxx|xxxxxxxxxx|xxxxxxxxxx|xxxxxxxxxx|xxxxxxxxxx|
NICO |----------|----------|----------|----------|----------|----------|----------|----------|----------|----------|
ORID |----------|----------|----------|----------|----------|----------|----------|----------|----------|----------|
PENC |xxxxxxxxxx|xxxxxxxxxx|xxx-xxxxxx|xxxxxxxxxx|xxxxxxxxxx|xxxxxxxxxx|xxxxxxxxxx|xxxxxxxxxx|xxxxxxxxxx|xxxxxxxxx-|
SNTR |xxxxxxxxxx|xxxxxxxxxx|xxxxxxxxxx|xxxxxxxxxx|xxxxxxxxxx|xxxxxxxxxx|xxxxxxxxxx|xxxxxxxxxx|xxxxxxxxxx|xxxxxxxxxx|
SOFI |xxxxxxxxxx|x-xxxxxxxx|xxx-x-xxxx|xxxxxxxxxx|xxxxxxxxxx|xxxxxxxxxx|xxxxxxxxxx|xxxxxxxxxx|xxxxxxxxxx|xxxxxxxxx-|
TUBI |----------|----------|----------|----------|----------|----------|----------|----------|----------|----------|
VASS |xxxxxxxxxx|xxxxxxxxxx|xxxxxxxxxx|xxxxxxxxxx|xxxxxxxxxx|xxxxxxxxxx|xxxxxxxxxx|xxxxxxxxxx|xxxxxxxxxx|xxxxxxxxxx|
XRSO |xxxxxxxxxx|xxxxxxxxxx|xxx-------|-xxxxxxxxx|xxxxxxxxxx|xxxxxxxxxx|xxxxxxxxxx|xxxxxxxxxx|xxxxxxxxxx|xxxxxxxxxx|

```
     200|       210|       220|       230|       240|       250|       260|       270|
AKYR     |xxxxxxxxxx|xxxxxxxxxx|xxxxxxxxxx|xxxxxxxxxx|xxxxxxxxxx|xxxxxxxxxx|xxxxxxxxxx|xxx
ANKR     |----------|----------|----------|----------|---------x|xxxxxxxxxx|xxxxxxxxxx|xxx
ANOP     |xxxxxxxxxx|xxxxxxxxxx|xxxxxxxxxx|xxxxxxxxxx|xxxxxxxxxx|xxxxxxxxxx|xxxxxxxxxx|xxx
ARKI     |xxxxxxxxxx|xxxxxxxxxx|xxxxxxxxxx|xxxxxxxxxx|xxxxxxxxxx|xxxxxxxxxx|xxxxxxxxxx|xxx
ATRS     |xxxxxxxxxx|xxxxxxxxxx|xxxxxxxxxx|xxxxxxxxxx|xxxxxxxxxx|xxxxxxxxxx|xxxxxxxxxx|xxx
DION     |xxxxx-----|-xxxxxxxxx|xxxxxxxxxx|xxx-----x-|xxxxxxxxxx|xxxx-xxxxx|xxxxxxxxxx|xxx
DUBR     |----------|----------|----------|----------|----------|----------|----------|---
GRAZ     |----------|----------|----------|----------|----------|----------|----------|---
KERY     |xxxxxxxxxx|xxxxxxxxxx|xxxxxxxxxx|xxxxxxxxxx|xxxxxxxxxx|xxxxxxxxxx|xxxxxxxxxx|xxx
KITH     |xxxxxxxxxx|xxxxxxxxxx|xxxxxxxxxx|xxxxxxxxxx|xxxxxxxxxx|xxxxxxxxxx|xxxxxxxxxx|xxx
KRYO     |xxxxxxxxxx|xxxxxxxxxx|xxxxxxxxxx|xxxxxxxxxx|xxxxxxxxxx|xxxxxxxxxx|xxxxxxxxxx|xxx
MATE     |----------|----------|----------|----------|----------|----------|----------|---
MENA     |xxxxxxxxxx|xxxxxxxxxx|xxxxxxxxxx|xxxxxxxxxx|xxxxxxxxxx|xxxxxxxxxx|xxxxxxxxxx|xxx
METH     |xxxxxxxxxx|xxxxxxxxxx|xxxxxxxxxx|xxxxxxxxxx|xxxxxxxxxx|xxxxxxxxxx|xxxxxxxxxx|xxx
MLOS     |xxxxxxxxxx|xxxxxxxxxx|xxxxxxxxxx|xxxxxxxxxx|xxxxxxxxxx|xxxxxxxxxx|xxxxxxxxxx|xxx
NEAP     |xxxxxxxxxx|xxxxxxxxxx|xxxxxxxxxx|xxxxxxxxxx|xxxxxxxxxx|xxxxxxxxxx|xxxxxxxxxx|xxx
NICO     |----------|----------|----------|----------|----------|----------|----------|---
ORID     |----------|----------|----------|----------|----------|----------|----------|---
PENC     |------xxxx|xxxxxxxxxx|xxxxxxxxxx|xxxxxxxxxx|xxxxxxxxxx|xxxxxxxxxx|xxxxxxxxxx|xxx
SNTR     |xxxxxxxxxx|xxxxxxxxxx|xxxxxxxxxx|xxxxxxxxxx|xxxxxxxxxx|xxxxxxxxxx|xxxxxxxxxx|xxx
SOFI     |x-----xxxx|xxxxxxxxxx|xxxxxxxxxx|xxxxxxxxxx|xxxxxxxxxx|xxxxxxxxx-|xxxxxxxxxx|xxx
TUBI     |----------|----------|----------|----------|----------|----------|----------|---
VASS     |xxxxxxxxxx|xxxxxxxxxx|xxxxxxxxxx|xxxxxxxxxx|xxxxxxxxxx|xxxxxxxxxx|xxxxxxxxxx|xxx
XRSO     |xxxxxxxxxx|xxxxxxxxxx|xxxxxxxxxx|xxxxxxxxxx|xxxxxxxxxx|xxxxxxxxxx|xxxxxxxxxx|xxx
```

Appendix D

Regional Filtering Results

Aegean Filter

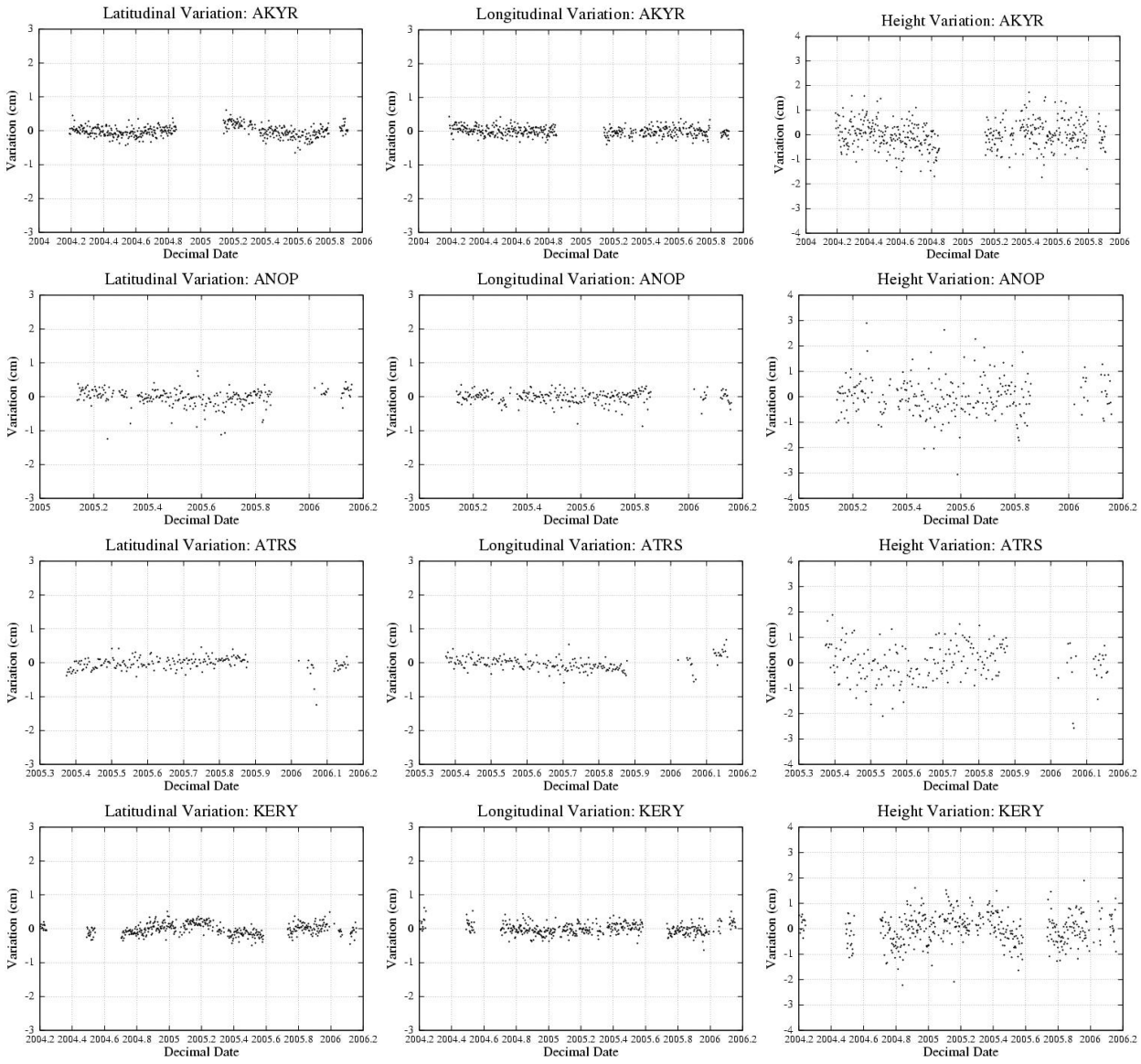

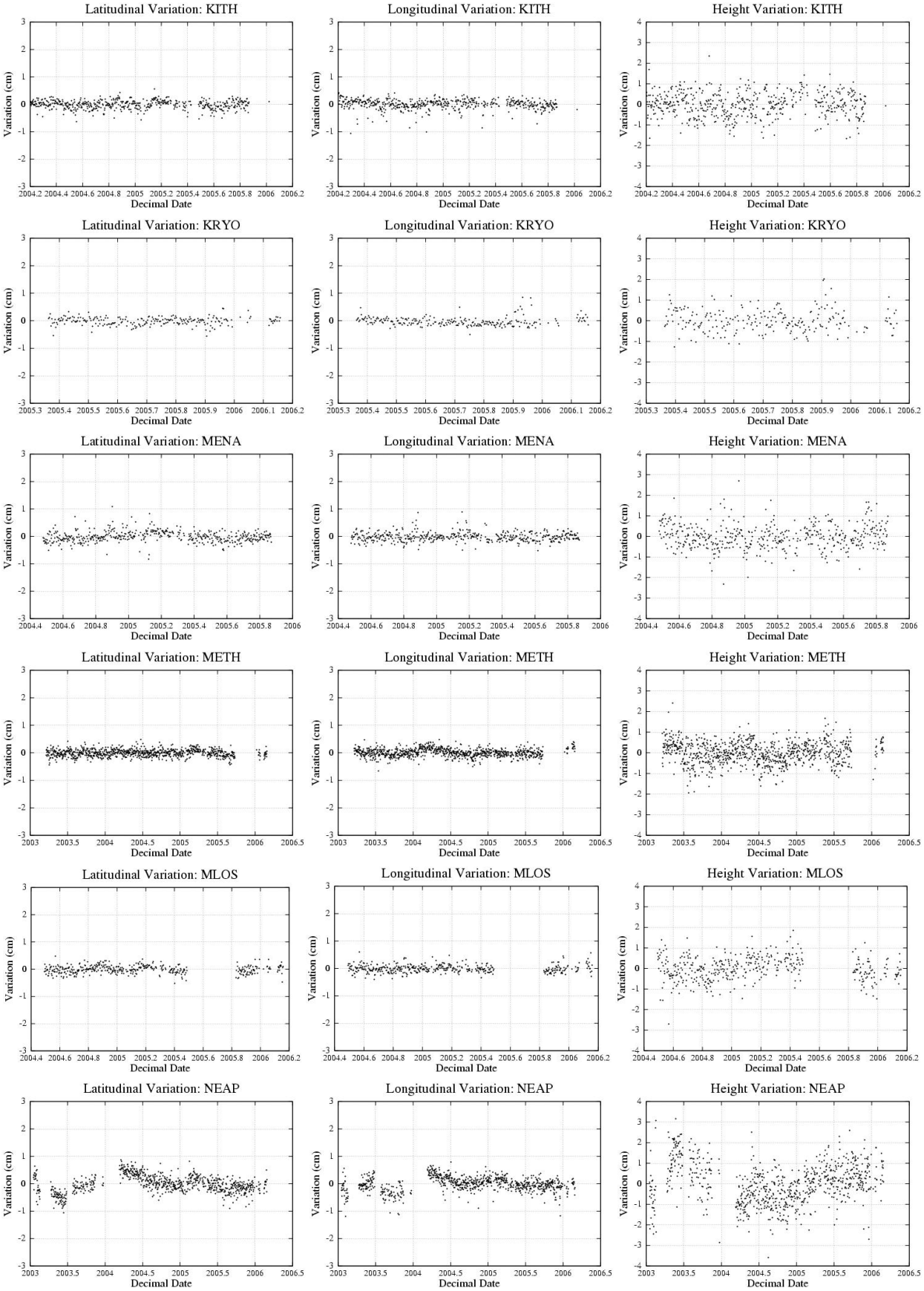
Latitudinal Variation: KITH
Longitudinal Variation: KITH
Height Variation: KITH
Latitudinal Variation: KRYO
Longitudinal Variation: KRYO
Height Variation: KRYO
Latitudinal Variation: MENA
Longitudinal Variation: MENA
Height Variation: MENA
Latitudinal Variation: METH
Longitudinal Variation: METH
Height Variation: METH
Latitudinal Variation: MLOS
Longitudinal Variation: MLOS
Height Variation: MLOS
Latitudinal Variation: NEAP
Longitudinal Variation: NEAP
Height Variation: NEAP
Variation (cm)
Decimal Date

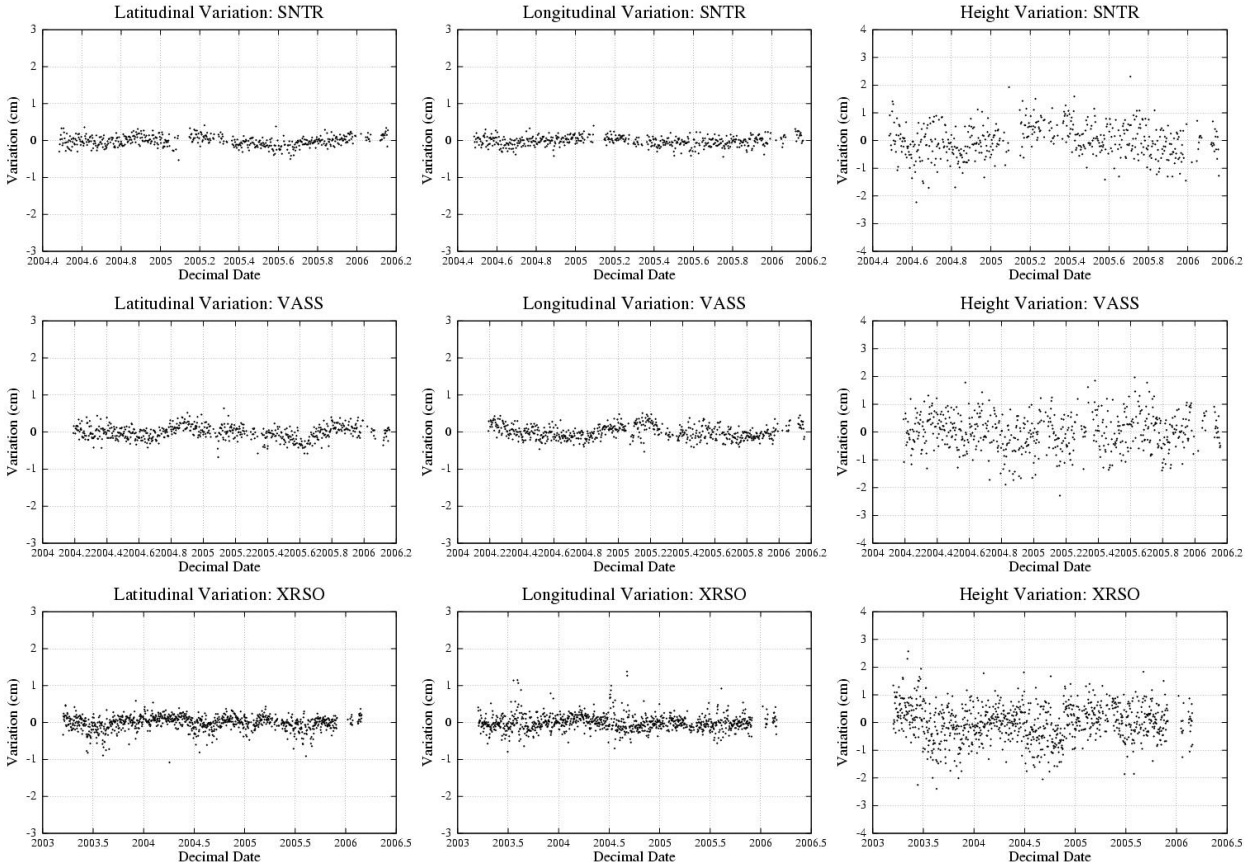
Latitudinal Variation: SNTR
Longitudinal Variation: SNTR
Height Variation: SNTR
Latitudinal Variation: VASS
Longitudinal Variation: VASS
Height Variation: VASS
Latitudinal Variation: XRSO
Longitudinal Variation: XRSO
Height Variation: XRSO
Variation (cm)
Decimal Date

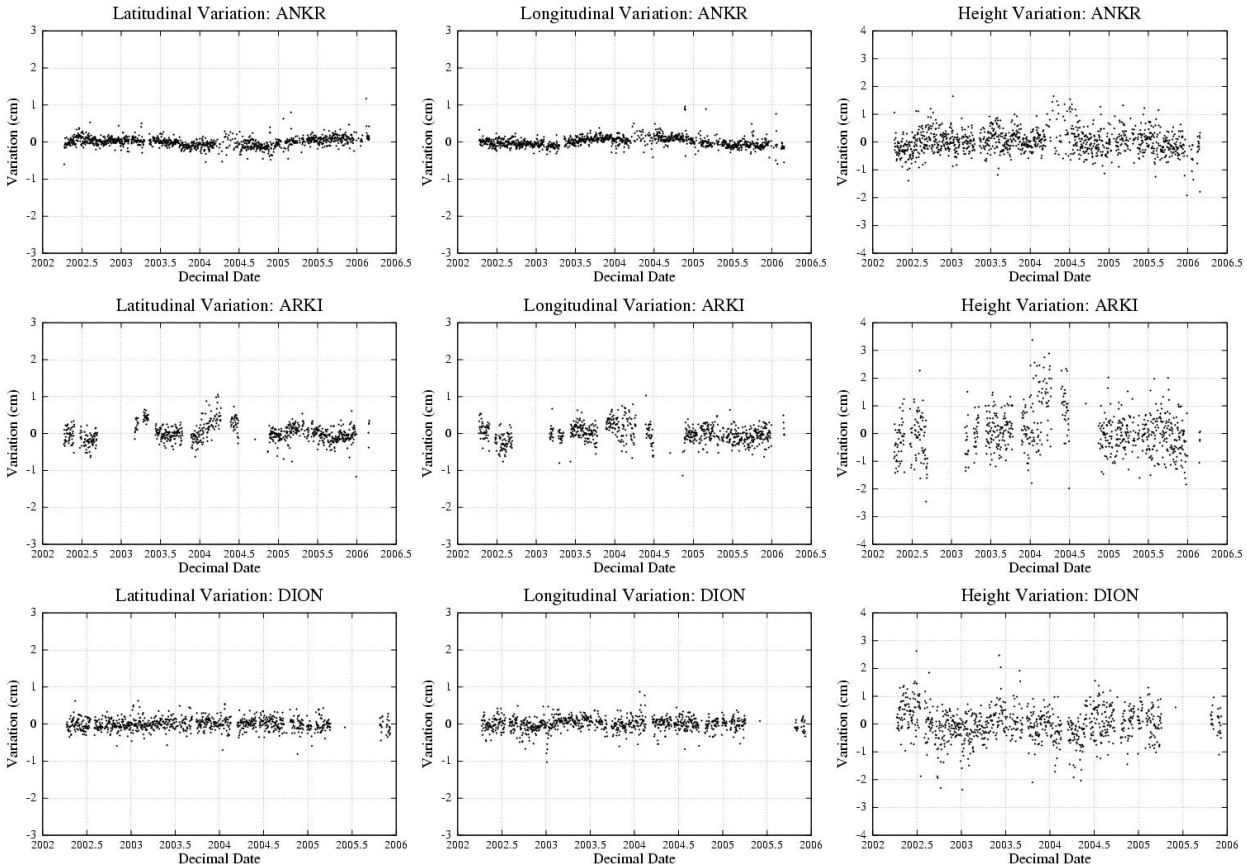
Latitudinal Variation: ANKR
Longitudinal Variation: ANKR
Height Variation: ANKR
Latitudinal Variation: ARKI
Longitudinal Variation: ARKI
Height Variation: ARKI
Latitudinal Variation: DION
Longitudinal Variation: DION
Height Variation: DION
Variation (cm)
Decimal Date

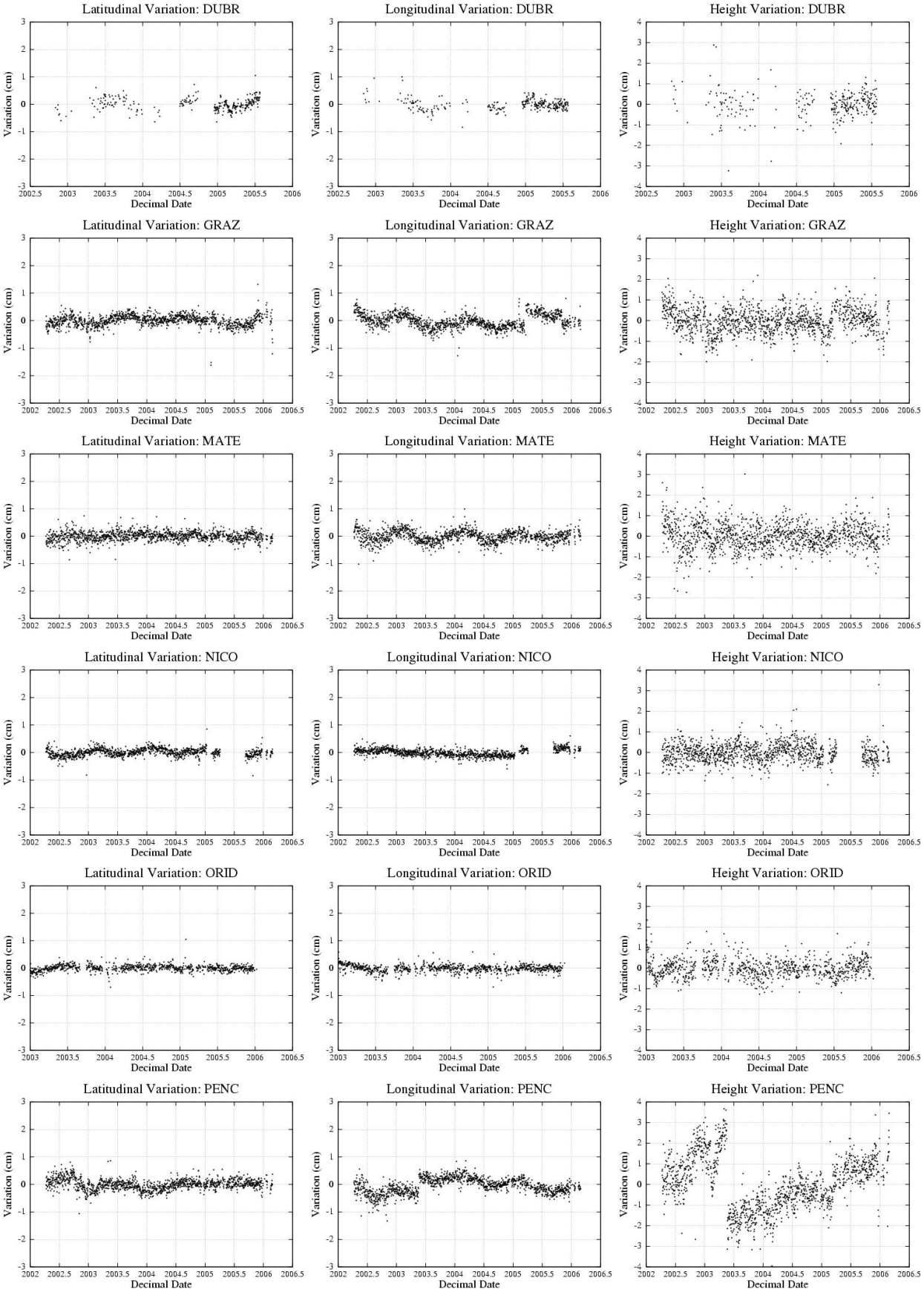
Latitudinal Variation: DUBR
Longitudinal Variation: DUBR
Height Variation: DUBR
Latitudinal Variation: GRAZ
Longitudinal Variation: GRAZ
Height Variation: GRAZ
Latitudinal Variation: MATE
Longitudinal Variation: MATE
Height Variation: MATE
Latitudinal Variation: NICO
Longitudinal Variation: NICO
Height Variation: NICO
Latitudinal Variation: ORID
Longitudinal Variation: ORID
Height Variation: ORID
Latitudinal Variation: PENC
Longitudinal Variation: PENC
Height Variation: PENC
Variation (cm)
Decimal Date

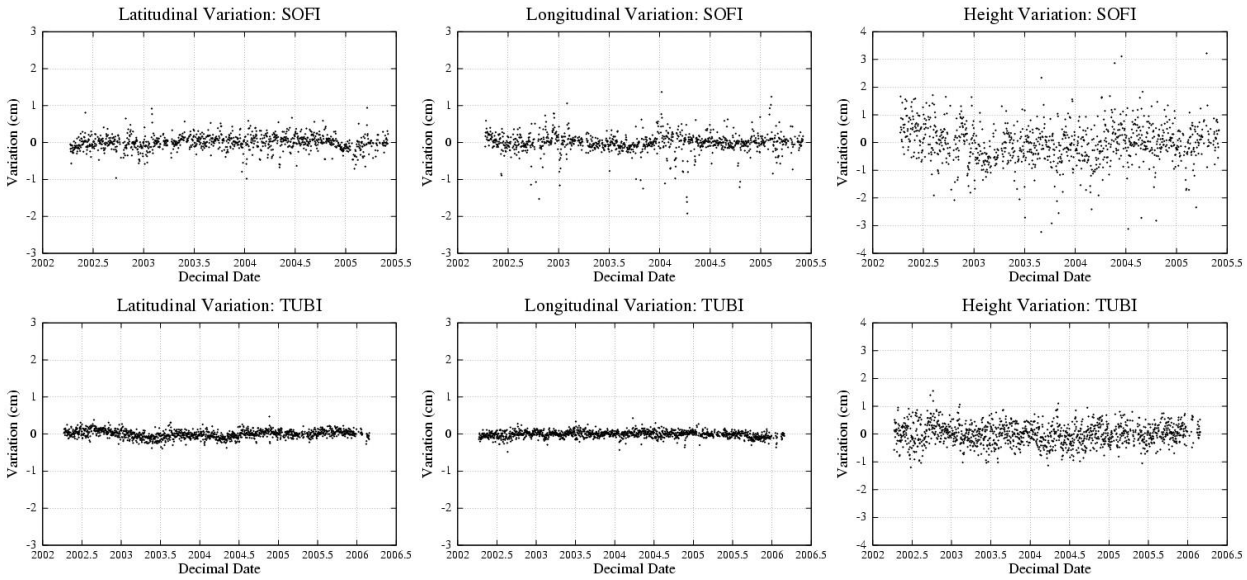
Latitudinal Variation: SOFI
Longitudinal Variation: SOFI
Height Variation: SOFI
Latitudinal Variation: TUBI
Longitudinal Variation: TUBI
Height Variation: TUBI
Variation (cm)
Decimal Date

Eurasian Filter

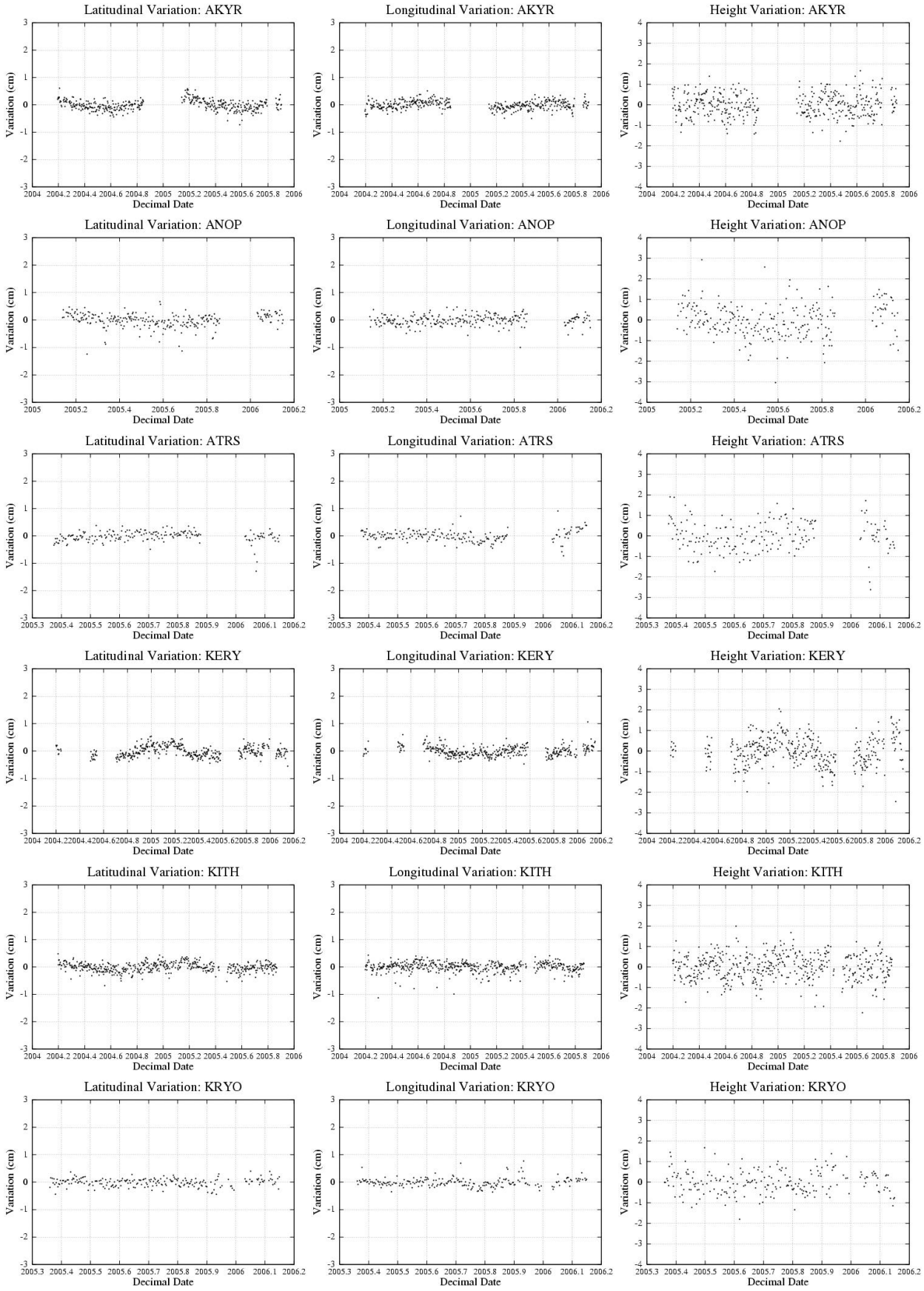

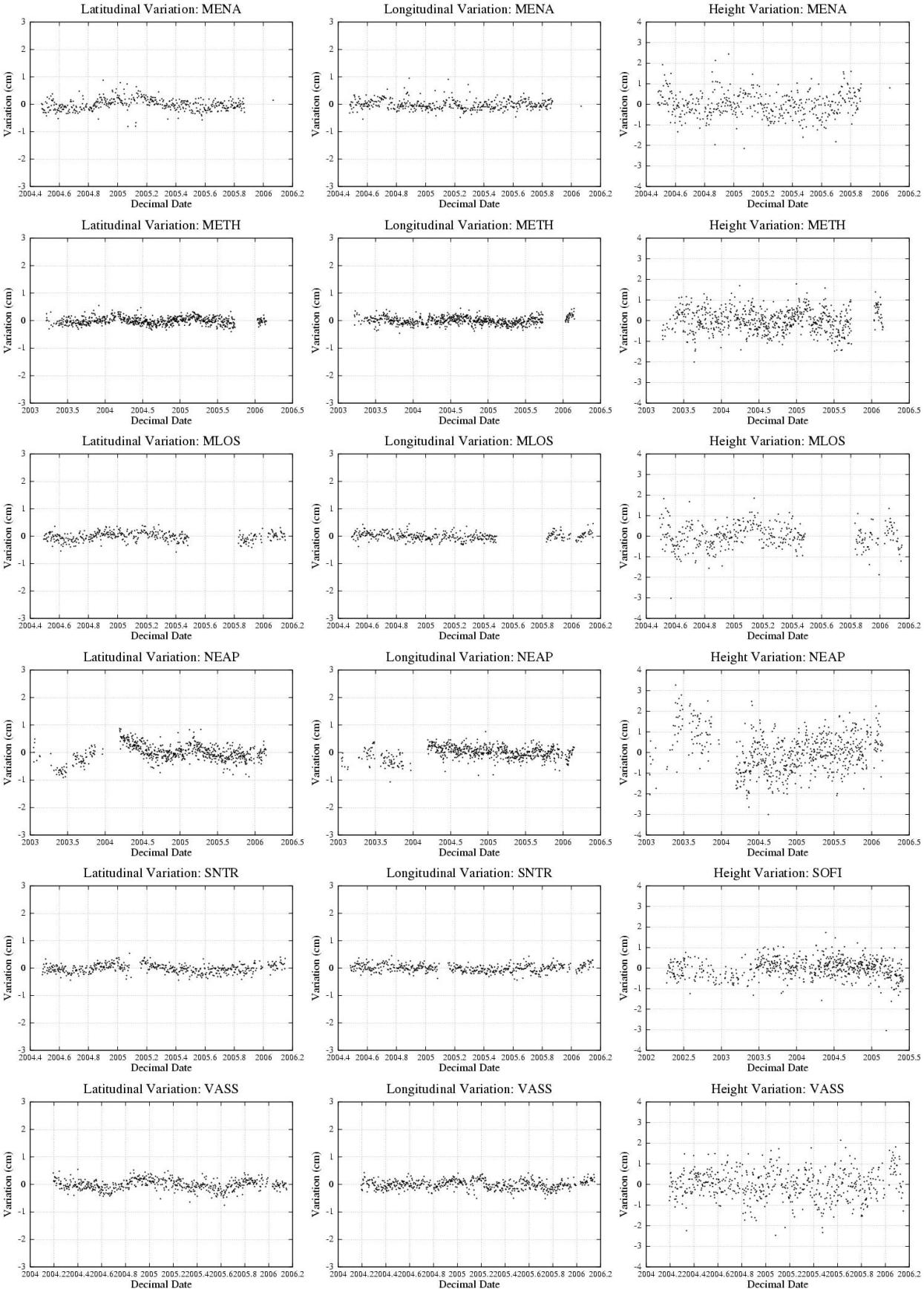
Latitudinal Variation: MENA
Longitudinal Variation: MENA
Height Variation: MENA
Latitudinal Variation: METH
Longitudinal Variation: METH
Height Variation: METH
Latitudinal Variation: MLOS
Longitudinal Variation: MLOS
Height Variation: MLOS
Latitudinal Variation: NEAP
Longitudinal Variation: NEAP
Height Variation: NEAP
Latitudinal Variation: SNTR
Longitudinal Variation: SNTR
Height Variation: SOFI
Latitudinal Variation: VASS
Longitudinal Variation: VASS
Height Variation: VASS
Variation (cm)
Decimal Date

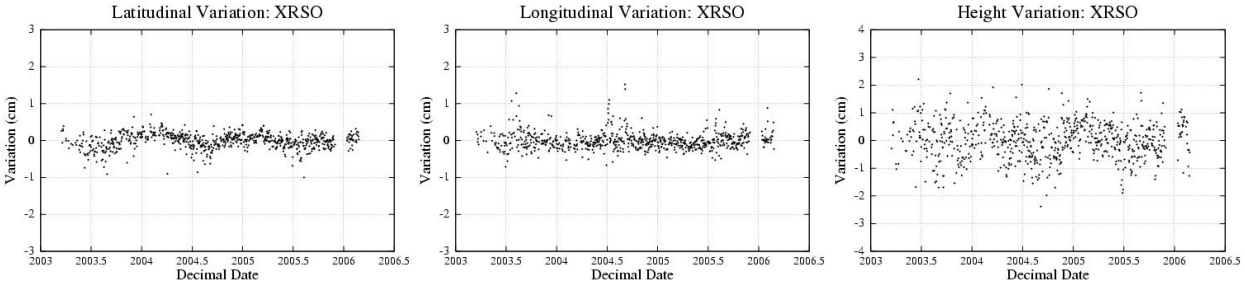
Latitudinal Variation: XRSO
Longitudinal Variation: XRSO
Height Variation: XRSO
Variation (cm)
Decimal Date

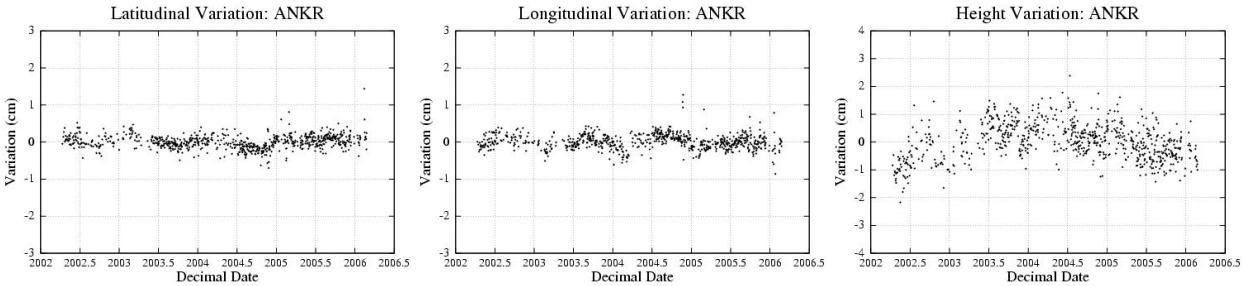
Latitudinal Variation: ANKR
Longitudinal Variation: ANKR
Height Variation: ANKR
Variation (cm)
Decimal Date

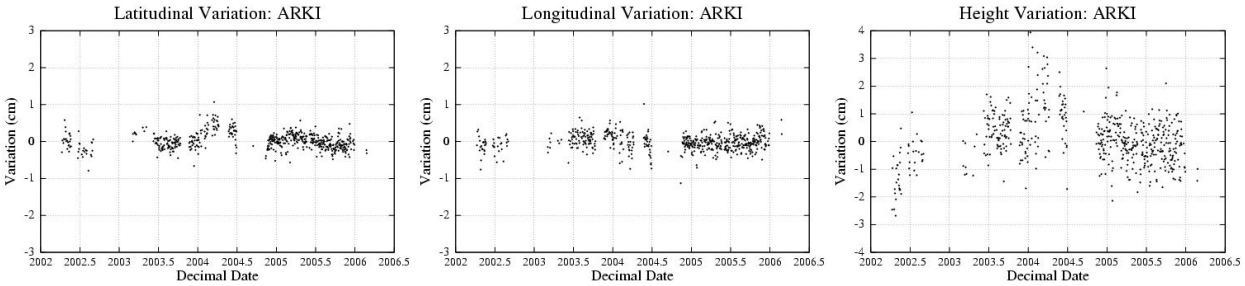
Latitudinal Variation: ARKI
Longitudinal Variation: ARKI
Height Variation: ARKI
Variation (cm)
Decimal Date

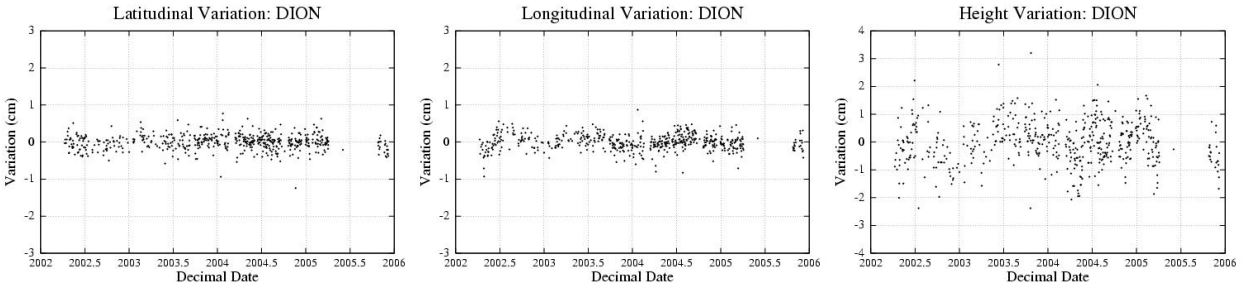
Latitudinal Variation: DION
Longitudinal Variation: DION
Height Variation: DION
Variation (cm)
Decimal Date

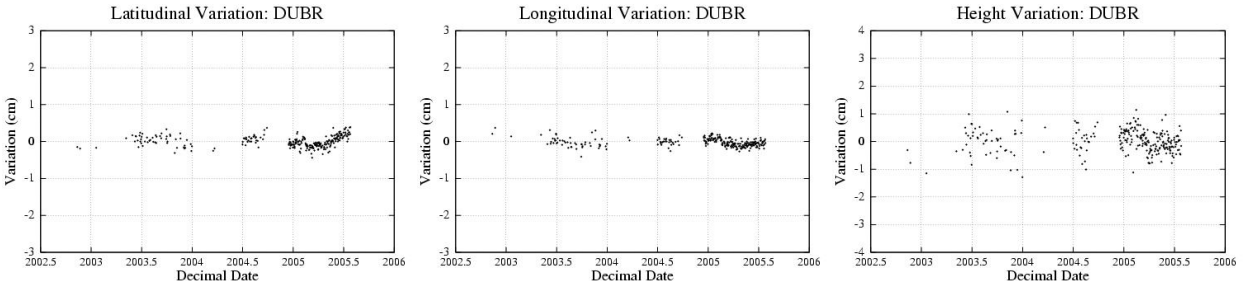
Latitudinal Variation: DUBR
Longitudinal Variation: DUBR
Height Variation: DUBR
Variation (cm)
Decimal Date

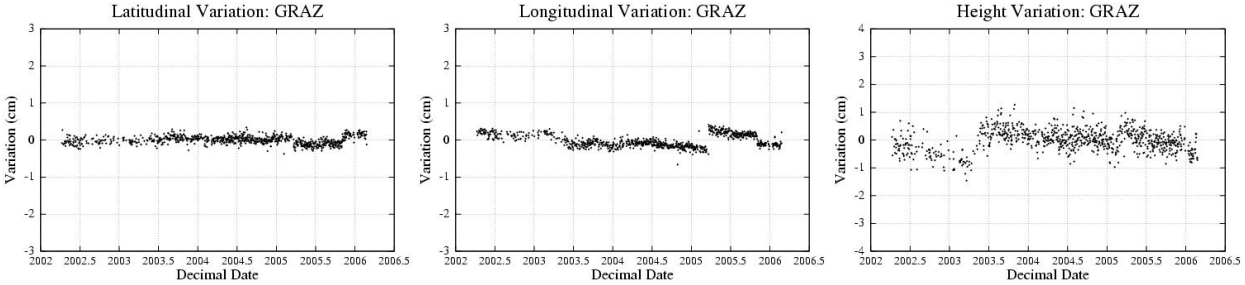
Latitudinal Variation: GRAZ
Longitudinal Variation: GRAZ
Height Variation: GRAZ
Variation (cm)
Decimal Date

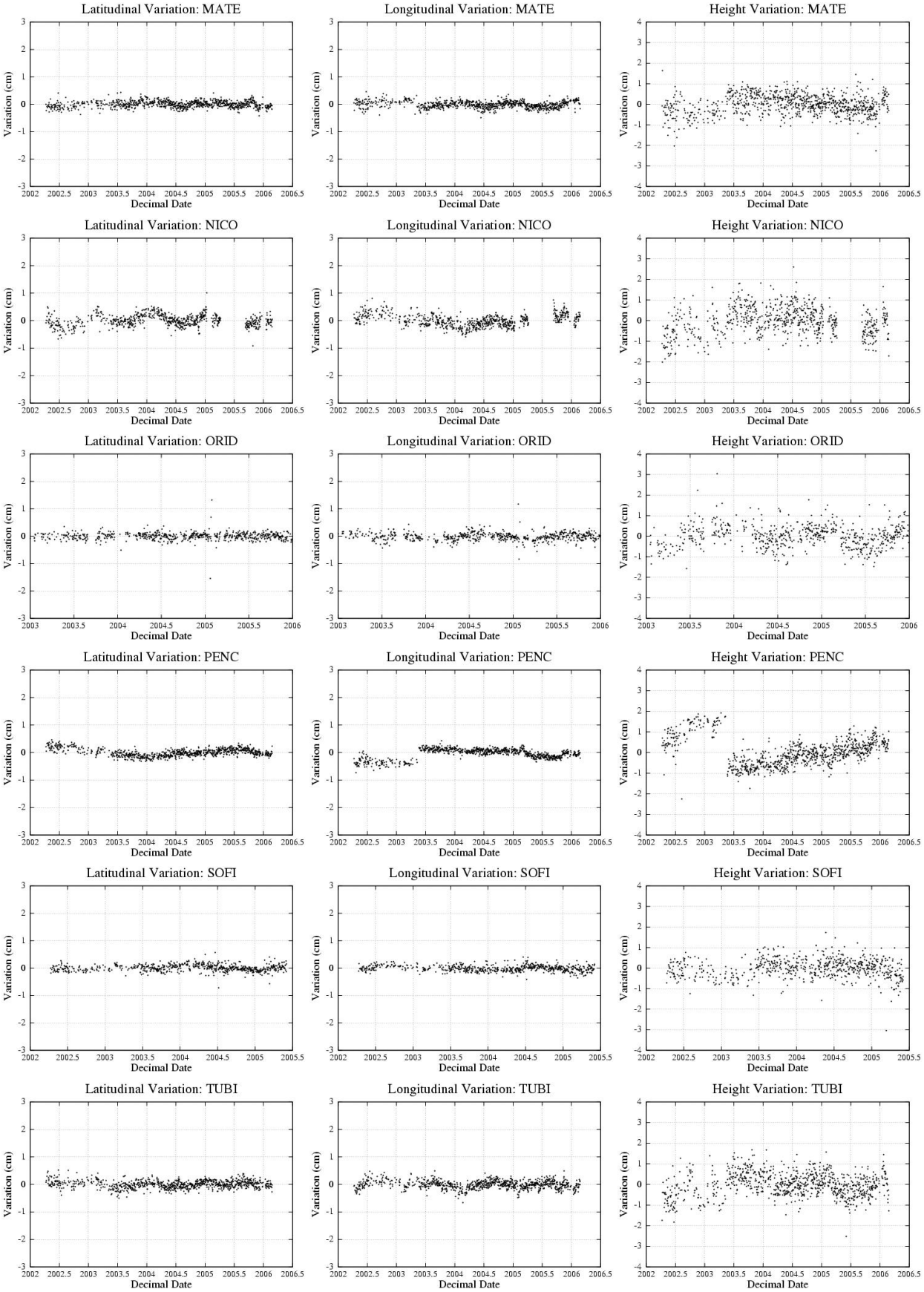
Latitudinal Variation: MATE
Longitudinal Variation: MATE
Height Variation: MATE
Latitudinal Variation: NICO
Longitudinal Variation: NICO
Height Variation: NICO
Latitudinal Variation: ORID
Longitudinal Variation: ORID
Height Variation: ORID
Latitudinal Variation: PENC
Longitudinal Variation: PENC
Height Variation: PENC
Latitudinal Variation: SOFI
Longitudinal Variation: SOFI
Height Variation: SOFI
Latitudinal Variation: TUBI
Longitudinal Variation: TUBI
Height Variation: TUBI
Variation (cm)
Decimal Date

0.1 Sigma Filter

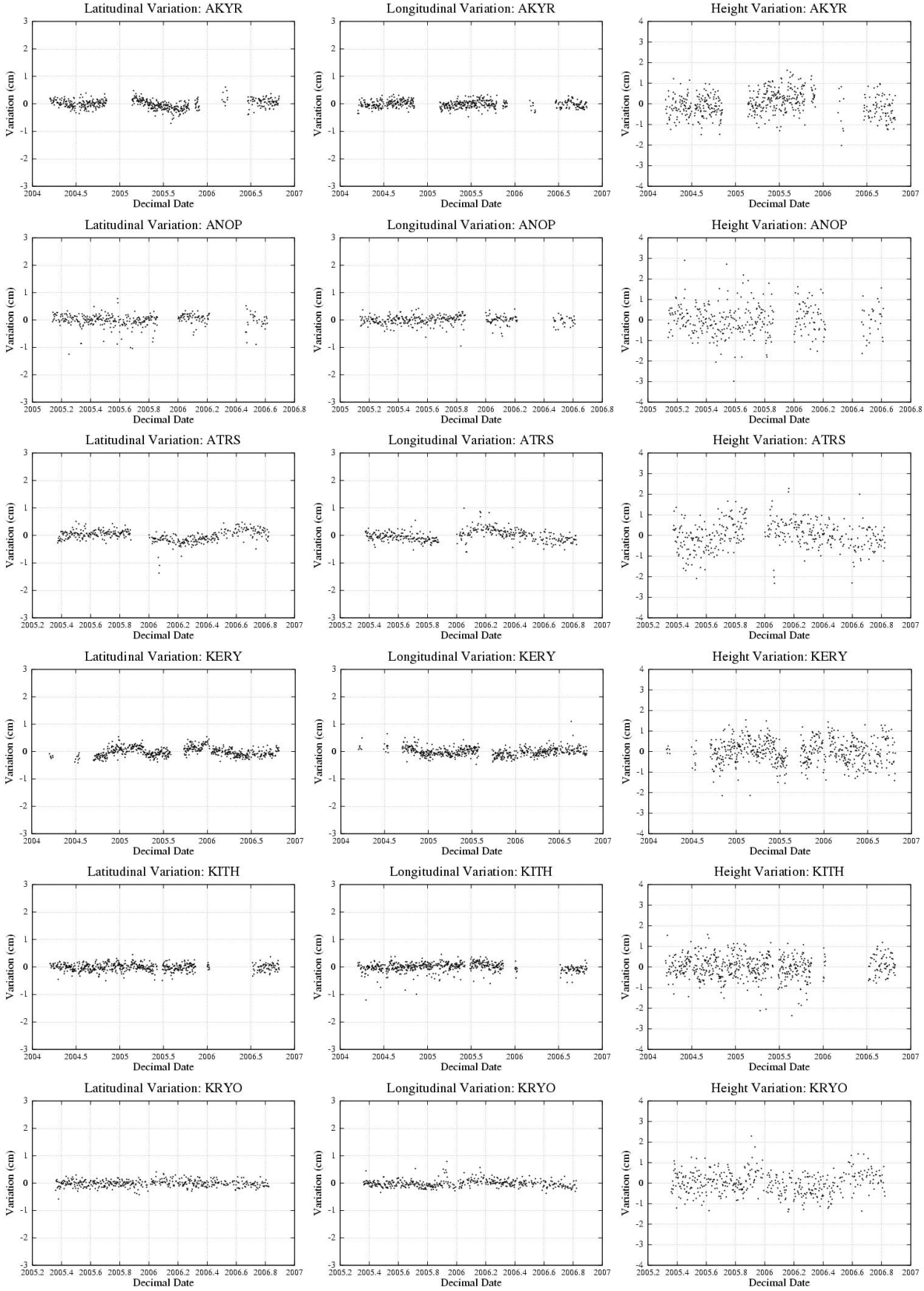

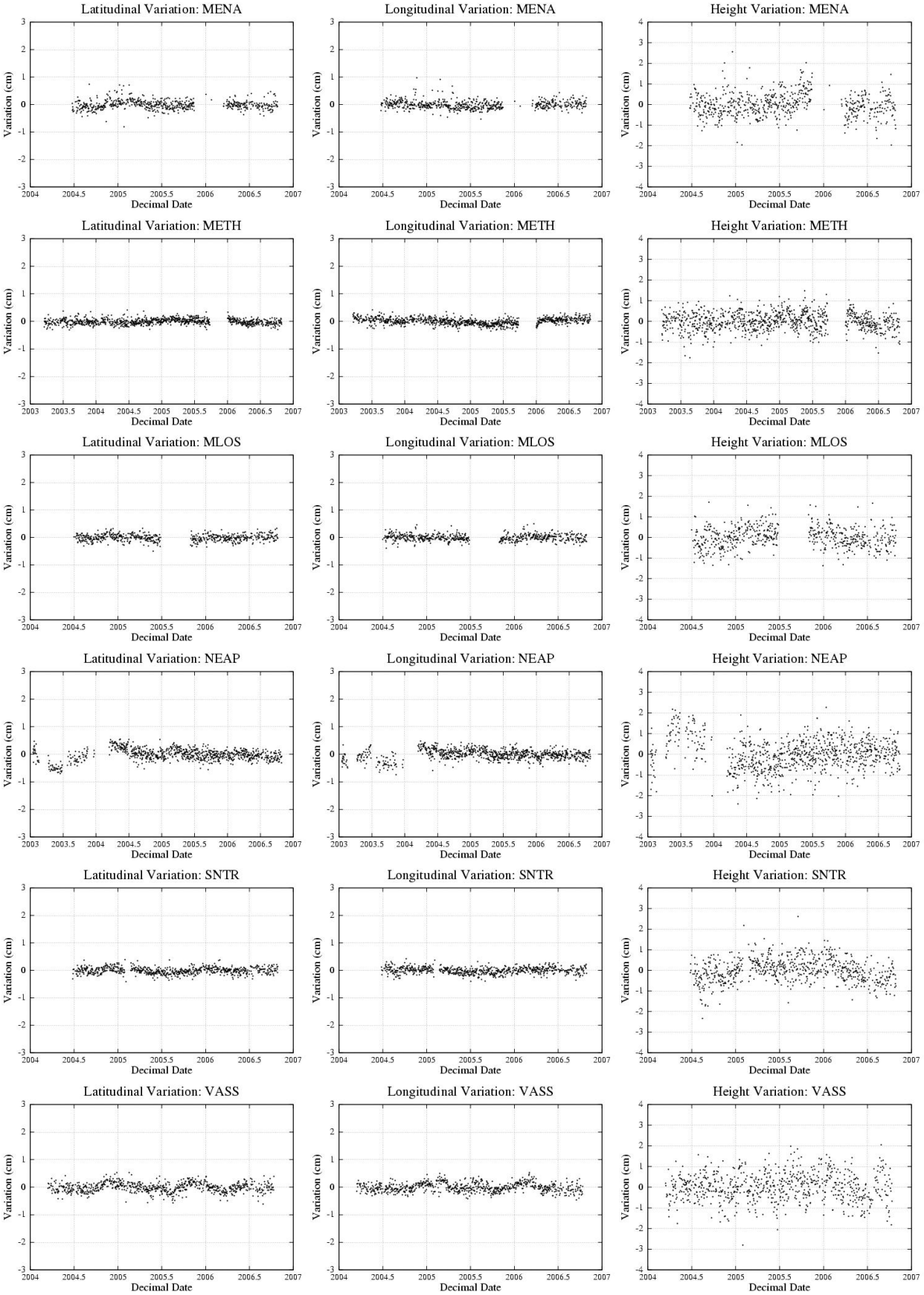
Latitudinal Variation: MENA
Longitudinal Variation: MENA
Height Variation: MENA
Latitudinal Variation: METH
Longitudinal Variation: METH
Height Variation: METH
Latitudinal Variation: MLOS
Longitudinal Variation: MLOS
Height Variation: MLOS
Latitudinal Variation: NEAP
Longitudinal Variation: NEAP
Height Variation: NEAP
Latitudinal Variation: SNTR
Longitudinal Variation: SNTR
Height Variation: SNTR
Latitudinal Variation: VASS
Longitudinal Variation: VASS
Height Variation: VASS
Variation (cm)
Decimal Date

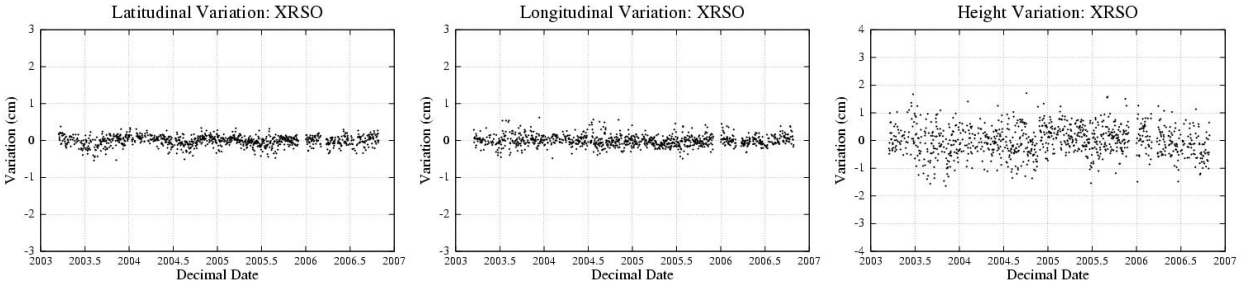
Latitudinal Variation: XRSO
Longitudinal Variation: XRSO
Height Variation: XRSO
Variation (cm)
Decimal Date

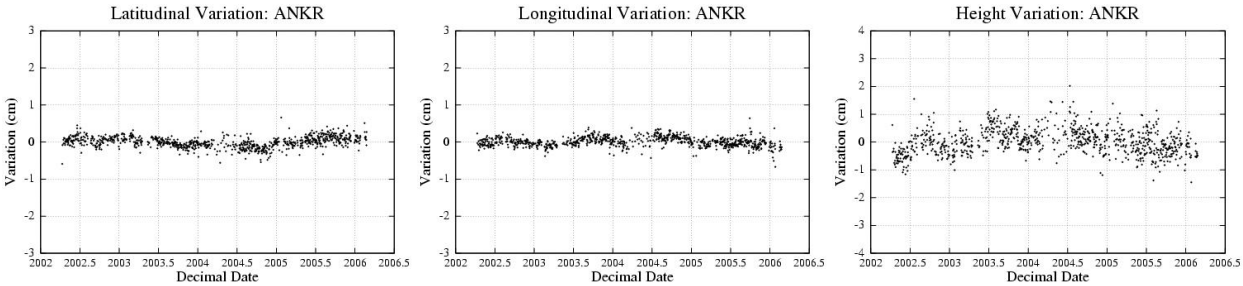
Latitudinal Variation: ANKR
Longitudinal Variation: ANKR
Height Variation: ANKR
Variation (cm)
Decimal Date

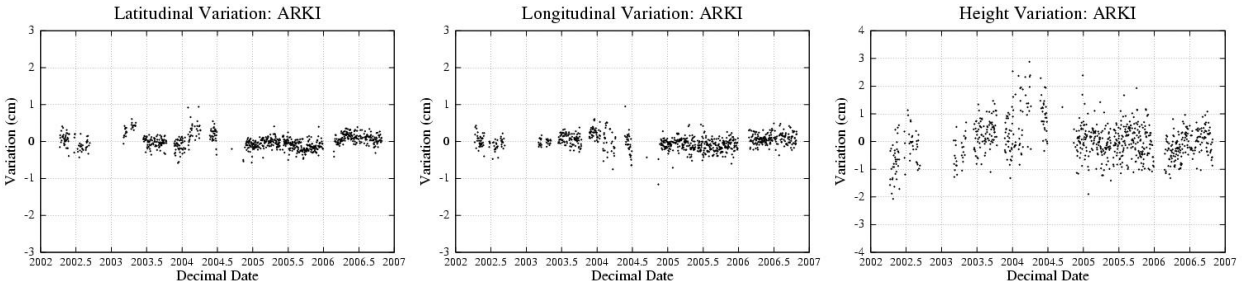
Latitudinal Variation: ARKI
Longitudinal Variation: ARKI
Height Variation: ARKI
Variation (cm)
Decimal Date

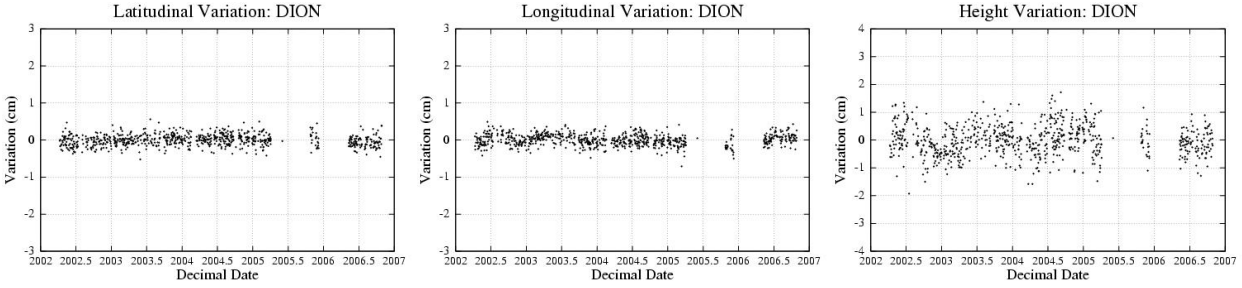
Latitudinal Variation: DION
Longitudinal Variation: DION
Height Variation: DION
Variation (cm)
Decimal Date

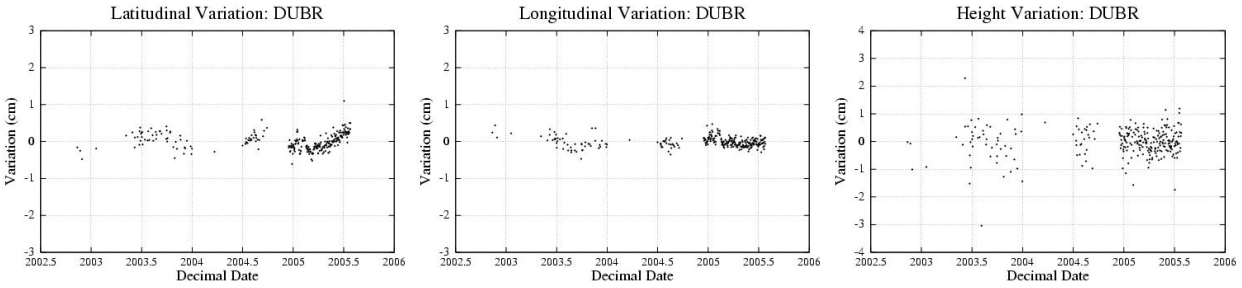
Latitudinal Variation: DUBR
Longitudinal Variation: DUBR
Height Variation: DUBR
Variation (cm)
Decimal Date

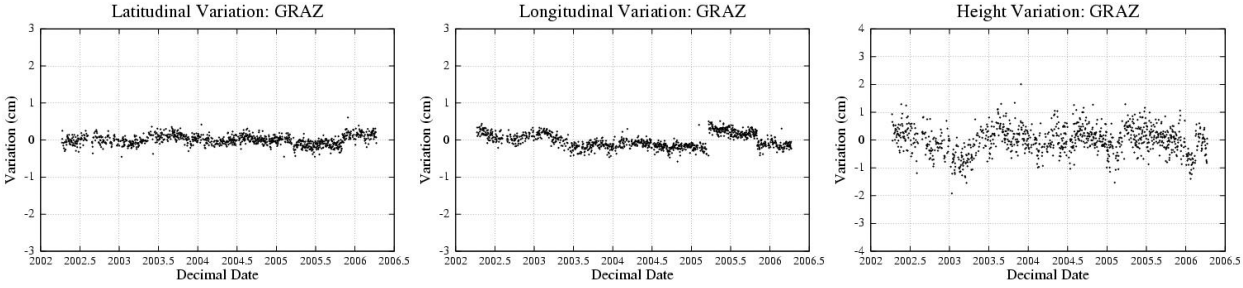
Latitudinal Variation: GRAZ
Longitudinal Variation: GRAZ
Height Variation: GRAZ
Variation (cm)
Decimal Date

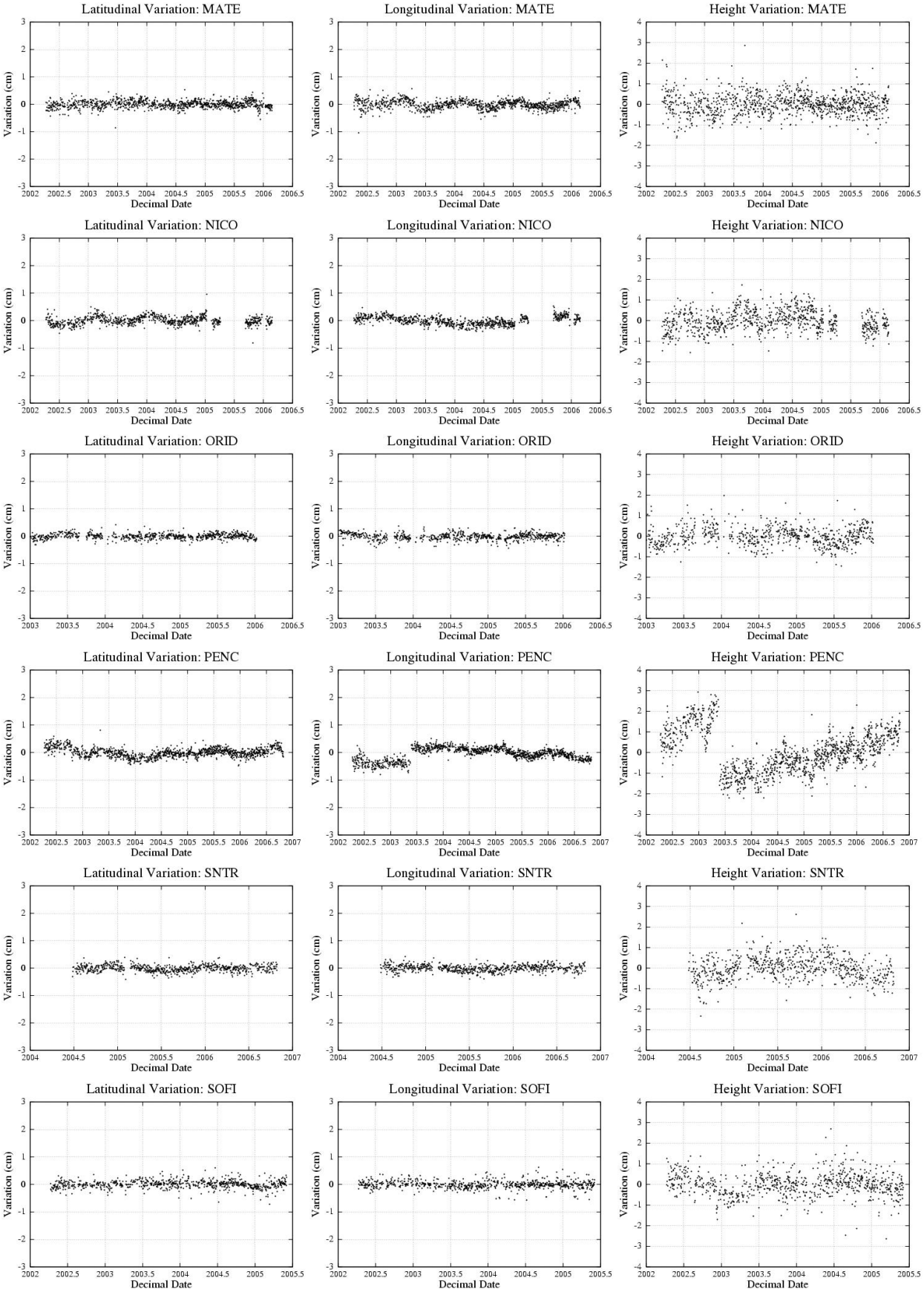
Latitudinal Variation: MATE
Longitudinal Variation: MATE
Height Variation: MATE
Latitudinal Variation: NICO
Longitudinal Variation: NICO
Height Variation: NICO
Latitudinal Variation: ORID
Longitudinal Variation: ORID
Height Variation: ORID
Latitudinal Variation: PENC
Longitudinal Variation: PENC
Height Variation: PENC
Latitudinal Variation: SNTR
Longitudinal Variation: SNTR
Height Variation: SNTR
Latitudinal Variation: SOFI
Longitudinal Variation: SOFI
Height Variation: SOFI
Variation (cm)
Decimal Date

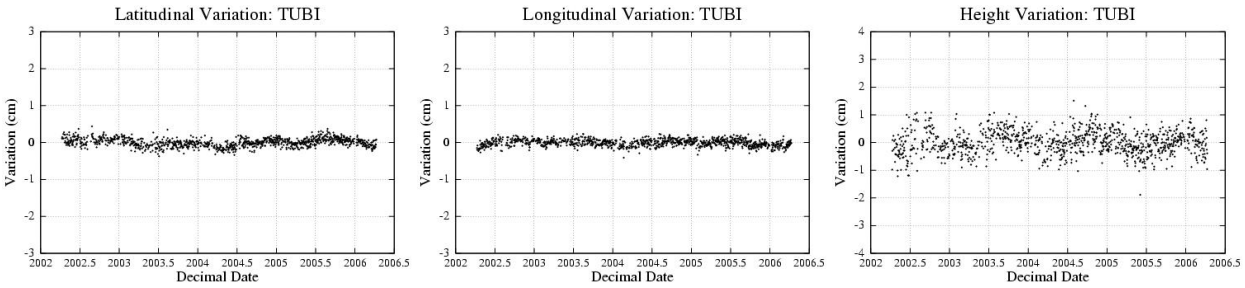
Latitudinal Variation: TUBI
Variation (cm)
Decimal Date
Longitudinal Variation: TUBI
Variation (cm)
Decimal Date
Height Variation: TUBI
Variation (cm)
Decimal Date

1.0 Sigma Filter

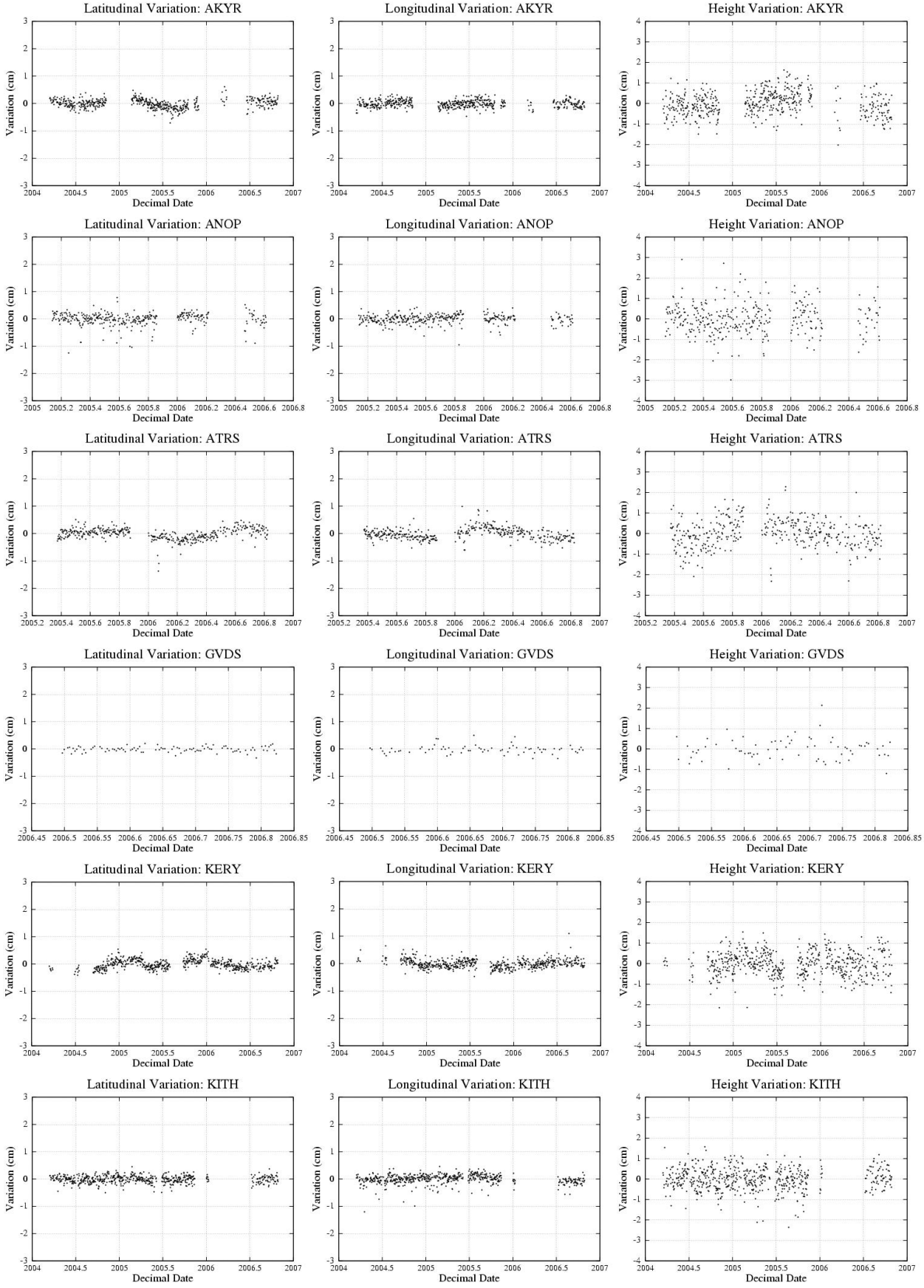

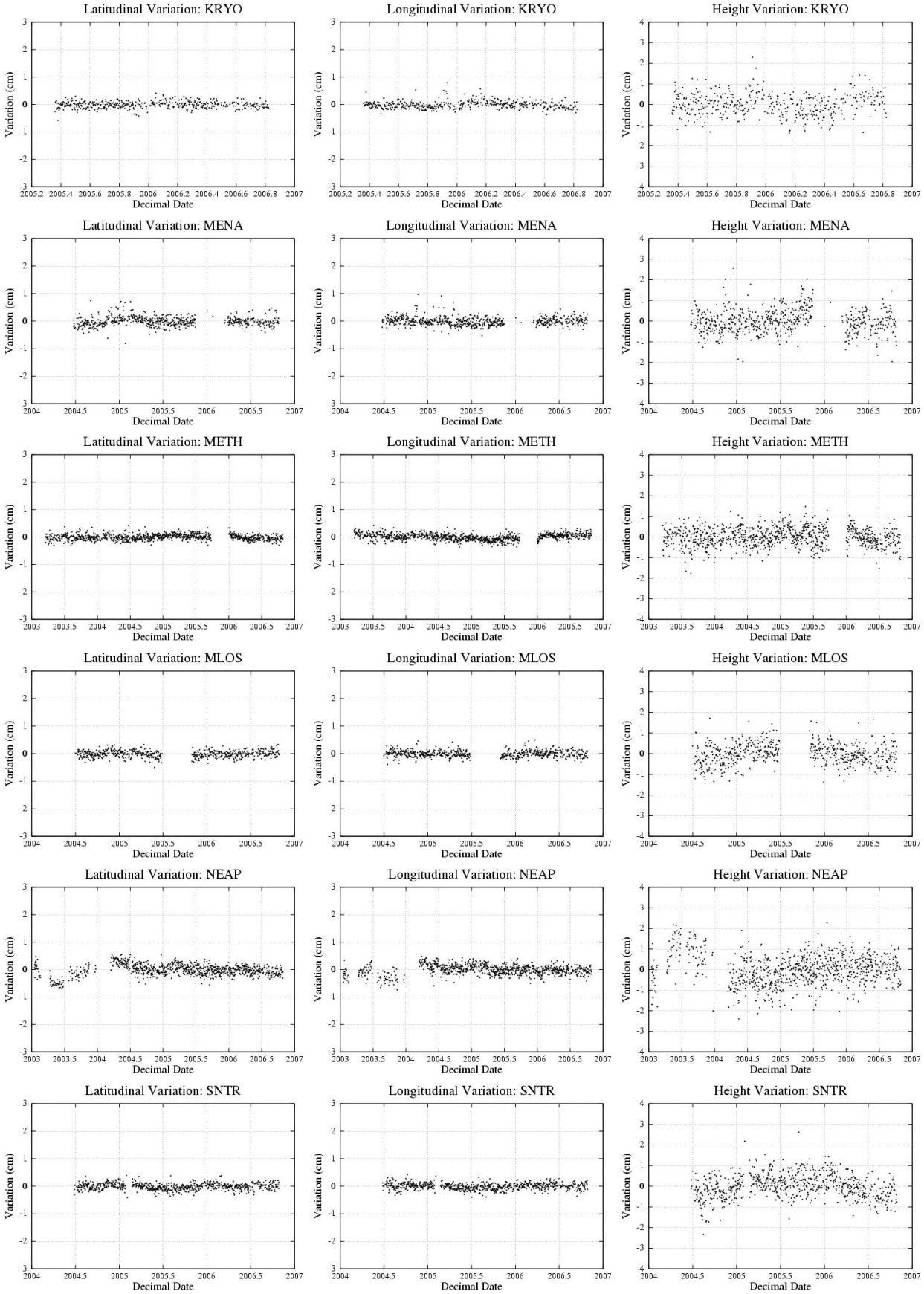
Latitudinal Variation: KRYO
Longitudinal Variation: KRYO
Height Variation: KRYO
Latitudinal Variation: MENA
Longitudinal Variation: MENA
Height Variation: MENA
Latitudinal Variation: METH
Longitudinal Variation: METH
Height Variation: METH
Latitudinal Variation: MLOS
Longitudinal Variation: MLOS
Height Variation: MLOS
Latitudinal Variation: NEAP
Longitudinal Variation: NEAP
Height Variation: NEAP
Latitudinal Variation: SNTR
Longitudinal Variation: SNTR
Height Variation: SNTR
Variation (cm)
Decimal Date

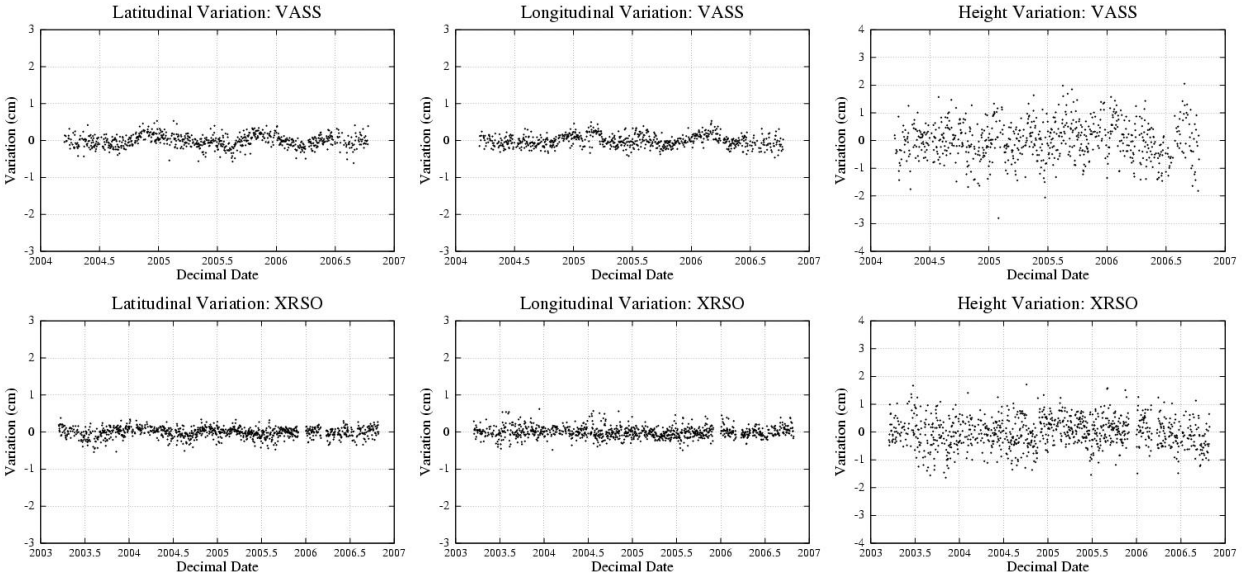
Latitudinal Variation: VASS
Longitudinal Variation: VASS
Height Variation: VASS
Latitudinal Variation: XRSO
Longitudinal Variation: XRSO
Height Variation: XRSO
Variation (cm)
Decimal Date

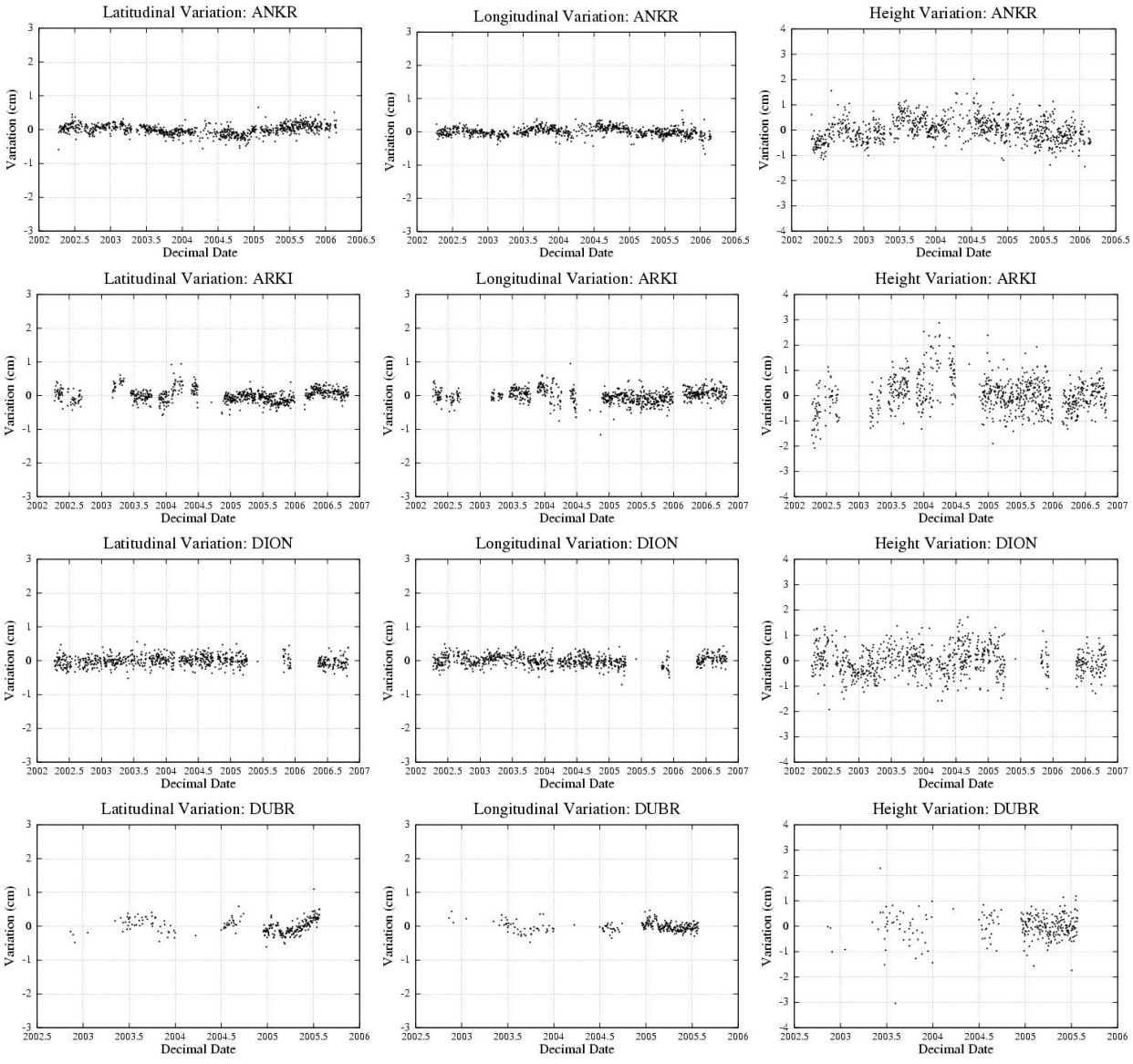
Latitudinal Variation: ANKR
Longitudinal Variation: ANKR
Height Variation: ANKR
Latitudinal Variation: ARKI
Longitudinal Variation: ARKI
Height Variation: ARKI
Latitudinal Variation: DION
Longitudinal Variation: DION
Height Variation: DION
Latitudinal Variation: DUBR
Longitudinal Variation: DUBR
Height Variation: DUBR
Variation (cm)
Decimal Date

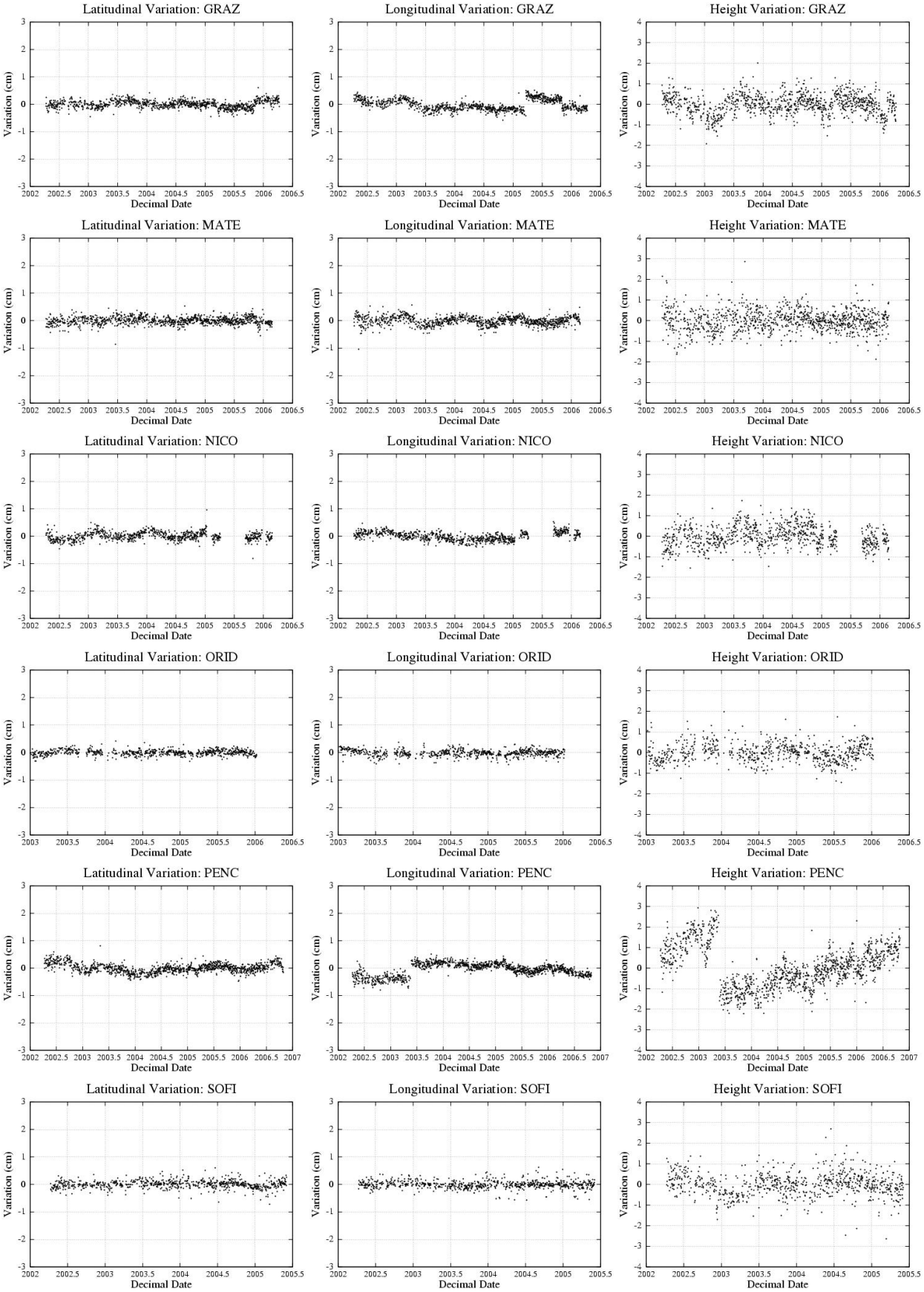
Latitudinal Variation: GRAZ
Longitudinal Variation: GRAZ
Height Variation: GRAZ
Latitudinal Variation: MATE
Longitudinal Variation: MATE
Height Variation: MATE
Latitudinal Variation: NICO
Longitudinal Variation: NICO
Height Variation: NICO
Latitudinal Variation: ORID
Longitudinal Variation: ORID
Height Variation: ORID
Latitudinal Variation: PENC
Longitudinal Variation: PENC
Height Variation: PENC
Latitudinal Variation: SOFI
Longitudinal Variation: SOFI
Height Variation: SOFI
Variation (cm)
Decimal Date

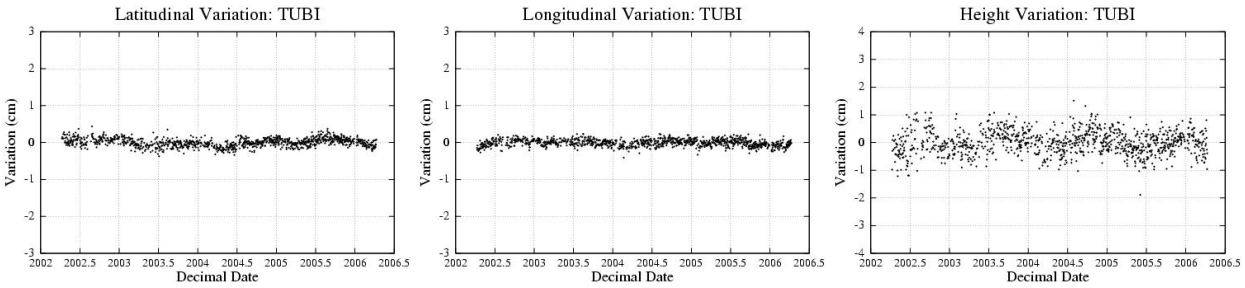
Latitudinal Variation: TUBI
Variation (cm)
Decimal Date
Longitudinal Variation: TUBI
Variation (cm)
Decimal Date
Height Variation: TUBI
Variation (cm)
Decimal Date

Appendix E

Filtered Baseline Method

Easting Variations

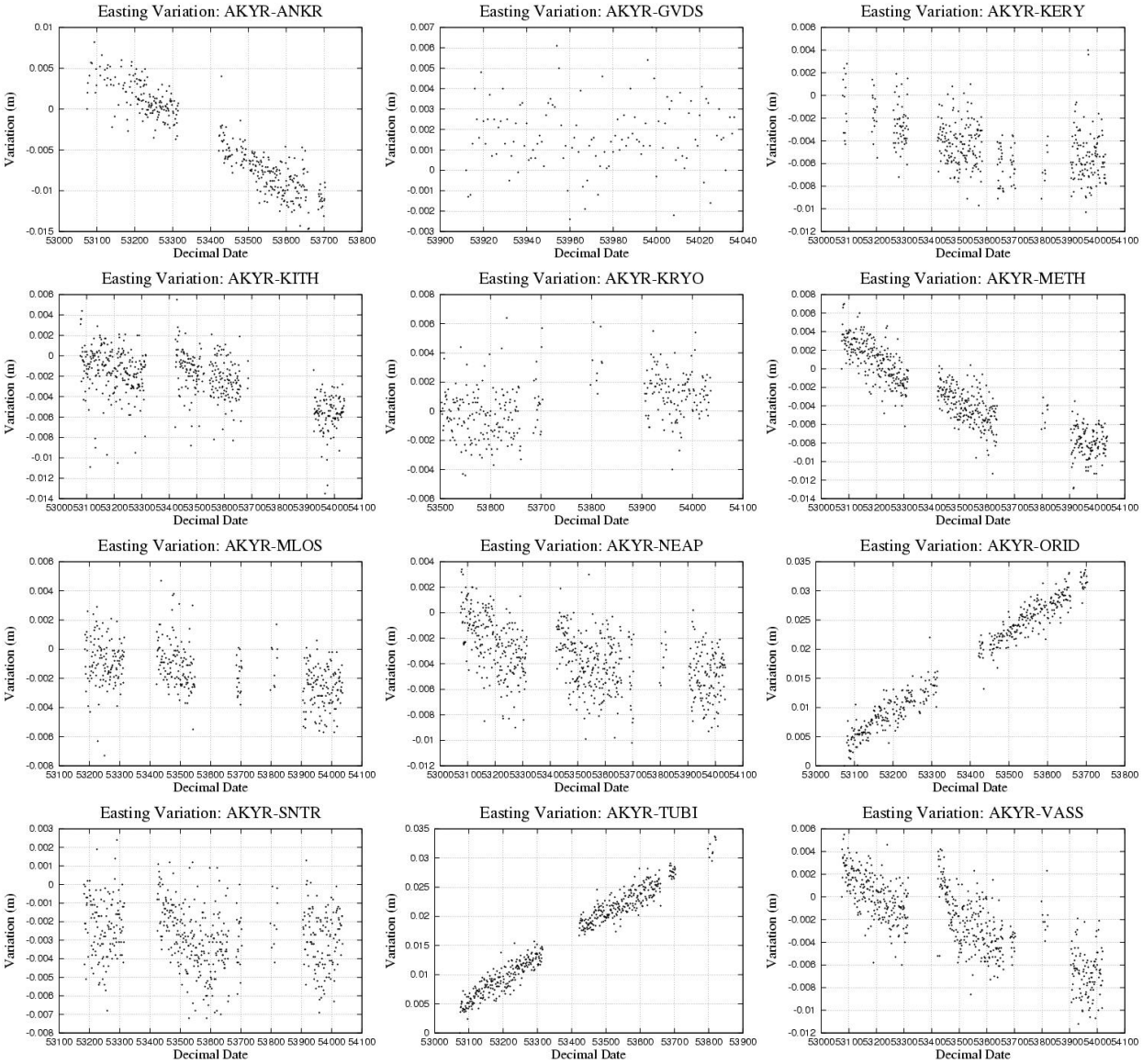

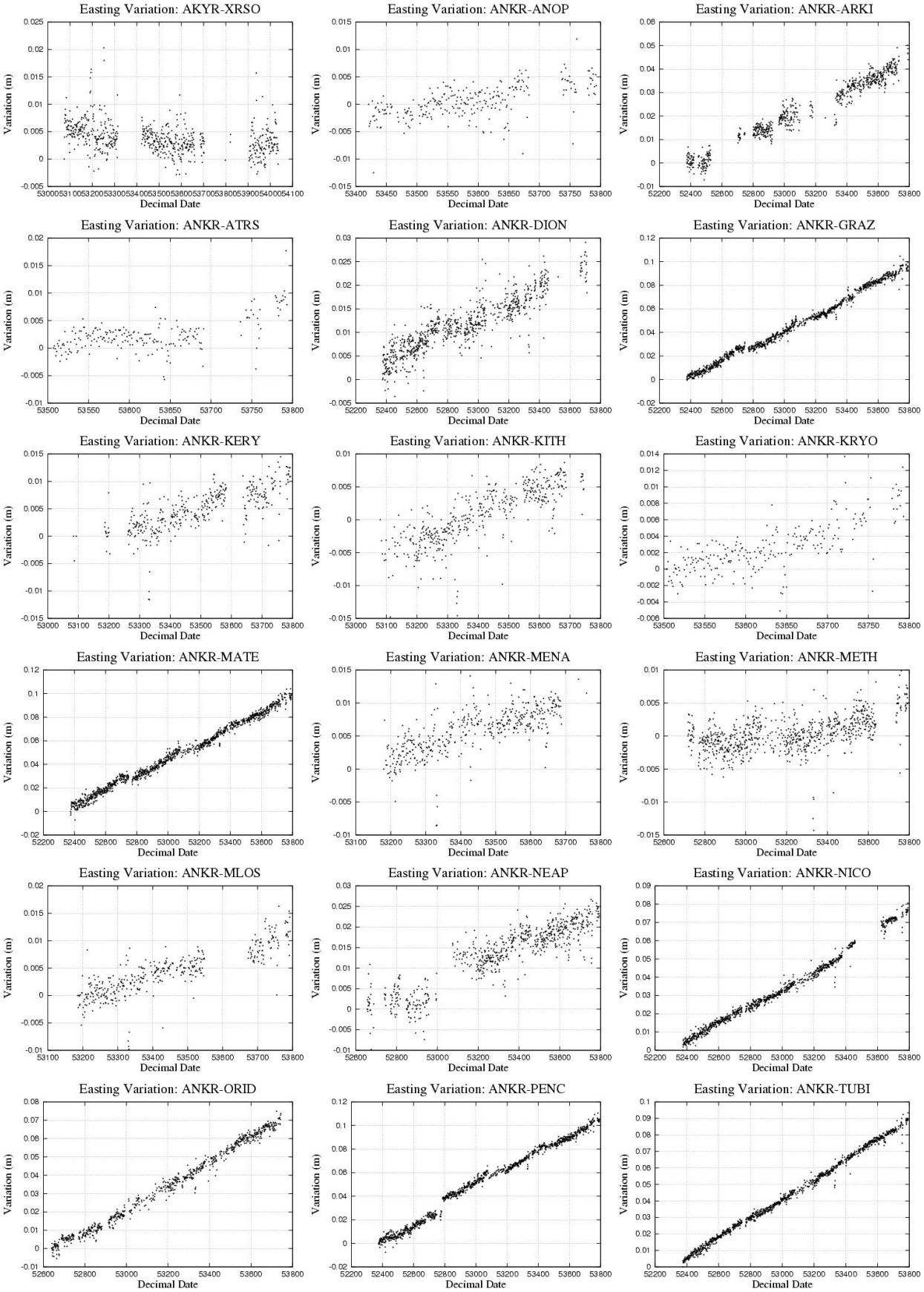
Easting Variation: AKYR-XRSO
Easting Variation: ANKR-ANOP
Easting Variation: ANKR-ARKI
Easting Variation: ANKR-ATRS
Easting Variation: ANKR-DION
Easting Variation: ANKR-GRAZ
Easting Variation: ANKR-KERY
Easting Variation: ANKR-KITH
Easting Variation: ANKR-KRYO
Easting Variation: ANKR-MATE
Easting Variation: ANKR-MENA
Easting Variation: ANKR-METH
Easting Variation: ANKR-MLOS
Easting Variation: ANKR-NEAP
Easting Variation: ANKR-NICO
Easting Variation: ANKR-ORID
Easting Variation: ANKR-PENC
Easting Variation: ANKR-TUBI
Variation (m)
Decimal Date

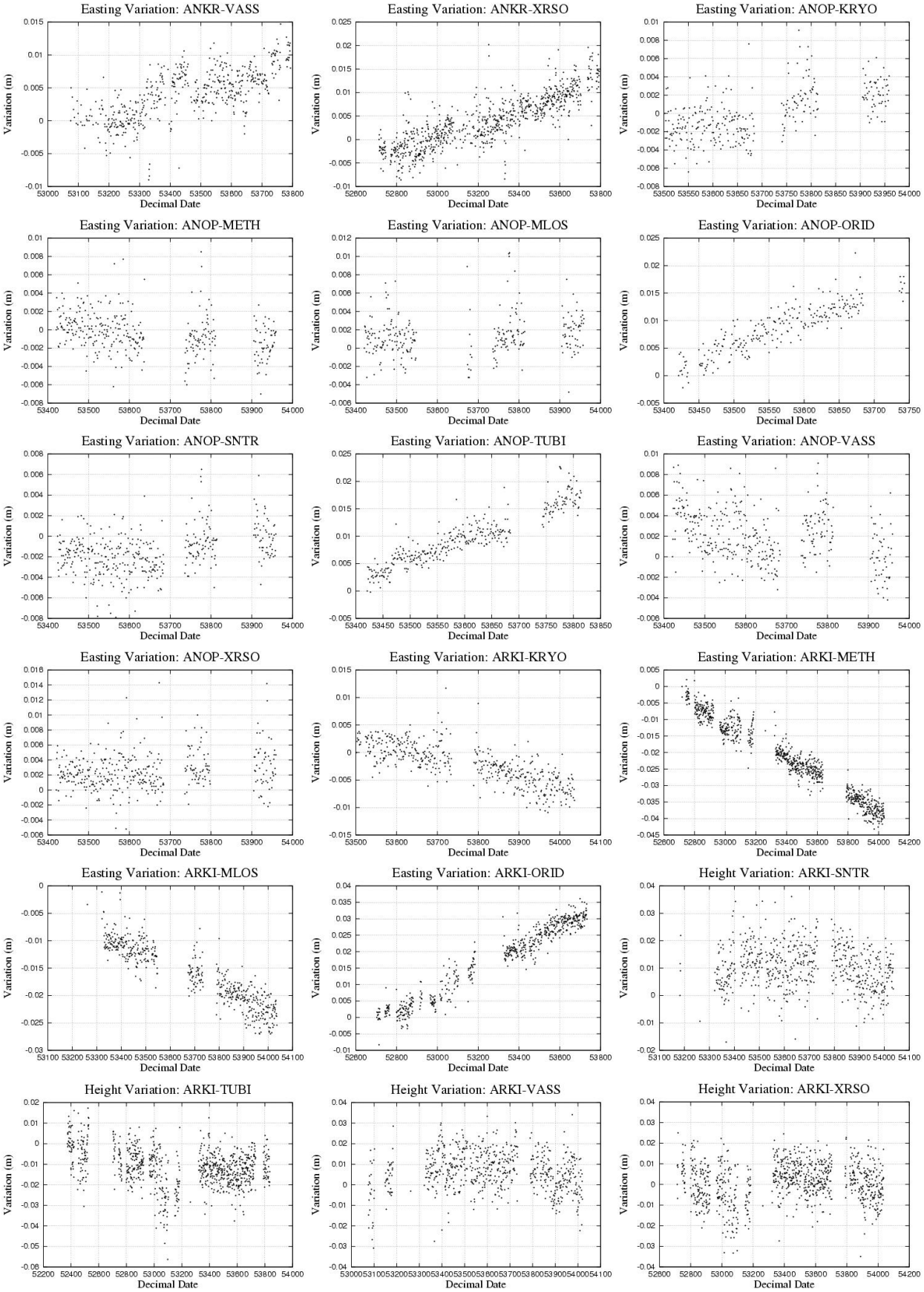
Easting Variation: ANKR-VASS
Easting Variation: ANKR-XRSO
Easting Variation: ANOP-KRYO
Easting Variation: ANOP-METH
Easting Variation: ANOP-MLOS
Easting Variation: ANOP-ORID
Easting Variation: ANOP-SNTR
Easting Variation: ANOP-TUBI
Easting Variation: ANOP-VASS
Easting Variation: ANOP-XRSO
Easting Variation: ARKI-KRYO
Easting Variation: ARKI-METH
Easting Variation: ARKI-MLOS
Easting Variation: ARKI-ORID
Height Variation: ARKI-SNTR
Height Variation: ARKI-TUBI
Height Variation: ARKI-VASS
Height Variation: ARKI-XRSO
Variation (m)
Decimal Date

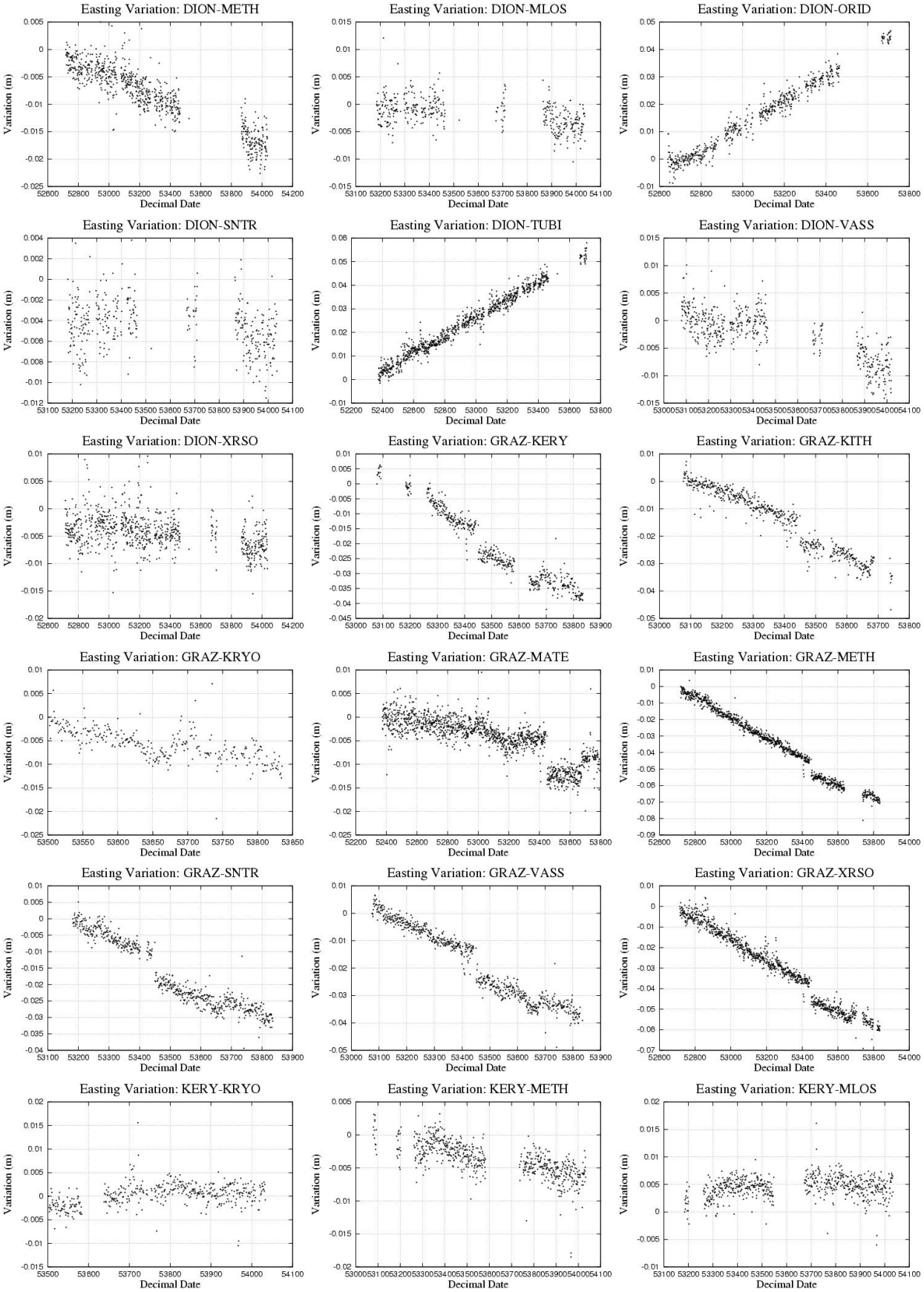
Easting Variation: DION-METH
Easting Variation: DION-MLOS
Easting Variation: DION-ORID
Easting Variation: DION-SNTR
Easting Variation: DION-TUBI
Easting Variation: DION-VASS
Easting Variation: DION-XRSO
Easting Variation: GRAZ-KERY
Easting Variation: GRAZ-KITH
Easting Variation: GRAZ-KRYO
Easting Variation: GRAZ-MATE
Easting Variation: GRAZ-METH
Easting Variation: GRAZ-SNTR
Easting Variation: GRAZ-VASS
Easting Variation: GRAZ-XRSO
Easting Variation: KERY-KRYO
Easting Variation: KERY-METH
Easting Variation: KERY-MLOS
Variation (m)
Decimal Date

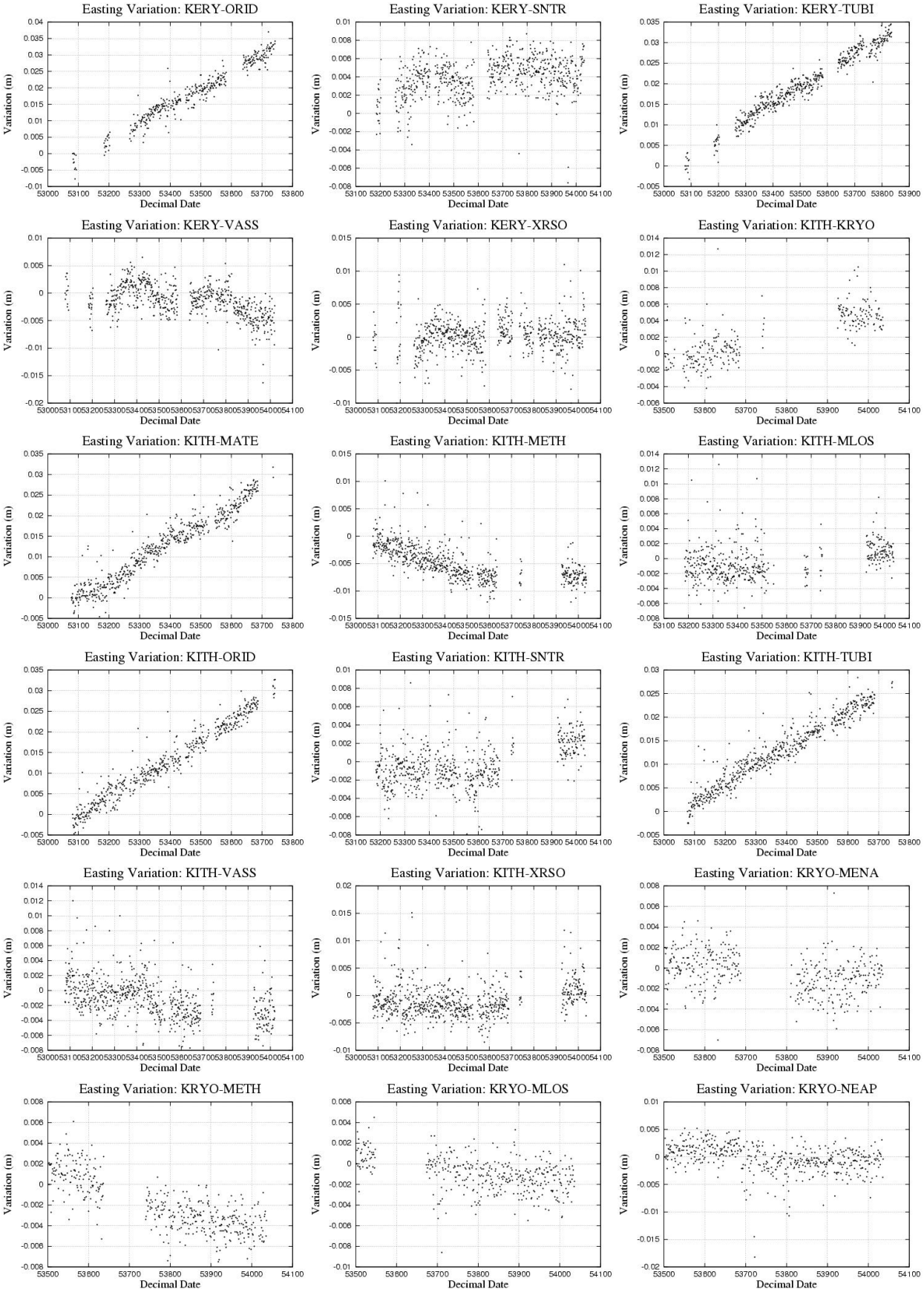
Easting Variation: KERY-ORID
Easting Variation: KERY-SNTR
Easting Variation: KERY-TUBI
Easting Variation: KERY-VASS
Easting Variation: KERY-XRSO
Easting Variation: KITH-KRYO
Easting Variation: KITH-MATE
Easting Variation: KITH-METH
Easting Variation: KITH-MLOS
Easting Variation: KITH-ORID
Easting Variation: KITH-SNTR
Easting Variation: KITH-TUBI
Easting Variation: KITH-VASS
Easting Variation: KITH-XRSO
Easting Variation: KRYO-MENA
Easting Variation: KRYO-METH
Easting Variation: KRYO-MLOS
Easting Variation: KRYO-NEAP
Variation (m)
Decimal Date

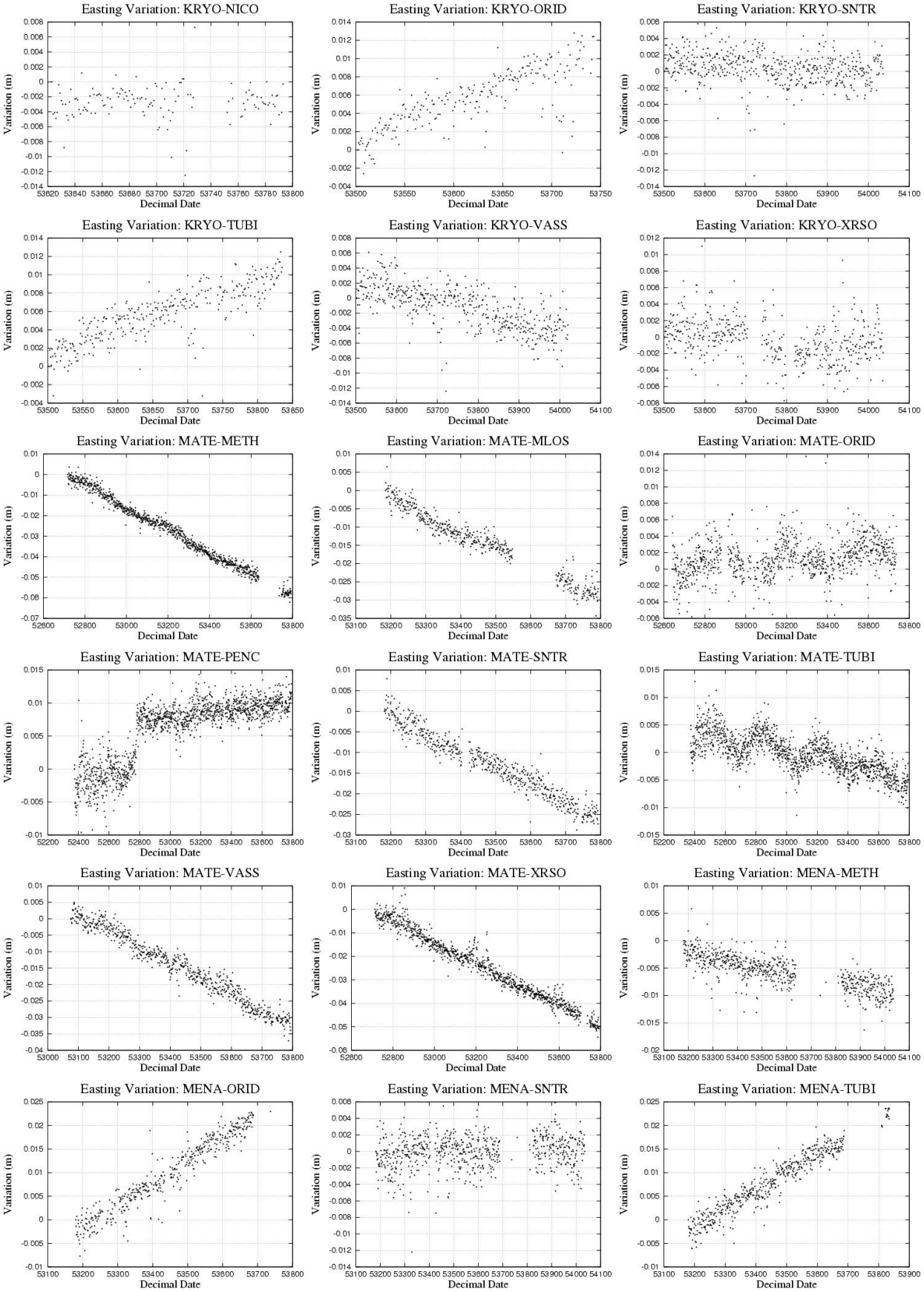
Easting Variation: KRYO-NICO
Easting Variation: KRYO-ORID
Easting Variation: KRYO-SNTR
Easting Variation: KRYO-TUBI
Easting Variation: KRYO-VASS
Easting Variation: KRYO-XRSO
Easting Variation: MATE-METH
Easting Variation: MATE-MLOS
Easting Variation: MATE-ORID
Easting Variation: MATE-PENC
Easting Variation: MATE-SNTR
Easting Variation: MATE-TUBI
Easting Variation: MATE-VASS
Easting Variation: MATE-XRSO
Easting Variation: MENA-METH
Easting Variation: MENA-ORID
Easting Variation: MENA-SNTR
Easting Variation: MENA-TUBI
Variation (m)
Decimal Date

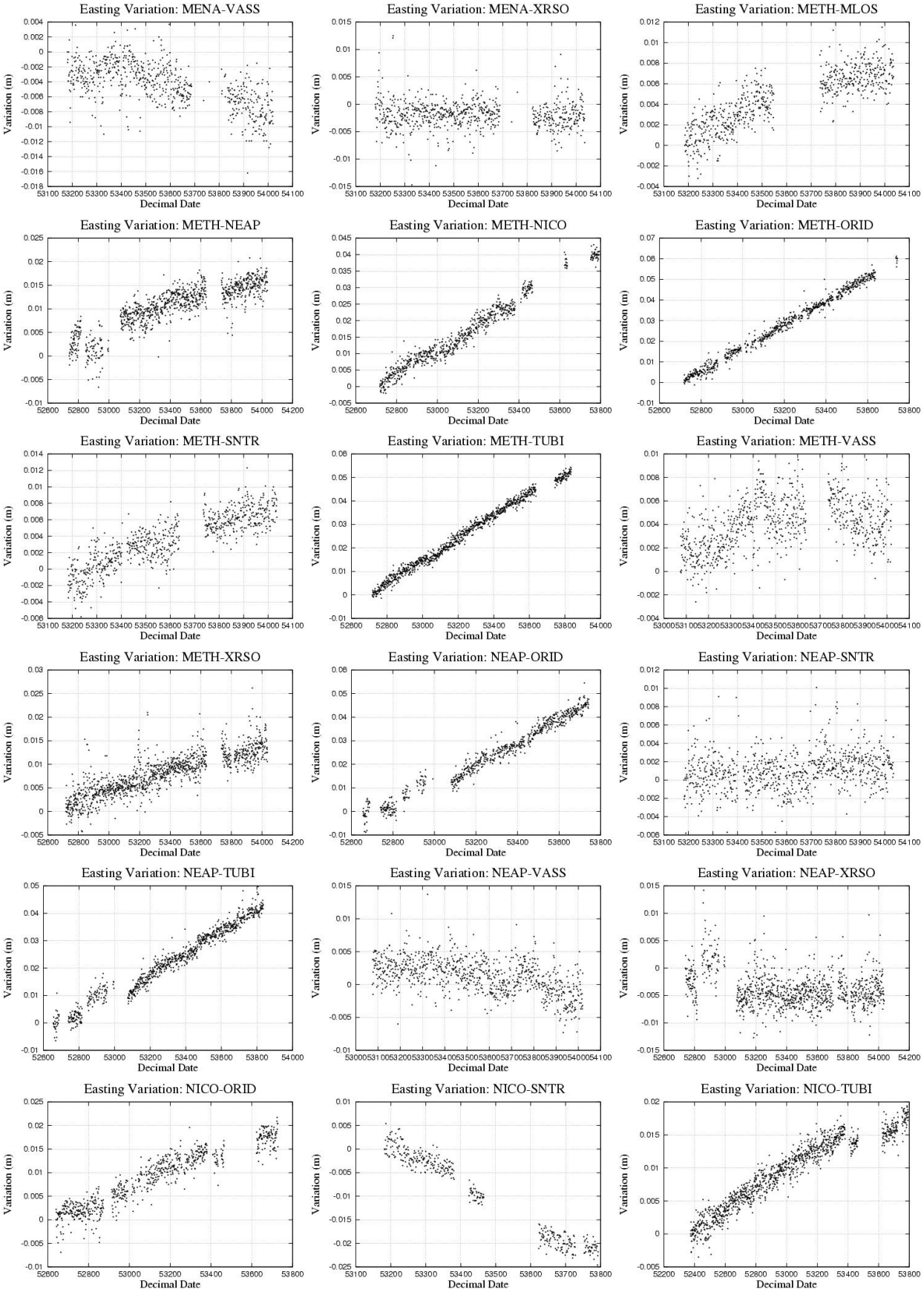
Easting Variation: MENA-VASS
Easting Variation: MENA-XRSO
Easting Variation: METH-MLOS
Easting Variation: METH-NEAP
Easting Variation: METH-NICO
Easting Variation: METH-ORID
Easting Variation: METH-SNTR
Easting Variation: METH-TUBI
Easting Variation: METH-VASS
Easting Variation: METH-XRSO
Easting Variation: NEAP-ORID
Easting Variation: NEAP-SNTR
Easting Variation: NEAP-TUBI
Easting Variation: NEAP-VASS
Easting Variation: NEAP-XRSO
Easting Variation: NICO-ORID
Easting Variation: NICO-SNTR
Easting Variation: NICO-TUBI
Variation (m)
Decimal Date

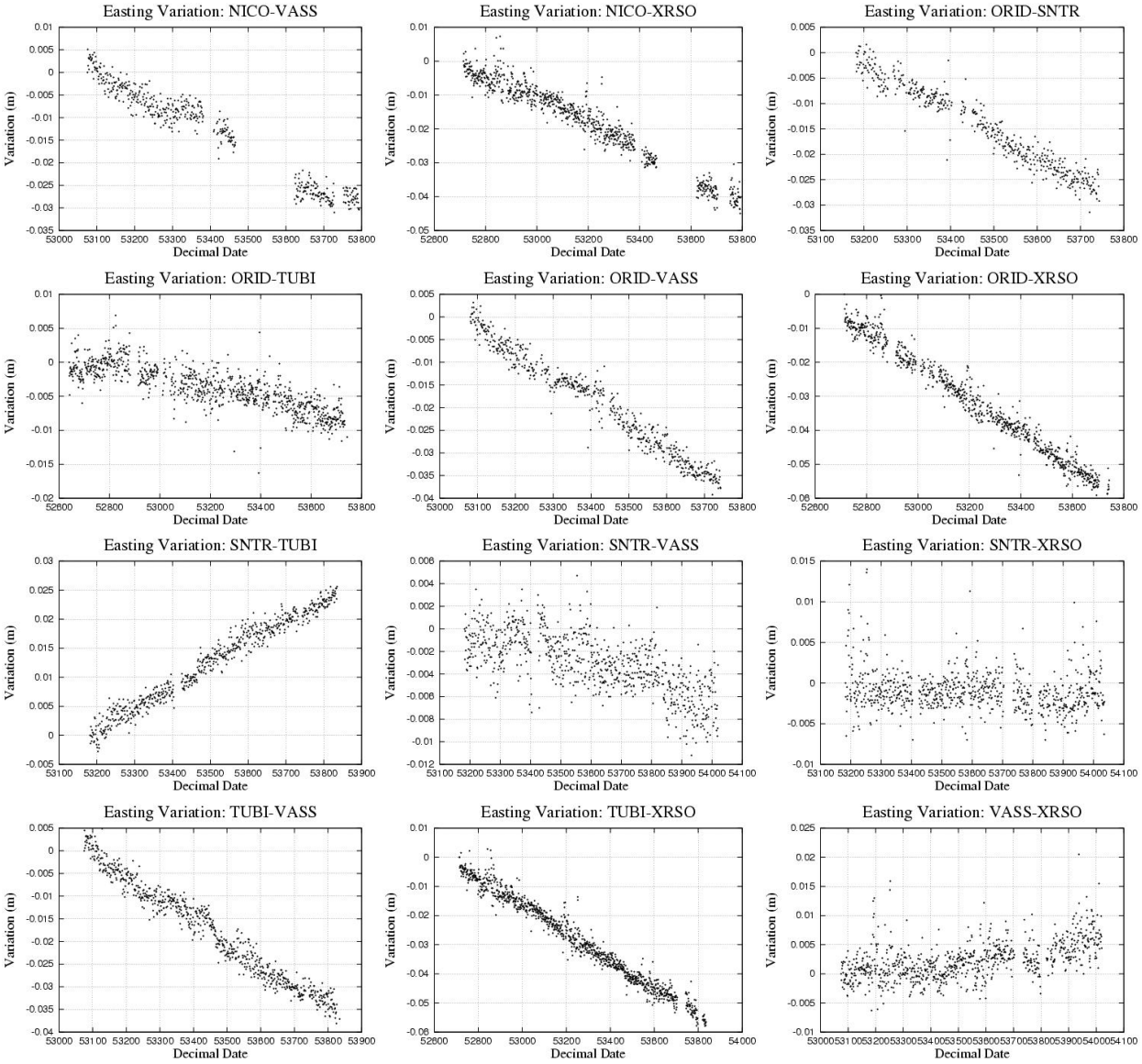
Easting Variation: NICO-VASS
Easting Variation: NICO-XRSO
Easting Variation: ORID-SNTR
Easting Variation: ORID-TUBI
Easting Variation: ORID-VASS
Easting Variation: ORID-XRSO
Easting Variation: SNTR-TUBI
Easting Variation: SNTR-VASS
Easting Variation: SNTR-XRSO
Easting Variation: TUBI-VASS
Easting Variation: TUBI-XRSO
Easting Variation: VASS-XRSO
Variation (m)
Decimal Date

Northing Variations

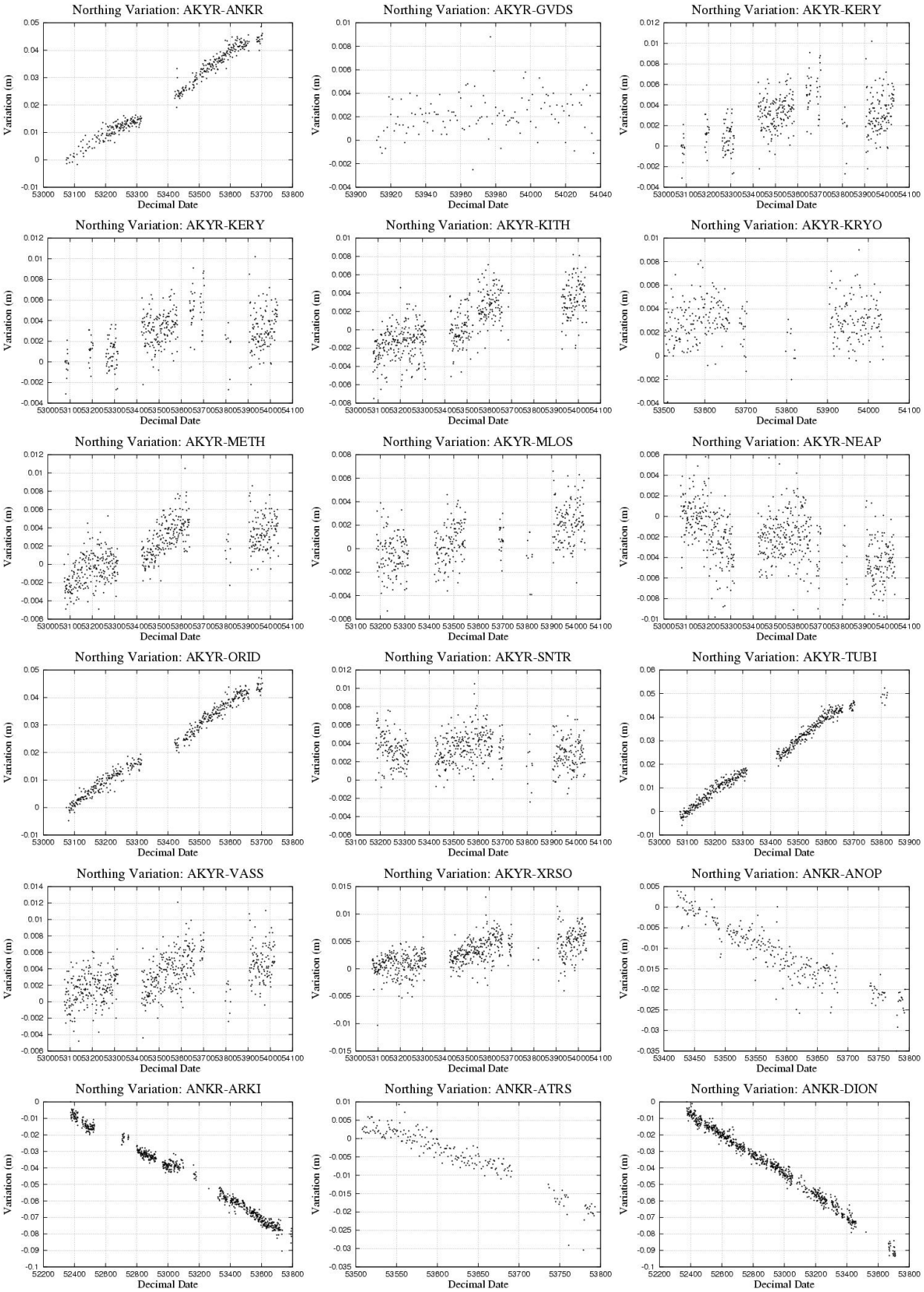

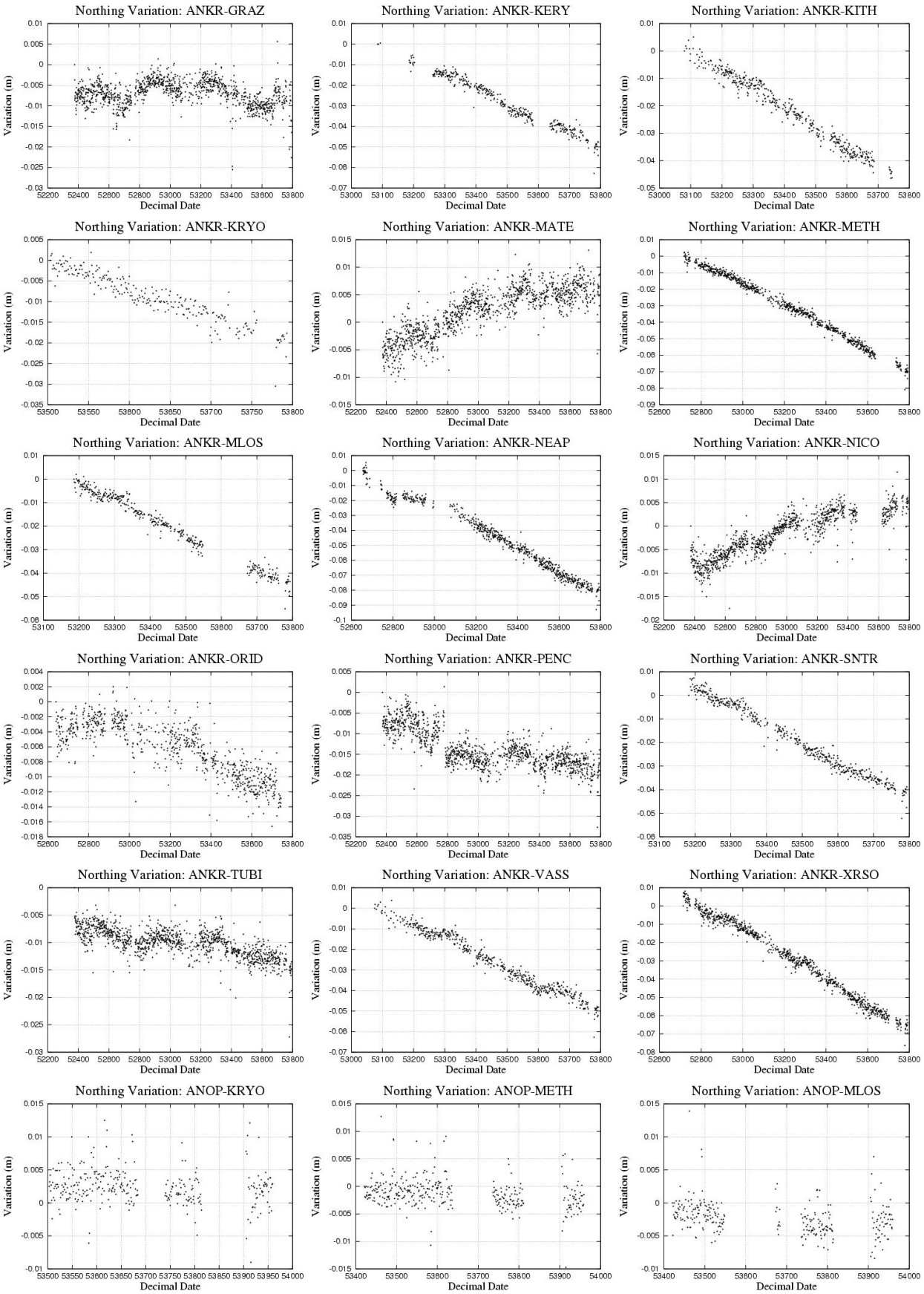
Northing Variation: ANKR-GRAZ
Northing Variation: ANKR-KERY
Northing Variation: ANKR-KITH
Northing Variation: ANKR-KRYO
Northing Variation: ANKR-MATE
Northing Variation: ANKR-METH
Northing Variation: ANKR-MLOS
Northing Variation: ANKR-NEAP
Northing Variation: ANKR-NICO
Northing Variation: ANKR-ORID
Northing Variation: ANKR-PENC
Northing Variation: ANKR-SNTR
Northing Variation: ANKR-TUBI
Northing Variation: ANKR-VASS
Northing Variation: ANKR-XRSO
Northing Variation: ANOP-KRYO
Northing Variation: ANOP-METH
Northing Variation: ANOP-MLOS
Variation (m)
Decimal Date

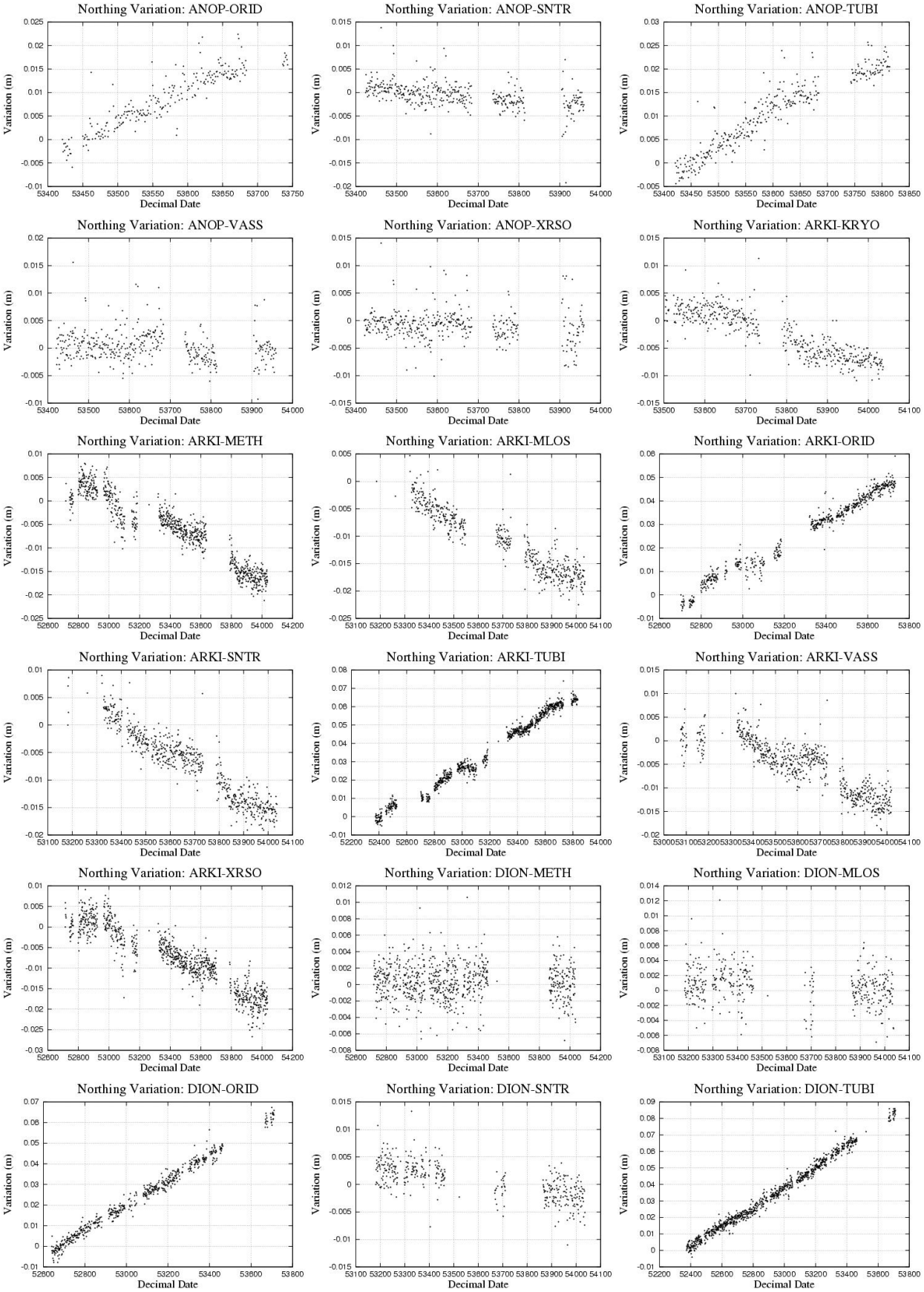
Northing Variation: ANOP-ORID
Northing Variation: ANOP-SNTR
Northing Variation: ANOP-TUBI
Northing Variation: ANOP-VASS
Northing Variation: ANOP-XRSO
Northing Variation: ARKI-KRYO
Northing Variation: ARKI-METH
Northing Variation: ARKI-MLOS
Northing Variation: ARKI-ORID
Northing Variation: ARKI-SNTR
Northing Variation: ARKI-TUBI
Northing Variation: ARKI-VASS
Northing Variation: ARKI-XRSO
Northing Variation: DION-METH
Northing Variation: DION-MLOS
Northing Variation: DION-ORID
Northing Variation: DION-SNTR
Northing Variation: DION-TUBI
Variation (m)
Decimal Date

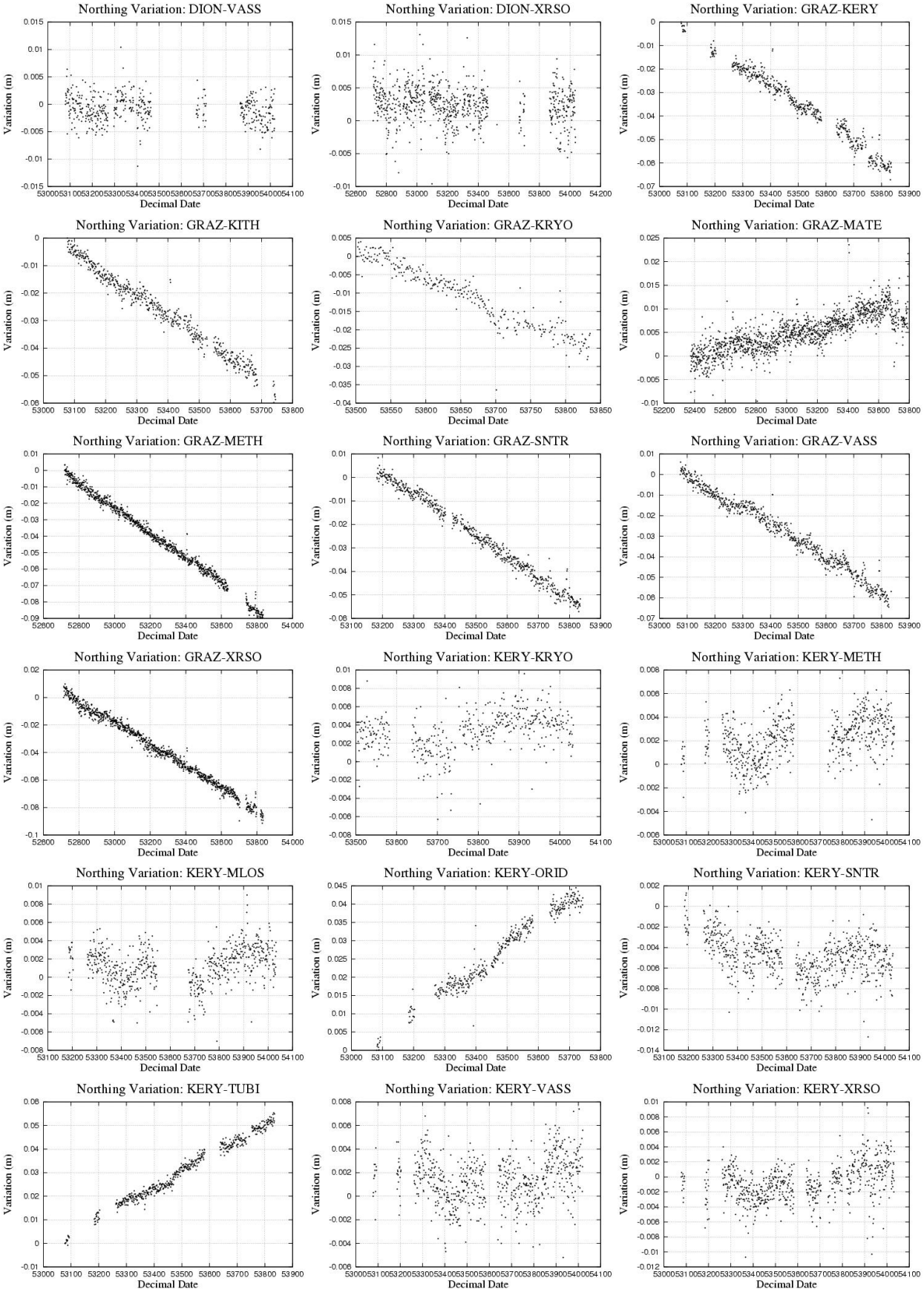
Northing Variation: DION-VASS
Northing Variation: DION-XRSO
Northing Variation: GRAZ-KERY
Northing Variation: GRAZ-KITH
Northing Variation: GRAZ-KRYO
Northing Variation: GRAZ-MATE
Northing Variation: GRAZ-METH
Northing Variation: GRAZ-SNTR
Northing Variation: GRAZ-VASS
Northing Variation: GRAZ-XRSO
Northing Variation: KERY-KRYO
Northing Variation: KERY-METH
Northing Variation: KERY-MLOS
Northing Variation: KERY-ORID
Northing Variation: KERY-SNTR
Northing Variation: KERY-TUBI
Northing Variation: KERY-VASS
Northing Variation: KERY-XRSO
Variation (m)
Decimal Date

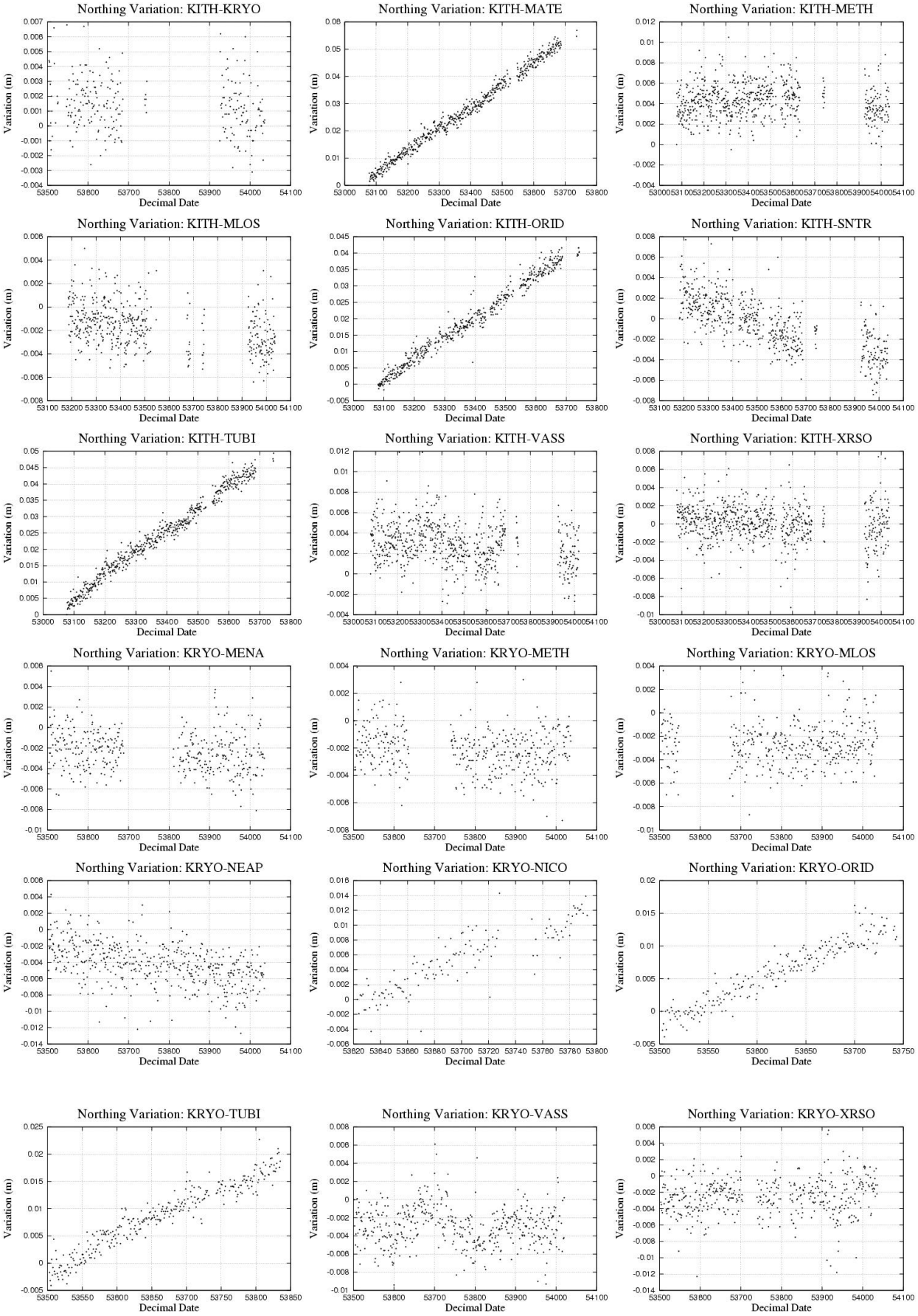
Northing Variation: KITH-KRYO
Northing Variation: KITH-MATE
Northing Variation: KITH-METH
Northing Variation: KITH-MLOS
Northing Variation: KITH-ORID
Northing Variation: KITH-SNTR
Northing Variation: KITH-TUBI
Northing Variation: KITH-VASS
Northing Variation: KITH-XRSO
Northing Variation: KRYO-MENA
Northing Variation: KRYO-METH
Northing Variation: KRYO-MLOS
Northing Variation: KRYO-NEAP
Northing Variation: KRYO-NICO
Northing Variation: KRYO-ORID
Northing Variation: KRYO-TUBI
Northing Variation: KRYO-VASS
Northing Variation: KRYO-XRSO
Variation (m)
Decimal Date

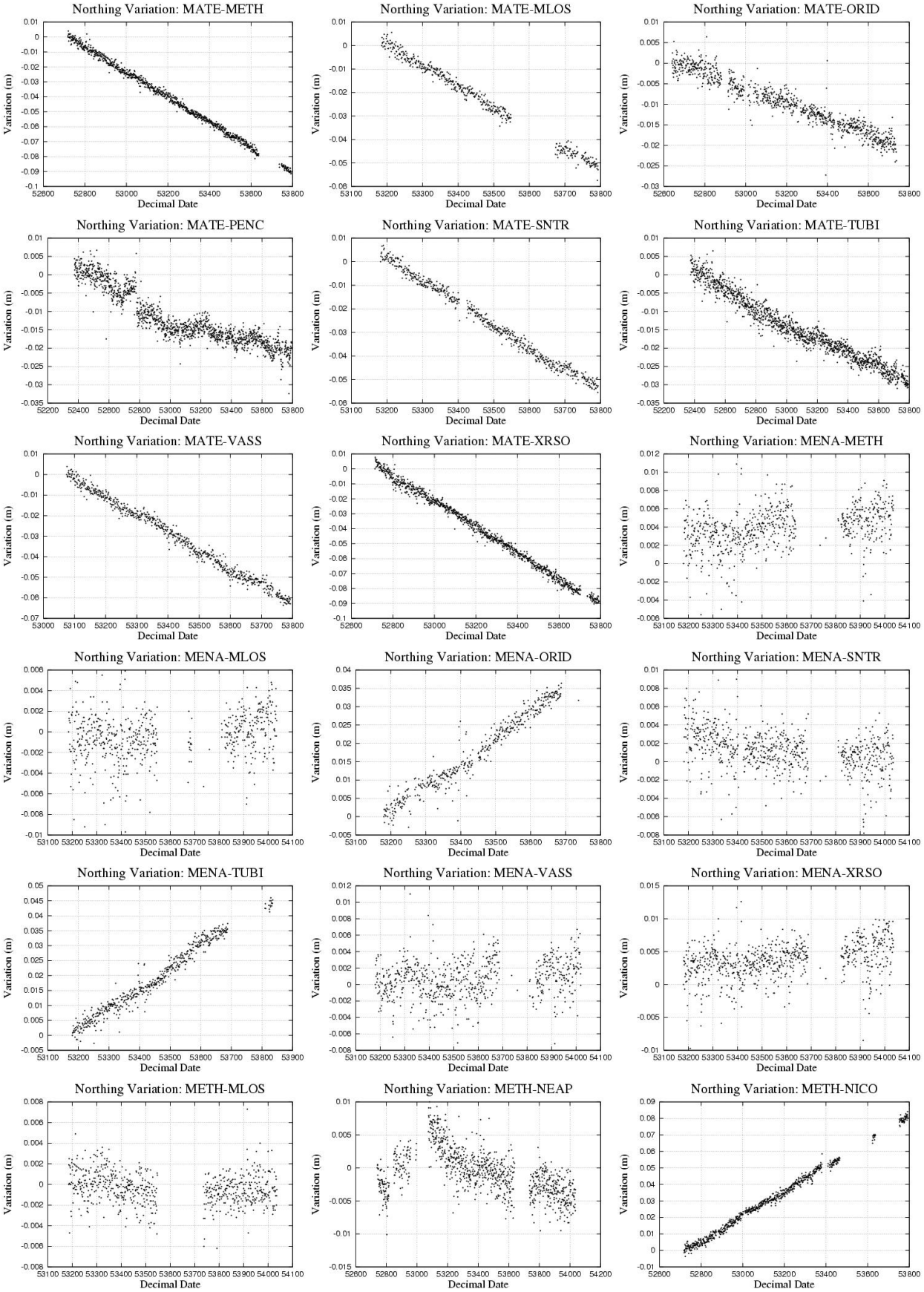
Northing Variation: MATE-METH
Northing Variation: MATE-MLOS
Northing Variation: MATE-ORID
Northing Variation: MATE-PENC
Northing Variation: MATE-SNTR
Northing Variation: MATE-TUBI
Northing Variation: MATE-VASS
Northing Variation: MATE-XRSO
Northing Variation: MENA-METH
Northing Variation: MENA-MLOS
Northing Variation: MENA-ORID
Northing Variation: MENA-SNTR
Northing Variation: MENA-TUBI
Northing Variation: MENA-VASS
Northing Variation: MENA-XRSO
Northing Variation: METH-MLOS
Northing Variation: METH-NEAP
Northing Variation: METH-NICO
Variation (m)
Decimal Date

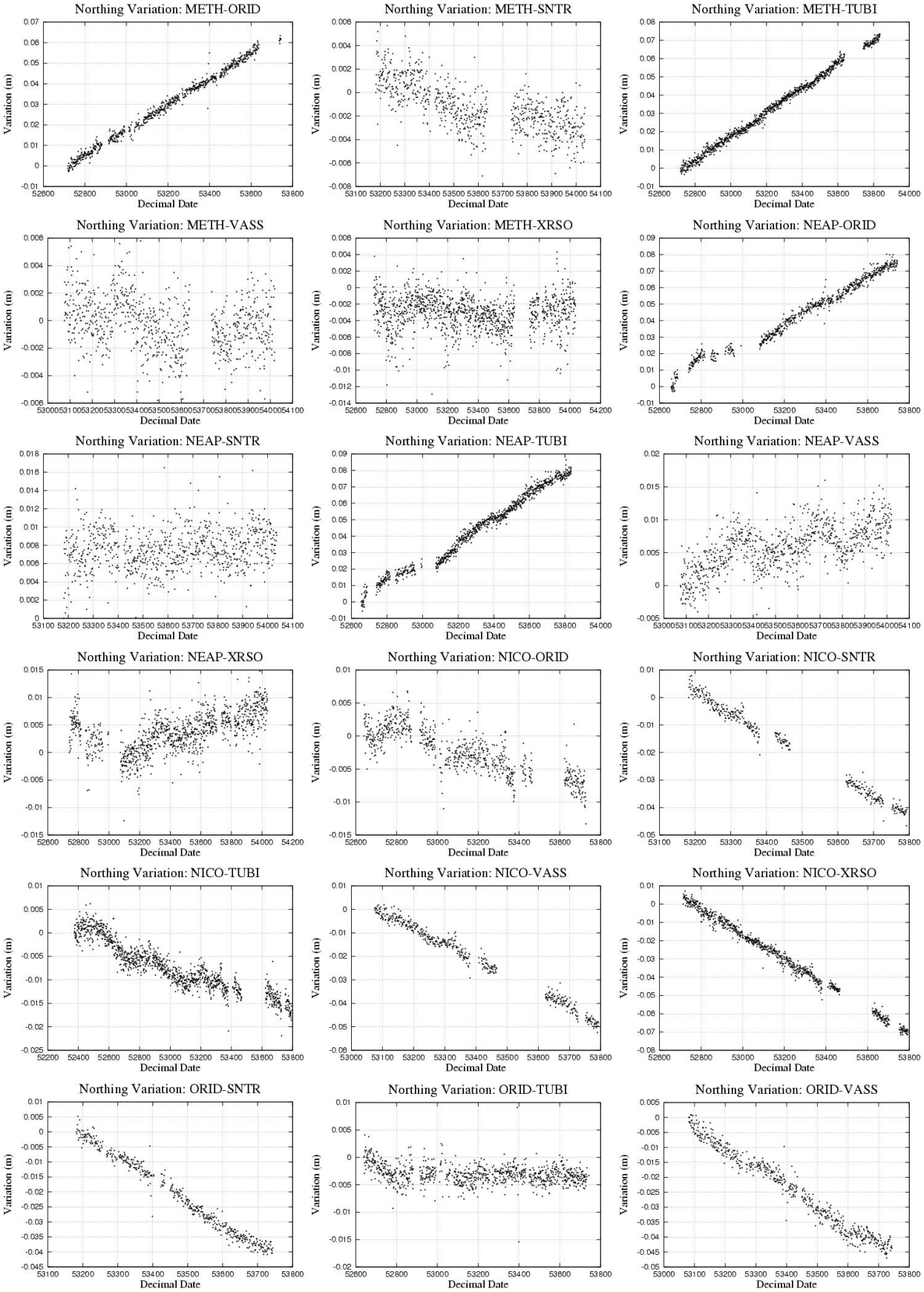
Northing Variation: METH-ORID
Northing Variation: METH-SNTR
Northing Variation: METH-TUBI
Northing Variation: METH-VASS
Northing Variation: METH-XRSO
Northing Variation: NEAP-ORID
Northing Variation: NEAP-SNTR
Northing Variation: NEAP-TUBI
Northing Variation: NEAP-VASS
Northing Variation: NEAP-XRSO
Northing Variation: NICO-ORID
Northing Variation: NICO-SNTR
Northing Variation: NICO-TUBI
Northing Variation: NICO-VASS
Northing Variation: NICO-XRSO
Northing Variation: ORID-SNTR
Northing Variation: ORID-TUBI
Northing Variation: ORID-VASS
Variation (m)
Decimal Date

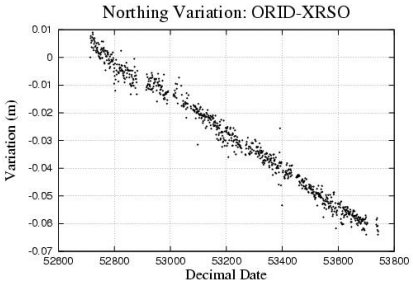
Northing Variation: ORID-XRSO
Variation (m)
Decimal Date

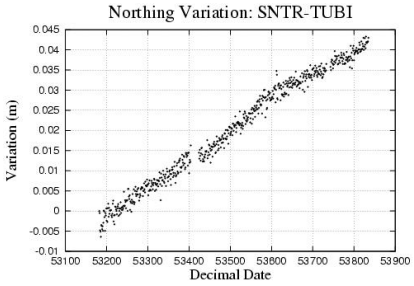
Northing Variation: SNTR-TUBI
Variation (m)
Decimal Date

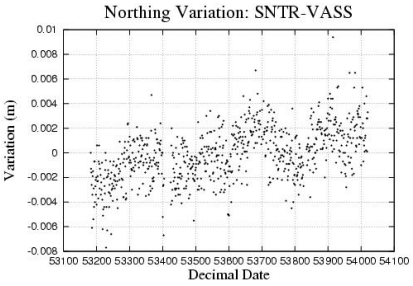
Northing Variation: SNTR-VASS
Variation (m)
Decimal Date

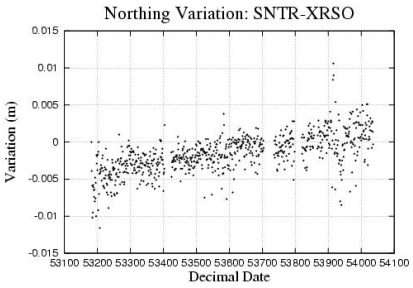
Northing Variation: SNTR-XRSO
Variation (m)
Decimal Date

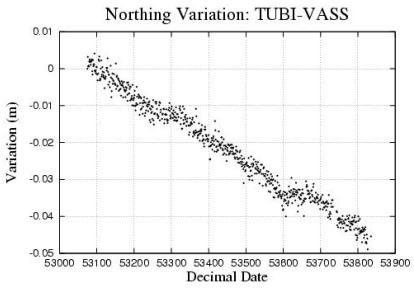
Northing Variation: TUBI-VASS
Variation (m)
Decimal Date

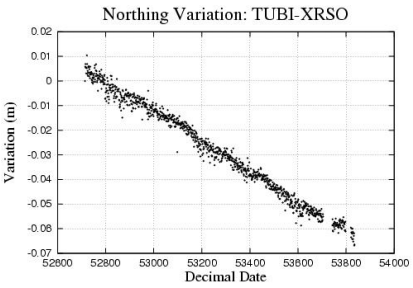
Northing Variation: TUBI-XRSO
Variation (m)
Decimal Date

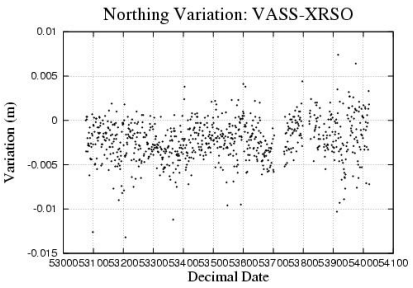
Northing Variation: VASS-XRSO
Variation (m)
Decimal Date

Vertical Variations

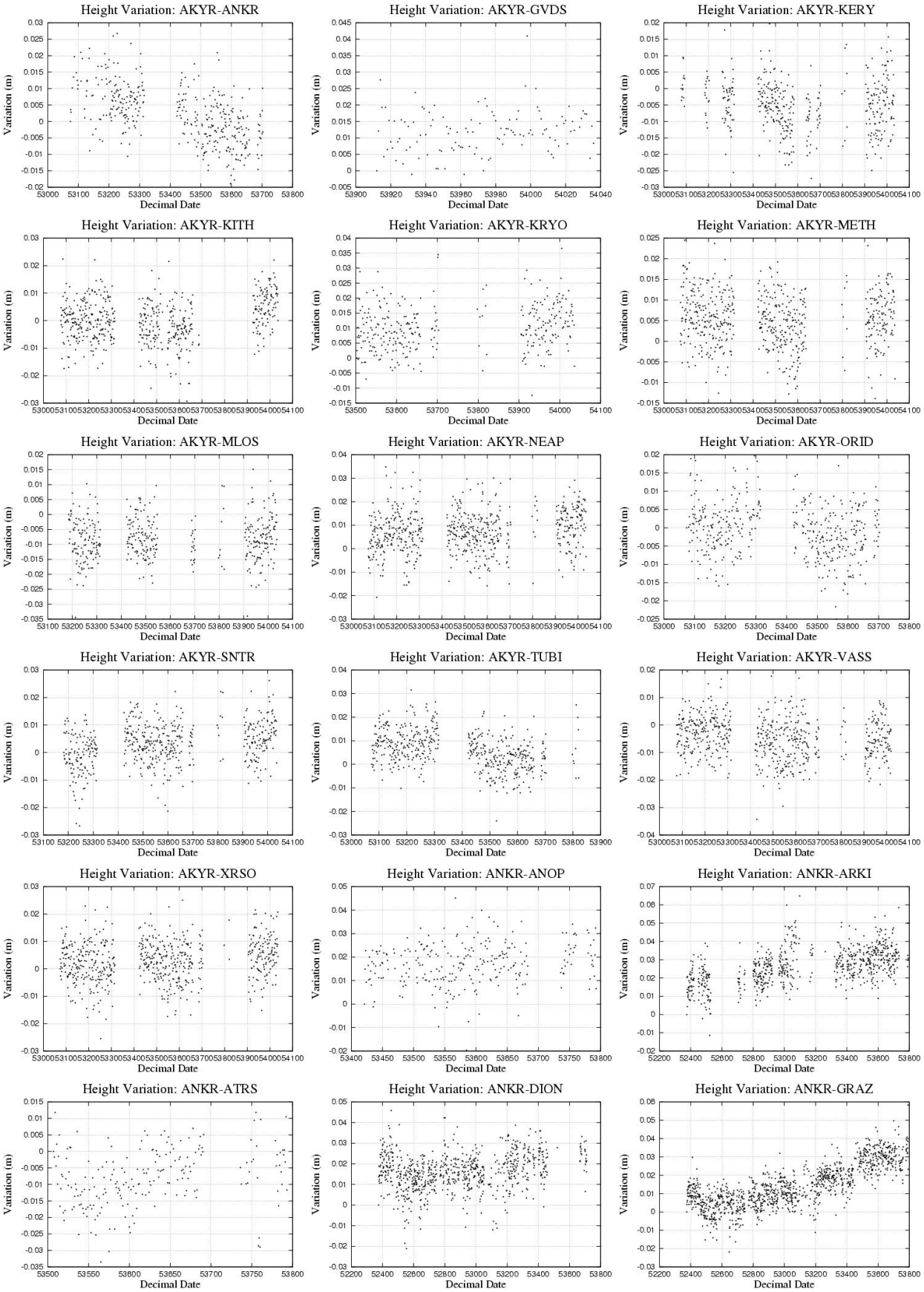

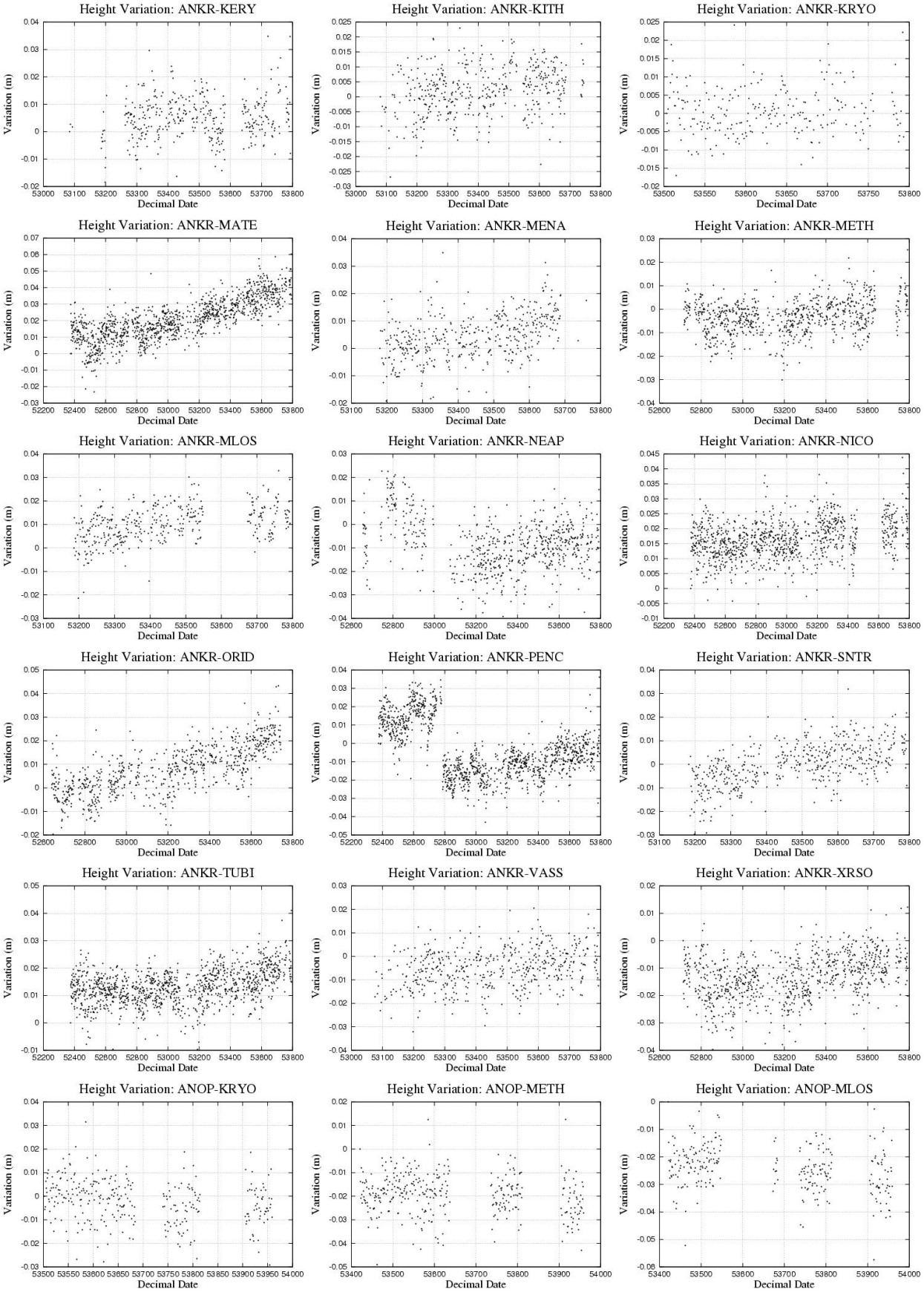
Height Variation: ANKR-KERY
Height Variation: ANKR-KITH
Height Variation: ANKR-KRYO
Height Variation: ANKR-MATE
Height Variation: ANKR-MENA
Height Variation: ANKR-METH
Height Variation: ANKR-MLOS
Height Variation: ANKR-NEAP
Height Variation: ANKR-NICO
Height Variation: ANKR-ORID
Height Variation: ANKR-PENC
Height Variation: ANKR-SNTR
Height Variation: ANKR-TUBI
Height Variation: ANKR-VASS
Height Variation: ANKR-XRSO
Height Variation: ANOP-KRYO
Height Variation: ANOP-METH
Height Variation: ANOP-MLOS
Variation (m)
Decimal Date

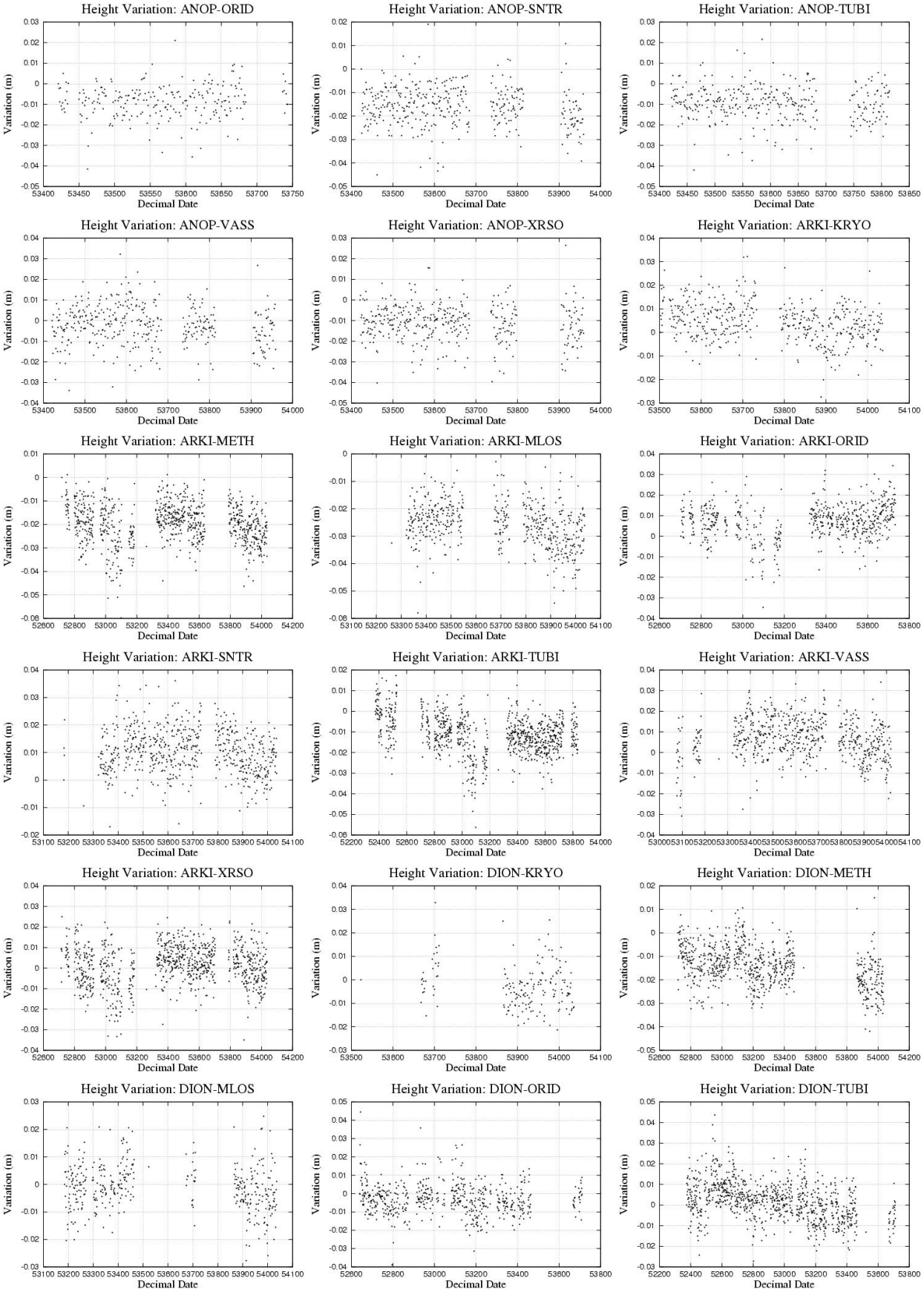
Height Variation: ANOP-ORID
Height Variation: ANOP-SNTR
Height Variation: ANOP-TUBI
Height Variation: ANOP-VASS
Height Variation: ANOP-XRSO
Height Variation: ARKI-KRYO
Height Variation: ARKI-METH
Height Variation: ARKI-MLOS
Height Variation: ARKI-ORID
Height Variation: ARKI-SNTR
Height Variation: ARKI-TUBI
Height Variation: ARKI-VASS
Height Variation: ARKI-XRSO
Height Variation: DION-KRYO
Height Variation: DION-METH
Height Variation: DION-MLOS
Height Variation: DION-ORID
Height Variation: DION-TUBI
Variation (m)
Decimal Date

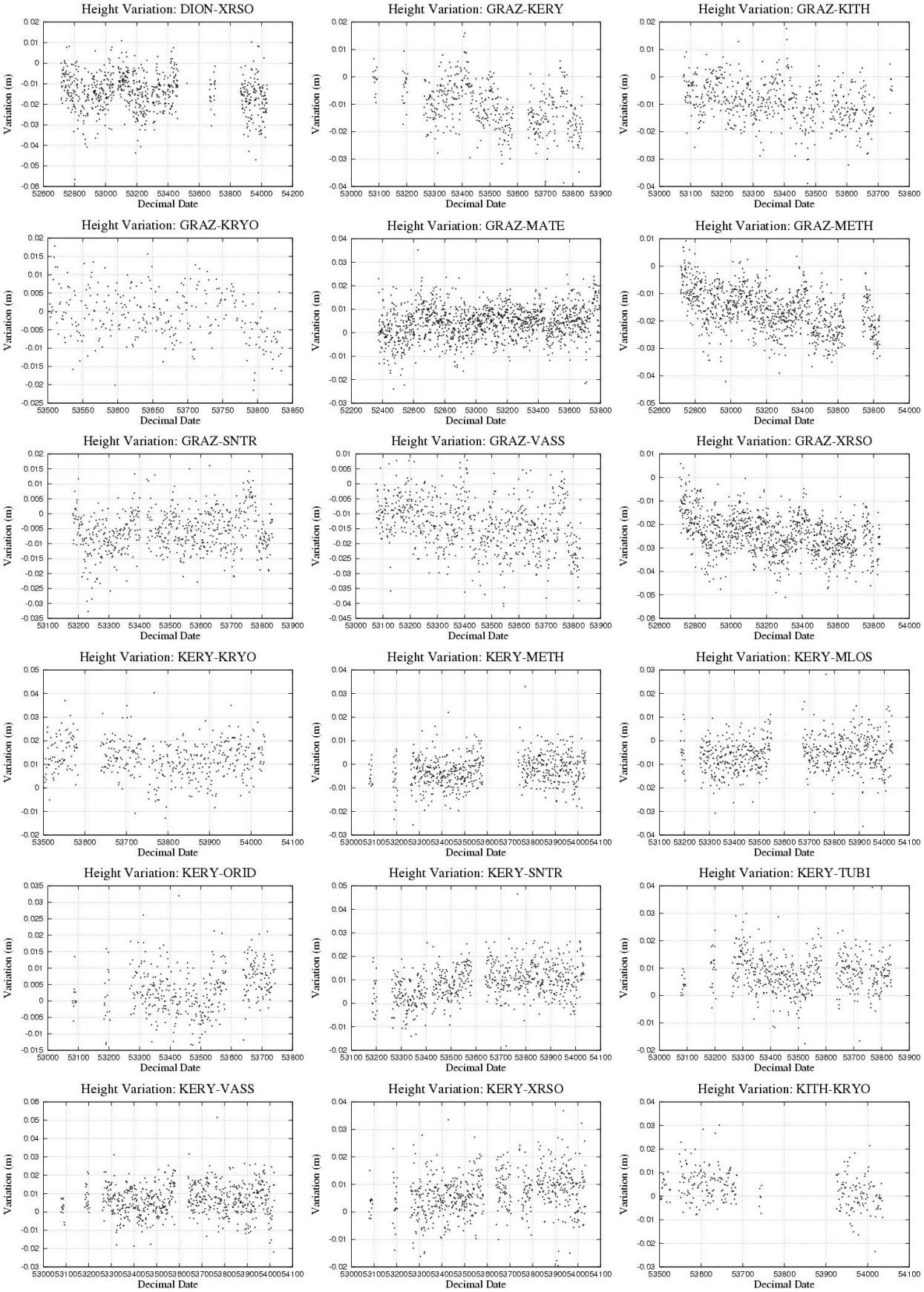
Height Variation: DION-XRSO
Height Variation: GRAZ-KERY
Height Variation: GRAZ-KITH
Height Variation: GRAZ-KRYO
Height Variation: GRAZ-MATE
Height Variation: GRAZ-METH
Height Variation: GRAZ-SNTR
Height Variation: GRAZ-VASS
Height Variation: GRAZ-XRSO
Height Variation: KERY-KRYO
Height Variation: KERY-METH
Height Variation: KERY-MLOS
Height Variation: KERY-ORID
Height Variation: KERY-SNTR
Height Variation: KERY-TUBI
Height Variation: KERY-VASS
Height Variation: KERY-XRSO
Height Variation: KITH-KRYO
Variation (m)
Decimal Date

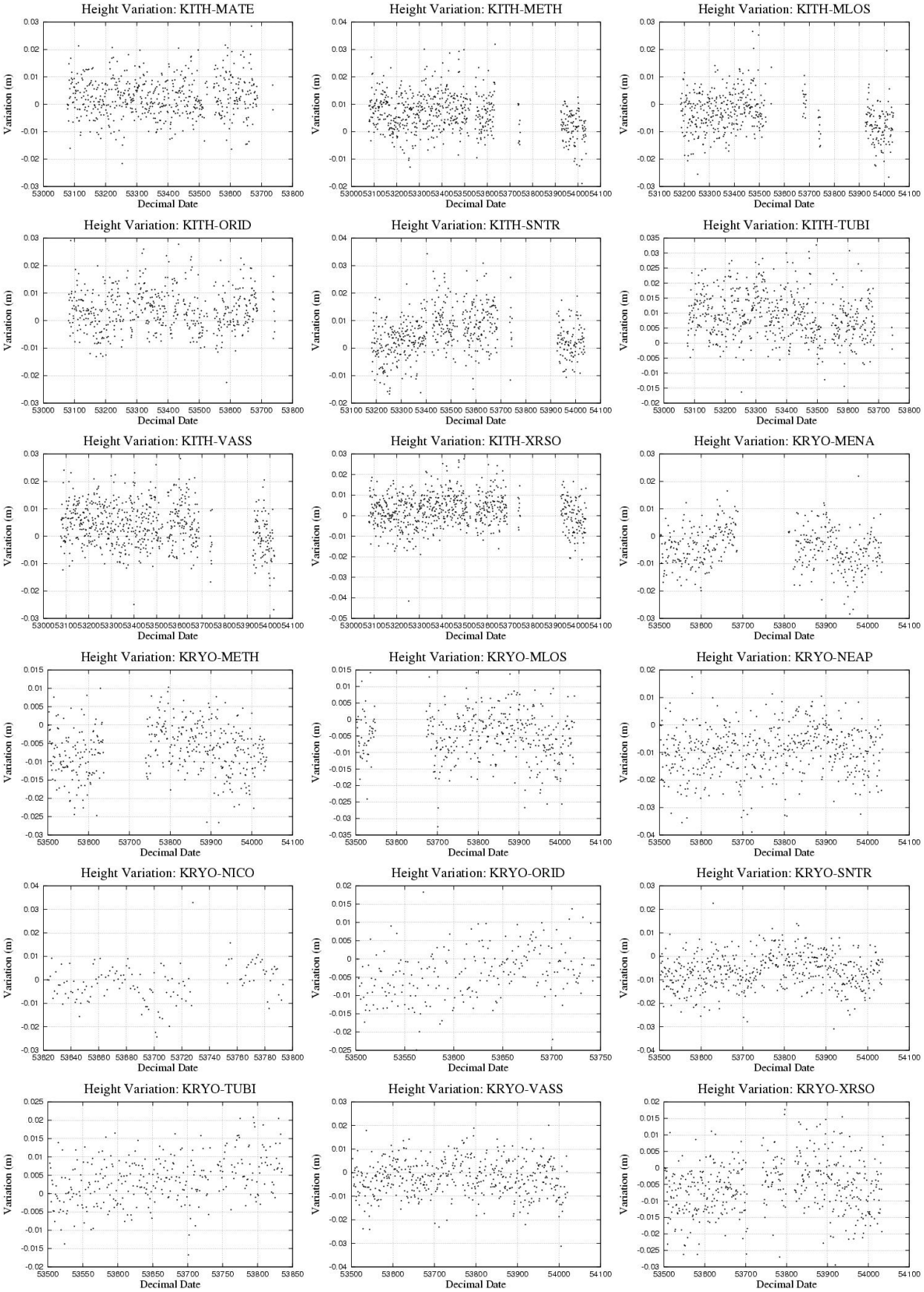
Height Variation: KITH-MATE
Height Variation: KITH-METH
Height Variation: KITH-MLOS
Height Variation: KITH-ORID
Height Variation: KITH-SNTR
Height Variation: KITH-TUBI
Height Variation: KITH-VASS
Height Variation: KITH-XRSO
Height Variation: KRYO-MENA
Height Variation: KRYO-METH
Height Variation: KRYO-MLOS
Height Variation: KRYO-NEAP
Height Variation: KRYO-NICO
Height Variation: KRYO-ORID
Height Variation: KRYO-SNTR
Height Variation: KRYO-TUBI
Height Variation: KRYO-VASS
Height Variation: KRYO-XRSO
Variation (m)
Decimal Date

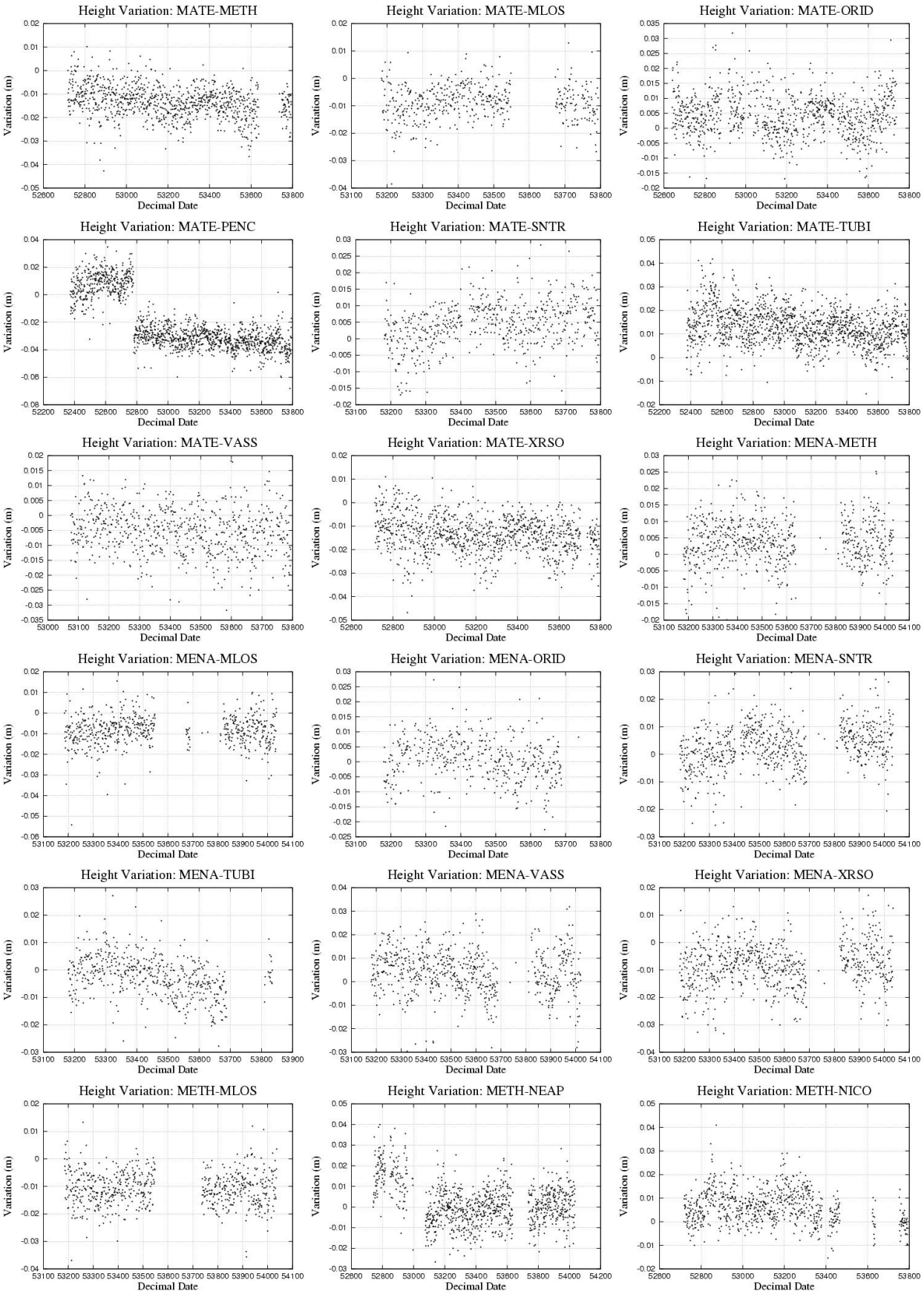
Height Variation: MATE-METH
Height Variation: MATE-MLOS
Height Variation: MATE-ORID
Height Variation: MATE-PENC
Height Variation: MATE-SNTR
Height Variation: MATE-TUBI
Height Variation: MATE-VASS
Height Variation: MATE-XRSO
Height Variation: MENA-METH
Height Variation: MENA-MLOS
Height Variation: MENA-ORID
Height Variation: MENA-SNTR
Height Variation: MENA-TUBI
Height Variation: MENA-VASS
Height Variation: MENA-XRSO
Height Variation: METH-MLOS
Height Variation: METH-NEAP
Height Variation: METH-NICO
Variation (m)
Decimal Date

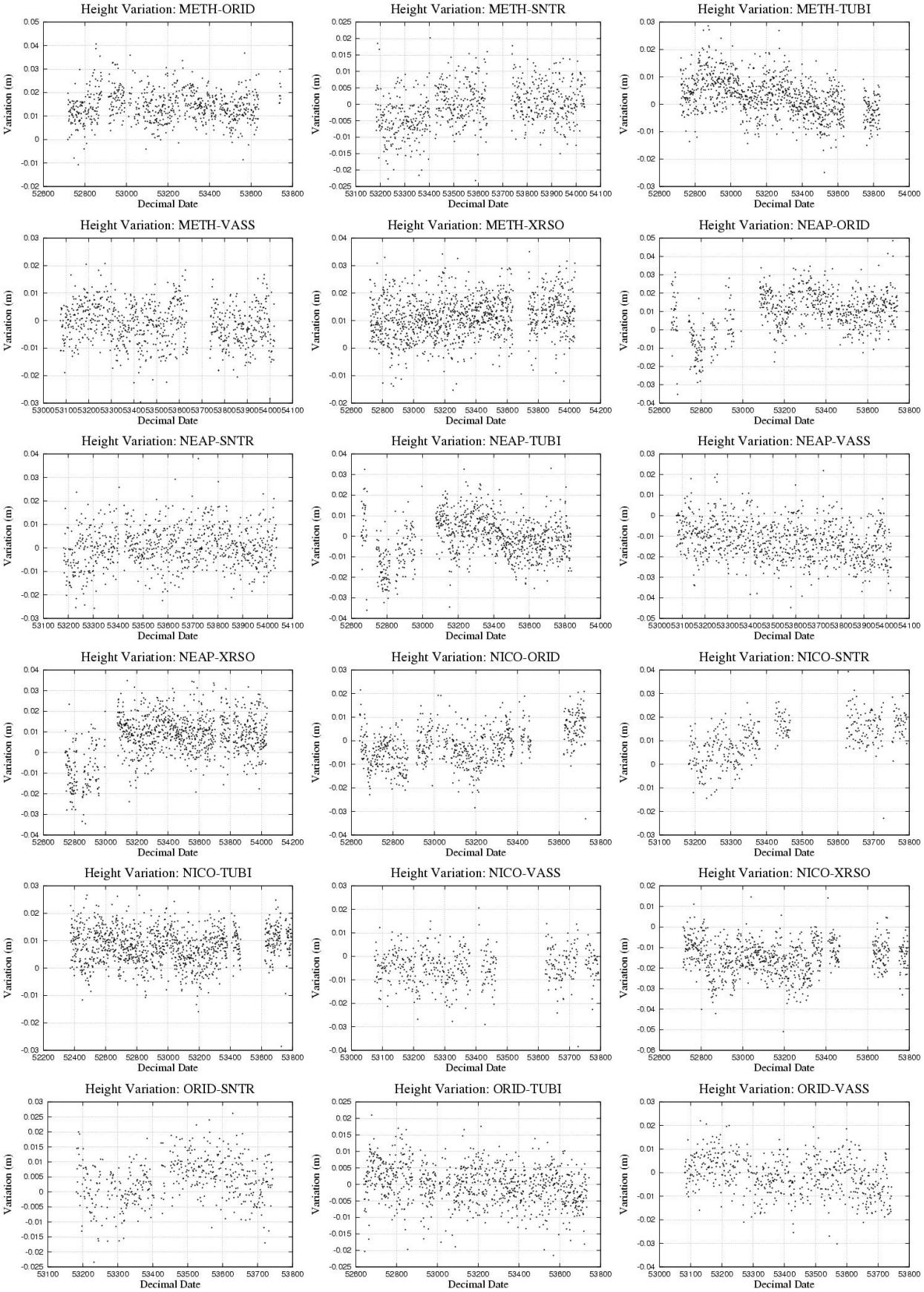
Height Variation: METH-ORID
Height Variation: METH-SNTR
Height Variation: METH-TUBI
Height Variation: METH-VASS
Height Variation: METH-XRSO
Height Variation: NEAP-ORID
Height Variation: NEAP-SNTR
Height Variation: NEAP-TUBI
Height Variation: NEAP-VASS
Height Variation: NEAP-XRSO
Height Variation: NICO-ORID
Height Variation: NICO-SNTR
Height Variation: NICO-TUBI
Height Variation: NICO-VASS
Height Variation: NICO-XRSO
Height Variation: ORID-SNTR
Height Variation: ORID-TUBI
Height Variation: ORID-VASS
Variation (m)
Decimal Date

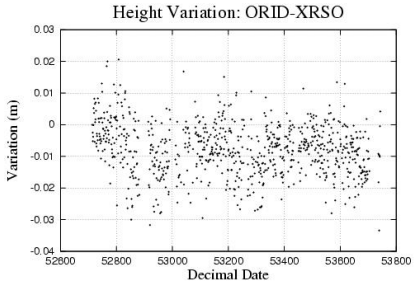
Height Variation: ORID-XRSO
Variation (m)
Decimal Date

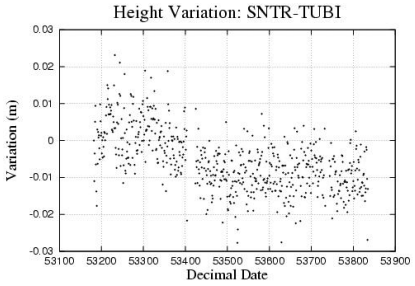
Height Variation: SNTR-TUBI
Variation (m)
Decimal Date

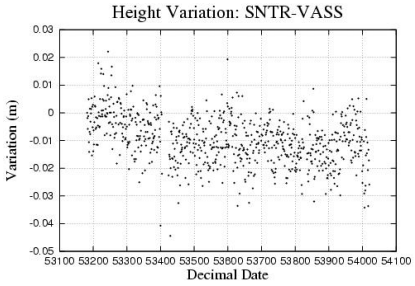
Height Variation: SNTR-VASS
Variation (m)
Decimal Date

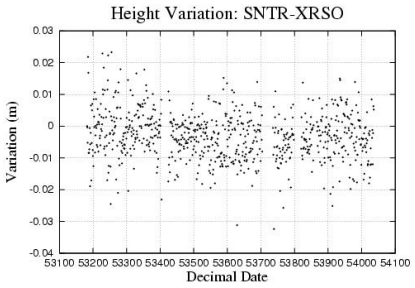
Height Variation: SNTR-XRSO
Variation (m)
Decimal Date

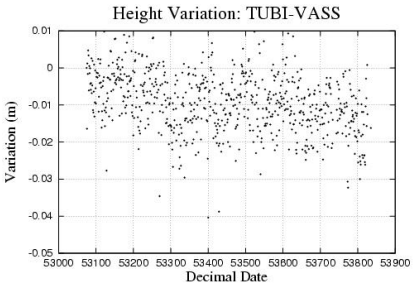
Height Variation: TUBI-VASS
Variation (m)
Decimal Date

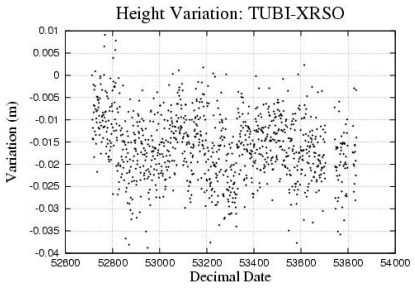
Height Variation: TUBI-XRSO
Variation (m)
Decimal Date

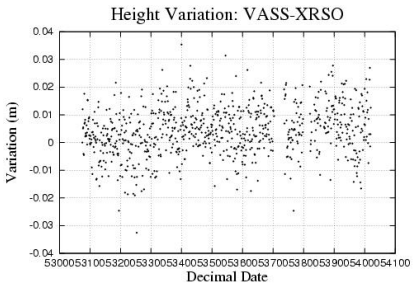
Height Variation: VASS-XRSO
Variation (m)
Decimal Date

Appendix F

Curve Fitting Technique

The equation we're looking to solve for is:

$$y = A\sin(\omega t + \varphi)$$

1.

From this we seek to estimate the parameters A (the amplitude) and φ (the phase angle)

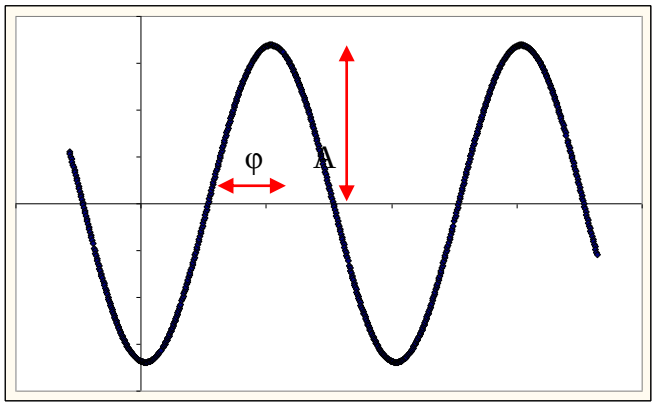

From 1. we can derive:

$$y = A[\sin\omega t\cos\varphi + \sin\varphi\cos\omega t]$$
$$y = A\cos\varphi\sin\omega t + A\sin\varphi\cos\omega t$$
$$y = b\sin\omega t + a\cos\omega t$$

In the process we estimate the coefficients "a" and "b" from the data, and then use these estimates to solve for A and φ through the equations:

$$b = A\cos\varphi$$

2.

$$a = A\sin\varphi$$

3.

Therefore:

$$\frac{a}{b} = \frac{A\sin\varphi}{A\cos\varphi} = \tan\varphi$$

Therefore:

$$\varphi = \tan^{-1}\left(\frac{a}{b}\right)$$

Squaring 2. and 3. gives:

$$b^2 = A^2\cos^2\varphi^2$$
$$a^2 = A^2\sin^2\varphi^2$$

Adding these gives:

$$a^2 + b^2 = A^2\cos^2\varphi + A^2\sin^2\varphi = A^2\left(\cos^2\varphi + \sin^2\varphi\right)$$

As:

$$\left(\cos^2\varphi + \sin^2\varphi\right) = 1$$

$$a^2 + b^2 = A^2$$

Therefore:

$$A = \sqrt{\left(a^2 + b^2\right)}$$

Data Estimation

The data set needs to first of all be detrended and all time tags have to be reduced (for example "t" needs equal t^o-2003).

The model is:

$$y = a\cos\omega t + b\sin\omega t + v$$
$$\omega = 2\pi f$$
$$f = \frac{1}{T}$$

T = 1 as the estimate is for an annual signal, therefore $f = 1$

This yields the following matrices:

$$\begin{bmatrix} a\cos\omega t_1 + b\sin\omega t_1 \\ a\cos\omega t_2 + b\sin\omega t_2 \\ \vdots \\ a\cos\omega t_n + b\sin\omega t_n \end{bmatrix} \begin{bmatrix} a \\ b \end{bmatrix} = \begin{bmatrix} y_1 \\ y_2 \\ \vdots \\ y_n \end{bmatrix} + \begin{bmatrix} v_1 \\ v_2 \\ \vdots \\ v_n \end{bmatrix}$$